



THE HONG KONG  
POLYTECHNIC UNIVERSITY

香港理工大學

Pao Yue-kong Library  
包玉剛圖書館

---

## Copyright Undertaking

This thesis is protected by copyright, with all rights reserved.

**By reading and using the thesis, the reader understands and agrees to the following terms:**

1. The reader will abide by the rules and legal ordinances governing copyright regarding the use of the thesis.
2. The reader will use the thesis for the purpose of research or private study only and not for distribution or further reproduction or any other purpose.
3. The reader agrees to indemnify and hold the University harmless from and against any loss, damage, cost, liability or expenses arising from copyright infringement or unauthorized usage.

If you have reasons to believe that any materials in this thesis are deemed not suitable to be distributed in this form, or a copyright owner having difficulty with the material being included in our database, please contact [lbsys@polyu.edu.hk](mailto:lbsys@polyu.edu.hk) providing details. The Library will look into your claim and consider taking remedial action upon receipt of the written requests.

**Modeling and Control of a Direct Expansion  
(DX) Variable-air-volume (VAV) Air  
Conditioning (A/C) System**

**Chen Wu**

**A thesis submitted in partial fulfillment of the requirements  
for the Degree of Doctor of Philosophy**

Department of Building Services Engineering  
The Hong Kong Polytechnic University

October 2005



Pao Yue-kong Library  
PolyU · Hong Kong

*To my family*

## **Certificate of Originality**

I hereby declare that this thesis is my own work and that, to the best of my knowledge and belief, it reproduces no material previously published or written, nor material that has been accepted for the award of any other degree or diploma, except where due acknowledgement has been made in the text.

Chen Wu

Department of Building Services Engineering

The Hong Kong Polytechnic University

Hong Kong SAR, China

July, 2005

## **Abstract**

A direct expansion (DX) variable-air-volume (VAV) air conditioning (A/C) system, a typical type of air-cooled packaged A/C systems found in commercial buildings, consists of a VAV air-distribution sub-system and a DX refrigeration plant. Such a system offers more advantages than a conventional chilled-water based VAV A/C system, such as higher energy efficiency and generally costing less to own and operate. Currently, the major deterrence to its wider application is to continuously match the output cooling capacity from its DX refrigeration plant with the varying cooling load in its VAV air-distribution sub-system. However, the development of both variable-speed compressor and electronic expansion valve (EEV) technologies offer a good opportunity to address the problem of capacity-load matching.

This thesis firstly reports on the development of an experimental rig for a DX VAV A/C system. The rig was operated by a computerized logging and control supervisory system. All major operating parameters can be real-time measured, monitored and recorded, using high-precision measuring devices/sensors. The setting up of the rig would help facilitate developing both a dynamic model and its experimental validation, and new control strategies for a DX VAV A/C system.

Secondly, a complete dynamic mathematical model for the experimental DX VAV A/C system has been developed based on the principle of mass and energy conservation, and using the correlations describing the operational performance of various components in the experimental DX VAV A/C system, which were either field-tested or available from manufacturers. Mathematical correlations representing

the control logics of various controllers were also included. The model was component-based and of partial-lumped-parameter type. It consisted of separate constituent sub-models for both the DX refrigeration plant and the VAV sub-system in the DX VAV A/C system. Both the steady-state and dynamic behaviors from both the DX refrigeration plant and the VAV sub-system can be simultaneously simulated by the model.

Thirdly, the experimental validation for the dynamic model developed using the experimental rig is presented. The open-loop responses from both the DX refrigeration plant and the dynamic sub-model representing the DX plant were compared and found in good agreement. Fourthly, the thesis reports on the simulated closed-loop responses from the DX VAV A/C system with all its conventional proportional-integral (PI) control loops being enabled, using the validated model. Simulation results demonstrated that the dynamic model developed can behave as expected in a similar manner to a real DX VAV A/C system with all its control loops enabled. This further confirmed that the model developed was correct and could be useful for studying control issues for a real DX VAV A/C system.

Finally, the development of a novel DDC-based feedforward capacity controller, for matching the output cooling capacity from the DX refrigeration plant with the varying cooling load in the VAV sub-system, is reported. The feedforward controller consisted of both a numerical calculation algorithm, which was fundamentally based on the principle of energy balance using a number of real-time measured system's operating parameters, and a dead-band for avoiding unstable compressor operation. Controllability tests for the feedforward controller have been carried out in the

experimental rig. Test results suggested that the novel feedforward controller developed was able to provide satisfactory control sensitivity and accuracy, resulting in a higher operating efficiency of, and better environmental control by, a DX VAV A/C system.

## **Acknowledgements**

I must express my sincere grateful thanks to my Chief Supervisor, Dr. Deng Shiming, Associate Professor from the Department of Building Services Engineering (BSE), The Hong Kong Polytechnic University, for his readily available supervision, invaluable suggestions, patient guidance and continuous help throughout the course of the project.

Special thanks go to The Hong Kong Research Grant Council (RGC) and The Hong Kong Polytechnic University for financially supporting this project. I would like also to thank the technicians in the HVAC Laboratory of the BSE Department for their assistances in experimental work.

Finally, I would like to express my deepest appreciation to my parents, my wife Ms. Wang Lifeng, and all other family members. I could not have completed my research work without their understandings, encouragement and support.



## Table of Contents

	<b>Page</b>
<b>Certificate of Originality</b>	<b>i</b>
<b>Abstract</b>	<b>ii</b>
<b>Acknowledgements</b>	<b>v</b>
<b>Table of Contents</b>	<b>vi</b>
<b>List of Figures</b>	<b>xi</b>
<b>List of Tables</b>	<b>xv</b>
<b>Nomenclature</b>	<b>xvi</b>
<b>Subscripts</b>	<b>xx</b>
<b>Chapter 1 Introduction</b>	<b>1</b>
<b>Chapter 2 Literature Review</b>	<b>6</b>
2.1 Introduction	6
2.2 Modeling of DX VAV A/C systems	8
2.2.1 Modeling of DX refrigeration plants	10
2.2.1.1 Correlations of the thermodynamics of refrigerants	10
2.2.1.2 Heat exchanger modeling	12
2.2.1.3 Compressor modeling	14
2.2.1.4 Expansion valve modeling	16
2.2.2 Modeling of VAV air-distribution sub-systems	17
2.2.2.1 Supply fan modeling	19
2.2.2.2 Air-distribution ductwork modeling	20
2.2.2.3 VAV terminal modeling	22
2.2.2.4 Air-conditioned space modeling	23
2.3 Fundamental issues for VAV A/C systems	23

2.3.1	Demanded control ventilation	25
2.3.2	Reset of supply air static pressure	26
2.3.3	Performance of humidity control	27
2.3.4	Advanced control for VAV A/C systems	29
2.4	Problems for DX VAV A/C systems	31
2.4.1	Capacity control	32
2.4.2	Humidity control	37
2.4.3	DDC for DX VAV A/C systems	39
2.5	Summary	41
<b>Chapter 3</b>	<b>Proposition</b>	<b>45</b>
3.1	Background	45
3.2	Project title	46
3.3	Aims and objectives	47
3.4	Research methodologies	47
<b>Chapter 4</b>	<b>Development of an Experimental Rig for DX VAV A/C Systems</b>	<b>50</b>
4.1	Introduction	50
4.2	Detailed descriptions of the experimental rig and its major components	51
4.2.1	DX refrigeration plant	51
4.2.2	VAV air-distribution sub-system	55
4.3	Instrumentation and data acquisition system (DAS)	57
4.3.1	Sensors/measuring devices for temperatures, pressures and flow rates	57
4.3.2	Data acquisition system and calculation	59
4.4	LabVIEW logging & control supervisory program	61
4.5	Conventional control loops in the experimental rig	62
4.6	Summary	64
<b>Chapter 5</b>	<b>Dynamic Modeling of the Experimental DX VAV A/C System</b>	<b>66</b>

5.1	Introduction	66
5.2	Development of the sub-model for the DX refrigeration plant	67
5.2.1	Variable-speed compressor	69
5.2.2	Electronic expansion valve (EEV)	72
5.2.3	Condenser	74
5.2.3.1	Refrigerant side of the desuperheating region	75
5.2.3.2	Refrigerant side of the two-phase region	76
5.2.3.3	Refrigerant side of the subcooling region	79
5.2.3.4	Receiver, fittings and refrigerant line	81
5.2.3.5	Air side of the condenser	82
5.2.4	DX Evaporator (cooling coil)	86
5.2.4.1	Refrigerant side of the two-phase region	87
5.2.4.2	Refrigerant side of the superheating region	90
5.2.4.3	Air side of the evaporator	93
	5.2.4.3.1 Wet-cooling of air in <i>Veal2</i>	93
	5.2.4.3.2 Dry-cooling of air in <i>Veal</i>	96
5.3	Development of the sub-model for the VAV air-distribution sub-system	98
5.3.1	Air-conditioned spaces	100
5.3.2	Supply air fan	101
5.3.3	Return air and outdoor air dampers	103
5.3.4	VAV terminals	104
5.3.5	Plenum box	110
5.3.6	Hydraulic calculation for air-distribution ductwork	110
5.4	Numerical solution procedure	111
5.5	Summary	117
<b>Chapter 6</b>	<b>Model Validation</b>	<b>119</b>
6.1	Introduction	119
6.2	Overview of model validation	120
6.3	Experimental validation for the sub-model of DX refrigeration plant	124
6.4	Summary	133

<b>Chapter 7</b>	<b>Simulated Closed-loop Responses Using the Validated Model</b>	<b>134</b>
7.1	Introduction	134
7.2	Operating conditions to obtain closed-loop responses	135
7.3	Simulated results and analysis	137
7.4	Summary	152
<b>Chapter 8</b>	<b>A Novel DDC-based Feedforward Capacity Controller for the DX VAV A/C System</b>	<b>154</b>
8.1	Introduction	154
8.2	Development of the novel DDC-based feedforward capacity controller	157
8.2.1	Numerical calculation algorithm (NCA) using real-time measured operating parameters	158
8.2.2	The dead-band for avoiding unstable compressor operation	162
8.2.2.1	Problems for controlling compressor speed based only on the NCA	162
8.2.2.2	Introduction of the dead-band	166
8.2.3	Complete control for the DX VAV A/C system	167
8.3	Approach to realize the feedforward controller in the experimental station	168
8.4	Controllability tests for the feedforward controller developed	170
8.4.1	Results of Test 01	172
8.4.2	Results of Test 02	181
8.5	Summary	189
<b>Chapter 9</b>	<b>Conclusions and Future Work</b>	<b>192</b>
9.1	Conclusions	192
9.1.1	The problem encountered	
9.1.2	The experimental rig and dynamic mathematical model developed	193
9.1.3	Model validation and simulated closed-loop responses	194

9.1.4	Novel feedforward capacity controller	195
9.1.5	Main contributions	196
9.2	Proposed future work	197
<b>References</b>		<b>199</b>
<b>Appendix A Photos of the Experimental Rig</b>		<b>214</b>
<b>Appendix B Publications Arising From the Thesis</b>		<b>221</b>

## List of Figures

	<b>Page</b>
<b>Chapter 4</b>	
Figure 4.1	The schematic diagram of the complete experimental rig 53
Figure 4.2	The schematic diagram of the DX refrigeration plant 54
<b>Chapter 5</b>	
Figure 5.1	The conceptual model of the experimental DX VAV A/C system 68
Figure 5.2	Conceptual model of the VAV air-distribution sub-system 99
Figure 5.3	Control logics of pressure-independent VAV terminals 106
Figure 5.4	Schematic diagram of the hydraulic network for the ductwork in the experimental DX VAV A/C system 111
Figure 5.5	Flow chart for the numerical solution procedure of the complete model for the experimental DX VAV A/C system 115
Figure 5.6	Flow chart for the numerical solution procedure of the sub-model for VAV air-distribution sub-system 116
<b>Chapter 6</b>	
Figure 6.1	Comparison between the measured and the simulated performances for the supply fan at different speeds 121
Figure 6.2	Comparison between the measured and the simulated air flow rates passing through terminal's damper 123
Figure 6.3	Open-loop responses of the sub-model and the plant (degree of refrigerant superheat) after being subjected to a step-change of compressor speed 129
Figure 6.4	Open-loop responses of the sub-model and the plant (cooling capacity) after being subjected to a step-change of compressor speed 129
Figure 6.5	Open-loop responses of the sub-model and the plant (evaporating pressure) after being subjected to a 130

	step-change of compressor speed	
Figure 6.6	Open-loop responses of the sub-model and the plant (condensing pressure) after being subjected to a step-change of compressor speed	130
Figure 6.7	Open-loop responses of the sub-model and the plant (compressor power input) after being subjected to a step-change of compressor speed	131
Figure 6.8	Open-loop responses of the sub-model and the plant (dry-bulb air temperature at evaporator exit) after being subjected to a step-change of compressor speed	131
Figure 6.9	Open-loop responses of the sub-model and the plant (wet-bulb air temperature at evaporator exit) after being subjected to a step-change of compressor speed	132
Figure 6.10	Open-loop responses of the sub-model and the plant (sensible heat ratio) after being subjected to a step-change of compressor speed	132
 <b>Chapter 7</b>		
Figure 7.1	Simulated closed-loop responses (space air temperatures)	144
Figure 7.2	Simulated closed-loop responses (VAV terminal's damper opening)	145
Figure 7.3	Simulated closed-loop responses (air flow rate of VAV terminal)	145
Figure 7.4	Simulated closed-loop responses (space air moisture content)	146
Figure 7.5	Simulated closed-loop responses (space air relative humidity)	146
Figure 7.6	Simulated closed-loop response (total supply air flow rate)	147
Figure 7.7	Simulated closed-loop response (supply air static pressure)	147
Figure 7.8	Simulated closed-loop response (supply fan speed)	148
Figure 7.9	Simulated closed-loop response (supply air dry-bulb temperature)	148

Figure 7.10	Simulated closed-loop response (compressor speed)	149
Figure 7.11	Simulated closed-loop response (degree of refrigerant superheat at evaporator exit)	149
Figure 7.12	Simulated closed-loop response (EEV opening)	150
Figure 7.13	Simulated closed-loop response (evaporating pressure)	150
Figure 7.14	Simulated closed-loop response (condensing pressure)	151
Figure 7.15	Simulated closed-loop response (supply air moisture content)	151
Figure 7.16	Simulated closed-loop response (cooling capacity)	152
 <b>Chapter 8</b>		
Figure 8.1	Measured total supply air flow rate	164
Figure 8.2	Measured compressor speed regulated by NCA only based feedforward controller	165
Figure 8.3	Measured degree of refrigerant superheat	165
Figure 8.4	Measured EEV opening	166
Figure 8.5	Interface of the L&C program for testing the feedforward controller developed	169
Figure 8.6	Interface of the self-programming module for testing the feedforward controller developed	170
Figure 8.7	Space air temperatures <i>vs.</i> time (Test 01)	175
Figure 8.8	VAV terminal openings <i>vs.</i> time (Test 01)	175
Figure 8.9	VAV terminal air flow rates <i>vs.</i> time (Test 01)	176
Figure 8.10	Supply fan speed <i>vs.</i> time (Test 01)	176
Figure 8.11	Supply air pressure <i>vs.</i> time (Test 01)	177
Figure 8.12	Total supply air flow rate <i>vs.</i> time (Test 01)	177
Figure 8.13	Compressor speed <i>vs.</i> time (Test 01)	178
Figure 8.14	EEV opening <i>vs.</i> time (Test 01)	178
Figure 8.15	Refrigerant superheat at the exit of evaporator <i>vs.</i> time (Test 01)	179
Figure 8.16	Plant's cooling capacity <i>vs.</i> time (Test 01)	179
Figure 8.17	Supply air temperature <i>vs.</i> time (Test 01)	180
Figure 8.18	Air relative humidity in both Spaces <i>vs.</i> time (Test 01)	180



Figure 8.19	Space air temperatures <i>vs.</i> time (Test 02)	183
Figure 8.20	VAV terminal openings <i>vs.</i> time (Test 02)	184
Figure 8.21	VAV terminal air flow rates <i>vs.</i> time (Test 02)	184
Figure 8.22	Supply fan speed <i>vs.</i> time (Test 02)	185
Figure 8.23	Supply air pressure <i>vs.</i> time (Test 02)	185
Figure 8.24	Total supply air flow rate <i>vs.</i> time (Test 02)	186
Figure 8.25	Compressor speed <i>vs.</i> time (Test 02)	186
Figure 8.26	EEV opening <i>vs.</i> time (Test 02)	187
Figure 8.27	Refrigerant superheat at the exit of evaporator <i>vs.</i> time (Test 02)	187
Figure 8.28	Plant's cooling capacity <i>vs.</i> time (Test 02)	188
Figure 8.29	Supply air temperature <i>vs.</i> time (Test 02)	188
Figure 8.30	Air relative humidity in both Spaces <i>vs.</i> time (Test 02)	189

## **Appendix A**

Photo 1	Overview of the experimental rig (1)	214
Photo 2	Overview of the experimental rig (2)	214
Photo 3	Condensing unit of the DX plant	215
Photo 4	DX cooling coil in the VAV air-distribution sub-system	215
Photo 5	Outdoor air induction	216
Photo 6	Box of VAV terminal	216
Photo 7	Controller of VAV terminal	217
Photo 8	Load generation unit inside conditioned spaces	217
Photo 9	Air sampling device	218
Photo 10	Manometers for measuring supply air static pressure	218
Photo 11	SCR, SSR and VFD	219
Photo 12	Control panel	219
Photo 13	Logging & control supervisory program	220
Photo 14	Self-programming module (SPM)	220

## List of Tables

	<b>Page</b>
<b>Chapter 4</b>	
Table 4.1	Details of the variable-speed compressor and EEV 54
Table 4.2	Geometric parameters of heat exchangers 55
Table 4.3	Details of the VAV terminals and supply air fan 57
<b>Chapter 6</b>	
Table 6.1	Coefficients for the equation of terminal's damper 122
<b>Chapter 7</b>	
Table 7.1	Controllers' control parameters for obtaining closed-loop response 137
Table 7.2	Set points for various operating parameters 137
<b>Chapter 8</b>	
Table 8.1	Control parameters of the PI feedback controllers in the experimental DX VAV A/C system 171
Table 8.2	Operating conditions of the two controllability tests 172

## Nomenclature

Variable	Description	Unit
$A$	opening of damper/EEV; or heat transfer area	$m^2$
$B$	proportional gain of differential-pressure sensor	V/Pa
$B_0$	refrigerant boiling characteristic number	DL
$B_m$	integrated refrigerant thermo-physical property	DL
$C_0$	refrigerant convection characteristic number	DL
$C_1, C_2 \sim C_6$	constants in Equations (5.95) to (5.101)	DL
$C_p$	specific heat at constant pressure	kJ/(kg.K)
$C_v$	flow coefficient of EEV	DL
$D$	tube diameter	m
$D_c$	tube collar diameter	m
$D_h$	hydraulic tube diameter	m
$De$	deviation of controlled parameter	CD
$DV$	direct-current voltage	V
$e$	rotor eccentricity	m
$F$	input frequency of VFD	Hz
$Fr$	<i>Froude</i> number	DL
$f$	refrigerant turbulent skin-friction coefficient	DL
$g$	air moisture content	kg/(kg dry-air)
$g_r$	refrigerant mass flux	kg/(s.m <sup>2</sup> )
$g_z$	air moisture content of conditioned space	kg/(kg dry-air)
$h$	enthalpy	kJ/kg
$j$	<i>Colburn</i> factor	DL
$j_1, j_2, j_3 \sim j_8$	correlation number	DL
$K$	pressure loss coefficient of damper	DL
$K_p$	proportional gain of PI controller	CD
$l$	stroke of cylinder	m
$l_e$	tube length of each flow circuit	m

$LMTD$	log mean temperature difference	K
$m$	mass flow rate	kg/s
$M$	mass	kg
$MC$	moisture removal capacity	kg/s
$M_r$	mass of residual refrigerant	kg
$N$	fan speed	r/min.
$NR$	number of tube row	DL
$Nu$	<i>Nusselt</i> number	DL
$n$	compressor speed	r/s
$P$	pressure	Pa
$P_B$	proportional band of thermostat controller	°C
$Pr$	<i>Prandtl</i> number	DL
$PH$	total pressure head	Pa
$PI_f$	fin pitch	m
$PI_L$	louver pitch	m
$PL$	number of electrode couple for motor	DL
$PLS$	pulse number output from EEV's controller	DL
$\Delta P$	pressure difference	Pa
$Q$	heat transfer rate	W
$q$	heat transfer flux	W/m <sup>2</sup>
$R_0$	combined thermal resistance from the tube wall, surface contact and fouling	(m.K)/W
$Re$	<i>Reynolds</i> number	DL
$R_{dam}$	flow resistance of damper	(Pa.s <sup>2</sup> )/m <sup>6</sup>
$R$	radius of cylinder	m
$r$	the radius of rotor	m
$s$	slip factor of the motor	DL
$S_1$	transverse tube pitch	m
$S_2$	longitudinal tube pitch	m
$T$	temperature	K
$T_s$	air temperature sensed by thermostat	°C

$T_z$	air temperature of conditioned space	°C
$t_c$	time constant	s
$t_i$	integral time of PID controller	s
$U$	overall heat transfer coefficient	W/(m <sup>2</sup> .K)
$V$	space volume of heat transfer region	m <sup>3</sup>
$V_z$	volume of conditioned space	m <sup>3</sup>
$\dot{V}$	air volumetric flow rate	m <sup>3</sup> /s
$\dot{V}_{com}$	refrigerant volumetric flow rate of compressor	m <sup>3</sup> /s
$\dot{V}_{com,t}$	theoretical volumetric flow rate of compressor	m <sup>3</sup> /s
$W$	electrical work to compressor	W
$w_{com}$	indicated specific work to compressor	J/kg
$w_{com,t}$	isentropic specific work of compressor	J/kg
$x$	refrigerant dryness fraction	DL
$Z$	refrigerant void fraction	DL

*Greek symbols*

$\alpha$	convective heat transfer coefficient	W/(m <sup>2</sup> .K)
$\beta$	compression index	DL
$\delta t$	sampling time of controller	s
$\varepsilon$	rotor relative eccentricity	DL
$\phi$	offset adjustment parameter of PID controller	CD
$\varphi$	leakage factor of damper	DL
$\gamma$	refrigerant latent heat of vaporization	kJ/kg
$\eta_{el}$	electric coefficient of compressor	DL
$\eta_f$	fin efficiency	DL
$\eta_i$	indicated coefficient of compressor	DL
$\eta_{mec}$	mechanical coefficient of compressor	DL
$\eta_{motor}$	motor coefficient of compressor	DL
$\eta_s$	surface coefficient of tube-fin	DL
$\lambda$	compressor's displacement coefficient,	DL

$\lambda_f$	thermal conductivity of fin metal	W/(m.K)
$\lambda_l$	leakage coefficient of compressor	DL
$\lambda_r$	thermal conductivity of refrigerant	W/(m.K)
$\lambda_p$	pressure loss coefficient of compressor	DL
$\lambda_T$	temperature coefficient of compressor	DL
$\lambda_v$	volumetric coefficient of compressor	DL
$\mu$	dynamic viscosity	kg/(m.s)
$\omega_0$	constant rotation speed of motor	degree(°)/s
$\omega$	rotational speed of actuator motor	degree(°)/s
$\theta$	damper inclination angel	degree (°)
$\theta_h$	actuator-damper hysteresis angle	degree (°)
$\theta_l$	louver angle	degree (°)
$\rho$	density	kg/m <sup>3</sup>
$\omega$	moisture generation rate	kg/s
$v_a$	air velocity	m/s
$\xi$	dehumidifying augmentation factor	DL
$\zeta$	slip rate of refrigerant	DL

Note: DL = Dimensionless  
 CD = Controller-dependent

## Subscripts

<i>a</i>	air
<i>c</i>	condenser/ condensing
<i>com</i>	compressor
<i>des</i>	desuperheating region
<i>dr</i>	dry-cooling
<i>e</i>	evaporator/evaporating
<i>f</i>	fin
<i>fa</i>	fresh air
<i>i</i>	inside tube
<i>l</i>	liquid refrigerant
<i>max</i>	maximum
<i>min</i>	minimum
<i>o</i>	outside tube
<i>r</i>	refrigerant
<i>ra</i>	return air
<i>sb</i>	subcooling region
<i>sh</i>	refrigerant superheat
<i>sly</i>	supply air
<i>sp</i>	superheating region
<i>stp</i>	static pressure
<i>tp</i>	two-phase region
<i>tu</i>	tube
<i>v</i>	vapor refrigerant
<i>wall</i>	enclosure wall
<i>wt</i>	wet-cooling

# **Chapter 1**

## **Introduction**

A direct expansion (DX) variable-air-volume (VAV) air-conditioning (A/C), or a DX VAV A/C system, a typical type of air-cooled packaged A/C systems found in commercial buildings, is composed of an air-cooled DX refrigeration plant and a VAV air-distribution sub-system. The evaporator in the DX refrigeration plant is used directly as a DX cooling coil in the VAV air-distribution sub-system to simultaneously cool and dehumidify the air passing through the DX cooling coil. Conditioned air is then forced through the air-distribution ductwork by a supply fan, and sent into conditioned-spaces with air flow rates being regulated by their respective VAV terminals.

A DX VAV A/C system offers more advantages than a conventional chilled-water based VAV A/C system. These include high energy efficiency, no problem of freezing, and lower cost to own and maintain because no chilled water pumps and piping are required. A DX VAV A/C system can also offer independent zoning-control of space air temperature to meet different requirements of thermal control. The major deterrence to the wider use of DX VAV A/C systems, however, has been the difficulty to match the output cooling capacity from its DX refrigerant plant with the varying cooling load in its VAV air-distribution sub-system.

In a DX VAV A/C system, continuously-varying supply air flow rate over a wide range due to its VAV operation requires corresponding changes in the output cooling capacity from its DX refrigeration plant. The accurate capacity regulation for a DX



refrigeration plant using the conventional control methods such as cycling on-off, hot-gas bypass and staging-control is hard to achieve. Consequently, the control stability for supply air temperature, which is critical for realizing independent zoning-control of space air temperatures, is much more difficult to obtain in a DX VAV A/C system, than in a conventional chilled-water based VAV A/C system by using high-resolution three-way modulating valves. Unfortunately, the related in-depth reported research work on DX VAV A/C systems can be hardly identified in open literatures. Therefore, it is necessary to embark on a study on developing new capacity control strategies that can help eliminate the problem of capacity-load matching in a DX VAV A/C system, through mathematical modeling and experimental work.

The thesis begins with in Chapter 2 a critical literature review on various issues related to the modeling and control for DX VAV A/C systems. An extensive review on the modeling of individual components in either a DX refrigeration plant or a VAV A/C system, which revealed that a complete dynamic mathematical model for DX VAV A/C systems cannot be identified, is firstly presented. This is followed by reviewing fundamental issues related to VAV A/C systems, such as demanded control ventilation, reset of supply air static pressure, and the performance of humidity control, etc. Thirdly, a number of important issues where further in-depth research work in the operating and control of a DX VAV A/C system is required have been identified and reported.

Chapter 3 presents the research proposal which covers the background, the project title, aims and objectives, and research methodologies adopted in the research work

for a DX VAV A/C system.

Chapter 4 presents the development of an experimental rig for DX VAV A/C systems. The experimental rig consisted of a DX refrigeration plant having a variable-speed rotor compressor and an EEV, and a VAV air-distribution sub-system including two identical conditioned spaces. The schematic diagrams for the experimental rig and the detailed explanations for its major components and instrumentation are included. The speeds of the rotor compressor, supply air fan and condenser cooling fan may be varied using variable-frequency drives (VFD). Various high-accuracy measuring devices/sensors are detailed. A logging & control supervisory program specifically developed for this experimental rig using LabVIEW programming platform is presented. The introduction of twelve conventional feedback control loops provided in the experimental rig to create and maintain any required experimental conditions is also included. The availability of the experimental rig is expected to be helpful in successfully carrying out the research work for DX VAV A/C systems as proposed in Chapter 3.

Chapter 5 reports on the development of a representative, dynamic mathematical model for the experimental DX VAV A/C system. The model consisted of two constituent sub-models for its DX refrigeration plant and its VAV air-distribution sub-system, respectively. The complete dynamic model for the experimental DX VAV A/C system was component-based and consisted of a set of ordinary differential equations and algebraic correlations. In addition, the numerical solution procedure to solve the dynamic model is explained. Preliminary tests of the complete model suggested that the model was stable and behaved as expected.

Chapter 6 presents the experimental validation for the dynamic model of the experimental DX VAV A/C system, using the experimental rig described in Chapter 4. Experimental work to obtain the open-loop responses of the DX refrigeration plant after being subjected to step changes in its major operating parameters has been carried out. Experimental open-loop responses for all major operational parameters from the DX plant agreed well with the simulated open-loop responses from the dynamic sub-model representing the DX refrigeration plant, suggesting that the dynamic model has been successfully experimentally validated.

Chapter 7 presents a simulation study on the closed-loop responses of the DX VAV A/C system with all its conventional PI feedback control loops being enabled, using the validated dynamic model. The responses obtained suggested that the validated dynamic model would behave in a similar manner to that a real DX VAV A/C system would, when all its control loops were put into operation. This further confirmed that the model developed was correct and could be helpful for studying control issues for DX VAV A/C systems.

Chapter 8 reports on the development of a novel direct-digital-control (DDC) based feedforward capacity controller, for matching the output cooling capacity from the DX refrigeration plant with the varying cooling load in the VAV air-distribution sub-system. The feedforward controller consisted of both a numerical calculation algorithm, which was fundamentally based on the principle of energy balance using a number of real-time measured system's operating parameters, and a dead-band for avoiding unstable compressor operation. Controllability tests for the feedforward

controller have been carried out in the experimental rig. Test results suggested that the novel feedforward controller was able to provide satisfactory control sensitivity and accuracy, resulting in a higher operating efficiency of, and better environmental control by a DX VAV A/C system.

Finally, the conclusions of this thesis and the proposed future work are presented in Chapter 9.

## **Chapter 2**

### **Literature Review**

#### **2.1 Introduction**

Faced with the next possible energy crises and the pursuing of high quality living and working environment, the Heating, Ventilation and Air Conditioning (HVAC) industry is struggling to achieve higher energy efficiency, while improving the thermal comfort control in air-conditioned spaces. It has been reported that energy used for building cooling and heating accounted for more than half of the total energy use in commercial and public buildings in many parts of the world [Lam 2000]. Direct-expansion (DX) air conditioning (A/C) systems find wide applications in those light commercial and low rise residential buildings, such as supermarkets, schools, offices and villas. According to Department of Energy (DOE), USA, packaged rooftop A/C systems, a typical type of DX A/C system, consumed about one-third of the total heating and cooling energy use in commercial buildings, over one quadrillion BTU per year in the US [Bordick and Gilbride 2002]. Therefore, it is important to improve the operating efficiency of DX A/C systems, as this would significantly contribute to sustainable development.

A DX A/C system usually provides basic air conditioning functions including air distribution, fresh air induction, filtration, and cooling/heating of the conditioned air. The evaporator in its refrigeration plant is of DX type and is used directly as a cooling coil to simultaneously cool and dehumidify the air passing through it. A DX A/C system includes air-distribution ductwork. This distinguishes itself from a

residential small-size window-type or split-type air conditioner. Meanwhile, a DX A/C system makes use of its evaporator to handle directly the conditioned air. This again distinguishes itself from a conventional central chilled-water based A/C system where chilled water is used in a cooling coil for cooling and dehumidifying.

DX A/C systems vary in size from 1.5 to over 100 tons of cooling capacity, and are dominated by the systems having the cooling capacity below 10 tons. These smaller DX systems accounted for about 50% of the total installed DX cooling capacity in the US [Kenneth 1997 and Jabobs 2002]. The majority of existing DX A/C systems has been operated with air-distribution sub-systems of constant air volume (CAV). Over the years, DX A/C systems have been regarded as a least-cost alternative solution when the use of central chilled water-based A/C systems became less economic. With the increased diversification of building functions and the impacts from potential shortage of energy supply, more and more attentions have been paid to DX A/C systems because of their application flexibility and higher energy efficiency. On the other hand, the use of variable-air-volume (VAV) air-distribution sub-system can help save much energy from reduced fan power consumption during part-load operation. It also provides independent zoning control to meet different requirements for thermal comfort.

Therefore, a DX VAV A/C system, which is a direct integration of a DX refrigeration plant and a VAV air-distribution sub-system, is expected to be much more flexible and energy-efficient [Qian and Zheng 2003]. Such a system combines the advantages of both a DX refrigeration plant and a VAV air-distribution system.

Therefore studying the operating performance of, and developing appropriate control strategies for DX VAV A/C systems become more and more important.

This chapter presents a critical literature review on various issues related to the modeling and control for DX VAV A/C systems. An extensive review on the modeling for individual components in either a DX refrigeration plant or a VAV A/C system, which revealed that a complete dynamic mathematical model for DX VAV A/C systems cannot be identified, is firstly presented. This is followed by reviewing fundamental issues related to VAV A/C systems, such as demanded control ventilation, reset of supply air static pressure, and the performance of humidity control, etc. Thirdly, a number of important issues where further in-depth research work in the operating and control of a DX VAV A/C system is required have been identified and reported.

## **2.2 Modeling of DX VAV A/C systems**

The research work based on mathematical modeling, over recent years, has gained more and more recognition because it could not only save the cost of research and development, but also help understand the operating characteristics of a physical system under study over its entire operating range. In the field of HVAC and refrigeration, simulation-based research has become more and more popular. It can be applied to system design, optimization and developing new control methods. It can help to investigate the operational performance of a system, to verify the feasibility of a new control strategy, to detect and diagnose the faults of a system, etc.

Simulation-based research can be classified into the following two types, lumped- and distributed-parameter simulation. Distributed-parameter mathematical modeling can reflect well the distribution characteristic of a system's parameters, which is particularly useful in, for example, studying the air flow field of evaporator. However carrying out distributed-parameter simulation research is time-consuming, with perhaps poor calculation stability. On the other hand, although lumped-parameter simulation research is relatively simple and is hard to reflect the detailed distribution of parameters along the dimension of a system component, it is more useful in studying the overall performance of a system, and consequently usually more effective in carrying out research work related to system control. Furthermore, simulation may also be classified into dynamic and steady-state modeling. Steady-state modeling should be sufficiently accurate for most long-term system simulations or for design optimization. However, it is not suitable for control application where it is necessary to investigate system's transient responses to sudden disturbance. Dynamic modeling is required when carrying out research work related to the control for a physical system.

A DX VAV A/C system consists of a constituent DX refrigeration plant and a VAV air-distribution sub-system. There have been previously reported studies on developing separate mathematical models for the two constituent parts. These are separately reviewed in this section.



### **2.2.1 Modeling of DX refrigeration plants**

Various approaches have been used to model a DX refrigeration plant. Some models described in detail all phenomena involved, while others applied simplification. Often, a DX refrigeration plant may be considered as consisting of four basic components, and then component-based modeling was possible. With the availability of both models representing various components and correlations for refrigerants, a DX refrigeration plant may be finally represented by a set of ordinary differential equations and algebraic correlations. An extensive survey of earlier development of dynamic and steady-state models of DX refrigeration systems has been reported by Welsby et al. [1988]

#### **2.2.1.1 Correlations of the thermodynamics of refrigerants**

In accordance with the Montreal Protocol, R22 will be gradually phased out by 2020. Currently, more environmental friendly alternative refrigerants, such as R134a, R410a and R407c, have been widely used in HVAC&R systems. This is particularly true in those developed countries and regions.

In practice, the working fluid in the refrigeration circuit of a DX refrigeration plant is the mixture of refrigerant and lubricating oil or contaminants. The compositions perhaps vary from case to case, affecting the thermodynamic properties of a pure refrigerant. In order to well understand the effects of thermo-physical properties on the performance of a refrigeration plant, Martz et al. [1996] and Hesse and Kruse

[1988] attempted to predict the thermodynamics of oil refrigerant mixtures through mathematic modeling. However, because the exact molecular composition of lubricating oil was diversified and often difficult to be ascertained, the preciseness and application of their models for oil refrigerant mixtures in the simulation-based research were limited. On the other hand, the modification of a refrigerant thermodynamic model considering the presence of oil would make the dynamic simulation for a DX A/C system much more complicated, but would be of little help to study its control performance of the system.

In 1981 Chan and Haselden [1981a, 1981b, 1981c] published a set of computer subroutines for refrigerant thermodynamic properties. These have been widely used because they were based on the recommendations of a Working Party set up by International Institute of Refrigeration (IIR) and hence were authoritative. In order to incorporate a model representing the thermodynamic properties of a particular refrigerant into the dynamic simulation model of a refrigeration system, in 1986, Cleland [1986] published a set of curve-fitting polynomial equations of refrigerants that were computationally much quicker than those by Chan and Haselden. The Cleland equations agreed well with those by Chan and Haselden with deviations of about 0.25%, which was tolerable for simulation-based research. Because the above mentioned equations for refrigerants were all explicit, iteration was often inevitable.. Based on the Sectional Smooth Technique, Ding et al. [1992] and Zhang et al. [2000] developed an implicit cubic linear function for refrigerant thermodynamic properties that can avoid iteration. In 1994, Cleland [1994] extended his curve-fitting correlations, which were firstly proposed in 1986 and have been widely accepted since, to include the correlations for refrigerant R134a. His correlations were based

on the data set for R134a published by the IIR [International Institute of Refrigeration 1992] and the range of saturation temperature was  $-40\text{ }^{\circ}\text{C}$  to  $70\text{ }^{\circ}\text{C}$ .

### **2.2.1.2 Heat exchanger modeling**

The modeling of heat exchangers has always been in the spotlight for simulation-based research work for HVAC&R systems. Diversified approaches have been employed to establish the models for condensers and evaporators. Important studies include the fully lumped-parameter models by Chi and Didion [1982], and Vargas and Parise [1995], the fully distributed-parameter models by MarcArthur [1984], and Bensafi et al [1997]. However, partially lumped-parameter models by Deng [2000] and Domanski [1991] used a different approach where for example an evaporator was divided into three zones, i.e., two-phase, superheat and sub-cooling zone. Three zones were modeled separately based on the different heat transfer and fluid flow characteristics. This approach can adequately represent the overall thermal characteristics in a heat exchanger in operation to carry out research work for system's control, meanwhile its simulation stability and computational speed may be well ensured.

During modeling a heat exchanger, its heat transfer and fluid flow characteristics are embodied by mathematical correlations of heat transfer coefficients and the total pressure drop. For a refrigerant-to-air heat exchanger using various inside micro-fin tube for heat transfer enhancement, its air-side heat transfer resistance may account for over 80% of the total heat transfer resistance. Hence, the correlations of the air-

side heat transfer coefficient would significantly affect the modeling accuracy for the overall heat transfer. A set of relatively simple correlations for the average heat transfer coefficient for a plate-finned tube was developed by Turaga et al [1988]. The experimental comparison by Corberan and Melon [1998] showed that the correlations for a multiple-row heat exchanger having flat fin provided by Gray and Webb [1986] agreed well with the experimental data. It was recommended that an air-side heat transfer coefficient for wavy and louvered fins, which were widely used in air conditioning & refrigeration installations now, could be evaluated using the coefficient for a flat fin and multiplying it by an enhancement factor appropriate to a given fin design. Webb [1990] developed an enhancement factor correlation for wavy fins that can take into account the flow conditions and geometric variables of a heat exchanger. Currently, the most commonly enhanced surface used in DX A/C systems is of louvered fin type that can provide a higher average heat transfer coefficient. Wang et al. [1999 and 2000] proposed general heat transfer correlations for louvered fin geometry having round tube configuration under dry and wet conditions, respectively. A total of 49 samples of louvered fin-and-tube heat exchangers with different geometric parameters, including louver pitch, louver height, longitudinal tube pitch, transverse tube pitch, tube diameter, and fin pitch were included in the correlations developed.

The refrigerant pressure drop through a heat exchanger was often neglected or a fixed value was assumed in lumped-parameter models. In fact, the refrigerant pressure drop in a heat exchanger, particularly in an evaporator, greatly impacted on the performance of a refrigeration system, as this would directly affect the evaporating or condensing pressure. More importantly, this would also affect the

compressor suction pressure and the degree of superheat of refrigerant, and hence the refrigerant state before compressor suction. The refrigerant state at suction was very important to calculate the refrigerant mass flow rate passing through a compressor, and then the cooling capacity of a system. The uncertainty of refrigerant flow rate would reduce the accuracy of simulation for a DX refrigeration system. According to the correlations by Pierre [1964], the refrigerant pressure drop through a heat exchanger was proportional to the square of refrigerant flow rate. Therefore, the approach assuming a fixed refrigerant pressure drop was probably too rough for system's simulation-based research. This was particularly true for a DX refrigeration system using a variable-speed compressor. Although there have been many reports studying the pressure drop for various refrigerants including R134a inside a heat exchanger [Cavallini et al. 2001], a general average pressure drop correlation has been in fact hard to derive because the average pressure drop would be closely related to the configuration of inside tube surface, and actual heat exchanger's geometry such as circuitry arrangements etc.

### **2.2.1.3 Compressor modeling**

Compared to an evaporator or a condenser, the dynamics of a compressor may be negligible, quasi-steady modeling was therefore usually applied. This was achieved by assuming that a compressor reached its specified operating speed instantly. Generally, a polytropic compression process was assumed and the mathematical model of compressor can be established by using traditional theoretical

thermodynamic approach [Domanski and McLinden 1992, Jolly et al. 1990, Matthew and Banasal 1998]. A model so developed was suitable for system simulation, and particularly for energy performance analysis and the investigations related to system control. When modeling, the volumetric and electric efficiencies were usually represented by an empirical correlation or determined using the actual performance data with the aid of curve fitting/regression analysis. The latter that can achieve better approximation than the former one, required a set of detailed tested performance data of compressor from manufacturers or on-situ tests.

Due to high efficiency, low noise, low torque variations, high reliability and tolerance to refrigerant droplets [ASHRAE Handbook 2000], scroll compressors whose capacity ranging from 3 to 50 kW have been increasingly used in residential and commercial air conditioning installations. Many mathematical models for scroll compressor can be found in open literature. However, most of them were too complex, as they were intended for the purpose of compressor design. These models usually took into account the geometry of scrolls, the scroll dynamics, deformations, internal leakage, etc., requiring therefore large number of parameters from manufacturer [Dutta and Yanagisawa 2001 and Park et al. 2002].

For research work related to the control of a DX refrigeration system, the model for its scroll compressor should be simple in structure and fast in response for easy incorporation into the complete model of a DX VAV A/C system. In fact, its accuracy to represent refrigerant mass flow rate and discharge temperature was mostly important for simulation-based research work for control. It was reported by

Eric et al. [2002] that the heating up of refrigerant at the suction of a hermetic scroll compressor can cause refrigerant temperature to increase by up to 35 K. Fortunately, the pressure drops at both the suction and the discharge were insignificant and can therefore almost be neglected. These characteristics of a scroll compressor were the major differences between a scroll compressor and other types of non-hermetic compressor, and should be taken into consideration when modeling.

#### **2.2.1.4 Expansion valve modeling**

Two types of expansion valves commonly used in DX A/C systems are a thermal expansion valve (TEV) and an electronic expansion valve (EEV). The latter has the advantages of rapid response owing to electronic signal transmission, zero activating superheat, nearly linear valve characteristic, a wide coverage of flow rate, easy realization of programmed control, etc. It is expected that an EEV would gain a wider application in DX A/C systems in future. Therefore, an EEV is indispensable if the advantages of a DX A/C system having a variable-speed compressor are to be maximized. As an essential component in a DX A/C system, an EEV acts as a throttling device where the expansion of refrigerant takes place, and usually regulates the refrigerant flow rate such that its desired degree of superheat at the exit of an evaporator can be maintained. Commonly, a steady-state model can be applied to an expansion valve due to its very small thermal inertia. Refrigerant expansion is generally treated as an isenthalpic process when modeling an expansion valve. Refrigerant mass flow passing through an expansion valve is usually calculated by

an empirical correlation. Deng [2000] presented a relatively simple model for an expansion valve. The model simply considered the refrigerant mass flow rate proportional to the degree of refrigerant superheat, however the actual fluid-flow characteristic in an expansion valve was hard to be represented by the model. MacArthur [1984] represented an expansion valve by an orifice equation. One representative model of expansion valves was developed by Damasceno and Rooke [1990], based on the specifications given by manufacturer and empirical fitting for one set of distributor nozzle and tube sizes. The refrigerant mass flow rate passing through an expansion valve,  $m_{r, TXV}$ , similar to that flowing through an orifice, was given by:

$$m_{r, TXV} = [C_{TXV}(\Delta T_{oper} - \Delta T_{sat}) + C_{bleed}] (\rho_r \Delta P_{TXV})^{0.5} \quad (2.1)$$

where,  $\Delta T_{oper}$  was the actual degree of superheat,  $\Delta T_{sat}$  the required degree of superheat to initiate the valve,  $\rho_r$  the refrigerant density and  $\Delta P_{TXV}$  the available refrigerant pressure drop across the valve. The flow area coefficient,  $C_{TXV}$ , was calculated based on the experimental performance data of the valve.

### 2.2.2 Modeling of VAV air-distribution sub-systems

Many studies on VAV A/C systems can be found in open literature. Most of the research work reported focused on the control and optimization to improve thermal environmental control while lowering energy use. Simulation-based research was the main approach used to investigate the operational performance of VAV A/C systems



and to evaluate the effectiveness of different control strategies. Well-known simulation packages such as TRANSYS [Klein et al. 1990], DOE-2 [LBL 1982], HAVACSIM+ [NTIS 1986], BLAST [UI 1983], EnergyPlus [EnergyPlus 2004], etc., provided good platforms to simulate VAV A/C systems. Generally, DOE-2 and BLAST were more suitable for evaluating the energy use performance of a VAV A/C system, while HAVACSIM+ and TRANSYS relatively suitable for developing long-time-span issues of control strategies. These general program packages already provided the sub-models of basic components in a VAV A/C system. However, as pointed out by Underwood [Underwood 2000] who was involved in developing component sub-models for TRNSYS, one remarkable restriction of these simulation packages was that most of component models available were steady-state or quasi-steady-state, making them not suitable for investigating short-time-span control issues such as system's control stability analysis. When specific operating characteristics and control issues were investigated, it would become necessary to make modifications to specific components and to programs' structure.

Apart from the general program packages such as TRANSYS, a number of practical, simple but precise models for VAV A/C systems to meet specific research requirements have also been developed. For example, Zaheer and Zheng [1994] developed a transient model of a two-zone VAV A/C system consisting of 328 nonlinear time-varying equations. House [1995] carried out a simulation study for a VAV A/C system for studying its optimal control. These specifically developed models were different from or improved from those in the general program packages, and often used for specific purpose.

### 2.2.2.1 Supply fan modeling

Carrado and Mazza [1991] established a model of a constant-speed supply fan that can account for the influence of its inlet vane angle on its operating parameters. The model normalized the air flow rate, fan total pressure rise and fan power consumption respectively. Fan performance law was directly applied by fitting two polynomials of normalized air flow rate and fan pitch angle. As to a variable speed supply fan, its pressure-volume flow characteristics can be described, in general, by a family of constant-speed curves for pressure rise versus volumetric flow rate. According to the first fan performance law [ASHRAE 2000], for fans operating at similar dynamic conditions, their volumetric flow rates at different speeds are proportional to the change of fan speed; their fan pressure rises are proportional to the square of, and their fan power consumptions to the cubic of the change of fan speed, respectively. Hence, using the performance data from a fan manufacturer and the well-known least-square curve-fitting technique, the fan characteristics at different speeds can be developed based on the performance data at its rated speed and expressed by a set of polynomials. In order to get better approximation with the experimental performance data, Mei and Levermore [2002] adopted a ten-neuron sigmoid artificial neural network (ANN) improved model to represent the characteristics of a fan whose speed was controlled by varying supply voltage.

The dynamics of a fan-motor system lies in the electromagnetic and mechanical inertia of the system. When a varying voltage is supplied to a fan motor to change fan speed, the fan speed does not immediately reach its steady-state regime mainly due to the electro-motive force induced to the armature of the motor. Therefore when

carrying out a control strategy analysis, the dynamics of the fan whose speed is controlled by varying supply voltage, should be taken into consideration. Mei and Levermore [2002] used a first-order differential equation with different time constants in different operational areas to describe the dynamics of a fan-motor system. Moreover, two first-order differential equations, which showed the detailed relationships among the armature current, voltage applied to the motor, voltage drop and motor speed, were used by Zaheer-Uddin and Zheng [1994] to simulate the transient behaviors of a fan motor. For a fan whose speed is controlled by varying frequency using variable frequency drive (VFD), its dynamics can be neglected due to the fact that the speed of a standard squirrel-cage motor is direct proportional to the input power frequency and fan speed change can reach its steady-state regime in a fraction of second.

#### **2.2.2.2 Air-distribution ductwork modeling**

Modeling of the air ductwork in an A/C system should also be given adequate attention because not only it plays a significant role in the energy balance of the system, but also the transport behavior of the working fluid inside the ductwork influences system's control characteristics.

Tobias [1973] developed a classic dynamic thermodynamic distributed-parameter model for duct and pipe, which took the thermal capacitances of the air and duct wall into consideration simultaneously and was governed by two partial differential

equations. However, it was not suitable for incorporation into a large-scale model of a complete A/C system because this would significantly increase the complexity of the model, and hence reduce the model's reliability, without greatly improving modeling accuracy, for the complete A/C system. A lumped-parameter model for air ductwork should be the first choice to be integrated into the complete model for the A/C system. Jacob [1987] divided the whole air ductwork into a number of segments and assumed the air distribution to be linear and the duct wall temperature to be uniform along each duct segment. The duct wall temperature varied from segment to segment. Hence a dynamic model for air duct was represented by a simple first-order differential equation and an algebraic equation. However, the transport delay which should be considered in the modeling of large ductwork, was neglected in this dynamic lumped-parameter model. Clark [1985] took the air transport delay into consideration, but assumed that the thermal losses to ambient occurred at a steady-state rate at all times and the air temperature at the duct exit was in equilibrium with the average duct wall temperature. Such a simplification would greatly decrease the model accuracy when the external heat transfer resistance was relatively large, for example, in air duct with external thermal insulation. The dynamic model for pipe and duct developed by Klein [1994], which was adopted by the program TRANSYS, did not either take the duct wall thermal capacitance into account unfortunately.

Because the pressure response is instantaneous, its dynamic effects are generally neglected when developing the hydraulic model of air ductwork. The Hardy Cross method [Fox 1983] has been often used to calculate the pressure-volume flow balance in a large-scale duct network, based on the mass conservation and pressure

balance. Through balancing the fan pressure rise and the system pressure losses, the airflow rate can be determined.

### **2.2.2.3 VAV terminal modeling**

When studying the energy performance for VAV A/C systems, a large percentage of existing models often used a simple steady-state damper model to represent a VAV terminal. A VAV terminal box was simply treated as a variable flow resistance, with its pressure loss coefficient being a function of the inclination angle of the damper inside the VAV box. Such simplifications were believed to have little effect on the investigation of the energy use performance of a VAV A/C system [Lebrun 1995]. However, a VAV A/C system was highly dynamic because of the inevitable interactions among the zone temperature control loops, the supply air static pressure control loop and the supply air temperature control loop. Therefore the dynamic performance of VAV terminals should be essential for analyzing the stability and investigating the effectiveness of different control strategies.

Hung [1999] developed a typical VAV terminal model taking nonlinearities of a constant-speed damper, actuator hysteresis, installed flow characteristic of the damper, and zone time constant varying with air flow rate into consideration. Khoo and Levermore [1998] derived a representative dynamic VAV terminal model based on a commercially available European terminal unit including an integral flow controller and actuator gear. The dynamic terminal model contained detailed sub-

modules for a flow controller, variable-speed actuator, damper linkages with hysteresis, damper, fan and air velocity sensor.

#### **2.2.2.4 Air-conditioned space modeling**

Generally, two types of mathematical methods have been used in modeling air-conditioned spaces or buildings. One was the frequency domain method, such as Fourier transformation; the other the time domain method, such as transfer function [Stephenson and Mitalas 1971], thermal response factors [Stephenson and Mitalas 1967], and state space method [Hong and Jiang 1997]. Masato et al. [2000] derived a simplified dynamic model for an air-conditioned space for control analysis, which can provide an indicative temperature distribution inside the space. The whole space under study was divided into five zones and the dynamics of each zone described by a lumped-parameter model. Another representative model for an air-conditioned space was described by Wang [1999]. A multi-zone building was represented with a network of equivalent thermal resistance, thermal capacitance and air volume.

### **2.3 Fundamental issues for VAV A/C systems**

In 1990s', more and more VAV A/C systems were installed as a promising alternative to CAV A/C systems because of their ability not only to meet the challenge of increasing thermal load differences among different conditioned zones, but also to operate with high efficiency. Firstly, a VAV system can serve multiple zones without simultaneous heating and cooling, which was energy inefficient, as prohibited by many building codes or standards. Individual zone temperatures can be

maintained at their respective settings by varying the amount of supply air to each zone. At the same time, the conditioned air can be filtered centrally to enhance the air quality in each zone. Secondly, a VAV system can help save fan energy significantly during part load operation that occurred most of the operating time. It was reported that the energy cost for operating a VAV system can be reduced by up to 20~30% because of the overwhelm energy saving from fan operation, when compared to a conventional CAV A/C system [Thomas 1997].

Unfortunately, the following performance deficiencies can be often found in VAV A/C systems: (1) Poor mixing of supply air and zone air; (2) Inadequate air circulation; (3) Dumping; (4) Reduced ventilation rates as load decreased [Coad 1996]. Wang [1999] pointed out that such problems may be alleviated by resetting the supply air temperature during part-load operation and developed a control strategy that utilized the air flow rate set-points of pressure-independent terminal controllers as the cooling load indicators for individual zones. The control strategy can avoid poor ventilation and meanwhile save as much fan energy as possible. In certain cases, the set point of the supply air temperature can be reset to a higher value according to certain pre-determined algorithms, in order to further optimize system's energy efficiency. For example, once the air flow rate passing through the cooling coil is below a threshold value, then the set point of the supply air temperature should be increased so that the total energy consumption by the refrigeration plant and the supply fan may be further reduced. On the other hand, there existed other studies aiming to ensure the stable and reliable operation of a VAV system. Janu et al. [1995] pointed out that the maintenance of indoor positive pressure through outdoor air flow rate optimization control could not only save

energy, but also help stabilize the indoor air temperature control. Seem et al. [2000] proposed a new control strategy where the outdoor air damper was left fully open and only the exhaust and recycling air dampers were linked and modulated together to prevent outdoor air from entering an air handling unit (AHU) through the exhaust air outlet, which can happen in conventional VAV AHU damper controlled systems.

### **2.3.1 Demanded control ventilation**

The main purpose for the control of a VAV A/C system is to maximize its energy efficiency while maintaining the required thermal environment in a conditioned space. Indoor air quality in working/living environment has a significant impact on the health and productivity of occupants. The minimum outdoor air flow rate, i.e., 7.5L/s per person, has been specified by an ASHRAE Standard. Alternatively, the concentration of indoor contaminants should be held below acceptable limits according to the ASHRAE Standard. Conditioning outdoor air can result in higher energy costs, and therefore it is important to bring in and condition only as much air as required. Bringing in more outdoor air than required will lead to energy waste.

Apparently, common outside air (OA) ventilation control strategies including fixed minimum OA percentage or fixed minimum OA rate during the entire operation range, do not prove to be a cost-effective way to ensure good IAQ. Demanded control ventilation (DCV) may provide an alternative to realize optimized indoor air quality while minimizing energy costs [Schell 1998 and Pavlovas 2004]. DCV modulates the outdoor air flow rate based on measured indoor pollutant level,



usually CO<sub>2</sub>. When occupancy is high in buildings a CO<sub>2</sub> -based DCV system can increase ventilation to ensure IAQ, and vice versa. Donnini et al. [1991] carried out a comparative study on two floors of an office building in Montreal. One floor was equipped with a CO<sub>2</sub> -based DCV system, while the other served by a conventional ventilation control system. The study lasted for one year, during which energy demand was monitored. It was found that in the floor having the DCV system, 12% of the annual energy consumption was saved. Zamboni et al [1991] carried out a field study in auditoriums having CO<sub>2</sub> -based DCV systems in Norway and Switzerland. It was reported that required heating energy use was reduced by 15% during one week of testing in the winter and the required cooling energy use by 75% in the summer. According to the principle of DCV, Shelquist and Randy [2001] designed a digital direct control (DDC) system that can meet the ASHRAE Standard 62-1999 while optimizing energy efficiency by using a ventilation reset strategy. Wang [1999] proposed an optimization control of outdoor air flow by combining the enthalpy control with DCV. However, the concentration of non-occupant-generated contaminants, such as volatile organic compounds (VOCs), may not be controlled with a CO<sub>2</sub> -based DCV system. Such a critical issue for DCV systems deserves more attention and should be properly treated for an acceptable level of IAQ [Davidge 1991].

### **2.3.2 Reset of supply air static pressure**

Fan energy consumption accounts for a large portion of the total energy use in a VAV system. Typically, a VAV fan is controlled based on the fixed static pressure

set point to meet the maximum flow requirement, which is apparently not energy efficient during part load operation. Lowering the energy consumption for a VAV fan is a main consideration to increase the energy efficiency of a VAV system. One of the most common measures to lower the fan energy consumption is to minimize the supply air static pressure. In order to supply an appropriate amount of air to individual zones, and to minimize the static pressure, the static pressure should be reset and controlled to be just adequate for the most heavily loaded zone over all operation ranges. Wang and Burnett [1998] developed a strategy for on-line reset of static pressure and evaluated its economics and feasibility in a real building. Lorenzetti and Norford [1994] also described a static pressure reset control strategy where static pressure set point can be continuously minimized to provide only the required air flow rate. Using the feedback of local zone flow control loops, Englander and Norford [1992] proposed and evaluated two methods of controlling a supply fan to minimize duct static pressure without sacrificing occupant comfort or adequate ventilation. On the other hand, Tung and Deng [1997] proposed a new concept to modulate the speed of a VAV fan, to save fan energy. The supply fan speed was continuously adjusted to its lowest possible level through the summation of the air flow rate passing through each VAV terminal.

### **2.3.3 Performance of humidity control**

It is common that an HVAC system operates most of the time at a part-load condition. It is hard for a conventional VAV system to maintain both dry-bulb and wet-bulb temperatures of the air in a conditioned space at their desired settings simultaneously. Traditionally, a VAV system focuses on the control of space air

temperature, with space air humidity control left uncontrolled. With an elevated demand for healthy and productive living/working environment and thermal comfort, humidity control will become more and more important for a VAV system.

At part load conditions the sensible heat ratio line in a psychrometric chart will become steeper than that at design/full load condition. Firstly, the internal moisture-removal demand in an occupied space remains relatively constant when the sensible heat load reduces during part load operation, lowering the sensible heat ratio (SHR) in an A/C space. Secondly, the necessary and continuous intake of outdoor air into an occupied space for acceptable indoor air quality worsens the problem of humidity control. Assuming that the minimum outdoor air intake at all time is 20% of the total supply air flow rate at design/full load, during half load operation, the ratio of the outdoor air would increase to 40% of the total. In other words, ventilation requirement dictates an increased portion of outdoor air during part load operation. Thirdly, it is common to have a part load condition where the ambient air dry-bulb temperature is lower and its dew point temperature is higher than those at design outdoor condition. The higher is the moisture content of outdoor air, the higher the latent load of a system. Therefore, these require the cooling and dehumidifying coil in a VAV system to operate at a new ratio of heat to mass transfer and hence, the slope of the coil ratio line should be correspondingly steeper at part load conditions [Shaw and Luxion 1988]. Unfortunately, the flow rate of the coolant in a cooling and dehumidifying coil is usually controlled to decrease with the reduction of thermal load. The reduction of coolant flow rate would weaken the coil's capability for moisture removal. Such an existing contradiction makes it hard for a conventional VAV system to realize effective humidity and temperature control

simultaneously unless additional air handling equipment or processes are employed. Attempts to solve such a problem, such as using low coil face velocity [Shaw and Luxion 1993], have been reported. In fact, when the SHR in individual zones served by a single AHU deviates greatly from that in design condition, it is almost impossible to maintain air humidity in all zones at their individual desired levels simultaneously without using terminal supplementary treatment process. However, for a single-zone VAV system or a multi-zone VAV system with similar zone SHR characteristics, it is possible to maintain the temperature and humidity at their desired settings simultaneously through the coincident modulation of the flow rate of the coolant and supply air. This will be further discussed in Section 2.4.2.

#### **2.3.4 Advanced control for VAV A/C systems**

A VAV A/C system is a nonlinear, multi-variable, time-varying, strong-coupled control object. The control characteristics of such a system vary much with the change of supply air volume. Hence, robust control schemes are required, if efficient and effective operations of VAV A/C systems are expected. The control stability should be given a high priority. Classic control algorithm such as proportional and integral (PI) control, which is based on the characteristics of a control object, is hard to achieve desirable control results for a VAV system having extremely varying operational characteristics. With the rapid development of powerful and flexible DDC technologies, advanced control based on artificial intelligence, such as fuzzy control [Alcalá et al. 2005, He et al. 2005 and Angelov 2003], neural network

[Mahmoud and Ben-Nakhi 2003], system identification [Desta et al. 2005], find increasingly wide applications in HVAC systems.

The neural network technology is based on the operating mechanism of a human brain and has a strong ability to approximate a nonlinear function. It is usually used to model complicated, nonlinear control objects, and then performs identification and optimization. A general regression neural network (GRNN) for identification and control was employed in a feedforward-feedback controller for a VAV system [Ahemd et al 1998a, 1998b and 1998c]. A memory-based neural network was selected to capture the input-output regression characteristics of the VAV system. It was testified that GRNN possessed simplicity, robustness and excellent capability in system identification. Another adaptive robust neural network controller was developed by Song and Hu [2002] and applied to a VAV system to deal with model uncertainty and control disturbance due to the incomplete knowledge of the physical VAV system. A robust adaptive training algorithm was provided to update weights of the neural network on-line to take care of non-linearity and changes of the system. In recent years fuzzy control has been viewed as a strong alternative to the standard PID control in various applications including VAV systems due to its robustness, fast time response and easy implementation. The core part of fuzzy control is its control rules that are derived from experience of experts and the previous knowledge about a control object. So et al. [1997] designed a new self-learning fuzzy controller in which the control policy was adaptable to changes in a control process and in the environment. Therefore the controller can always operate at its optimal settings. Wu and Cai [2000] developed an Adaptive Neuro-Fuzzy (ANF) method for the supply air pressure control in a VAV system. The simulation results showed that ANF

exhibited improved robustness when the VAV system encountered significant disturbances.

## **2.4 Problems for DX VAV A/C systems**

As mentioned in Section 2.1, as the size of A/C system decreases, the use of DX cooling becomes attractive because of lower capital cost. On the other hand, a DX A/C system incorporating VAV operation, i.e., a DX VAV A/C system, can provide flexible zoning control, with ease future zone reconfiguration, which are commonly seen in a conventional chilled water based VAV A/C system. Moreover, it is expected that a DX VAV A/C system is energy-efficient and can help reduce peak demand. Firstly, compared to a chilled water-based system, a DX A/C system can operate at a higher evaporating temperature because of the non-presence of an intermediate heat transfer medium. The difference in evaporating temperatures between DX A/C systems and chilled water-based systems can be about 10 °C at full load and up to 16 °C at part load [Kirkman 1984]. It was estimated that energy savings could range from 1% to 2% per degree F rise in evaporating temperature in a refrigeration system [AEC 1989]. Secondly, it was reported that fan energy use could account for 40% of the annual total energy use for a rooftop DX A/C system located in mild climates [Wilson 1995]. Therefore the incorporation of VAV air-distribution into a DX VAV A/C system, can save a large amount of fan energy use during part load operation, helping improve the energy efficiency of a DX VAV A/C system.

However, there were a number of problems associated with DX VAV A/C systems. These included capacity control and humidity control. These will be detailed in sections 2.4.1 and 2.4.2, respectively. In addition, Coad [1984] pointed out that the existence of uneven air flow pattern or temperature-stratified air stream may pose an uneven thermal loading which is the rate of heat transfer per unit area of a coil face, on a DX cooling coil. A DX cooling coil may be robust to moderately uneven thermal loading with reasonably high average face velocities at its design conditions. However, the face velocity of a cooling coil in a DX VAV A/C system may be greatly reduced during part load operation. With air face velocity reduced, the effects of uneven thermal loading may be magnified. The expansion valve in the DX VAV A/C system may become prone to hunting and unstable operations may result in. Thus great care should be taken in designing a DX VAV A/C system to ensure even air flow patterns and thorough mixing of air streams before reaching its DX coil. An even loaded and well designed evaporator and a properly sized expansion valve must be provided in all DX VAV A/C systems.

### **2.4.1 Capacity control**

To maintain a constant supply air temperature is critical for a VAV A/C system to decouple or isolate its different control loops and to realize desirable zoning thermal comfort control. If the supply air temperature changes continuously, air temperatures in different zones may never be stabilized. A zone air temperature sensor will not respond instantaneously to a change in supply air temperature. It would typically take some times (up to 20 minutes) before a VAV terminal unit damper is

repositioned to alter the supply air flow rate to a zone in a corrective manner. If the control of air temperature downstream of a DX coil is poor, the supply air temperature may probably have changed again during this period of time, hence another cycle from zone temperature sensor to repositioning the damper in the VAV terminal will be started. Furthermore, such cyclic changes in supply volume flow rate will be accompanied by a cyclic variation in noise level from supply diffusers [Shepherd 1999].

Capacity change for a chilled water cooling coil with a three-port modulating valve can reach 0.1% of its full capacity, and the ratio of maximum capacity to minimum can reach 20:1 to 50:1. Thus a stable control of supply air temperature is relatively easy to realize in a conventional chilled-water based VAV A/C system.

For a DX VAV A/C system, the matching between the output cooling capacity from its DX refrigeration plant and the continuous varying cooling load in its VAV subsystem due to VAV operation is critical to maintain a constant supply air temperature in the DX VAV A/C system. However, currently the capacity control for a DX A/C system with a reciprocating compressor is typically by either cylinder unloading or hot gas bypass. A DX A/C system with either a scroll or a screw-type compressor may mostly use hot gas bypass, discharge or inlet throttling of refrigerant flow. Medium-to-large sized DX A/C systems usually include multiple compressors to further realize staging capacity control, while a DX A/C system of small size usually makes use of frequent cycling on/off to modulate its cooling capacity, which would dramatically reduce the life and increase the noise level of its



condensing unit. Apparently, purely staging capacity control or frequent cycling on/off will lead to the fluctuation of supply air temperature, and hot-gas bypass capacity control will result in energy inefficient operation because it imposes an artificial thermal load on a DX system.

A control method that could minimize the problem of inability to match the cooling capacity of the refrigeration plant with the varying thermal load in the VAV subsystem for a DX VAV A/C system was reported [Avery 1996]. The method used several small DX coils with face dampers that would be closed when a coil was deactivated. These small DX coils were connected with the same number of independent condensing units, so that the matching problem could be minimized through staging cooling capacity control. However, such a method was equivalent to distributing the total heat load evenly among several smaller DX A/C systems. Therefore, its initial cost was high and its overall energy efficiency remained a concern. In addition, its control system was much more complicated and hence its reliability could not be ensured. In fact the problem of capacity matching still exists within each stage. Haessig [1995] proposed an electronic hot gas bypass control method to address the cooling capacity matching within each stage. In the approach proposed by Haessig, an electronic temperature sensor monitored the change of supply air temperature, and accordingly a digital controller modulated the amount of hot gas bypassed into the evaporator. Hot refrigerant gas offset continuously the redundancy of cooling capacity between stages. Although this hot gas bypass approach can maintain the supply air temperature precisely at its set point and have a better energy performance than using electric or hydronic reheat, its energy

efficiency at part load condition was still poor because the energy consumed by the compressor stayed almost constant at all loads.

Variable refrigerant volume (VRV) technology may be a promising alternative to achieve precise cooling capacity matching while maximizing energy saving in a DX VAV A/C system. Variable speed compressor coupled with EEV in a VRV A/C system can modulate precisely the refrigerant flow rate and hence system's cooling capacity, making the accurate matching between output cooling capacity and varying VAV thermal load possible. It was reported that through the modulation of compressor speed, the output cooling capacity from a residential split-type DX A/C system could be varied ranging between 50 and 100% of its full capacity in proportion to the change in room temperature [Lida et al. 1982]. Currently with the advance of variable speed compressor and EEV technologies, inverter-aided A/C systems can vary their cooling outputs between 20% and 100% of full load. Moreover, the use of variable speed compressor for capacity control may offer the potential for greater energy savings during part load operations. On the other hand, the energy performance of a conventional DX A/C system with single speed compressor at part load condition is degraded dramatically [Silver et al. 1990]. During part load operation, the condensing and evaporating pressures/temperatures of a DX A/C system will respectively decrease and increase with a lower compressor speed, which would substantially increase its coefficient of performance (COP) [Scalabrin and Bianco 1994]. Yang and Lee [1991] presented an analysis for an inverter-driven variable speed air conditioning system used in a hot and humid region. The results indicated that the use of variable-speed compressor could provide an annual energy saving of 20%. It was reported in 1985 that an inverter-

driven A/C system developed by Mitsubishi Electric Corporation in Japan could achieve 35% energy savings compared to single speed compressor A/C system [Nakashima et al. 1985]. Furthermore, it can be expected that the pull-down time needed for an A/C system to reach a temperature setting during start-up can be reduced because a compressor can operate initially at its highest speed.

However in the past variable speed compressors were generally regarded to be suitable only for use in small-scale A/C systems, but not in medium- or large-scaled A/C systems due to the lack of insufficient development and component integration. Fortunately, in recent years medium- to large-scaled variable speed compressors have gained great improvement in various aspects and been widely used in medium-capacity multi-evaporator A/C systems, particularly in Japan [Youn et al. 2001 and Urashima 1993]. In order to demonstrate the benefit and feasibility of variable speed technology used in large-scale centrifugal chiller systems, Lenarduzzi and Yap [1998] established a demonstration installation of variable speed compressor in retrofitting a chilled-water based A/C system. The system was monitored for one cooling season and the results showed that variable speed drive technology could also work successfully in large-scale A/C systems. It was estimated that approximately 41% of energy saving has been achieved for this particular site and the power quality and total harmonic distortion problem induced could be neglected. Therefore, the VRV technology featured with variable speed compressor and EEV has been proven to be an energy efficient and practical way to realize capacity control and has many other advantages such as soft start-up, rapid responding, simple system controls, easy maintenance, etc. Reasons for few application of VRV technology in DX VAV A/C systems may include the unfamiliarity with the variable speed technology and its

potential benefits for use in DX VAV A/C systems, relatively high initial cost and limited related studies.

#### **2.4.2 Humidity control**

A DX VAV A/C system is the integration of a DX refrigeration plant and a VAV air-distribution sub-system. The difficulty in controlling space humidity by a VAV A/C system, as discussed in Section 2.3.3, exists in a DX VAV A/C system. For conventional DX A/C systems where cooling equipment cycles on and off in response to a thermostat, due to ventilation requirement, outdoor air and its moisture load may enter a building without dehumidifying, raising indoor humidity level. Such a problem is amplified in mild, humid climates at part load operation [Doty 2001]. In fact, during the off period of a DX coil, some condensate remaining on the surface of a DX coil or its condensate pan can re-evaporate into occupied spaces, deteriorating further the system's dehumidifying ability, because a supply fan must keep running to intake outdoor air for ventilation. Over-sizing which can often be found in DX A/C systems would also further make the situation much worse.

Even with a correctly sized conventional DX A/C system, the problem of humidity control associated with part-load operation remained, albeit not to the same extent. It was concluded that supplementary dehumidification during part-load operation was necessary and indispensable for conventional DX A/C systems with single speed compressor to maintain a healthy, comfort working/living environment, not to

mentioned a DX VAV A/C system [Lsiburek 2002]. Several enhanced dehumidification technologies can be used in DX A/C systems. These include thermally activated desiccant systems, heat pipe technology, and dual-path systems that pre-treat ventilation air, etc. These approaches would inevitably make the operation and control of a DX A/C system more complicated and consequently increase its capital cost. As a general guideline, the dehumidifying or moisture-removal capacity of a DX A/C system increases when lowering both its evaporating temperature and the air face velocity across a DX coil. The previous field studies by Shirey [1993] and Khatter [1999] have demonstrated the impacts of supply air flow rate and evaporating temperature on dehumidification. Khattar presented a demonstration installation in a supermarket and made use of cylinder unloading for capacity control. A low DX coil temperature was maintained even at part load operation through compressor capacity control, which was based on suction pressure.

VAV air-distribution together with VRV technology provides an easy-to-implement and practical way for a DX A/C system to enhance its dehumidification ability. The application of VAV air-distribution technology in DX A/C systems makes it easy to change the air face velocity, and the use of a variable speed compressor allows the easy modulation of evaporating temperature. Hence, for single-zone or multi-zone configuration with similar zone SHR characteristics, a DX VAV A/C system incorporating VRV technology is able to achieve accurate temperature and humidity control. Kalman et al. [1995] presented a control strategy in which the speed of a variable-speed compressor was regulated in accordance with the change of space temperature, while that of supply fan in accordance with the space relative humidity. A PID control algorithm, where the controller parameters could be derived

analytically based on a simulation model developed for the system, was used in this study. The feasibility to control the space temperature and relative humidity simultaneously by the coincident variation of compressor speed and evaporator fan speed, respectively, was verified experimentally. Similarly, Andrade and Bullard [2002] investigated by means of simulation the roles of supply air and refrigerant flow rate, and their interactions on the performance of an air conditioner equipped with a variable-speed supply fan and compressor. Andrade and Bullard pointed out that varying the indoor blower speed could provide the necessary humidity control by adjusting the evaporator surface temperature to meet latent loads at any compressor speed. In addition, how the overall system efficiency of the air conditioner was affected by changes in compressor and blower speeds was also discussed.

### **2.4.3 DDC for DX VAV A/C systems**

With the development of DDC technology which is flexible and powerful, various artificial intelligent control methods become practical for HVAC systems. DDC is an extremely fast and accurate process in which a microprocessor-based controller continuously monitors/collects information from the environment or plants, performs calculations based on internal programming and database information, and provides corrective control action [Reeves 1996]. It possesses powerful ability of calculation and measurement so that various sophisticated control algorithms can be implemented through DDC. Unlike traditional controls, a DDC controller can follow program instructions and manage many control loops simultaneously. It can easily

allow a control decision process to simultaneously take multiple input parameters into account. To date DDC has found wide application in HVAC systems. DDC not only is used to collect information for system's monitoring and central supervision, but also provides a new approach for desirable VAV A/C systems' control. For example in the study by Tung and Deng [1996], with the help of DDC and network communication technology, the speed of supply fan was adjusted to its lowest possible level using summation of air flow through VAV terminals as the control signal. In a DDC-based variable-water-volume (VWV) system combined with a VAV A/C system [Ahmed 1991], the speed of a water pump could be set immediately using the pump characteristics information and the calculated total system flow rate and pressure head.

A controller for a DX A/C system with a variable speed compressor, which was based on a mathematical model and featured with DDC, has been developed by Deng [2002]. Cooling capacity was modulated through varying compressor speed, using a set of real-time measured operating parameters in its refrigerant circuit. Such a control scheme could not only avoid the use of problematic measurement of air conditions immediately downstream of the evaporator coil for control action, but also have quick and robust response to disturbance. As early as in 1987 Atkinson [1987] pointed out that with the help of DDC the air distribution control for a DX VAV A/C system may be simplified by using standard velocity measurement devices and by scaling, summing, or subtracting these signals as required. Similarly, Okada et al. [1992] also took the advantages of DDC to develop an air distribution controller for a residential VAV A/C system. By determining the required air volume for each room and calculating the necessary air pressure rise for each duct branch,

the maximum air pressure rise was selected as the required fan discharge pressure. The opening of a VAV terminal's damper was then set according to the necessary flow resistance, and the speed of supply fan according to the summation of required air flow rate for each room. It was reported that compared to constant static pressure control, the control method developed could save up to 50% of fan power consumption. It can be expected that with the aid of DDC and the enhancement of the quality of various digital sensing device, the control of a DX VAV A/C system could become more accurate and effective.

## **2.5 Summary**

DX A/C systems, most of which are conventionally CAV operated, account for large portion of energy used for space cooling of buildings. DX VAV A/C systems which integrate a VAV air-distribution sub-system and a DX refrigeration plant, are believed to be highly energy-efficient, and can help reduce peak demand. It can also provide flexible independent zoning control, with easy future space or zone reconfiguration. However, the literature review reported in this chapter suggested that there has been inadequate research and development for DX VAV A/C systems. The in-depth reported research on the modeling and control of DX VAV A/C systems was limited in open literatures.

Although various simulation-based studies for either DX refrigeration plants or VAV A/C systems, separately, were often reported, and the mathematical models for components in either DX refrigeration plants or VAV air-distribution sub-systems



were readily available, the model specific for a complete DX VAV A/C systems cannot be identified in literatures. Simulation-based research has been regarded as an efficient and effective means to investigate operating characteristics and control performance for various HVAC&R systems including DX VAV A/C systems. Dynamic modeling was necessary in carrying out research work related to the control of DX VAV A/C systems. When modeling conventional chilled-water-based VAV A/C systems, the dynamics of cooling coil, chiller and water distribution system were usually neglected and much of effort focused on the dynamics of air distribution. On the other hand, the modeling of a DX refrigeration plant apparently did not include components in an air-distribution sub-system and hence would not take the interaction between the refrigeration plant and air-distribution sub-system into account. However, when investigating the control performance of a DX VAV A/C system, the dynamics of its DX refrigeration plant and its VAV air-distribution sub-system should all be considered. Consequently the model to be developed for a DX VAV A/C system is expected to become much more complicated. Therefore, much needs to be done in developing a representative, accurate and generalized model for a DX VAV A/C system.

The air distribution in a DX VAV A/C system is similar to that in a conventional chilled-water based VAV A/C system, and therefore similar problems are faced. Various control strategies to ensure reliable and efficient operation of a conventional VAV A/C system may be referred to and incorporated into a DX VAV A/C system. Demanded control ventilation has been proved to be an efficient way to ensure good IAQ while reducing energy use. Resetting supply air static pressure provides an attractive way to further lower fan energy consumption. Moreover, resetting supply

air temperature can help alleviate some inherent performance deficiencies during low part load operation.

The major problem for the wider application for a DX VAV A/C system has been the matching between the output cooling capacity from its DX refrigeration plant and the varying cooling load in its VAV air-distribution sub-system. Staging capacity control or frequent cycling on-off the plant will lead to the fluctuation of supply air temperature whose stability is critical to realize a desirable zoning thermal control. Capacity control using hot gas bypass is energy inefficient because it imposes an artificial thermal load.

Much research work including field studies has proven that VRV technology featured with a variable-speed compressor and EEV, can help achieve the matching between the output cooling capacity with the varying cooling load. Meanwhile, the joint use of a variable-speed compressor and a variable-speed fan can alleviate the humidity control problem encountered for DX A/C systems and even provide accurate simultaneous temperature and humidity control for single-zoned DX A/C systems. However, the use of variable-speed compressors in DX VAV A/C systems has been scarcely reported in open literature. With the advancement of variable-frequency drive technology, the use of variable-speed compressor is considered to be a promising alternative for DX VAV A/C systems. Therefore, it is necessary to investigate the control characteristics and energy performance of, and to develop feasible and effective control strategies and algorithms for, DX VAV A/C systems with variable-speed compressor.

A DX VAV A/C system with a variable-speed compressor is a nonlinear, multi-variable, time-varying and strong-coupled control object. Its control characteristics vary much with the changes of supply air flow rate and refrigerant flow rate. The use of classic control approaches such as a PID control may not yield desirable control results. New approaches such as the advanced DDC and other artificial intelligent control methodologies should be actively explored for application in DX VAV A/C systems.

## **Chapter 3**

### **Proposition**

#### **3.1 Background**

From the literature review presented in Chapter 2, it is clear that the use of a DX VAV A/C system is to be preferred since such a system combines the advantages from both a DX A/C system and VAV operation. However, it is understood that the main technical deterrence to the wider application of a DX VAV A/C system lies in matching the output cooling capacity from its DX refrigeration plant with the varying cooling load in its VAV air-distribution sub-system. The capacity control methods presently adopted by DX A/C systems, such as on-off cycling refrigeration plant, hot-gas bypass, staging-control are not totally satisfactory because of either poor control accuracy or poor energy efficiency. On the other hand, previous related studies indicated that the use of variable-refrigerant-volume (VRV) technology featured with a variable-speed compressor and an EEV in a DX VAV A/C system would help to solve the matching problem.

The simulation-based research has been increasingly recognized as an efficient and powerful means to study the operating performance, and to develop advanced control strategies for HVAC installations. The literature review presented in Chapter 2 also revealed that although there have been a large number of reported studies on separate modeling DX refrigeration plants and VAV A/C systems, a complete dynamic model developed specifically for a complete DX VAV A/C system, which should take into account the dynamic behaviors of both its DX refrigeration plant and its VAV

air-distribution sub-system simultaneously, cannot be identified in open literature. For those well-known simulation program packages such as TRNSYS and HAVACSIM<sup>+</sup> which could provide simulation platform for large-scaled VAV A/C systems, one of their restrictions is that many of the component models available in the packages are steady-state or quasi-steady-state, making them not suitable for studying the transient behavior of a DX VAV A/C system and its related control issues.

A DX VAV A/C system is a nonlinear, strong-coupling, time-varying and multivariable control object, and more complex to control its output cooling capacity than the conventional chilled-water based VAV A/C system. The use of a variable-speed compressor and an EEV in a DX VAV A/C system, would further complicate the control of DX VAV A/C systems. Furthermore, the wide variation range of supply air flow rate in a DX VAV A/C system requires a robust capacity controller to maintain its supply air temperature. On the other hand, because the control characteristics of supply air temperature in a DX VAV A/C system are completely different from that of return air temperature entering an evaporator, the capacity controller currently used for a domestic variable-frequency air conditioner, should not be simply reproduced for a DX VAV A/C system.

### **3.2 Project title**

This thesis focuses on two major issues related to the development of a DX VAV A/C system having a variable-speed compressor and an EEV: 1) building up a

complete dynamic mathematical model of a DX VAV A/C system; 2) developing a capacity controller to address the capacity-load matching problem. The proposed research project is therefore entitled “Modeling and control of a direct-expansion (DX) variable-air-volume (VAV) air conditioning (A/C) system”.

### **3.2 Aims and objectives**

The objectives of the proposed project are:

- 1) To set up an experimental DX VAV A/C rig having a variable-speed compressor and an EEV;
- 2) To develop a representative, dynamic mathematical model for the experimental DX VAV A/C system, and to experimentally validate the model;
- 3) To develop a DDC-based novel capacity controller for the DX VAV A/C system to solve the problem of capacity-load matching.

### **3.3 Research methodologies**

An experimental DX VAV A/C rig will be firstly set up. High-accuracy measuring and control devices including a data acquisition system (DAS) and PI programmable controllers, will be used in the experimental rig. All measurements will be computerized. All measured parameters can be real-time monitored and curve-data

displayed, recorded and processed. The DAS and all controllers in the experimental rig can be digitally communicated with a supervisory computer.

A complete dynamic mathematical model will be developed for the experimental DX VAV A/C system, in parallel to setting up the experimental rig. The model will be component-based and of partial-lumped-parameter type. The model will be developed based on the principle of mass and energy conservation, and using the correlations describing the operational performance of various components in the experimental DX VAV A/C system, which will be either field-tested or available from manufacturers. Mathematical correlations representing the control logics of various controllers will be also included. The model will consist of two constituent sub-models for its DX refrigeration plant and its VAV air-distribution sub-system, respectively, taking into account the dynamic behaviors of both the constituent DX plant and the constituent VAV sub-system simultaneously.

The dynamic model developed for the experimental DX VAV A/C system will be experimentally validated using the experimental rig. Open-loop responses of the major operating parameters of the DX refrigeration plant and the sub-model for the plant after being subjected to step-changes in operating conditions will be compared.

Using the validated model, the simulated closed-loop responses of the experimental DX VAV A/C system, after being subjected to step changes from space internal cooling load and space air temperature set-point and with its conventional PI (proportional-integral) control loops enabled, will be studied. This is to further

confirm that the model developed could behave as expected for a real DX VAV system.

Finally, with the help of the powerful calculation and processing capacity of DDC, a novel capacity controller for regulating compressor speed will be developed for the experimental DX VAV A/C system. The controller will be based on the principle of energy balance and some real-time measured key operating parameters in the DX VAV A/C system. The novel controller will be implemented in the experimental rig. Controllability tests will be carried out to see whether the expected control sensitivity and accuracy may be achieved.



## **Chapter 4**

### **Development of an Experimental Rig for DX VAV A/C Systems**

#### **4.1 Introduction**

An experimental DX VAV A/C rig has been developed and set up in the HVAC Laboratory of Department of Building Services Engineering in The Hong Kong Polytechnic University. The primary purpose of setting up the experimental rig was to enable the research work on the modeling and control for DX VAV A/C systems. In addition, other related research work on DX-based A/C systems may also be carried out using this experimental rig, with appropriate modifications.

The experimental rig to be set up resembles a typical DX VAV A/C system, including two identical spaces conditioned by the DX VAV A/C system. Advanced technologies such as an electronic expansion valve, variable-speed compressor, as well as a computerized data measuring, logging and control system have been incorporated into the experimental rig.

This chapter reports on the development and setting up of the experimental rig. Detailed descriptions of the experimental rig and its major components are firstly presented. This is followed by describing the computerized measuring devices and data acquisition. Finally, the computer supervisory program used to operate and control the experimental rig is detailed.

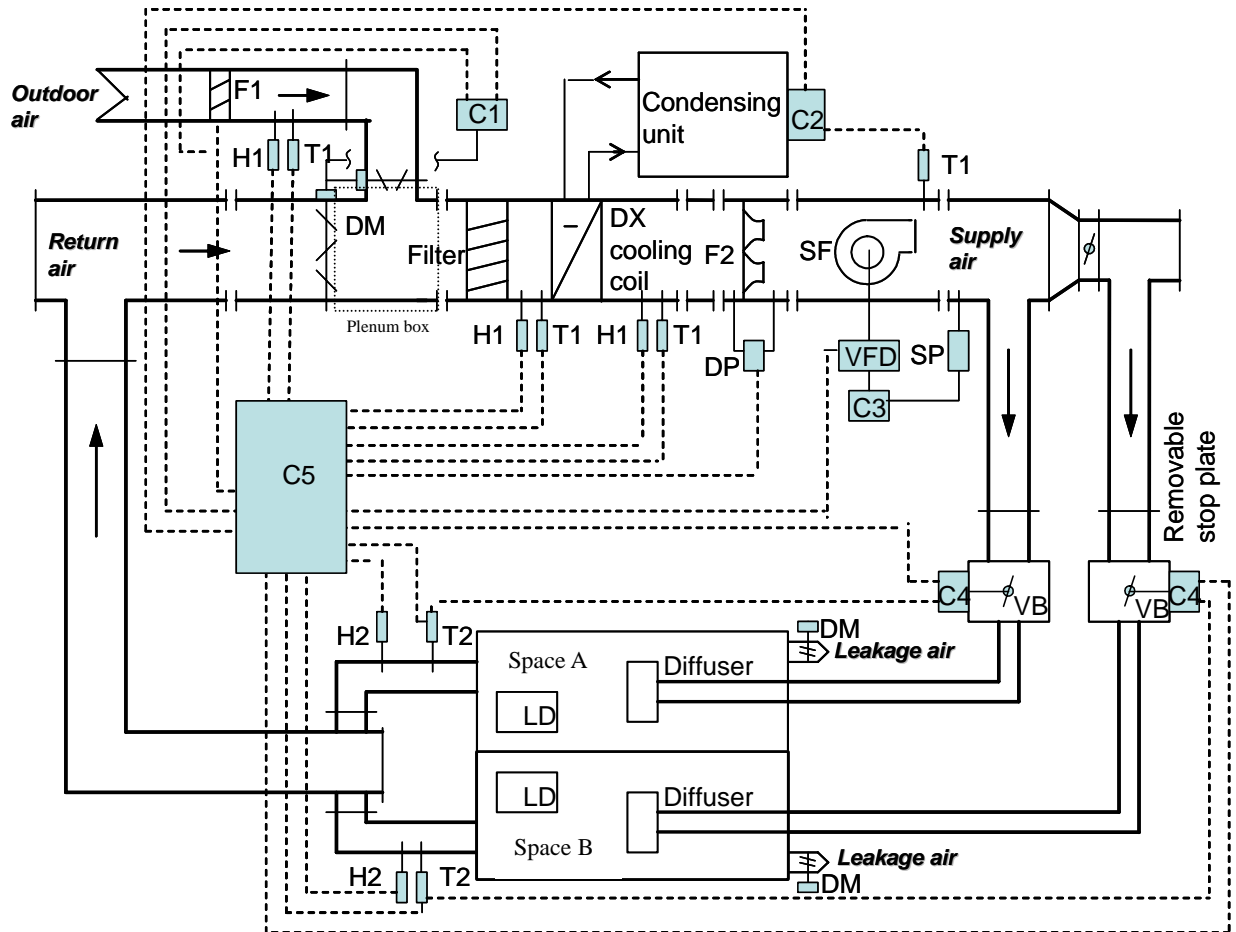
## **4.2 Detailed descriptions of the experimental rig and its major components**

The experimental rig for DX VAV A/C systems is mainly composed of two parts, i.e., a DX refrigeration plant and a VAV air-distribution sub-system which includes two identical spaces served by the DX VAV A/C system. The schematic diagrams of both the complete experimental rig and the DX refrigeration plant are shown in Figure 4.1 and 4.2, respectively.

### **4.2.1 DX refrigeration plant**

As shown in Figure 4.2, the major components in the DX refrigeration plant include a variable-speed rotor compressor, an EEV, a high-efficiency tube-louver-finned DX evaporator and an air-cooled tube-plate-finned condenser. The evaporator is placed inside the VAV air-distribution sub-system, to work as a DX air cooling coil. The design air face velocity for the DX cooling coil is 2.5m/s. The nominal output cooling capacity from the DX refrigeration plant is 9.9 kW (~2.8 RT). The actual output cooling capacity from the DX refrigeration plant can however be modulated from 15% to 110% of the nominal capacity. Other details of the compressor and EEV can be found in Table 4.1. The geometrical parameters of the condenser and evaporator are shown in Table 4.2. Both condenser fan and compressor are driven by variable-frequency drives (VFD). The EEV includes a throttling needle valve, a step motor and a pulse generator. It is used to maintain the degree of refrigerant superheat at the evaporator exit. The working fluid of the DX plant is refrigerant R22, with a total charge of 5.3 kg.

In addition, two three-way connectors and two flexible joints, whose locations are indicated in Figure 4.2, are reserved in the refrigerant pipeline for the purpose of possibly modifying the rig for other related studies. A condenser air duct, which is not normally required in real applications, is used to duct the condenser cooling air carrying the rejected heat from the condenser to outside Laboratory. The condenser fan, housed inside the condenser air duct, can also be variable-speed operated. An electrical heater controlled by Solid State Relay (SSR) is used to adjust the temperature of the cooling air entering the condenser for various experimental purposes. A refrigerant mass flow meter is installed upstream the EEV. Other necessary accessories and control devices, such as an oil separator, a refrigerant receiver, a sight glass and safety devices, are provided in the experimental rig to ensure its normal and safe operation.



C1-controller of outdoor/return air damper	C2-controller of condensing unit	C3-controller of supply fan
C4-controller of VAV terminal	C5-data acquisition and control unit	DP-differential pressure transducer
DM-damper	LD-load generating unit	F1-hot film anemometer
F2-supply air flow rate measuring apparatus	H1-air wet-bulb temperature sensor	H2-air humidity meter
SP-static pressure measuring device	SF-supply fan with motor outside duct	T1 -air dry-bulb temperature sensor
T2-air dry-bulb temperature sensor	VB-pressure independent VAV terminals	VFD-variable frequency drives

Figure 4.1 The schematic diagram of the complete experimental rig

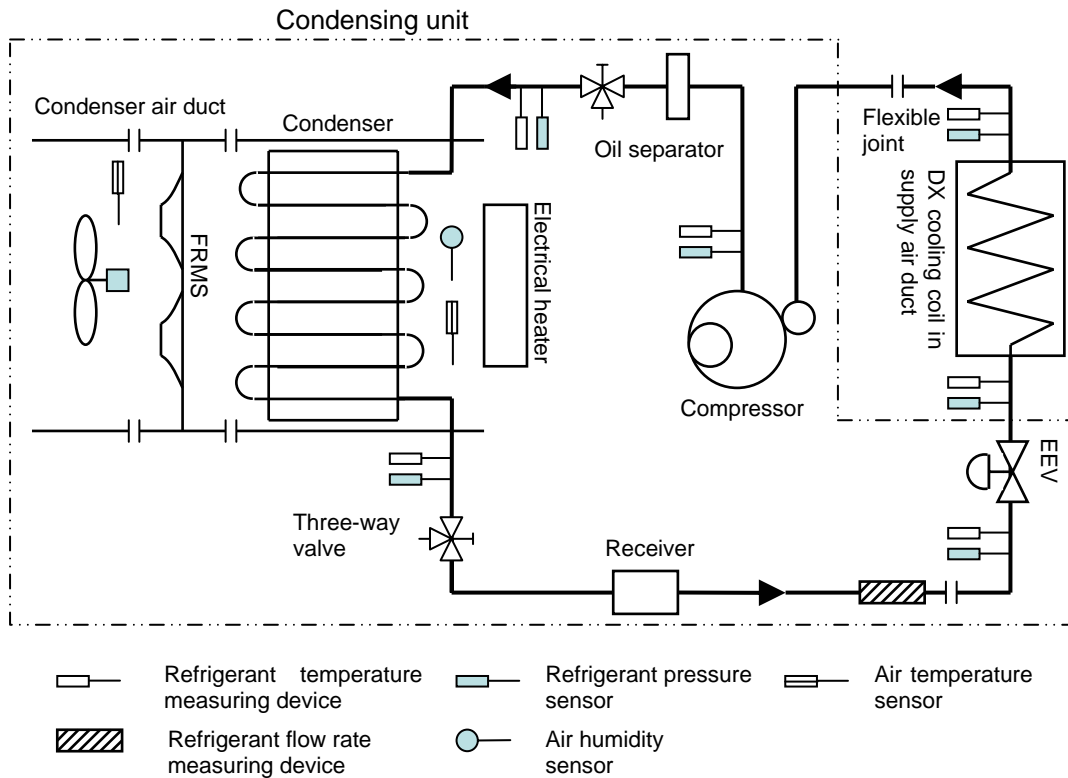


Figure 4.2 The schematic diagram of the DX refrigeration plant

Table 4.1 Details of the variable-speed compressor and EEV

Compressor:	
Model:	HITACHI THS20MC6-Y
Allowable Frequency range:	15~110 Hz
Rated Capacity:	9900 W at 90Hz
Displacement:	3.04 ml/rev
EEV:	
Model:	SAGINOMIYA DKV-18D15
Pulse range:	0~480 Pulse
Rated capacity:	10500 W
Port diameter:	1.8 mm

Table 4.2 Geometric parameters of heat exchangers

Configuration	Evaporator	Condenser
Transverse tube pitch:	25 mm	25 mm
Longitude tube pitch:	21.65 mm	21.65 mm
Fin pitch:	2.0 mm	2.0 mm
Fin thickness	0.15 mm	0.15 mm
Outside tube diameter:	9.52 mm	9.52 mm
Inside tube diameter:	8.86 mm	8.86 mm
Louver height:	1.07 mm	~
Louver pitch:	2.35 mm	~
Length of the windward area:	420 mm	650 mm
Height of the windward area:	450 mm	800 mm
Number of the windward transverse tube:	18	30
Number of the tube row:	6	4
Number of refrigerant loop:	4	5

#### 4.2.2 VAV air-distribution sub-system

The VAV air-distribution sub-system in the experimental DX VAV A/C rig is schematically shown in Figure 4.1. It includes an air-distribution ductwork with return and outdoor air dampers, a variable-speed centrifugal supply air fan with motor placed outside the duct, two pressure-independent VAV terminals and two conditioned spaces. The supply air fan is driven by a variable-frequency drive and its

speed regulated according to the supply air static pressure. Two VAV terminals are installed in two branch supply air ducts to serve the two spaces (A and B), respectively. The pressure-independent VAV terminal includes a VAV box with damper, a flow controller with built-in Pitot tube for measuring air flow rate passing through the terminal, a constant-speed damper actuator and a thermostat for measuring space air temperature. The terminal is featured with DDC technology and can signal the degree of opening of its damper. The details of the supply air fan and the VAV terminals are tabulated in Table 4.3.

The size of each of the two adjacent identical spaces is 3.9m (L) × 3.4m (W) × 2.9m (H). The spaces are separated by a removable partition so that a larger simulated air conditioned space may become available when and as necessary. Inside each space there is a sensible heat and moisture load generating unit (LGU). The unit is intended to simulate the cooling load in a conditioned space. Its heat and moisture generation rate as regulated by either Silicon Control Resistance (SCR) or SSR may be varied manually or automatically with a pre-set pattern through operator's programming. In addition, a leakage outlet with a residual-pressure relief damper is installed in each space so that a positive internal pressure of not more than 20 Pa can be maintained at all time. In the VAV air-distribution sub-system of the experimental DX VAV A/C system, return air from both spaces mixed with outdoor air in a plenum box upstream of an air filter. The mixed air is then filtrated and then cooled and dehumidified by the DX cooling coil. Afterwards, the cooled and dehumidified air passes through the supply air fan, to be supplied to the two spaces, via the two VAV terminals, to deal with the cooling load from LGUs.

Table 4.3 Details of the VAV terminals and supply air fan

	Brand	Model	Note
<b>VAV Box</b>	ROYAL	TU-1	Diameter: 149 mm; rated flow rate: 170-1019 m <sup>3</sup> /h
<b>Flow controller</b>	BELIMO	VRD-2	Control input: DC 0-10 V
<b>Actuator</b>	BELIMO	NM24-V	Control signal: DC 6.0 ± 4 V
<b>Supply air fan</b>	KRUGER	BSB 315	Nominal flow rate: 1700m <sup>3</sup> /h; total pressure head: 1100 Pa

### 4.3 Instrumentation and data acquisition system (DAS)

The instrumentation for the experimental DX VAV A/C system is also shown in Figure 4.1 and Figure 4.2. The rig is fully instrumented for measuring all of its operating parameters, which may be classified into three types, i.e., temperature, pressure and flow rate. Since all measurements are to be computerized, all sensors and measuring devices are able to output direct current (DC) signal of 4-20 mA or 1-5 V, which are transferred to a DAS for logging and recording.

#### 4.3.1 Sensors/measuring devices for temperatures, pressures and flow rates

Eleven sets of air temperature and humidity measuring sensors are located in the air-distribution subsystem of the experimental rig. To minimize the influence of uneven distribution of air parameters inside the air duct, standard air-sampling devices are provided to ensure measuring accuracy. Air relative humidity is



indirectly measured via measuring air dry-bulb and wet-bulb temperatures. As shown in Figure 4.2, there are five temperature sensors for measuring refrigerant temperatures in the DX refrigeration plant. To ensure fast response of the sensors for facilitating the study of transient behaviors of the DX refrigeration plant, these temperature sensors are inserted into the refrigerant circuit, and are thus in direct contact with the refrigerant. The temperature sensors for air and refrigerant are of platinum Resistance Temperature Device ( RTDs ) type, using three-wire Wheatstone bridge connection and with the pre-calibrated accuracy of  $\pm 0.1\text{ }^{\circ}\text{C}$  . The specifications of the RTDs are: CHINO Pt100/0 $^{\circ}\text{C}$ -3W, Class A, SUS  $\Phi$  3.2-150L.

Refrigerant pressures in various locations in the DX refrigeration plant are measured using pressure transmitters with an accuracy of  $\pm 0.13\%$  of full scale reading (Model: SETRA C206). The atmospheric pressure is measured with a barometer having an accuracy of  $\pm 0.05\text{kPa}$  ( Model: VAISALA PTB-101B).

There are two sets of air flow rate measuring apparatus (FRMA) in the VAV air-distribution sub-system. One set of FRMA is used to measure the total supply air flow rate, i.e., the air flow rate passing through the DX cooling coil. The other is for measuring the air flow rate passing through the condenser. The two sets of FRMA are constructed in accordance with ANSI/ASHRAE Standards 41.2, consisting of nozzles of different sizes, diffusion baffles and a manometer with a measuring accuracy of  $\pm 0.1\%$  of full scale reading (Model: ROSEMOUNT 3051). The number of nozzles in operation can be altered automatically.

On the other hand, outdoor air flow rate is measured using a hot-film anemometer with a reported accuracy of  $\pm 0.1\text{m/s}$  (Model: E+E 70-VT62B5 ). The anemometer is installed 500mm, which is longer than the recommended length of entrance of 200 mm by its manufacturer, downstream of the outdoor air inlet, to ensure the measuring accuracy of outdoor air flow rate. The power consumption of the variable-speed compressor is measured using a pulse-width-modulation (PWM) digital power meter with a reported uncertainty of  $\pm 2\%$  of reading (Model: EVERFINE PF9833). The refrigerant mass flow rate passing through the EEV is measured by a Coriolis mass flow meter with a reported accuracy of  $\pm 0.25\%$  of full scale reading (Model: KROHNE MFM1081K+F). The supply air static pressure is measured using a manometer with a reported accuracy of  $\pm 0.1\%$  of full scale reading (Model: ROSEMOUNT 3051).

In order to ensure the measuring accuracy for the temperatures of the air flowing inside an air duct, standardized air sampling devices recommended by the ISO Standard: 5151 are used in the experimental rig.

#### **4.3.2 Data acquisition system and calculation**

A data acquisition unit (Model: AGLIENT 34970A/34902A) is used in this experimental rig. It provides 48 channels for monitoring various types of system parameters. The DC signal from various measuring devices/sensors can be scaled into their real physical values of the measured parameters using a logging & control supervisory program which is developed using LabVIEW programming platform.

The minimum data sampling interval is one second. It should be noted that the flow rates of both supply air and condenser air are calculated using the air static pressure drops across their respective nozzles. The outdoor air flow rate is evaluated by multiplying the measured air velocity with the sectional area of the outdoor air duct. The output cooling capacity from the DX VAV A/C system is calculated based on the enthalpy-difference of air across the DX cooling coil.

The volumetric air flow rate passing through a single nozzle is calculated as follows:

$$q_v = K_2 C_d A \sqrt{1000 P_v V'_n} \quad (4.1)$$

where

- $q_v$  = volumetric flow rate, m<sup>3</sup>/s;
- $K_2$  = a constant of 1.414;
- $C_d$  = nozzle flow coefficient;
- $A$  = nozzle throat area, m<sup>2</sup>;
- $P_v$  = air static pressure drop across the nozzle, Pa;
- $V'_n$  = specific volume of moisture air, m<sup>3</sup>/kg.

The output cooling capacity from the experimental DX VAV A/C system is then calculated by:

$$\phi_c = \frac{q_v (h_{a1} - h_{a2})}{V'_n} \quad (4.2)$$

where

- $\phi_c$  = output cooling capacity, W;
- $q_v$  = supply air flow rate, m<sup>3</sup>/s;
- $h_{a1}$  = air enthalpy upstream the DX cooling coil, J/kg;
- $h_{a2}$  = air enthalpy downstream the DX cooling coil, J/kg;
- $V'_n$  = specific volume of moisture air, m<sup>3</sup>/kg.

Based on the uncertainty of individually measured variables, the uncertainty for the output cooling capacity,  $\text{Error}_{\text{cp}}$ , can then be determined using the classic root-sum-square formula:

$$\text{Error}_{\text{cp}} = \sqrt{\sum (U_N \times C_s)^2} \quad (4.3)$$

where

$U_N$  = individual uncertainty of the individually measured input variables:  $q_v, h_{a1}, h_{a2}, V_n$

$C_s$  = sensitivity coefficient, the partial derivative of the cooling capacity with respect to the measured input variables

The uncertainty of the output cooling capacity was estimated at approximately 3~4%, depending largely on the accuracy of both air temperatures and air flow rate measurements.

#### **4.4 LabVIEW logging & control supervisory program**

As pointed out earlier, the main purpose of setting up this experimental DX VAV A/C system is for experimentally investigating the modeling and control for DX VAV A/C systems. Therefore, a computer supervisory program which is capable of performing simultaneously data-logging and parameter-controlling is required. It needs to communicate with not only the data acquisition unit, but also conventional standalone digital programmable PI controllers which are to be detailed in Section 4.5. A commercially available programming package, LabVIEW, provides a powerful programming and graphical platform for data acquisition and analysis, as well as for control application.

A data logging & control supervisory program has been developed using LabVIEW,

with all measured parameters real-time monitored, curve-data displayed, recorded and processed. The program can also perform the retrieval, query and trend-log graphing of historical data for measured parameters. The program runs on a personal computer (PC).

On the other hand, the LabVIEW-based logging & control supervisory program enables the PC to act as a central supervisory control unit for different low-level control loops, which will be discussed in Section 4.5, in the experimental rig. The PC can therefore not only modify the control settings of those standalone microprocessor-based PI controllers, but also deactivate any of these controllers. The LabVIEW-based logging & control supervisory program also provides an independent self-programming module (SPM) by which new control algorithms may be implemented easily through programming. A SPM performs in a similar manner to a central processing unit of a physical digital controller. The variables available from all measured parameters can be input to, and processed according to a specified control algorithm in a SPM to produce required control outputs. Once a SPM is initiated to replace a given standalone controller, the controller must be deactivated, but works as a digital-analog converter to receive the control output from the SPM. An analogue control signal is then produced by the controller to initiate the related actuator for necessary control action.

#### **4.5 Conventional control loops in the experimental rig**

Totally, there are twelve conventional control loops in this experimental rig. These loops use PI controllers which are of digital programmable type with RS-485

communication port (Model: YOKOGAWA UT350-1). The controller's proportional band, integral times, and set points are all allowed to be reset.

Among the twelve control loops, four are for varying heat and moisture generation rate of the LGUs located in the two spaces. Electrical power input to the LGU is regulated using SSR or SCR according to the instructions from their respective control loops, to simulate the space cooling load. In addition, there is one control loop for maintaining the condenser inlet air temperature at its setting through regulating electrical power input by SSR.

The remaining seven conventional PI control loops are as follows: supply air temperature by regulating the compressor speed; supply air static pressure by regulating the supply fan speed; condensing pressure by regulating the condenser fan speed; refrigerant superheating by regulating EEV opening; outdoor air flow rate by jointly regulating both outdoor and return air dampers' openings; air temperatures in Space A and B by regulating their VAV terminals' air flow rates, respectively. These seven control loops can be activated by using either the conventional physical digital PI controller available in the experimental rig or a SPM specifically for any new control algorithm to be developed.

The control of supply air temperature is used as an example for illustration. When the conventional PI controller is enabled, the controller measures the supply air temperature using the temperature sensor and then compares the measured with its set point. A deviation is processed in the controller according to a pre-set PI control

algorithm and an analogue control signal of 4~20 *mA* is produced and sent by the PI controller to the VFD for compressor motor to regulate its speed. On the other hand, such a conventional PI controller may be replaced by a SPM to be specifically developed based on a new control algorithm for compressor speed control. The SPM may take the advantages of using simultaneously multiple input variables, e.g., supply air temperature and its set point, evaporating and condensing pressure, degree of refrigerant superheat, etc. Control outputs can then be created using the SPM according to the new control strategy and algorithm, and communicated to the physical digital PI controller which now works only as a digital-analog converter. An analog control signal is then generated and sent to the VFD of compressor for its speed control.

#### **4.6 Summary**

An experimental rig for a DX VAV A/C system has been developed and set up. The rig consists of two parts: a DX refrigeration plant having a variable-speed compressor and EEV; and a VAV air-distribution sub-system including two identical conditioned spaces. Two LGUs are placed inside the two conditioned spaces, one in each space, for simulating its cooling load.

The experimental rig has been fully instrumented using high quality sensors/measuring devices. Totally forty-three operating parameters in the rig can be measured and monitored simultaneously and twelve conventional PI feedback control loops are provided. Two sets of air flow rate measuring apparatus are

constructed in accordance with ANSI/ASHRAE 41.2. Sensors for measuring refrigerant properties are in direct contact with refrigerant, and a Corioli mass flow meter is used for measuring the refrigerant flow rate passing through the EEV.

A logging & control (L&C) supervisory program has been developed specifically for this experimental rig using LabVIEW programming platform. All parameters can be real-time measured, monitored, curve-data displayed, recorded and processed by the L&C program. The LabVIEW-based L&C program provides an independent self-programming module (SPM) by which any new control algorithms to be developed may be implemented.

The availability of such an experimental rig for a DX VAV A/C system is expected to be extremely useful in developing both a dynamic mathematical model for a DX VAV A/C system and its experimental validation, and a novel capacity controller for matching the output cooling capacity from the DX refrigeration plant with the varying cooling load in the VAV air-distribution sub-system in a DX VAV A/C system.

Photos showing the experimental rig are shown in Appendix A.



## **Chapter 5**

### **Dynamic Modeling of the Experimental DX VAV A/C System**

#### **5.1 Introduction**

Simulation study has become increasingly popular for the past few decades. Its applicability in design optimization and developing control strategies for various refrigeration and air conditioning installations, has widely been accepted by the HVAC industry. It is well-known that the operation of a DX VAV A/C system is dynamic in nature and the interaction among the system's various control loops is intense. Therefore, there has been a strong need for a dynamic mathematical model that could accurately predict the transient behavior of a DX VAV A/C system. A good dynamic model can be significantly useful in configuring complex and advanced control and developing better control strategies. As pointed out in Chapter 2, although there have been many reported studies on separate modeling DX refrigeration plants and VAV A/C systems, a complete dynamic mathematical model specifically for a DX VAV A/C system cannot be identified in the open literature.

This chapter reports on the development of a complete dynamic mathematical model for the experimental DX VAV A/C system. The model developed is expected to be greatly helpful for developing advanced control strategies for DX VAV A/C systems. It is to be component-based, and takes into consideration the dynamic behaviors of both the DX refrigeration plant and the VAV air distribution sub-system in the DX VAV A/C system simultaneously. The dynamic model has been developed based on the principle of mass and energy conservation, and using the correlations describing

the operational performance of various components in the experimental DX VAV A/C system, which are either field-tested or available from manufacturers. Mathematical correlations representing the control logics of various controllers are also included. The complete dynamic model for the experimental DX VAV A/C system includes two constituent sub-models for the DX refrigeration plant and the VAV air-distribution sub-system, respectively.

The schematic diagram of the experimental DX VAV A/C system modeled is shown in Figure 4.1, and was described in detail in Chapter 4. The model was established by zoning the DX VAV A/C system, and the complete conceptual model which depicts the zoning of the DX VAV A/C system is shown in Figure 5.1. Each zone was treated as a stirred tank; and the dynamic model so developed is of partial-lumped-parameter type.

When presenting the sub-models in Sections 5.1 and 5.2, reference is made to Figure 5.1 for symbols representing the zones and subscripts indicating the locations in the DX VAV A/C system.

## **5.2 Development of the sub-model for the DX refrigeration plant**

The major components in the DX refrigeration plant included a variable-speed rotor compressor, air-cooled plate-finned condenser, electronic expansion valve (EEV), louver-finned DX evaporator, receiver and other fittings such as filter and dryer. For simplicity, the fittings and the refrigerant line between the receiver and EEV were

treated as one single component where only the heat transfer between refrigerant and surrounding environment was considered when modeling. The heat gain by or loss from other refrigerant lines within the refrigeration plant was either neglected due to good thermal insulation or given fixed values. The space volumes of refrigeration lines were added to their adjacent zones.

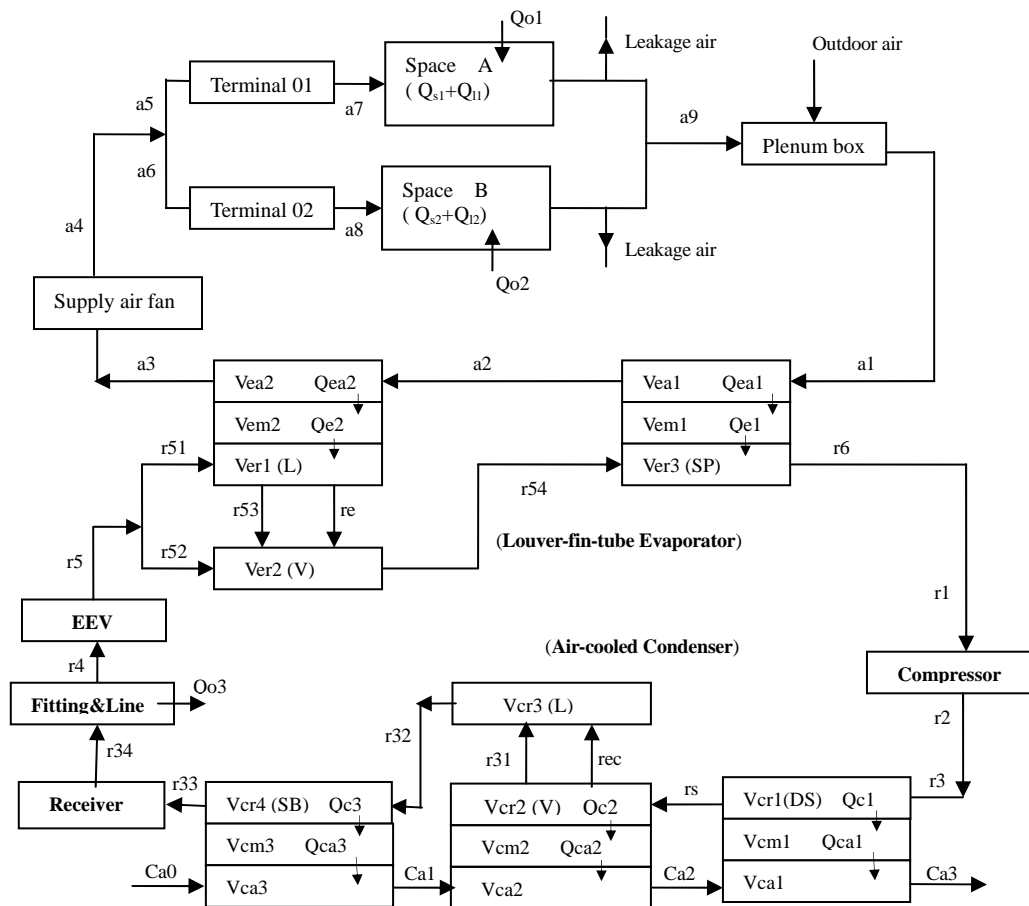


Figure 5.1 The conceptual model of the experimental DX VAV A/C system

When modeling, the DX evaporator was divided into two regions, i.e., a two-phase and a superheating region; and the air-cooled condenser into three regions, i.e., a desuperheating region, a two-phase region and a subcooling region. Both the evaporator and the condenser were approximated to be ideal counter-flow heat exchangers. The log mean temperature difference method was applied to each region

of the heat exchangers to determine their heat transfer rates. The moving-boundary method was used to deal with the refrigerant flows within both evaporator and condenser.

The well-known *A.C. Cleland* correlations [Cleland 1986], and the air state correlations recommended by ASHRAE [ASHRAE 2001] were used to describe various thermodynamic and thermophysical properties of refrigerant R22 and air, respectively.

### 5.2.1 Variable-speed compressor

A variable speed rotor compressor is used in the DX refrigeration plant. It is well known that compared to an evaporator and condenser, the transient characteristics of a compressor can be normally neglected. Therefore a compression process is often modeled as a steady-state process when building dynamic models. Generally, a polytropic compression can be assumed; and the compressor speed is assumed to reach its specified speed instantly. Therefore, in modeling the variable speed rotor compressor, this general approach has been adopted.

The refrigerant mass flow rate leaving the compressor is assumed to be equal to that at the compressor inlet:

$$m_{r1} = m_{r2} \quad (5.1)$$

and is calculated by:

$$m_{r1} = \rho_{r1} \dot{V}_{com} \quad (5.2)$$

Knowing the compressor's displacement coefficient,  $\lambda$ , the refrigerant volumetric flow rate passing through the compressor can be determined by:

$$\dot{V}_{com} = \dot{V}_{com,t} \times \lambda \quad (5.3)$$

The compressor's theoretical volumetric flow rate is evaluated by:

$$\dot{V}_{com,t} = n\pi r^2 l \varepsilon (2 - \varepsilon) \quad (5.4)$$

where,  $\dot{V}_{com,t}$  is the theoretical displacement volumetric flow rate;  $l$  the stroke of cylinder;  $r$  the radius of rotor; and  $\varepsilon$  the relative eccentricity of rotor:

$$\varepsilon = \frac{e}{R} \quad (5.5)$$

where  $e$  is the rotor eccentricity and  $R$  is the radius of cylinder.

The compressor speed can be calculated from the frequency of its motor drive:

$$n = \frac{F \times (1 - s)}{PL} \quad (5.6)$$

where  $F$  is the input frequency of the variable-frequency drive for compressor's motor;  $s$  the slip factor of the motor with a value between 2% and 6%; and  $PL$  the number of electrode couple of the motor.

The overall displacement coefficient,  $\lambda$ , is determined by:

$$\lambda = \lambda_v \lambda_p \lambda_r \lambda_l \quad (5.7)$$

where,  $\lambda_p$  is the pressure loss coefficient with a value approximately of 1.0;  $\lambda_l$  the leakage coefficient, 0.98~0.92; the compressor volumetric coefficient,  $\lambda_v$ , given by:

$$\lambda_v = 1 - 0.015 \times \left[ \left( \frac{P_{r2}}{P_{r1}} \right)^{\frac{1}{\beta}} - 1 \right] \quad (5.8)$$

and the temperature coefficient is

$$\lambda_T = 2.57 \times 10^{-3} \times T_{rs} + 1.06 \times 10^{-3} \times (T_{r6} - T_{r54}) \quad (5.9)$$

The compression index,  $\beta$ , is assumed to be constant at 1.18; the theoretical isentropic work done by the compressor is given by:

$$w_{com,t} = \frac{\beta}{\beta - 1} \frac{P_{r1}}{\rho_{r1}} \left\{ \left( \frac{P_{r2}}{P_{r1}} \right)^{\frac{\beta}{\beta - 1}} - 1 \right\} \quad (5.10)$$

The indicated work of compressor is,

$$w_{com} = \frac{w_{com,t}}{\eta_i} \quad (5.11)$$

The indicated coefficient,  $\eta_i$ , is evaluated by:

$$\eta_i = \frac{\lambda_T \lambda_l}{1.5 \times \Delta p_{dm} \times \left( \frac{P_{r2}}{P_{r1}} \right)^{\frac{1}{N}} + \frac{(h_{r2} - h_{r1}) / v_{r1}}{1}} \quad (5.12)$$

where,  $\Delta p_{dm}$  is the compressor discharge pressure loss:

$$\Delta p_{dm} = 25 \times (T_{rs} - 273.15)^{-1.01} \times 10^{-0.15 \frac{P_{r2}}{P_{r1}}} \quad (5.13)$$

Taking into account the energy loss inside the motor and transmission assembly, the total electrical work input to the compressor,  $W$ , is given as follows:

$$W = \frac{w_{com,t} m_{r1}}{\eta_{el}} \quad (5.14)$$

The electric coefficient is,

$$\eta_{el} = \eta_i \eta_{mec} \eta_{motor} \quad (5.15)$$

where  $\eta_{mec}$  is the mechanical coefficient with a value between 0.7 and 0.85;  $\eta_{motor}$  is the motor coefficient with a value of 0.8.

Based on the principle of energy conservation, the enthalpy of the vapor refrigerant exiting the compressor is evaluated by:

$$h_{r2} = h_{r1} + w_{com} \quad (5.16)$$

Therefore, the state of vapor refrigerant discharging from the compressor can be determined after knowing the refrigerant enthalpy and pressure. It should be noted here that the heat exchange between the compressor shell and the surroundings has been embedded in both the overall displacement coefficient and the electric coefficient. It should be further noted that to ensure the generalization of the system model developed, the compressor was modeled using the principle of energy and mass balance, rather than using curve-fitting its performance data. Such a modeling approach has been commonly adopted [Jolly et al. 1990, Chen et al. 2005, Deng 2002].

### **5.2.2 Electronic expansion valve (EEV)**

When investigating the transient behavior or analyzing the control stability of a refrigeration system, a dynamic model instead of a steady-state model for an expansion valve should be preferred. The dynamics of a thermal expansion valve (TEV) is caused mainly by the thermal capacitance of its temperature bulb which produces a pressure force for moving its needle valve. However, an EEV is usually driven by a stepping-motor and is program-controlled. The transmission of an electronic control signal may be regarded as instantaneous. Hence, its dynamics should mainly lie in the action of the stepping-motor which needs a certain amount of time to achieve the required valve opening.

The process in an EEV may be regarded as an isenthalpic throttling one. Hence, the enthalpy after the throttling process through the EEV is assumed to be equal to that before the EEV, i.e.,

$$h_{r5} = h_{r4} \quad (5.17)$$

The refrigerant flow through the EEV is represented by an orifice equation, and its mass flow rate is calculated by:

$$m_{r5} = C_v A_{EEV} \sqrt{\rho_{r4} \Delta P_{EEV}} \quad (5.18)$$

The refrigerant pressure drop across the EEV is

$$\Delta P_{EEV} = P_{r4} - P_{r5} \quad (5.19)$$

The flow coefficient of the EEV is given by [Chen 1999]:

$$C_v = 0.82 - 0.053 \times \chi_{r5} \quad (5.20)$$

Generally, an EEV has a linear inherent flow characteristic. The valve opening is assumed to be linear with the actual pulse output of the EEV's PI controller,  $PLS$ , i.e.,

$$A_{EEV} = K_{EEV} \times PLS \quad (5.21)$$

where  $K_{EEV}$  is the valve opening per unit of pulse output and obtainable from the performance data of the EEV.

PI control algorithm is adopted by the EEV controller and the pulse output is modulated in response to the degree of refrigerant superheat at the evaporator exit.

The theoretical pulse output of the EEV,  $PLS_1$ , is obtained by:

$$PLS_1 = k_{p,EEV} De_{sh} + \frac{k_{p,EEV}}{t_{i,EEV}} \int (De_{sh}) dt + \phi_{EEV} \quad (5.22)$$

where  $De_{SH}$  is the difference between the set point and the actual value of



refrigerant's degree of superheat;  $\phi_{EEV}$  the offset adjustment parameter for a particular EEV. The actual pulse output,  $PLS$ , derived as follows:

$$PLS = PLS_1 \quad \text{when} \quad ABS(PLS_1 - PLS_0) \leq CR \times \delta t ; \quad (5.23)$$

$$PLS = PLS_0 + CR \times \delta t \quad \text{when} \quad ABS(PLS_1 - PLS_0) > CR \times \delta t ; \quad (5.24)$$

where  $PLS_0$  is the actual pulse output of the EEV controller at the last sampling point, and  $CR$  the fixed pulse changing rate of the EEV's stepping-motor.

### 5.2.3 Condenser

The condenser in the DX plant is air-cooled and of plate-fin-tube type. Its zoning is shown in Figure 5.1. Counter-flow heat exchange is assumed between the refrigerant and cooling air. According to the state of refrigerant, the condenser is divided, when modeling, into three regions, i.e., a desuperheating region, a two-phase region and a subcooling region. The desuperheating region is represented by  $V_{cr1}$ . The two-phase region is further separated into two zones, i.e., a vapor zone,  $V_{cr2}$ , and a liquid zone,  $V_{cr3}$  where the liquid refrigerant is saturated. The subcooling region is represented by  $V_{cr4}$ . The superheated vapor refrigerant discharged from the rotor compressor is firstly cooled to become saturated vapor refrigerant in  $V_{cr1}$  and then flows into the two-phase region. The saturated vapor refrigerant in  $V_{cr2}$  is then condensed and becomes saturated in  $V_{cr3}$ . The refrigerant becomes subcooled in  $V_{cr4}$ . Afterwards, the refrigerant from the condenser flows to the receiver where the liquid refrigerant is accumulated. The tube walls of the desuperheating, two-phase and subcooling regions are represented by the  $V_{cm1}$ ,  $V_{cm2}$  and  $V_{cm3}$ , respectively.  $V_{ca1}$ ,  $V_{ca2}$  and  $V_{ca3}$  are the assumed zones for cooling air carrying away the rejected heat from the refrigerant in the desuperheating, two-phase and subcooling regions, respectively.

### 5.2.3.1 Refrigerant side of the desuperheating region

Neglecting the refrigerant mass storage inside the desuperheating region, the mass balance on zone  $V_{cr1}$  gives:

$$m_{rs} = m_{r3} = m_{r2} \quad (5.25)$$

The heat loss from the insulated refrigerant line between the compressor and the condenser is neglected, hence,

$$h_{r3} = h_{r2} \quad (5.26)$$

The heat transfer rate in the desuperheating region is:

$$Q_{c1} = m_{r3} \times (h_{r3} - h_{rs}) \quad (5.27)$$

where the saturated vapor refrigerant enthalpy,  $h_{rs}$ , can be evaluated from the refrigerant saturated pressure,  $P_{rs}$ , using the R22 state correlations.

The counter-flow heat transfer is assumed to take place between the refrigerant and the tube wall. The heat transfer rate in the desuperheating region can also be evaluated by using the log mean temperature difference,  $LMTD_{c,des}$ , between the refrigerant and the corresponding tube wall,  $V_{cm1}$ . Hence,

$$Q_{c1} = \alpha_{c,des} \times A_{t,cr1} \times LMTD_{c,des} \quad (5.28)$$

$LMTD_{c,des}$  is calculated by:

$$LMTD_{c,des} = \frac{T_{r3} - T_{rs}}{\ln\left(\frac{T_{r3} - T_{cm1}}{T_{rs} - T_{cm1}}\right)} \quad (5.29)$$

where the temperature of saturated vapor refrigerant,  $T_{rs}$ , can be evaluated from  $P_{rs}$ ; and the temperature of superheated vapor refrigerant,  $T_{r3}$ , from  $P_{r3}$  and  $h_{r3}$ , both using the R22 state correlations.

The refrigerant flow inside the tube can be regarded to be fully developed turbulent.

The heat transfer coefficient in the desuperheating region,  $\alpha_{c,des}$ , is then calculated using the *Petukhov-Popov* Equation [Baughn and Roby 1992] as follows:

$$\alpha_{c,des} = \lambda_{r,c} \times \frac{Nu_{des}}{D_{i,c}} \quad (Re=10^4 \sim 5 \times 10^6, Pr=0.5 \sim 2000) \quad (5.30)$$

where  $\lambda_{r,c}$  is the thermal conductivity of refrigerant; the *Nusselt* number is:

$$Nu_{des} = \frac{\frac{f_c}{8} Re_{des} Pr_{des}}{1.07 + 12.7 \left(\frac{f_c}{8}\right)^{0.5} (Pr_{des}^{\frac{2}{3}} - 1)} \quad (5.31)$$

where the turbulent skin-friction coefficient,  $f_c$ , is:

$$f_c = [1.82 \times \lg(Re_{des}) - 1.64]^{-2} \quad (5.32)$$

Using Equations (5.25) to (5.32) the inside heat transfer area in the desuperheating region,  $A_{i,cr1}$ , can then be obtained.

### 5.2.3.2 Refrigerant side of the two-phase region

Similarly, the mass storage and thermal capacity of the vapor refrigerant in  $V_{cr2}$  is negligible. Therefore a mass balance of the zone yields:

$$m_{rs} = m_{r31} + m_{rec} \quad (5.33)$$

and an energy balance of the zone yields:

$$m_{rs} h_{rs} = m_{r31} h_{r31} + m_{rec} h_{rec} + Q_{c2} \quad (5.34)$$

The heat transfer rate in the two-phase region,  $Q_{c2}$ , is calculated using

$$Q_{c2} = \alpha_{c,tp} A_{c,tp} (T_c - T_{cm2}) \quad (5.35)$$

where the condensing temperature,  $T_c$ , can be evaluated from the condensing pressure,  $P_c$ , using the R22 state correlations. The corresponding convective heat transfer coefficient,  $\alpha_{c,tp}$ , can be derived by *Nusselt* heat transfer equation for laminar flow [Zhang 1986]:

$$\alpha_{c,tp} = 0.555 r_c^{\frac{1}{4}} B_m (T_c - T_{cm2})^{-\frac{1}{4}} D_{i,c}^{-\frac{1}{4}} \quad (5.36)$$

where  $r_c$  is the refrigerant latent heat of vaporization, and  $B_m$  the integrated refrigerant thermophysical property obtained by:

$$B_m = \left( 9.81 \frac{\rho_r^2 \lambda_r^3}{\mu_r} \right)^{\frac{1}{4}} \quad (5.37)$$

The internal heat transfer area in the two-phase region is available by subtracting the internal heat transfer areas in both the desuperheating and subcooling regions from the condenser's total internal heat transfer area:

$$A_{c,tp} = A_{i,c} - A_{i,cr1} - A_{i,cr4} \quad (5.38)$$

Correspondingly the space volume in the two-phase region can be calculated using

$$V_{c,tp} = \frac{A_{c,tp}}{A_{i,c} \times V} \quad (5.39)$$

The space volume of liquid zone in the two-phase region is obtained from:

$$V_{cr3} = (1 - Z_c) V_{c,tp} \quad (5.40)$$

$Z_c$  refers to the refrigerant void fraction and is calculated using the *Zivi* Equation [Zivi 1964]:

$$Z_c = \frac{1}{1 + \left( \frac{1}{\chi_c} - 1 \right) \times \zeta_c \times \frac{\rho_{v,c}}{\rho_{l,c}}} \quad (5.41)$$

where  $\chi_c$  is the refrigerant dryness fraction in the two-phase region, and the slip rate

of refrigerant,  $\zeta_c$ , is given as

$$\zeta_c = \left( \frac{\rho_{l,c}}{\rho_{v,c}} \right)^{1/3} \quad (5.42)$$

The density of saturated vapor refrigerant in the condenser,  $\rho_{v,c}$ , is obtained from condensing pressure,  $P_c$ , using the R22 state correlations.

Applying the mass balance to  $V_{cr3}$ :

$$m_{r32} = m_{r31} + m_{rec} - \frac{d(\rho_{l,c} V_{cr3})}{dt} \quad (5.43)$$

The density of saturated liquid refrigerant,  $\rho_{l,c}$ , is evaluated using linear interpolation between 1030.4 kg/m<sup>3</sup> at 24.3 bar and 1145.8 kg/m<sup>3</sup> at 13.9 bar of condensing pressure, which is the system's normal operating pressure range, i.e.,

$$\rho_{l,c} = 1145.8 + (1030.4 - 1145.8) \times \frac{P_c - 13.9}{24.3 - 13.9} \quad (5.44)$$

Applying the energy balance to  $V_{cr3}$ :

$$m_{r31} h_{r31} + m_{rec} h_{rec} + \rho_{l,c} h_{r32} \frac{d(V_{cr3})}{dt} + M_{r,c} \frac{d(h_{r32})}{dt} = m_{r32} h_{r32} \quad (5.45)$$

It should be noted that  $M_{r,c}$  is the total mass of residual liquid refrigerant in both the condenser and the receiver. When deriving the above ordinary-different equation, the residual liquid refrigerant in  $V_{cr3}$  is considered along with those in both  $V_{cr4}$  and the receiver, to respond to the change of energy for refrigerant flow. Such a treatment would help reflect more reasonably the dynamics of both the enthalpy of the liquid refrigerant in this region, and the condensing pressure.

$M_{r,c}$  is therefore obtained from:

$$M_{r,c} = M_{CH} - M_{r,e} - M_{r,cl} - M_{r,cr1} - M_{r,cr2} \quad (5.46)$$

where  $M_{CH}$  is the amount of refrigerant charged in the DX plant;  $M_{r,e}$  the mass of residual refrigerant in the evaporator; and  $M_{r,cl}$  the mass of residual refrigerant in the refrigerant line and fittings. By knowing the saturated liquid refrigerant enthalpy,  $h_{r32}$ , the saturated refrigerant pressure at the exit of the two-phase region which is regarded as the condensing pressure,  $P_c$ , can then be obtained using the R22 state correlations.

The rate of evaporation or condensation of refrigerant resulting from the pressure variation in the two-phase region is evaluated by [Deng 2000]:

$$m_{rec}\gamma_c = \rho_{l,c}V_{cr3} \frac{dh_{r32}}{dt} \quad (5.47)$$

By assuming a constant refrigerant pressure drop inside the two-phase region, i.e.,  $\Delta P_c$ , the refrigerant pressure at the entrance of the two-phase region,  $P_{rs}$ , is obtained by

$$P_{rs} = P_c + \Delta P_c \quad (5.48)$$

The pressure drops of vapor refrigerant inside both the desuperheating region and adjacent refrigerant lines are neglected, i.e.,

$$P_{r2} = P_{r3} = P_{rs} \quad (5.49)$$

### 5.2.3.3 Refrigerant side of the subcooling region

Normally, the receiver in a refrigeration plant is not fully filled with liquid

refrigerant. Liquid and vapor refrigerant co-exist at the saturated condition in the receiver. This inevitably causes the refrigerant to enter the receiver at a saturated state [Jolly et al. 2000]. Therefore, for a DX refrigeration plant with an appropriate amount of refrigerant charge, the subcooling of the refrigerant exiting the condenser equipped with receiver is required to compensate the refrigerant pressure drop between the condenser and the receiver so that the saturated liquid state for refrigerant entering the receiver can be achieved. The smaller the refrigerant pressure drop, the lower the refrigerant subcooling. If the refrigerant pressure drop can be neglected, the liquid refrigerant would leave a condenser at saturated state and there would not be a subcooling region in the condenser. In fact, the pressure drop between the receiver and the condenser in a small-sized refrigeration plant is usually small. Therefore the refrigerant subcooling in the condenser is low at approximately a range of 0~5 °C under normal operating conditions. Correspondingly the subcooling region in a condenser is small and the effect of small variation of refrigerant subcooling on the operating behavior of a refrigeration plant equipped with a receiver is insignificant. Therefore, for simplicity, it is assumed that a fixed 3% of the total space volume in the condenser is for the subcooling region.

The refrigerant mass storage in the subcooling region is neglected, i.e.,

$$m_{r33} = m_{r32} \quad (5.50)$$

The heat transfer in the subcooling region is

$$Q_{c3} = m_{r33} \times (h_{r33} - h_{r32}) \quad (5.51)$$

It can also be expressed by

$$Q_{c3} = \alpha_{c, sb} \times A_{i, cr4} \times LMTD_{c, sb} \quad (5.52)$$

The log mean temperature difference is evaluated by

$$LMTD_{c, sb} = \frac{T_{r32} - T_{r33}}{\ln\left(\frac{T_{r32} - T_{cm3}}{T_{r33} - T_{cm3}}\right)} \quad (5.53)$$

The refrigerant flow inside the tube can be regarded to be fully-developed turbulent. The heat transfer coefficient for the subcooled refrigerant is evaluated using the *Dittus-Boelter* Equation [Kay and London 1984]:

$$Nu_{sb} = 0.023 \times Re_{sb}^{0.8} \times Pr_{sb}^{0.3} \quad (Re=10^4 \sim 1.2 \times 10^5, Pr=0.7 \sim 100) \quad (5.54)$$

Because the enthalpy for subcooled refrigerant,  $h_{r33}$ , depends on the refrigerant temperature,  $T_{r33}$ , Equations (5.50) to (5.54) are implicit and the *Newton* iteration method is used to solve these equations. After obtaining the temperature of the subcooled refrigerant,  $T_{r33}$ , the refrigerant subcooling in condenser can be obtained by:

$$T_{sb} = T_{r32} - T_{r33} \quad (5.55)$$

#### 5.2.3.4 Receiver, fittings and refrigerant line

The receiver is simply treated as a refrigerant vessel where the excessive refrigerant in the plant is stored. The enthalpy of the refrigerant exiting the receiver is assumed to be equal to  $h_{r33}$ :

$$h_{r34} = h_{r33} \quad (5.56)$$

For the fittings and refrigerant line (F&L) between the EEV and the receiver, applying a mass balance yields:

$$m_{r34} = m_{r4} = m_{r5} \quad (5.57)$$

The energy balance equation for the F&L zone is as follows:

$$m_{r4} h_{r4} + Q_{o3} = m_{r34} h_{r34} \quad (5.58)$$



where,  $Q_{o3}$  is the assumed total heat transfer between the refrigerant in the pipe line, fittings and the receiver, and their respective ambient environments.

### 5.2.3.5 Air side of the condenser

It is assumed that the same overall heat transfer coefficient,  $U_{o,c}$ , between the tube-fin and cooling air is applied to all the regions in the condenser,

$$U_{o,c} = \frac{1}{\frac{1}{\alpha_{o,c}} + R_{0,c}} \quad (5.59)$$

where  $R_{0,c}$  is the combined total thermal resistance from the tube wall, surface contact and fouling. Generally, the contact and fouling thermal resistance could account for about 20% of the total thermal resistance in a heat exchanger. Therefore, it should not be neglected and a fixed value may be assumed. Furthermore, when deriving the actual average convective heat transfer coefficient between tube-fin and cooling air, the surface coefficient of the condenser tube-fin,  $\eta_{s,c}$ , which accounts for the non-homogeneous temperature distribution over the plate-fin, is used. The actual average convective heat transfer coefficient is therefore,

$$\alpha_{o,c} = \eta_{s,c} \alpha_{a,c} \quad (5.60)$$

The surface coefficient is evaluated by

$$\eta_{s,c} = 1 - \frac{A_{f,c}}{A_{tu,c}} (1 - \eta_{f,c}) \quad (5.61)$$

where  $A_{f,c}$  is the fin surface area;  $A_{tu,c}$  is the outside tube surface area. The fin efficiency,  $\eta_{f,c}$ , of the condenser's plate fin is calculated by the *Schmidt* Equation [Schmidt 1945]:

$$\eta_{f,c} = \frac{th(m_c' h_c')}{m_c' h_c'} \quad (5.62)$$

$$m_c' = \sqrt{\frac{2\alpha_{a,c}}{\lambda_{f,c} \delta_f}} \quad (5.63)$$

$$h_c' = 0.5D_{o,c} \left( \frac{S_{tr,c}}{D_{o,c}} - 1 \right) \left[ 1 + 0.35 \ln \left( \frac{1.063S_{tr,c}}{D_{o,c}} \right) \right] \quad (5.64)$$

where  $\lambda_{f,c}$  is fin's thermal conductivity;  $\delta_f$  is the fin thickness;  $S_{tr,c}$  is the transverse tube pitch;  $D_{o,c}$  is the condenser tube outside diameter. The air heat transfer coefficient for forced convection is calculated by the *McQuiston* Equation [McQuiston 1978]:

$$\alpha_{a,c} = 0.0014 + 0.2168 \text{Re}_{a,c}^{-0.4} \left( \frac{A_{o,c}}{A_{tu,c}} \right)^{-0.15} \quad (5.65)$$

where the *Reynolds* Number for air flow is

$$\text{Re}_{a,c} = \frac{\rho_a v_{a,\max} D_{o,c}}{\mu_a} \quad (5.66)$$

For the metal zone,  $V_{cm1}$ , in the desuperheating region, an energy balance gives:

$$Q_{c1} = Q_{ca1} + M_{cm1} C_{p,c,m} \frac{dT_{cm1}}{dt} \quad (5.67)$$

where the metal mass in  $V_{cm1}$  can be obtained from

$$M_{cm1} = \frac{A_{i,cr1}}{A_{i,c}} \times M_c \quad (5.68)$$

The air side total heat transfer area in the desuperheating region is

$$A_{o,de} = \frac{A_{i,cr1}}{A_{i,c}} A_{o,c} \quad (5.69)$$

The heat transfer between the condenser tube-fin and cooling air is thus evaluated by:

$$Q_{ca1} = U_{o,c} A_{o,de} LMTD_{c,de} \quad (5.70)$$

where the log mean temperature difference between the tube-fin and cooling air in the desuperheating region is

$$LMTD_{c,de} = \frac{(T_{cm1} - T_{ca2}) - (T_{cm1} - T_{ca3})}{\ln\left(\frac{T_{cm1} - T_{ca2}}{T_{cm1} - T_{ca3}}\right)} \quad (5.71)$$

Since the moisture content of cooling air forced across the condenser remains unchanged, applying mass and energy balances to the zone,  $V_{ca1}$ , gives

$$m_{ca3} = m_{ca2} \quad (5.72)$$

$$Q_{ca1} = m_{ca3} C_{p,a} (T_{ca3} - T_{ca2}) \quad (5.73)$$

where  $C_{p,a}$  is the specific heat of cooling air. Equations (5.69) to (5.73) are implicit and are used together to derive the temperature of cooling air exiting the condenser,  $T_{ca3}$ .

Similarly, for the metal zone,  $V_{cm2}$ , in the two-phase region, an energy balance gives:

$$Q_{c2} = Q_{ca2} + M_{cm2} C_{p,c,m} \frac{dT_{cm2}}{dt} \quad (5.74)$$

where the metal mass in  $V_{cm2}$  can be obtained from

$$M_{cm2} = \frac{A_{i,c} - A_{i,cr1} - A_{i,cr4}}{A_{i,c}} \times M_c \quad (5.75)$$

The air side total heat transfer area in the two-phase region is

$$A_{o,tp} = \frac{A_{i,c} - A_{i,cr1} - A_{i,cr4}}{A_{i,c}} \times A_{o,c} \quad (5.76)$$

The heat transfer between the condenser tube and cooling air is thus evaluated by:

$$Q_{ca2} = U_{o,c} A_{o,tp} LMTD_{c,tp} \quad (5.77)$$

where the log mean temperature difference between the tube-fin and cooling air in the two-phase region is

$$LMTD_{c,tp} = \frac{(T_{cm2} - T_{ca1}) - (T_{cm2} - T_{ca2})}{\ln\left(\frac{T_{cm2} - T_{ca1}}{T_{cm2} - T_{ca2}}\right)} \quad (5.78)$$

For the assumed zone,  $V_{ca2}$ , applying mass and energy balances also gives

$$m_{ca2} = m_{ca1} \quad (5.79)$$

$$Q_{ca2} = m_{ca2} C_{p,a} (T_{ca2} - T_{ca1}) \quad (5.80)$$

Knowing the inlet air temperature,  $T_{ca1}$ , the air temperature at the exit of the two-phase region,  $T_{ca2}$ , can then be obtained using the *Newton* iteration method.

For the metal zone  $V_{cm3}$  in the subcooling region, applying an energy balance yields:

$$Q_{c3} = Q_{ca3} + M_{cm3} C_{p,m} \frac{dT_{cm3}}{dt} \quad (5.81)$$

where the metal mass in  $V_{cm3}$  can be calculated from

$$M_{cm3} = \frac{A_{i,cr4}}{A_{i,c}} \times M_c \quad (5.82)$$

The air side total heat transfer area in the subcooling region is

$$A_{o,sb} = \frac{A_{i,cr4}}{A_{i,c}} \times A_{o,c} \quad (5.83)$$

The heat transfer between the condenser tube and cooling air is

$$Q_{ca3} = U_{o,c} A_{o,sb} LMTD_{c,sb} \quad (5.84)$$

and

$$LMTD_{c, sb} = \frac{(T_{cm3} - T_{ca0}) - (T_{cm3} - T_{ca1})}{\ln\left(\frac{T_{cm3} - T_{ca0}}{T_{cm3} - T_{ca1}}\right)} \quad (5.85)$$

Similar to that for  $V_{ca2}$ , for the zone  $V_{ca3}$  the following two equations can be established:

$$m_{ca1} = m_{ca0} \quad (5.86)$$

$$Q_{ca3} = m_{ca3} C_{p,a} (T_{ca1} - T_{ca0}) \quad (5.87)$$

where  $T_{ca0}$  is the temperature of air entering the condenser and should be an input parameter to the model to be developed.

#### 5.2.4 DX Evaporator (cooling coil)

The DX evaporator in the plant is of louver-fin-tube type, which is believed to be able to provide much better heat transfer than a traditional fin type such as plate or wavy fin. Counter-flow heat exchange between refrigerant and air is assumed. The zoning of the evaporator is also depicted in Figure 5.1. When modeling, the evaporator's refrigerant side is divided into two regions: a two-phase region and a superheated region. The former is further divided into a liquid zone and a vapor zone. All heat transfer between refrigerant and air taking place in the two-phase region is assumed to be taken up by the liquid refrigerant and, therefore, heat transfer only occurs in the liquid zone,  $V_{erl}$ . When the refrigerant pressure in the evaporator decreases, some liquid refrigerant would flash into vapor which flows to the vapor zone, this mass flow is denoted by  $m_{re}$ . This amount of vapor refrigerant mixes with

both the vapor refrigerant from  $V_{er1}$  due to evaporation, and the vapor refrigerant directly from the EEV in the vapor zone  $V_{er2}$ . The saturated vapor refrigerant is then superheated in zone  $V_{er3}$  before being sucked in by the compressor. Similar to that in the condenser,  $V_{em2}$  and  $V_{ea2}$  are the tube metal and assumed air zones in two-phase region in the evaporator, respectively;  $V_{em1}$  and  $V_{ea1}$  are the tube metal and assumed air zones in the superheated region in the evaporator, respectively.

#### 5.2.4.1 Refrigerant side of the two-phase region

Mass and energy balances on zone  $Ver1$  are represented by the following two ordinary differential equations:

$$m_{r51} - m_{r53} - m_{re} = \frac{\rho_{l,e} d(V_{er1})}{dt} \quad (5.88)$$

$$m_{r51} h_{r51} - m_{r53} h_{r53} - m_{re} h_{re} + Q_{e2} = \frac{\rho_{l,e} d(h_{l,e} V_{er1})}{dt} \quad (5.89)$$

where  $\rho_{l,e}$  is the density of saturated liquid refrigerant and may be normally assumed to have a linear relationship with the evaporating pressure;  $h_{l,e}$  is the enthalpy of saturated liquid refrigerant and is also dependent on the evaporating pressure. The refrigerant dryness fraction in the two-phase region of the evaporator,  $\chi_{r5}$ , is calculated by

$$\chi_{r5} = \frac{h_{r5} - h_{r51}}{h_{r52} - h_{r51}} \quad (5.90)$$

Hence, the mass flow rates of liquid and vapor refrigerant entering both the liquid zone and the vapor zone in the evaporator, respectively, are,

$$m_{r51} = (1 - \chi_{r5}) m_{r5} \quad (5.91)$$

and

$$m_{r52} = \chi_{r5} m_{r5} \quad (5.92)$$

The heat transfer rate between liquid refrigerant and the tube wall in the two-phase region is given as

$$Q_{e2} = \alpha_{e,tp} A_{e,tp} (T_{em2} - T_e) \quad (5.93)$$

The internal heat transfer area in the two-phase region is

$$A_{e,tp} = \frac{V_{e,tp}}{V_e} A_{i,e} \quad (5.94)$$

and

$$V_{e,tp} = \frac{1}{1 - Z_e} V_{er1} \quad (5.95)$$

where  $Z_e$  is the void fraction and calculated using the *Zivi Equation* [Zivi 1964 ].

The convective heat transfer coefficient in the refrigerant side in the two-phase region is determined using the *Kandlikar Equation* [Kandlikar 1990]:

$$\alpha_{e,tp} = \alpha_l C_1 C_0^{C_2} (25 Fr_l)^{C_5} + C_3 B_0^{C_4} F_{f1} \quad (5.96)$$

The assumed convective heat transfer coefficient for liquid refrigerant in the two-phase region,  $\alpha_l$ , is calculated by

$$\alpha_l = 0.023 \left\{ \frac{g_r (1 - \chi_e) D_{i,e}}{\mu_l} \right\}^{0.8} \frac{\text{Pr}_l^{0.4} \lambda_l}{D_{i,e}} \quad (5.97)$$

where  $g_r$  is the refrigerant mass flux, and  $\mu_l$  the dynamic viscosity of liquid refrigerant. The refrigerant convection characteristic number is

$$C_0 = \left( \frac{1 - \chi_e}{\chi_e} \right)^{0.8} \left( \frac{\rho_{v,e}}{\rho_{l,e}} \right)^{0.5} \quad (5.98)$$

The refrigerant boiling characteristic number is

$$B_0 = \frac{q_{e,tp}}{g_r \gamma_e} \quad (5.99)$$

where  $q_{e,tp}$  is the heat flux in the two-phase region. The refrigerant *Froude* number is

$$Fr_l = \frac{g_r^2}{9.8 \rho_{l,e}^2 D_{i,e}} \quad (5.100)$$

Further in Equation (5.96)  $F_{f1}$  is the dimensionless factor of refrigerant property, and is 2.20 for R22. For the constants  $C_1$  to  $C_5$  in Equation (5.96),

$$\text{when } C_0 \leq 0.65, C_1 = 1.1360, C_2 = -0.9, C_3 = 667.2, C_4 = 0.7, C_5 = 0.30; \quad (5.101)$$

$$\text{when } C_0 > 0.65, C_1 = 0.6683, C_2 = -0.2, C_3 = 1058.0, C_4 = 0.7, C_5 = 0.30. \quad (5.102)$$

The mass flow rate of evaporation,  $m_{re}$ , resulting from pressure variation is evaluated by:

$$\frac{dh_{l,e}}{dt} = \frac{\gamma_e m_{re}}{\rho_{l,e} V_{er1}} \quad (5.103)$$

and its enthalpy is described by:

$$h_{re} = h_{r53} \quad (5.104)$$

where  $h_{r53}$  is the enthalpy of saturated vapor refrigerant under the pressure of  $P_e - \Delta P_e$ . The refrigerant pressure drop in the two-phase region is evaluated by:

$$\Delta P_e = 5.986 \times 10^{-5} (q_e g_r)^{0.91} \frac{l_e}{D_{i,e}} + C_6 \quad (5.105)$$

where  $l_e$  is the tube length of each flow circuit in the evaporator.

Thermal capacitance and mass storage in the vapor zone,  $V_{er2}$ , are negligible.



Therefore, both a mass balance and an energy balance give:

$$m_{r52} + m_{r53} + m_{re} - m_{r54} = 0 \quad (5.106)$$

$$m_{r52}h_{r52} + m_{r53}h_{r53} + m_{re}h_{re} - m_{r54}h_{r54} = 0 \quad (5.107)$$

#### 5.2.4.2 Refrigerant side of the superheating region

Similarly, both mass storage and thermal capacitance of vapor refrigerant in the superheated region have been neglected. Mass and energy balances in  $V_{er3}$  yield,

$$m_{r54} - m_{r6} = 0 \quad (5.108)$$

$$m_{r54}h_{r54} - m_{r6}h_{r6} + Q_{er2} = 0 \quad (5.109)$$

The heat transfer between vapor refrigerant and the tube wall in the superheated region is evaluated by:

$$Q_{e1} = \alpha_{e,sp} A_{e,sp} LMTD_{ei,sp} \quad (5.110)$$

where the heat transfer area is:

$$A_{e,sp} = A_{i,e} - A_{i,tp} \quad (5.111)$$

and the log mean temperature difference is

$$LMTD_{ei,sp} = \frac{(T_{em1} - T_{r54}) - (T_{em1} - T_{r6})}{\ln\left(\frac{T_{em1} - T_{r54}}{T_{em1} - T_{r6}}\right)} \quad (5.112)$$

The convective heat transfer coefficient for vapor refrigerant in the superheated region is evaluated also using the *Petukhov-Popov* Equation, based on the properties of superheated refrigerant:

$$Nu_e = \frac{\frac{f_e}{8} Re_e Pr_e}{1.07 + 12.7 \left(\frac{f_e}{8}\right)^{0.5} (Pr_e^{\frac{2}{3}} - 1)} \quad (5.113)$$

$T_{r54}$  is the temperature of saturated vapor refrigerant under the pressure,  $P_{r54}$  :

$$P_{r54} = P_e - \Delta P_e \quad (5.114)$$

where the pressure drop in the two-phase region,  $\Delta P_e$ , is given using Equation (5.105). The pressure drop of vapor refrigerant in the superheated region is negligible, i.e.,

$$P_{r6} = P_{r54} \quad (5.115)$$

Since the temperature of superheated refrigerant,  $T_{r6}$ , is the function of  $h_{r6}$ , Equations (5.108) to (5.115) are implicit. Therefore, the *Newton* iteration method is used to solve the above equations together to obtain the value of  $T_{r6}$ . The mass flow rate of the refrigerant exiting the evaporator,  $m_{r6}$ , should be equal to that sucked in by the compressor, i.e.,

$$m_{r6} = m_{r1} \quad (5.116)$$

Finally, the degree of superheat of the refrigerant exiting the evaporator is evaluated by:

$$T_{sp} = T_{r6} - T_{r54} \quad (5.117)$$

The heat gain in the suction line between the compressor suction and the evaporator is simply represented by a fixed value of temperature rise of vapor refrigerant,  $\Delta T_s$ . Similarly, the refrigerant pressure drop is also represented by a fixed value,  $\Delta P_s$ . Such simplifications are reasonable in building a dynamic model which aims mainly at investigating the control rather than the design of a refrigeration plant. Hence,

$$T_{r1} = T_{r6} + \Delta T_s \quad (5.118)$$

$$P_{r1} = P_{r6} - \Delta P_s \quad (5.119)$$

Using the R22 state correlations, the density and enthalpy of the refrigerant at the compressor suction,  $\rho_{r1}$  and  $h_{r1}$ , are then evaluated from both  $P_{r1}$  and  $T_{r1}$ .

Energy balances on the tube-fin metal zones of  $V_{em2}$  and  $V_{em1}$ , respectively, would lead to:

$$Q_{ea2} - Q_{e2} = M_{em2} C_{p_{em}} \frac{dT_{em2}}{dt} \quad (5.120)$$

$$Q_{ea1} - Q_{e1} = M_{em1} C_{p_{em}} \frac{dT_{em1}}{dt} \quad (5.121)$$

The mass of the tube-fin metal in  $V_{em2}$  and  $V_{em1}$ , respectively, can be evaluated by:

$$M_{em2} = \frac{V_{e,tp}}{V_e} M_e \quad (5.122)$$

$$M_{em1} = M_e - M_{em2} \quad (5.123)$$

where  $M_e$  is the total mass of the tube-fin metal in the evaporator;  $C_{p_{em}}$  is the equivalent specific heat for the tube and fin metal.

The modeling for the refrigerant side in the evaporator would provide the refrigerant states at the compressor's suction, which is required by the model for compressor sub-model. It will also make available the evaporator's tube-fin metal surface temperatures which are to be used in modeling for the air side of the evaporator for determining its cooling and dehumidification capacity.

### 5.2.4.3 Air side of the evaporator

When modeling the air side of the evaporator, both the thermal capacitance and mass storage of air are considered negligible and hence the moisture and heat transfer between air and tube-fin is assumed to be steady-state. In the air sides of both the two-phase region,  $V_{ea2}$ , and the superheated region,  $V_{ea1}$ , wet-cooling of air occurs when the tube-fin surface temperature is below the dew-point temperature of air entering the respective regions; otherwise, dry-cooling of air occurs. The discussions on wet cooling of air in  $V_{ea2}$  and dry cooling of air in  $V_{ea1}$  are sufficient, since the dry cooling of air in  $V_{ea2}$  and wet-cooling of air in  $V_{ea1}$  may be similarly treated.

#### 5.2.4.3.1 Wet-cooling of air in $V_{ea2}$

Because the thermal capacitance and mass storage of air are negligible, mass and energy balances in  $V_{ea2}$  yield:

$$m_{a2} - m_{a3} = 0 \quad (5.124)$$

$$m_{a2}h_{a2} - m_{a3}h_{a3} - Q_{ea2} = 0 \quad (5.125)$$

where the enthalpies of moist air,  $h_{a2}$  and  $h_{a3}$ , can be calculated from air moisture content and temperatures using the air state equations from ASHRAE [ASHRAE 2001].

The heat transfer between air and tube-fin metal in the two-phase region can be

expressed as:

$$Q_{ea2} = U_{ea2} A_{ea2} LMTD_{ea2} \quad (5.126)$$

The overall heat transfer coefficient is:

$$U_{ea2} = \frac{1}{\frac{1}{\alpha_{e,wt1}} + R_{0,e}} \quad (5.127)$$

where  $R_{0,e}$  is the combined total thermal resistance from the evaporator tube wall, surface contact and fouling, and a constant value is assumed. The log mean temperature difference between the tube-fin and air is:

$$LMTD_{ea2} = \frac{T_{a2} - T_{a3}}{\ln\left(\frac{T_{a2} - T_{em2}}{T_{a3} - T_{em2}}\right)} \quad (5.128)$$

and the heat transfer area is:

$$A_{ea2} = \frac{A_{e,tp}}{A_{i,e}} A_{o,e} \quad (5.129)$$

The airside actual convective heat transfer coefficient during a dehumidifying process can be expressed as follows:

$$\alpha_{e,wt1} = \alpha_{e,wt} \times \eta_{s,ea2} \quad (5.130)$$

where  $\alpha_{e,wt}$  is the airside theoretical convective heat transfer coefficient for dehumidification. The fin surface efficiency is:

$$\eta_{s,ea2} = 1 - \frac{A_{f,e}}{A_{tu,e}} (1 - \eta_{f,ea2}) \quad (5.131)$$

The existence of condensate within fin channels may increase the non-uniformity of fin temperature, lowering the fin efficiency of an evaporator under a wet-cooling condition. The Hong-Webb Equation [Hong and Webb 1996] which takes into account the influence of condensate on heat transfer performance has been applied to

calculate the fin efficiency of the evaporator:

$$\eta_{f,ea2} = \frac{th(m_e' h_e') \cos(0.1m_e' h_e')}{m_e' h_e'} \quad (5.132)$$

$$m_e' = \sqrt{\frac{2\alpha_{s,ea2}\xi}{\lambda_{f,e}\delta_{f,e}}} \quad (5.133)$$

where  $h_e'$  can be calculated in the same way as that for the condenser's fin efficiency.

It is known the existence of a dehumidifying process would enhance the total heat transfer in an evaporator. Through adopting a dehumidifying augmentation factor,  $\xi$ , the effect of dehumidification on the total heat transfer can be taken into account. The airside theoretical convective heat transfer coefficient for dehumidification should be equal to the sensible convective heat transfer coefficient multiplied by a dehumidifying augmentation factor  $\xi$ , i.e.,

$$\alpha_{e,wt} = \alpha_{s,ea2} \times \xi \quad (5.134)$$

The dehumidifying augmentation factor is evaluated by:

$$\xi = 1 + 2.46 \times \frac{g_a - g_{em2}}{T_a - T_{em2}} \quad (5.135)$$

where  $g_{em2}$  is the moisture content of saturated air under temperature,  $T_{em2}$ ; and the average moisture content and temperature of air are:

$$g_a = 0.5 \times (g_{a2} + g_{a3}) \quad (5.136)$$

$$T_a = 0.5 \times (T_{a2} + T_{a3}) \quad (5.137)$$

Normally the thermal resistance in airside is approximately 5 to 10 times of that in refrigerant side. Consequently, the use of more accurate correlations for airside heat transfer coefficient would significantly impact on modeling accuracy. Therefore, the

following latest correlations provided by Wang [Wang et al. 2000] are selected to derive the sensible convective heat transfer coefficient for the louver-finned evaporator under wet-cooling conditions.

$$\alpha_{s,ea2} = j_{wt} \rho_{a,e} v_{a,\max} \frac{Cp_a}{Pr_{a,e}^{\frac{2}{3}}} \quad (5.138)$$

where  $j_{wt}$  is the *Colburn* factor, and calculated by:

$$j_{wt} = 9.717 Re_a^{j_1} \left( \frac{PI_{f,e}}{D_{c,e}} \right)^{j_2} \left( \frac{S_{2,e}}{S_{1,e}} \right)^{j_3} \left( \ln \left( 3 - \frac{PI_L}{PI_{f,e}} \right) \right)^{0.07162} NR_e^{-0.543} \quad (5.139)$$

where various correlation parameters are:

$$j_1 = -0.023634 - 1.2475 \left( \frac{PI_{f,e}}{D_{c,e}} \right)^{0.65} \left( \frac{S_{2,e}}{S_{1,e}} \right)^{0.2} NR_e^{-0.18} \quad (5.140)$$

$$j_2 = 0.856 \times e^{\tan \theta_l} \quad (5.141)$$

$$j_3 = 0.25 \ln(Re_a) \quad (5.142)$$

The process line in a psychrometric chart for air cooling and dehumidification taking place in a DX cooling coil can be determined by using the state points of both the incoming air and saturated air at the tube-fin surface temperature. Once the process line is determined, the moisture content of exiting air,  $g_{a3}$ , can be obtained from the exiting air temperature,  $T_{a3}$ . The moisture removal capacity of the evaporator,  $MC_{a2}$ , is then computed by the following equation:

$$MC_{a2} = m_{a2} (g_{a2} - g_{a3}) \quad (5.143)$$

#### 5.2.4.3.2 Dry-cooling of air in $V_{eal}$

Under a dry-cooling condition when the tube-fin surface temperature is above the

dew point temperature of incoming air, no water from moist air will be condensed.

Therefore, in a dry-cooling condition, all the calculations involved are simplified.

Mass and energy balances on  $V_{ea1}$  give:

$$m_{a2} - m_{a1} = 0 \quad (5.144)$$

$$g_{a2} - g_{a1} = 0 \quad (5.145)$$

$$m_{a1}h_{a1} - m_{a2}h_{a2} - Q_{ea1} = 0 \quad (5.146)$$

Similar to modeling the air side in the condenser, for  $V_{ea1}$ , the heat transfer between

air and tube-fin is expressed by:

$$Q_{ea1} = U_{ea1}A_{ea1}LMTD_{ea1} \quad (5.147)$$

$$U_{ea1} = \frac{1}{\frac{1}{\alpha_{e,dr}} + R_3} \quad (5.148)$$

$$A_{ea1} = A_{o,e} - A_{ea2} \quad (5.149)$$

$$LMTD_{ea1} = \frac{T_{a1} - T_{a2}}{\ln\left(\frac{T_{a1} - T_{em1}}{T_{a2} - T_{em1}}\right)} \quad (5.150)$$

where the airside actual convective heat transfer coefficient is:

$$\alpha_{e,dr} = \alpha_{s,ea1}\eta_{s,ea1} \quad (5.151)$$

The *Schmidt* Equation [Schmidt 1945] mentioned in the Section 5.2.3.5 is used to determine the evaporator's fin efficiency under dry-cooling conditions.

The correlations developed by Wang [Wang et al. 1999] for louver-finned evaporators under dry-cooling conditions have been adopted to calculate the airside theoretical heat transfer coefficient,  $\alpha_{s,ea1}$ ,

$$\alpha_{s,ea1} = j_{dr}\rho_{a,e}\nu_{a,\max}\frac{Cp_a}{Pr_{a,e}^{\frac{2}{3}}} \quad (5.152)$$



$$j_{dr} = 1.1373 \text{Re}_a^{j_5} \left( \frac{PI_f}{S_{2,e}} \right)^{j_6} (\tan \theta_l)^{j_7} \left( \frac{S_{2,e}}{S_{1,e}} \right)^{j_8} NR^{0.3545} \quad (5.153)$$

where various correlation parameters are:

$$j_5 = -0.6027 + 0.02593 \left( \frac{S_{2,e}}{D_{h,e}} \right)^{0.52} NR^{-0.5} \ln(\tan \theta_l) \quad (5.154)$$

$$j_6 = -0.4776 + 0.40774 \left[ \frac{NR^{0.7}}{\ln(\text{Re}_a) - 4.4} \right] \quad (5.155)$$

$$j_7 = -0.58655 \left( \frac{PI_f}{D_{h,e}} \right)^{2.3} \left( \frac{S_{2,e}}{S_{1,e}} \right)^{-1.6} NR^{-0.65} \quad (5.156)$$

$$j_8 = 0.0814[\ln(\text{Re}_a) - 3] \quad (5.157)$$

By solving these correlations and using air state equations, the temperature and moisture content of the air exiting the evaporator, i.e.,  $g_{a2}$  and  $T_{a2}$  can be obtained. These two air state parameters are important to the sub-model of the VAV air-distribution sub-system, which is reported in the next section.

### 5.3 Development of the sub-model for the VAV air-distribution sub-system

The DX evaporator in the refrigeration plant acts as a DX cooling coil in the air-distribution sub-system. The return air from conditioned spaces mixes with outdoor air in a plenum box which is part of the sub-system. The mixed air then flows across the DX cooling coil. The air exiting the cooling coil is then supplied to either of the conditioned spaces via its respective VAV terminal.

The conceptual model of the VAV air-distribution sub-system having two

conditioned spaces and their respective VAV terminals is shown in Figure 5.2. The major components in the VAV air-distribution sub-system include a supply air fan, two VAV terminals, two conditioned spaces, a plenum box and dampers. Moreover, the air-distribution ductwork is regarded as being hydraulically balanced, which helps determine the volumetric rate and static pressure of airflow at various locations.

The sub-model for the VAV-distribution sub-system is integrated with the sub-model of the DX refrigeration plant via the state parameters of the air passing through the DX cooling coil, or the DX evaporator. The operation of the VAV air-distribution sub-system is dynamic in nature because of the action of VAV terminals, the time lag of thermostats, and the thermal capacitance of conditioned spaces.

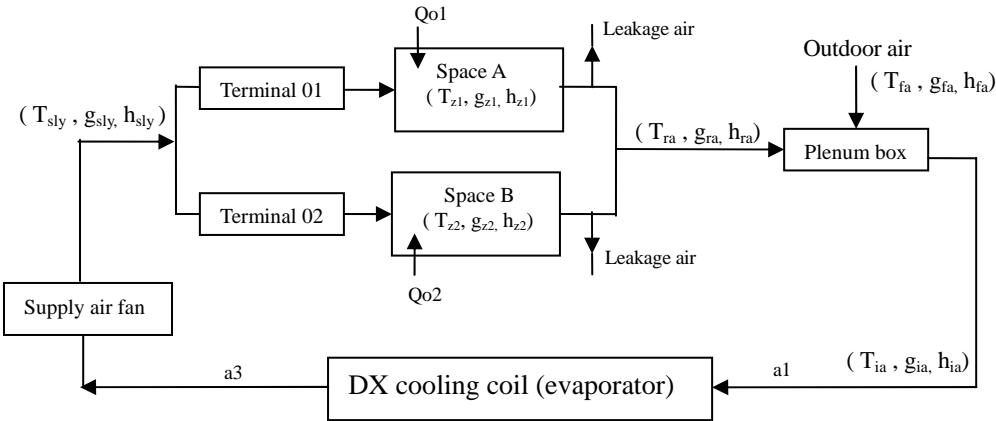


Figure 5.2 Conceptual model of the VAV air-distribution sub-system

### 5.3.1 Air-conditioned spaces

For the sake of simplicity, only one of the air-conditioned spaces, *Space A*, has been taken as an example to describe its modeling. It is assumed that throughout the whole conditioned-space, both indoor air temperature and moisture content are the same at their averages,  $T_z$  and  $g_z$ . The internal sensible heat gain in the conditioned-space from both occupants and equipment is represented by  $Q_{indoor}$ . The total sensible heat gain in the conditioned-space includes internal sensible heat gain and the heat transfer between indoor air and the internal surfaces of both space enclosure and indoor furniture,  $Q_{01}$ . A time lag of 10 minutes is assumed for space enclosure and indoor furniture to account for the influence caused by their thermal storage on the assumed surface temperature,  $T_{wall}$ . The space internal moisture load due to occupants and equipment is represented by  $\omega_{indoor}$ .

An energy balance for the conditioned space yields:

$$\rho_a V_z C_{pa} \frac{dT_z}{dt} = Q_{indoor} - \rho_a C_{pa} \dot{V}_a (T_z - T_{sly}) - Q_{01} \quad (5.158)$$

$$Q_{01} = U_{wall} A_{wall} (T_z - T_{wall}) \quad (5.159)$$

where  $T_{sly}$  is the supply air temperature and  $V_z$  is the volume of the conditioned-space.  $U_{wall}$  is the heat transfer coefficient between wall and air.

A moisture balance for the space yields:

$$\rho_a V_z \frac{dg_z}{dt} = \rho_a \dot{V}_a (g_z - g_{sly}) + \omega_{indoor} \quad (5.160)$$

where  $g_{sly}$  is the moisture content of supply air.

The temperature sensed by the thermostat in the conditioned-space is evaluated by:

$$\frac{dT_s}{dt} = \frac{1}{t_{c,t}}(T_z - T_s) \quad (5.161)$$

where  $t_{c,t}$  is the time constant of the temperature sensor in the thermostat.

### 5.3.2 Supply air fan

Based on the first fan law and using least-square curve-fitting, the pressure-flow characteristics of the variable-speed supply fan at different fan speeds have been developed from manufacturer's performance data, and expressed by a set of forth-order polynomial correlations relating fan pressure head to volumetric flow rate. For the supply fan, the relationship between its volumetric flow rate and its total pressure head at its rated rotational speed of 2200 rpm can be described by the following correlation through fitting and plotting, with the fitting goodness,  $R^2$ , being 0.9961,

$$PH_{fan} = 2593V_{fan}^4 - 5957.5V_{fan}^3 + 3388.3V_{fan}^2 - 543.91V_{fan} + 870.08 \quad (5.162)$$

where  $PH_{fan}$  is the fan's total pressure head, and  $V_{fan}$  is the fan's volumetric flow rate which is equal to the supply air flow rate,  $V_{sly}$ .

The first fan law that relates two dynamically similar operating conditions can give

the following correlations,

$$\frac{V_{rat}}{V_{ctl}} = \frac{N_{rat}}{N_{ctl}}; \quad (5.163)$$

$$\frac{PH_{rat}}{PH_{ctl}} = \left(\frac{N_{rat}}{N_{ctl}}\right)^2; \quad (5.164)$$

where  $N_{rat}$  is the rated rotational speed of a supply fan, and  $N_{ctl}$  is its actual operating speed.

The dynamic characteristics of a fan-motor assembly may be described by a first-order differential equation with a specific time constant,  $t_{c, fan}$ ,

$$\frac{dN_{ctl}}{dt} = \frac{1}{t_{c, fan}}(N_{ctl} - N_{ctl}^*) \quad (5.165)$$

where,  $N_{ctl}^*$  is the output from the supply air fan's PI controller.

A PI feedback controller is used for the variable-speed supply fan to regulate its rotational speed to maintain the supply air static pressure at a preset value. The PI controller has been modeled by the following equation which is discretised when being merged with the complete model for the DX VAV A/C system.

$$N_{ctl}^* = k_{p, fan} De_{stp} + \frac{k_{p, fan}}{t_{i, fan}} \int (De_{stp}) dt + \phi_{fan} \quad (5.166)$$

where  $De_{stp}$  is the deviation of the supply air static pressure.

For avoiding draughts in an occupied space, traditionally the temperature difference between supply air and space air is limited to within 8~10 °C, which is regarded as a maximum to enable good space air distribution for ceiling-mounting diffusers. For

an optimized system design, fan and duct heat gains must be limited to within 10% of the total cooling capacity of an A/C system. Therefore, considering the fact that a DX VAV A/C system has a relatively simple ductwork, the heat gains from the supply fan and ductwork is represented by an increase in supply air temperature, and its actual value varies linearly with the supply air flow rate between 1 and 2 °C.

### 5.3.3 Return air and outdoor air dampers

Legg (1986) established a series of experimentally validated mathematical expressions for different types of dampers. The pressure loss coefficient of a damper at an inclination angle,  $\theta$ , is given in the form:

$$\ln K_{\theta} = a + b\theta \quad (5.167)$$

For the outdoor air damper (a single flat plate damper with half-round spindle) used in the experimental DX VAV A/C system, Legg recommended that  $a=-2.13$  and  $b=0.1095$ . For the return air damper (an opposed flat-plate damper with crimped edges), the recommended values are  $a=-1.5$  and  $b=0.105$ .

Once the inclination angle of a damper is fixed, its flow resistance can then be determined by:

$$R_{dam} = \frac{\rho_a K_{\theta}}{2A_{dam}^2} \quad (5.168)$$

and the volumetric flow rate of air passing through the damper is:

$$\dot{V}_{dam} = \sqrt{\frac{\Delta P_{dam}}{R_{dam}}} \quad (5.169)$$

### 5.3.4 VAV terminals

In most of the previously reported studies, a VAV terminal was generally modeled using a simple steady-state mathematical expression for dampers. It was simply treated as a variable flow resistance, with its pressure loss coefficient relating to the inclination angle of the damper inside the VAV terminal. Such a simplification is acceptable for a simulation study aiming purely at system design. However when investigating the control issues for DX VAV A/C systems, one has to consider a VAV terminal's dynamic behaviors due to the presence of the hysteresis of actuator-damper linkage, the action of damper motor, the dead-band of its controller and the time lag of the temperature sensor in a thermostat. Therefore, the pressure-independent VAV terminals used in the experimental DX VAV A/C system need to be dynamically modeled.

A pressure-independent VAV terminal makes use of its built-in flow measuring device such as a *Pitot* tube or an *X*-grid to measure its actual volumetric air flow rate. The control signal from the thermostat installed in a space corresponds to the demanded air flow rate for a VAV terminal, which varies in response to the changes of space air temperature. Based on the deviation between the actual and demanded air flow rates, the flow controller within the VAV terminal, according to a pre-set control algorithm, sends a control signal to its damper motor. The opening of a VAV terminal's damper is varied by the motor to regulate the air flow rate supplied to the conditioned-space. Figure 5.3 shows the control logic of pressure-independent VAV terminals used in the experimental DX VAV A/C system.

The sensed space air temperature is compared to the temperature setting by the PI controller in the thermostat installed inside the conditioned-space, so that a temperature deviation is derived. The temperature deviation is processed by the controller as follows:

$$DV_s = DV_{\min} + \frac{(DV_{\max} - DV_{\min})(\Delta T_s + \frac{P_B}{2})}{P_B} + \frac{(DV_{\max} - DV_{\min})\delta t_s}{P_B * t_{i,s}} ST_s \quad (5.170)$$

$$\Delta T_s = T_s - T_{des} \quad (5.171)$$

where,  $ST_s$  is the summation of the discretised temperature error  $\Delta T_s$  over time;  $t_{i,s}$  is the integral time of the PI controller;  $P_B$  is the proportional band of the PI controller;  $\delta t_s$  is the time interval for sampling space air temperature.

$DV_{\min}, DV_{\max}$  are set to be *DC 0V* and *DC 10V* respectively;  $P_B$  is set to be  $2^\circ\text{C}$ .

The output control signal,  $DV_s$ , ranging *DC 0~10V*, is sent to the terminal's flow controller as the demanded voltage signal for the required volumetric air flow rate.



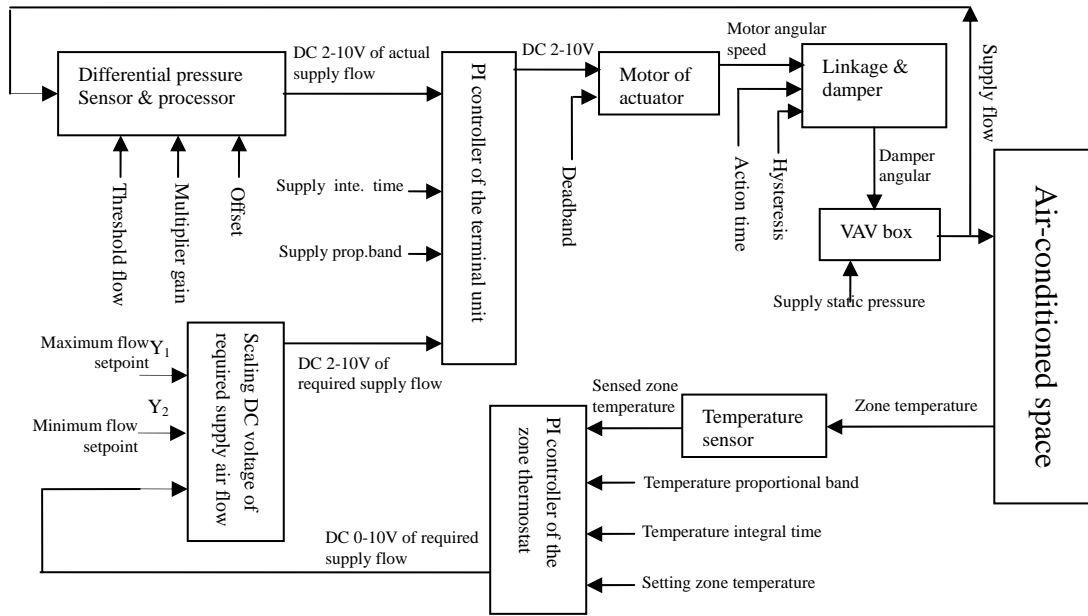


Figure 5.3 Control logics of pressure-independent VAV terminals

A *DC 0V* voltage output from the thermostat controller will require the terminal to supply the minimum air flow rate,  $\dot{V}_{\min}$ , and a *DC 10V* the maximum air flow rate,  $\dot{V}_{\max}$ . Usually, for the purpose of a terminal's versatility for various applications, the voltage signal created by the terminal assembly, which represents the terminal's actual air flow rate, should be expressed as a certain percentage of terminal's nominal air flow rate. The output voltage range for the terminal flow controller in the experimental DX VAV A/C system is *DC 2-10V*. Two scaling parameters,  $Y_1$  and  $Y_2$  for  $\dot{V}_{\min}$  and  $\dot{V}_{\max}$ , have been set by means of built-in potentiometers based on the following equations:

$$\dot{V}_{\max} = Y_1 \dot{V}_{nom} \quad (5.172)$$

$$\dot{V}_{\min} = Y_2 \dot{V}_{\max} \quad (5.173)$$

where  $Y_1=0.30\sim 1.0$ ;  $Y_2=0.0\sim 0.8$ .  $Y_1$  was set to be 0.85 during the commissioning

of the experimental DX VAV A/C system, and  $Y_2$  to be 0.30, which is required to meet ventilation requirement and to avoid air dumping.

Therefore, the voltage signals (*DC 0-10V*) output from the thermostat are scaled using  $Y_1$  and  $Y_2$  to create a reference voltage signal,  $DV_{ref}$ , to be the input to the terminal's flow controller.  $DV_{ref}$  will have the same range of *DC 2-10V* as that corresponding to the actual air flow rate,  $DV_{act}$ , passing through the terminal. The scaling is described as:

$$DV_{ref} = 2 + (10 - 2)[Y_1 Y_2 + (1 - Y_2) Y_1] \times \frac{DV_{dem}}{10} \quad (5.174)$$

The reference voltage signal is compared to that for the actual airflow volume rate,  $DV_{act}$ , and then a deviation signal is resulted in:

$$De_{flow} = DV_{ref} - DV_{act} \quad (5.175)$$

The deviation signal,  $De_{flow}$ , is then processed by the terminal's PI flow controller, which is modeled as:

$$DV_c = k_p De_{flow} + \frac{k_p}{t_i} \int De_{flow} dt + \phi_{flow} \quad (5.176)$$

where  $\phi_{flow}$  is set to be 6.0.

The output voltage signal for the terminal's actual airflow rate,  $DV_{act}$ , is regarded as

being linear with  $\dot{V}_a$ , i.e.,

$$DV_{act} = B\dot{V}_a + C \quad \text{when} \quad \dot{V}_{nom} \geq \dot{V}_a > \dot{V}_{thr}; \quad (5.177)$$

$$DV_{act} = 2 \quad \text{when} \quad \dot{V}_{thr} \geq \dot{V}_a \geq 0 \quad (5.178)$$

where  $B$  is a proportional coefficient; and  $\dot{V}_{thr}$  is a threshold airflow rate, below which the airflow measuring accuracy is rather poor using the terminal's built-in differential-pressure type measuring device. For the terminals in the experimental DX VAV A/C system  $\dot{V}_{thr}$  is approximately  $77 \text{ m}^3/\text{h}$ . On the other hand, the response for a differential-pressure sensor such as *Pitot* tube or *X-grid* to the variation of airflow rate can be considered as instantaneous. Therefore, the dynamics of the flow measuring devices was neglected when modeling.

A constant-speed actuator is used in the VAV terminal. The motor action of the actuator is described as follows:

$$DV_c > DV_+ : \quad \varpi = +\varpi_0 \quad (5.179)$$

$$DV_c < DV_- : \quad \varpi = -\varpi_0 \quad (5.180)$$

$$DV_+ > DV_c > DV_- : \quad \varpi = 0 \quad (5.181)$$

$$DV_c > DV_h : \quad DV_c = DV_h \quad (5.182)$$

$$DV_c < DV_l : \quad DV_c = DV_l \quad (5.183)$$

The following dead band within which there is no movement of actuator from  $DV_+$  to  $DV_-$  is adopted to prevent the actuator motor from hunting, as follows,

$$DV_+ = 6.23 \text{ V}; \quad DV_- = 5.77 \text{ V}; \quad (5.184)$$

$$DV_h = 10 \text{ V}; \quad DV_l = 2 \text{ V}; \quad (5.185)$$

and the constant rotational speed of the motor,  $\varpi_0$ , is set to be  $0.6 \text{ }^\circ/\text{s}$ .

There exists inevitably mechanical slack in the linkage between an actuator and a damper. Mechanical slack may become worse after the prolonged use of the damper. A hysteresis of constant angle-width,  $\theta_H$ , is therefore used to represent the damper's

linkage slack. Hysteresis occurs whenever a damper is requested to change its rotating direction. The actuator-damper hysteresis has been accounted for by means of the following algorithm described by Hung [1999]:

$$\text{Step 1: } \theta_h = \theta_h + \varpi \times \delta t \quad (5.186)$$

$$\text{Step 2: If } (\theta_h \geq +\theta_H), \text{ then } \theta_h = +\theta_H \quad (5.187)$$

$$\text{Step 3: If } (\theta_h \leq 0), \text{ then } \theta_h = 0 \quad (5.188)$$

$$\text{Step 4: If } [(\theta_h = +\theta_H) \& (\varpi = +\varpi_0)] \text{ or } [(\theta_h = 0) \& (\varpi = -\varpi_0)],$$

$$\text{then } \theta = \theta + \varpi \times \delta t \quad (5.189)$$

$$\text{Step 5: If } (\theta \geq \theta_{\max}), \text{ then } \theta = \theta_{\max} \quad (5.190)$$

$$\text{Step 6: If } (\theta \leq \theta_{\min}), \text{ then } \theta = \theta_{\min} \quad (5.191)$$

Here,  $\theta_{\min} = 0^\circ$ ; and the maximum inclination angle of the damper,  $\theta_{\max}$ , was set to be  $70^\circ$  during the commissioning of the experimental DX VAV A/C system because the damper should not be fully closed to meet the ventilation requirement.

Once the inclination angle,  $\theta$ , of the damper inside a terminal is determined, its flow resistance and air flow rate can be evaluated using its pressure loss coefficient following the similar way to that for an outdoor/return air damper mentioned in Section 5.3.3. The pressure loss coefficient of a terminal damper, which varies exponentially with its inclination angle, has been modeled following that used in the HVACSIM<sup>+</sup> program [Clark 1985].

$$K_d = K_{do} \left\{ \frac{W_f}{\left[ (1-\varphi) \left(1 - \frac{\theta}{\theta_c}\right) + \varphi \right]^2} + (1-W_f) \times \varphi^{\left[2 \left(1 - \frac{\theta}{\theta_c}\right) - 2\right]} \right\} \quad (5.192)$$

where  $W_f$  is the arbitrary weighting factor of a damper,  $\varphi$  the leakage factor of a

damper;  $\theta_c$  is the damper's angle at which a damper is fully closed;  $K_{do}$  is the pressure loss coefficient when the damper is fully opened.

### 5.3.5 Plenum box

The mixing of outdoor air and return air in the plenum box is assumed to be fully and adiabatic, and the air leakage from the plenum box is negligible. Therefore the energy and mass balance equations for the plenum box are as follows:

$$\dot{V}_{sly} = \dot{V}_{ra} + \dot{V}_{fa} \quad (5.193)$$

$$\dot{V}_{sly} h_{ia} = \dot{V}_{ra} h_{ra} + \dot{V}_{fa} h_{fa} \quad (5.194)$$

$$\dot{V}_{sly} g_{ia} = \dot{V}_{ra} g_{ra} + \dot{V}_{fa} g_{fa} \quad (5.195)$$

Using the air state equations, the dry-bulb temperature of the air entering the DX cooling coil,  $T_{ia}$ , can be obtained from  $h_{ia}$  and  $g_{ia}$ .

### 5.3.6 Hydraulic calculation for air-distribution ductwork

The air-distribution ductwork of the experimental DX VAV A/C system is regarded as being hydraulically balanced. A DX VAV A/C system's cooling capacity is relatively small, usually below 30 tons. Because there are only two VAV terminals, with a relatively simple ductwork, the VAV air-distribution sub-system's ductwork is treated as a serial-parallel hydraulic network. Such a treatment has been previously adopted [Wang 1999].

The schematic diagram of the hydraulic network for the ductwork in the

experimental DX VAV A/C system is shown in Figure 5.4. Each component in the network is treated as a flow resistance. The air branch ducts and VAV terminals serving the two spaces are treated as being parallelly-connected, as shown in Figure 5.4. Except for the dampers and VAV terminals, the flow resistances for all other components are given their respective fixed values, based on their field-tested performance data. By accounting the system pressure losses under the known pressure head from the supply fan, the airflow rate and air static pressure at different locations can be determined.

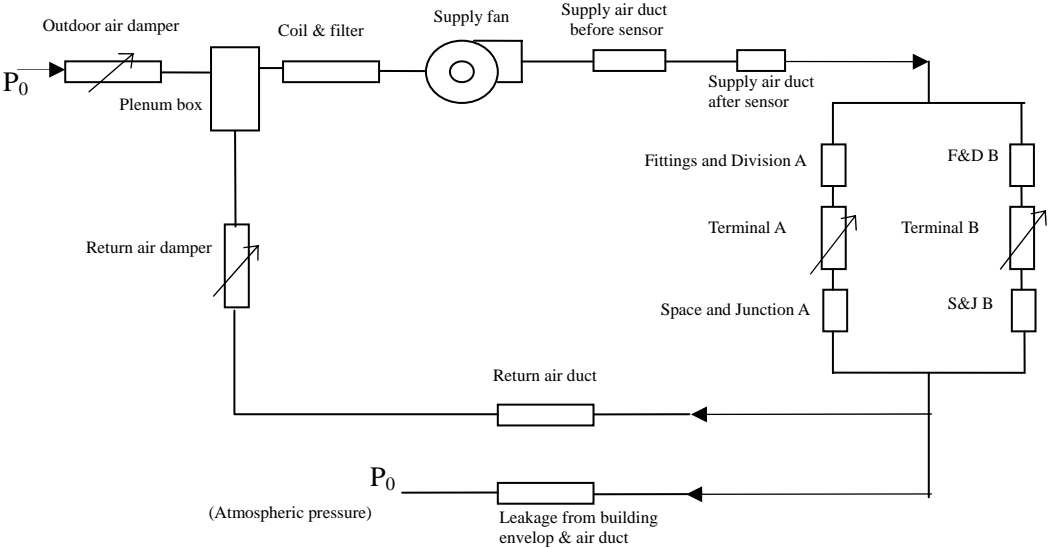


Figure 5.4 Schematic diagram of the hydraulic network for the ductwork in the experimental DX VAV A/C system

**5.4 Numerical solution procedure**

The complete dynamic model of the experimental DX VAV A/C system consists of a set of ordinary differential equations and algebraic correlations. In numerically solving the model, firstly, the geometric parameters of various system components

such as compressor, heat exchangers, VAV terminals should be input to the model. They were obtained from either manufacturers or field tests in the experimental rig. Secondly, the following parameters that describe the operational conditions of the DX VAV A/C system should also be available to the model: the ambient air temperature which is regarded as the temperature of both outdoor air and condenser inlet air; the set point of space air temperature; the conditioned-space's internal sensible heat and latent load; and the volumetric flow rate of condenser cooling air. Finally the initial values for such system parameters as evaporating and condensing pressures, degree of refrigerant superheat, space volume of evaporator's two-phase region, etc. should be assigned in order to start a transient simulation.

The numerical solution of the dynamic model starts from the inlet of evaporator, with its mass flow rate and enthalpy of refrigerant to be updated by the mathematical correlations for the EEV at the next simulation time step. The boundaries between different regions in heat exchangers, for example, the two-phase and superheating regions in evaporator are on the move during simulation because of the changes of space volumes in different regions. In the refrigerant side of the DX refrigeration plant, a constraint is that the refrigerant mass flow rate exiting evaporator must be equal to that given by the compressor's mathematical correlations. If such a constraint is not achieved, then split-half iteration for the refrigerant mass flow rate exiting evaporator is used. Once the above condition is satisfied, the degree of refrigerant superheat, and the heat transfer in the superheating region can be obtained. With the availability of refrigerant mass flow rate exiting the evaporator, the refrigerant mass flow rates at different locations in the evaporator except the evaporator's inlet, are reversely calculated. Knowing the state of refrigerant entering

the compressor allows the state of refrigerant at compressor discharge to be determined by using the compressor's mathematical correlations. The state parameters of refrigerant at the compressor discharge are then passed on to the mathematical expressions for condenser. With the states of refrigerant entering condenser updated for the current time step, various variables in condenser such as condensing pressure are then given their new current values by solving the related energy and mass balance equations. The updated pressure drop across the EEV and the current degree of refrigerant superheat are both utilized in the mathematical correlations for EEV to provide the new mass flow rate of refrigerant entering the evaporator at next time step. Therefore, mathematical correlations for different components in the DX refrigeration plant are linked together following the flow of refrigerant being circulated.

The air side of evaporator, which acts as the DX cooling coil, is part of the VAV air-distribution sub-system. The state parameters and mass flow rate of the air entering the DX evaporator were from the sub-model of air-distribution sub-system. During each simulation time step, tube-fin metal surface temperatures in both regions of evaporator are checked to see if they are below the corresponding air dew-point temperatures, thus determining whether the related wet-cooling or dry-cooling heat and mass transfer equations should be called upon for air handling in the regions. The moisture content and dry-bulb temperature of the airflow immediately downstream the evaporator, are then passed on to the sub-model of VAV air-distribution subsystem.

The *A.C. Cleland* correlations recommended by IIR (International Institute of



Refrigeration) for refrigerant R22 and the state correlations for air by ASHRAE are used to calculate the properties of refrigerant and air. The *Zivi* model is employed to evaluate the refrigerant void fraction in both evaporator and condenser. Evaluating refrigerant pressure loss across different system components is also performed during each time step. The speed of variable-speed compressor and the opening of EEV are available from the correlations describing the control algorithm of their respective controllers. The integration time step ( $\Delta T$ ) for the numerical solution is 0.1 second. The computational time required for a personal computer of 2.4 G Hz CPU speed to finish simulating an hour's operation of the DX VAV A/C system is approximately ten minutes. The flow chart illustrating the numerical solution procedure for the complete model of the experimental DX VAV A/C system is shown in Figure 5.5.

The mathematical correlations and equations forming the sub-model of VAV air-distribution sub-system are solved sequentially according to the flow direction of air stream and the logic sequence of the control action of respective controllers such as terminal's flow controller. The temperature and moisture content of supply air are determined from the state parameters of air leaving the DX cooling coil (evaporator), taking into account air temperature rise due to the heat gain from the supply fan. The flow rate and static pressure of supply air are determined from the pressure-flow rate balance of air ductwork. The supply fan speed, VAV terminal's damper openings and then supply air flow rate and static pressure remained unchanged within the control sampling time interval ( $\delta t$ ). Figure 5.6 shows the flow chart for the numerical solution procedure for the sub-model of air-distribution sub-system.

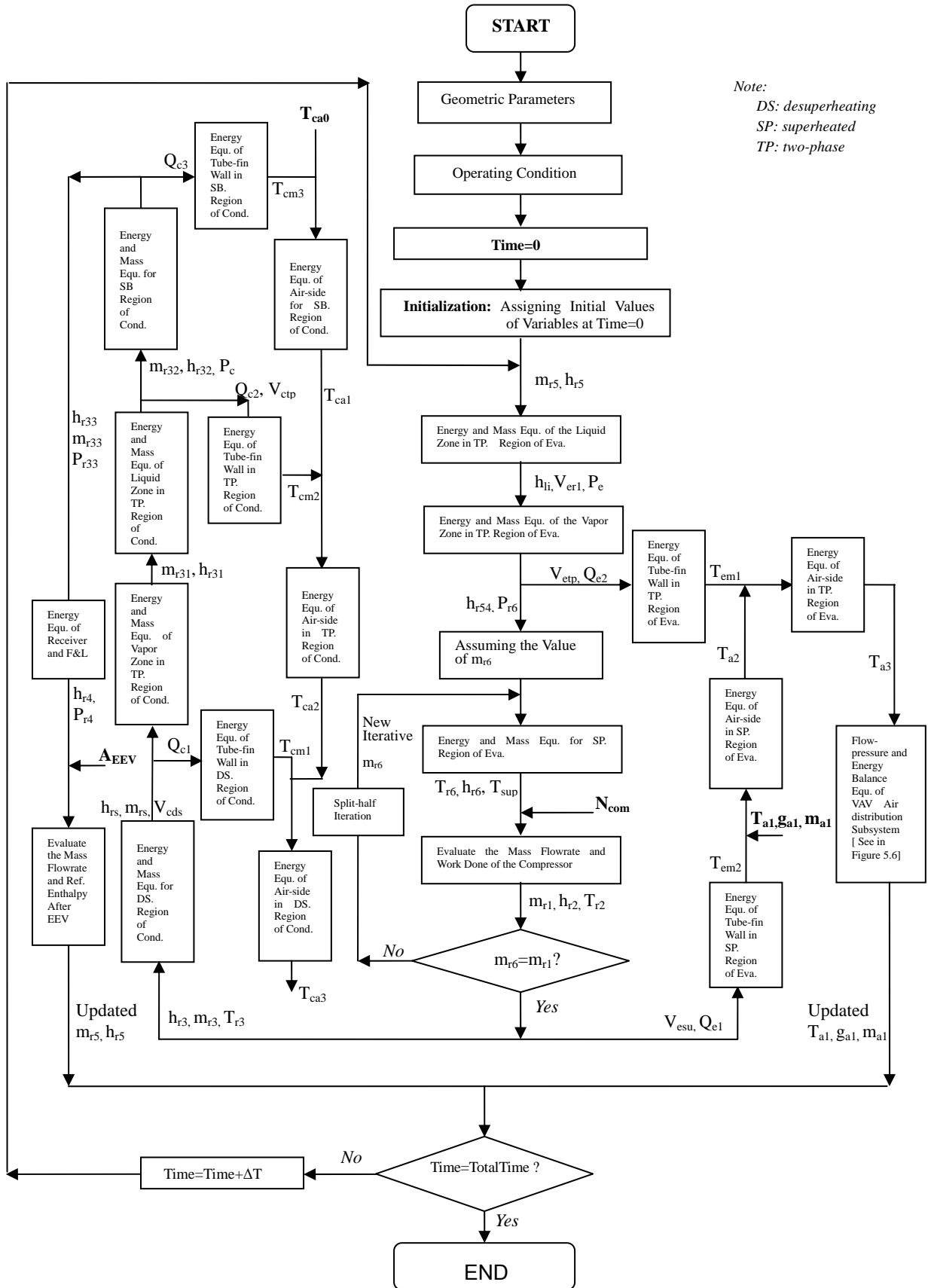


Figure 5.5 Flow chart for the numerical solution procedure of the complete model for the experimental DX VAV A/C system

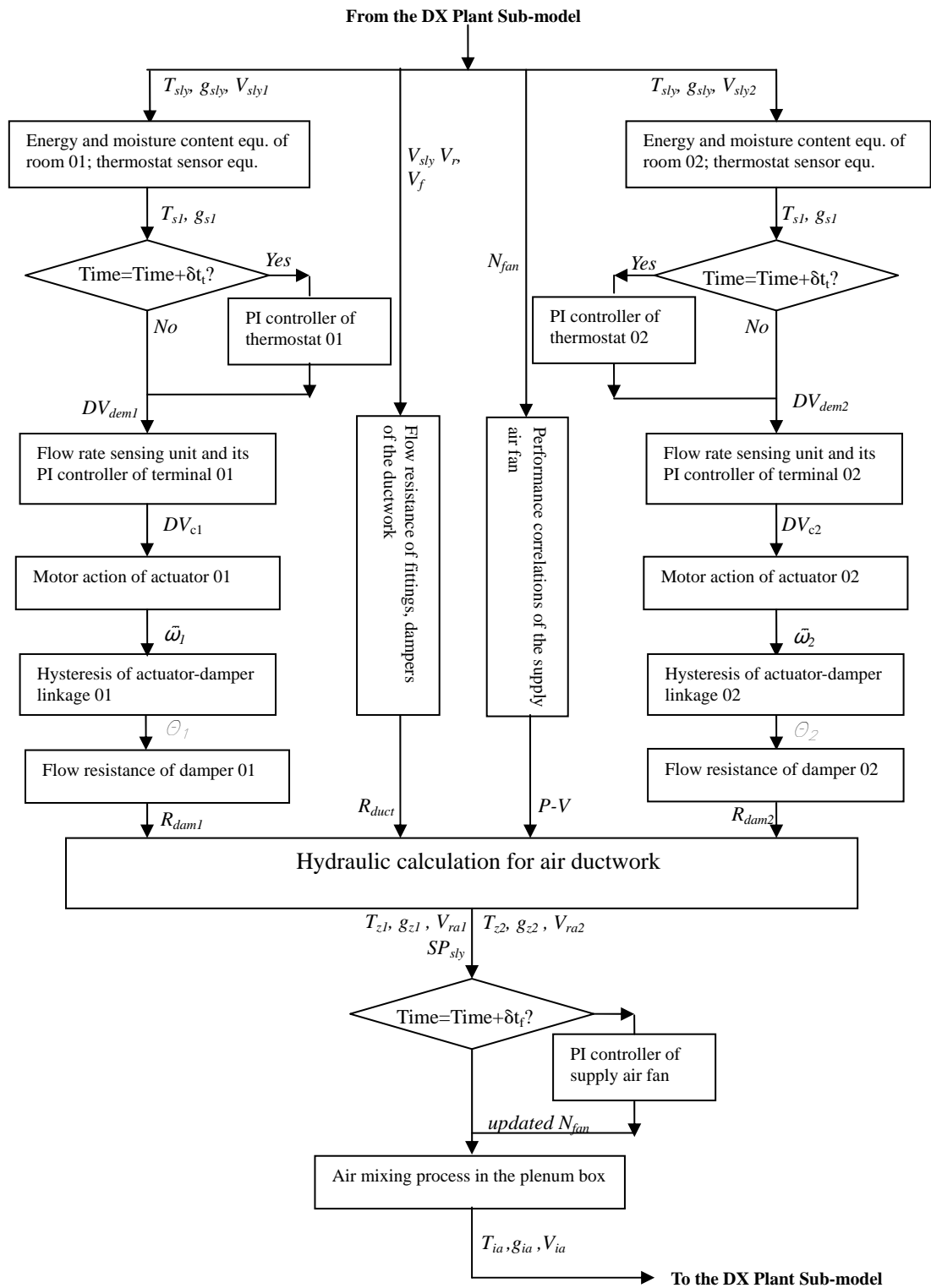


Figure 5.6 Flow chart for the numerical solution procedure of the sub-model for VAV air-distribution sub-system

## 5.5 Summary

A generalized dynamic mathematical model for the experimental DX VAV A/C system having two terminals serving two identical air-conditioned spaces has been developed based on the principle of mass and energy conservation, and using the correlations describing the operational performance of various components in the experimental DX VAV A/C system, which is either field-tested or available from manufacturers. Mathematical correlations representing the control logics of various controllers are also included.

The complete dynamic model developed for a DX VAV A/C system is component-based and of partial-lumped-parameter type. It consists of two constituent mathematical sub-models. One is for the DX refrigeration plant; the other for the VAV air-distribution sub-system. The components modeled in the DX refrigeration plant include a variable-speed rotor compressor, EEV, louver-fin-tube evaporator and air-cooled plate-finned-tube condenser. The evaporator and condenser are divided into different regions to be individually modeled. An averaged refrigerant pressure drop and a refrigerant void factor are adopted in modeling both evaporator and condenser. Both the evaporator and condenser are approximated as an ideal counter-flow heat exchanger. The air wet-cooling and dry-cooling conditions at the evaporator are separately considered when modeling the air handling process taking place in the DX evaporator.

The components modeled in the VAV air-distribution sub-system include a

variable-speed supply fan, pressure-independent VAV terminals, conditioned space, plenum box, return/outdoor air dampers, and air-distribution ductwork. The dynamic behaviors due to the hysteresis of actuator-damper linkage, the action of a damper motor, the dead-band of flow controller for VAV terminals, the time lag of temperature sensors, and the hysteretic action of the supply fan are all considered when modeling. Moreover, the air-distribution ductwork is treated as a simple serial-parallel hydraulically balanced network. The pressure-flow rate balance of the ductwork has been applied to determine the volumetric rate and static pressure of airflow at various locations within the ductwork.

The two sub-models are linked via the air handling process at the DX evaporator, or DX cooling coil. The final dynamic mathematical model of the experimental DX VAV A/C system consists of a set of first-order ordinary differential equations and algebraic correlations. The mathematical correlations and equations in the sub-model for the VAV air-distribution sub-system are solved sequentially according to the air flow direction and the logic sequence of the control action of respective controllers.

The dynamic mathematical model so developed is expected to be significantly useful in understanding the transient behaviors of, and in developing better control strategies for DX VAV A/C systems.

The complete dynamic model for the experimental DX VAV A/C system has been programmed using the Visual C++ programming language. The model will be subjected to an experimental validation, which is reported in Chapter 6.

## **Chapter 6**

### **Model Validation**

#### **6.1 Introduction**

Over the recent years it has been commonly recognized that a mathematical model developed for simulating a physical system should be experimentally validated, where at least a trend-wise agreement between simulated and experimental results should be achieved [Liu et al. 2003, Jabardo et al. 2002, Browne and Bansal 2002, Koury et al. 2001]. Generally experimental data may be from either field measurements or a purposely-built experimental rig. Very often, experimental data based on field measurements might hardly be free of uncontrollable disturbances from the ambient environment. The validity of the experimental data so obtained would then be in question and the validation work could become less creditable. Therefore using the experimental data from a laboratory-based experimental rig should be preferred when validating a mathematical model of a physical system, since the experimental conditions may be well controlled.

This chapter reports on the validation of the dynamic mathematical model developed for the experimental DX VAV A/C system reported in Chapter 5, using the experimental rig reported in Chapter 4. The open-loop responses from the DX refrigeration plant after being subjected to a step change in compressor speed, using both the dynamic mathematical model and the experimental rig, were obtained and compared for the purpose of model validation.

## 6.2 Overview of model validation

When modeling the DX VAV A/C system, as reported in Chapter 5, the majority of model development was for establishing the dynamic sub-model for the DX refrigeration plant. This part of model development took into accounts a large number of complex physical processes concurrently taking place. The dynamic sub-model of the DX refrigeration plant was built based on the first thermodynamic principle of energy and mass conservation. Therefore, although not easy to be assured, its simulation accuracy is crucial to accurately describing the performance of the DX VAV A/C system; and therefore its validation work should be an essential element of the model development.

On the other hand, modeling the VAV air-distribution sub-system was primarily based on the performance data of the components in the sub-system, and the control logics of various PI controllers. Semi-empirical correlations for the components in the VAV air-distribution sub-system were derived through curve-fitting components' performance data available from their respective manufacturers. Consequently, the accuracy of these semi-empirical correlations may be assured within their operating ranges. Therefore, it was normally not necessary to carry out further experiments for verifying the accuracy of these correlations. In certain cases, when components' performance data were not available from their manufacturers, in-situ tests were carried out to determine the values of coefficients in those semi-empirical correlations. Such treatments were commonly seen in previous studies [Wang 1999, Hung 1999] for establishing mathematical models of VAV A/C systems.

For example, for the variable-speed supply fan in the VAV air-distribution sub-system, its pressure-volumetric flow characteristics can be generally expressed by a family of curves at constant rotational speed and its performance data can be obtained from its manufacturer. As described in Section 5.3.2, the model of the variable-speed supply fan was developed using both a curve-fitting correlation (Equation 5.162) relating the pressure head to the volumetric flow rate of the supply fan at its rated rotational speed, and the first fan law. The accuracy of the model for the supply fan has been ascertained by comparing the simulated family of performance curves at different rotational speeds with those from its manufacturer, as shown in Figure 6.1. It can be observed that the model of the supply fan can well represent its pressure-volumetric flow characteristics at different fan rotational speeds.

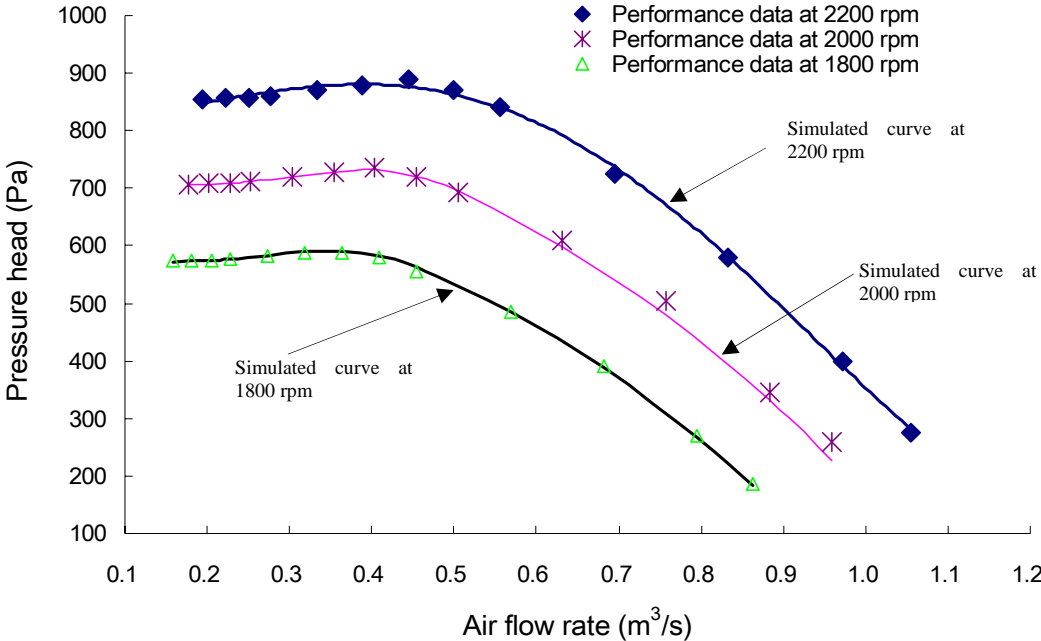


Figure 6.1 Comparison between the measured and the simulated performances for the supply fan at different speeds



For the VAV terminal which was an essential component in the VAV air-distribution sub-system, as another example, it was modeled using the mathematical expressions describing the process of its control actions and a generalized equation for its damper, as seen in Section 5.3.4. Coefficients in Equation (5.192) for the terminal damper were unavailable and had to be experimentally determined. However, the air volumetric flow rates passing through a VAV terminal at varying degrees of the opening of the terminal damper could be measured using the experimental rig. Those coefficients in Equation (5.192) can then be obtained by trial-and-error fitting of the measured data, and were shown in Table 6.1. As shown in Figure 6.2 which shows the comparison between the simulated results and the measured data, it can be seen that the accuracy for the terminal damper's model using the coefficients so obtained is satisfactory.

Table 6.1 Coefficients for the equation of terminal's damper

$K_{do}$	$W_f$	$\varphi$	$\theta$
0.02401	1	1	$\leq 2^\circ$
0.01764	0.014	0.002	$2^\circ$ to $15^\circ$
0.0735	0.78	0.00658	$15^\circ$ to $65^\circ$
1.8375	0.9999	0.00005	$> 65^\circ$

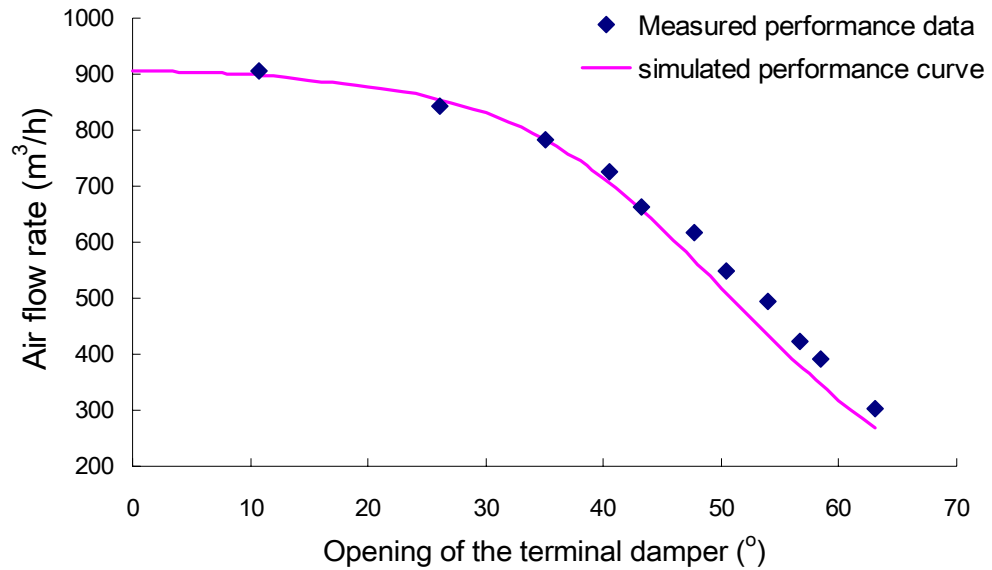


Figure 6.2 Comparison between the measured and the simulated air flow rates passing through terminal's damper

Therefore, in experimentally validating the complete dynamic mathematical model for the experimental DX VAV A/C system, only the experimental validation for the sub-model for the DX refrigeration plant including the air side of its DX evaporator has been carried out. After the dynamic sub-model of the DX refrigeration plant has been experimentally validated, the complete dynamic mathematical model for the DX VAV A/C system may be sufficiently regarded as being validated.

Preliminary tests for the complete dynamic mathematical model for the experimental DX VAV A/C system showed that the model's two constituent sub-models were stable and behaved as expected. This meant that the sub-model for the DX refrigeration plant was ready for experimental validation.

### 6.3 Experimental validation for the sub-model of DX refrigeration plant

Experimental work has been carried out to examine the open-loop steady-state and transient responses of the DX refrigeration plant, i.e., with all existing control loops disabled, after being subjected to step changes in its major operational conditions, such as the air flow rate passing through its evaporator and compressor speed, etc. During the experimental work, disturbances to the system's dynamic behaviors from other operational conditions other than the one subjected to a step-change were completely eliminated, and the experimental rig was operated for an adequately long time so that a steady-state operating condition was achieved. This section presents, as an example and in great detail, the open-loop steady-state and transient responses from both the DX plant and its sub-model after being subjected to a step-change in compressor speed, for the purpose of model validation.

During the experimental validation, the condenser cooling air flow rate was kept at  $3000 \pm 20 \text{ m}^3/\text{h}$ , and condenser inlet air temperature maintained at  $35.0 \pm 0.1 \text{ }^\circ\text{C}$ . The evaporator air flow rate was kept at  $1700 \pm 20 \text{ m}^3/\text{h}$ , and the dry-bulb and wet-bulb temperatures of air entering the evaporator maintained at  $23.0 \pm 0.1 \text{ }^\circ\text{C}$  and  $19.5 \pm 0.1 \text{ }^\circ\text{C}$ , respectively. The opening of the EEV was fixed at 230 *Pulse*, and the atmospheric pressure measured at 98.19 *kPa*. The experiment period was 1000 seconds. At the beginning of experiment, the compressor was running at 58 *Hz* ( $\sim 3400 \text{ rpm}$ ); and at  $t=300 \text{ s}$  the compressor speed was step-changed to 75 *Hz* ( $\sim 4500 \text{ rpm}$ ) via the variable-frequency driver in the experimental rig. The responses of the experimental rig before and after the step-change were monitored and logged at an interval of 3 seconds.

The same operating conditions were applied to the dynamic sub-model, and its dynamic responses were output at an interval of 1 second.

Steady-state and transient responses from both the sub-model and the DX plant after being subjected to the step change in compressor speed are compared in Figures 6.3 to 6.10. Figure 6.3 shows the time variation of the degree of refrigerant superheat at evaporator exit. It can be seen from the diagram that for the first 300 seconds, the steady-state responses from both the plant and sub-model agreed well, at around 6°C. When the step-change in compressor speed was introduced at 300 s, the plant's response was faster, with slight overshoot, than model's response. It took about 200 s for the plant to reach a new degree of refrigerant superheat at an average of 13.0 °C. However, on the other hand, it required 280 s for the sub-model's response to reach a new degree of refrigerant superheat at 12.8°C. The steady-state responses from both the DX plant and its sub-model approximately 300 s after the change agreed well, again, at around 13.0 °C.

It is interesting to note in Figure 6.4 that a peak value in cooling capacity occurred in both plant's and sub-model's responses soon after the step-change in compressor speed at  $t=300$  s. As a result of the sudden increase in compressor speed, evaporating pressure was quickly reduced and the averaged temperature difference between refrigerant and air increased. Accordingly, the degree of refrigerant superheat became greater. This meant that the effective heat transfer area in evaporator's two-phase region was reduced. Usually the heat transfer in evaporator's two-phase region can account for more than 90% of the total heat transfer, i.e., the total cooling

capacity in an evaporator. Because heat transfer was dependent on both heat transfer area and temperature difference, it was understandable that under a certain combination of reduced heat transfer area and increased temperature difference, a maximum heat transfer rate may result in. As seen in Figure 6.4, the plant's steady-state cooling capacity at  $t=300$  s before the step-change was around 6.71 kW; it reached its maximum at 7.28 kW at  $t=342$  s. Afterwards, it gradually reduced and finally settled at a slightly higher steady-state value of 6.82 kW. On the other hand, similar transient responses from the sub-model were observed, with the deviation of the steady-state responses from both the sub-model and the plant before and after the step-change being within 5%. This illustrates that the dynamic model developed was very powerful in being able to predict abrupt changes, e.g., a step change, in the system's cooling capacity. It should be pointed out that during the whole period of experiment, the opening of EEV was fixed and therefore the refrigerant mass flow rate passing through the EEV was in fact varied within a negligibly small range because of the exponential installation flow characteristic of the EEV in the DX refrigeration plant. This explained the cooling capacity of the plant did not significantly increase after the increase of compressor speed.

The steady-state and transient responses of evaporating pressure from both the plant and sub-model are illustrated in Figure 6.5. Before the step-change at 300 s, the steady-state responses from both the sub-model and the plant were stable, at 7.2 bar and an average of 7.0 bar, respectively. After the change was introduced at  $t=300$  s, the responses from both the sub-model and plant started to decrease, with that from the plant being more noticeable. However, the response of the sub-model demonstrated a good trend-wise agreement with that of the plant during the transient

period between 300 s and 600 s. The final steady-state responses from both the model and the plant were 6.1 *bar*, and an average of 5.8 *bar*, respectively, representing a percentage deviation of 6%.

Figure 6.6 shows the steady-state and transient responses of condensing pressure from both the plant and the sub-model after being subjected to the step-change in compressor speed. Both responses were stable at an average of 17.9 *bar* for plant and 17.75 *bar* for sub-model, respectively, before the step-change in compressor speed. After the change was introduced, both responses rapidly rose to their peak values within 40 seconds, and reached their new steady-state values at  $t=620$  s. Afterwards a good agreement between the two responses was observed.

It is also seen in Figure 6.6 that the condensing pressure at a higher compressor speed is higher than that at a lower compressor speed. This can be attributed mainly to the increase of compressor power input when compressor speed is increased, under fixed condenser cooling air flow rate and inlet air temperature, as illustrated in Figure 6.7. The figure shows the steady-state and transient responses of compressor power input from both the plant and the sub-model. The percentage deviations between the two responses in steady state periods (0~300 s, and 400~1000 s) were all within 5%. It can also be observed in Figure 6.7 that immediately after increasing compressor speed, an obvious peak value occurred in plant's response, but the same cannot be seen in the sub-model's response. The occurrence of such a peak might be attributed to such factors as instant electrical strikes caused by the sudden increase of compressor speed, which apparently cannot be reflected by the quasi-steady thermodynamic sub-model of compressor.

Figures 6.8 and 6.9 show the steady-state and transient responses of dry-bulb and wet-bulb air temperatures at the evaporator exit from both the sub-model and plant after being subjected to the step-change in compressor speed, respectively. The steady-state responses from sub-model in both figures were found to agree well with those of the plant. During the transition period, the plant's responses of both dry- and wet-bulb temperatures were slightly slower than those of the sub-model. This was possibly due to the time lag of air-sensing device including the platinum temperature sensors in the experimental rig.

On the other hand, it can be observed that the final steady-state dry-bulb air temperature exiting the DX evaporator was actually increased with the increased compressor speed, or the increased cooling capacity of the plant. As illustrated in Figure 6.5, the increase in compressor speed led to a reduction of evaporating pressure/temperature, and therefore a reduction of evaporator surface temperature. This consequently resulted in an improved plant's dehumidification capability. The equipment sensible heat ratio (SHR) of the plant became lower after increasing compressor speed, as illustrated in Figure 6.10. More of plant's cooling capacity was used for air dehumidification. Therefore, the final steady-state wet-bulb air temperature at evaporator exit was lower than that prior to the introduction of compressor speed increase at  $t=300$  s.

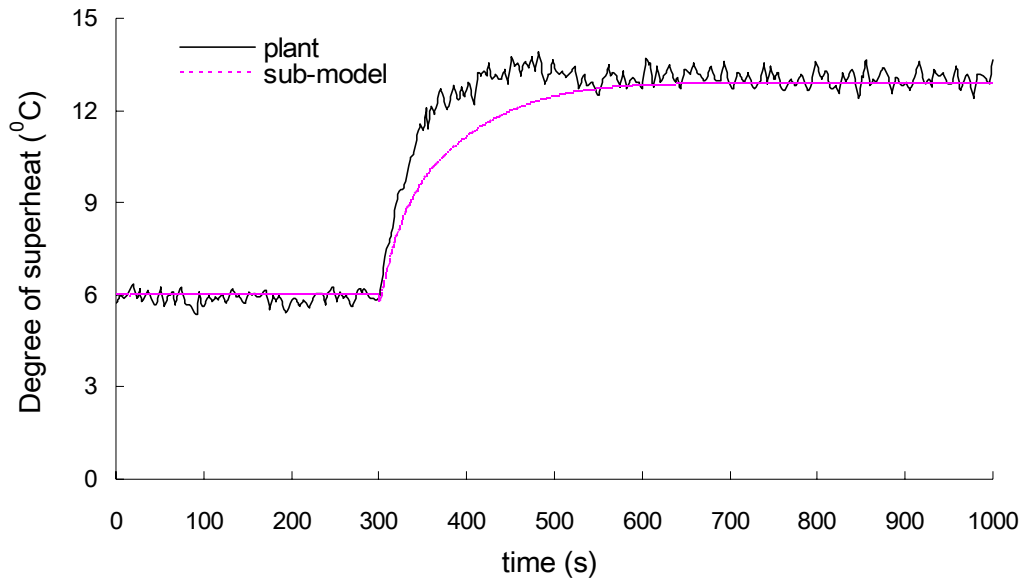


Figure 6.3 Open-loop responses of the sub-model and the plant (degree of refrigerant superheat) after being subjected to a step-change of compressor speed

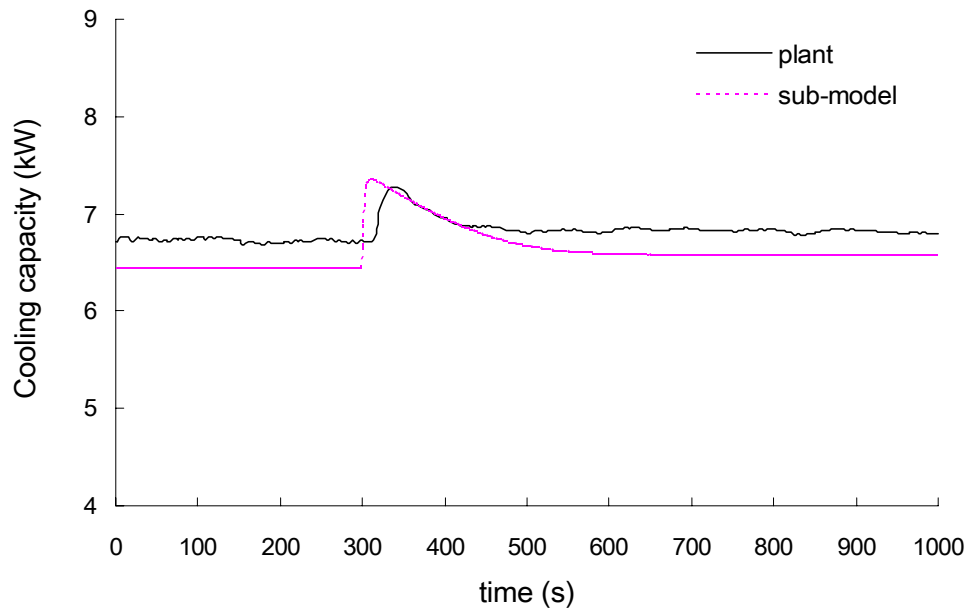


Figure 6.4 Open-loop responses of the sub-model and the plant (cooling capacity) after being subjected to a step-change of compressor speed



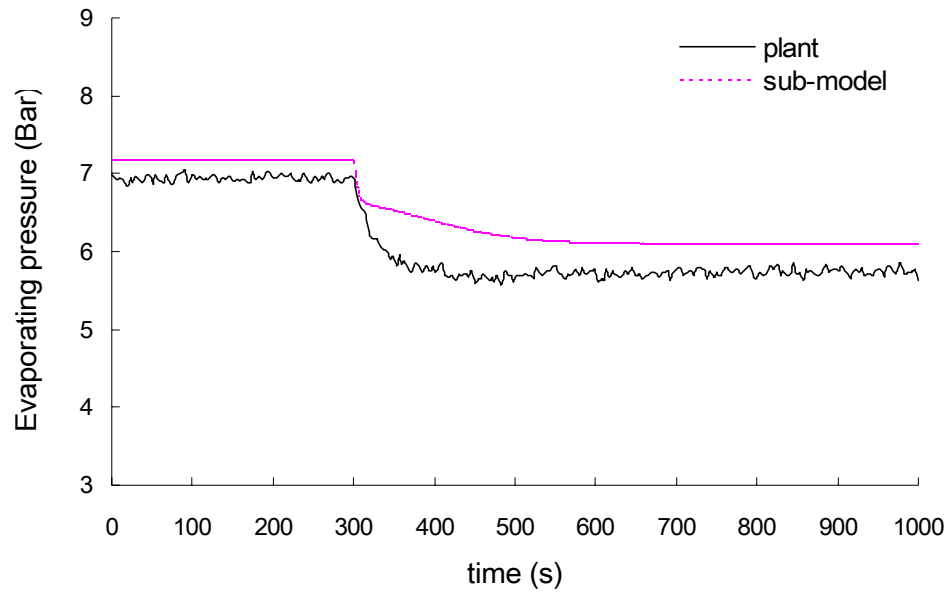


Figure 6.5 Open-loop responses of the sub-model and the plant (evaporating pressure) after being subjected to a step-change of compressor speed

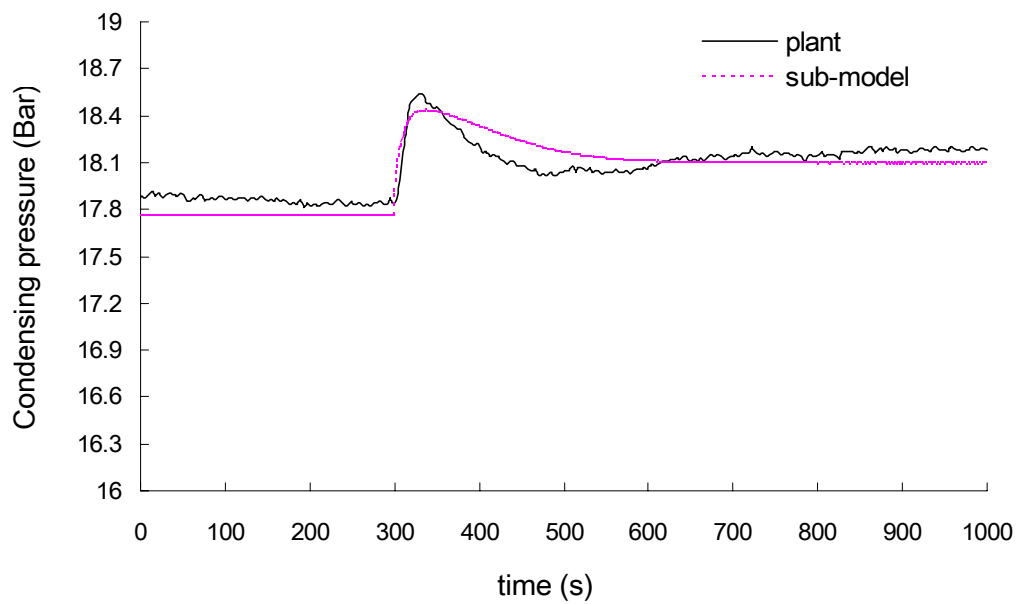


Figure 6.6 Open-loop responses of the sub-model and the plant (condensing pressure) after being subjected to a step-change of compressor speed

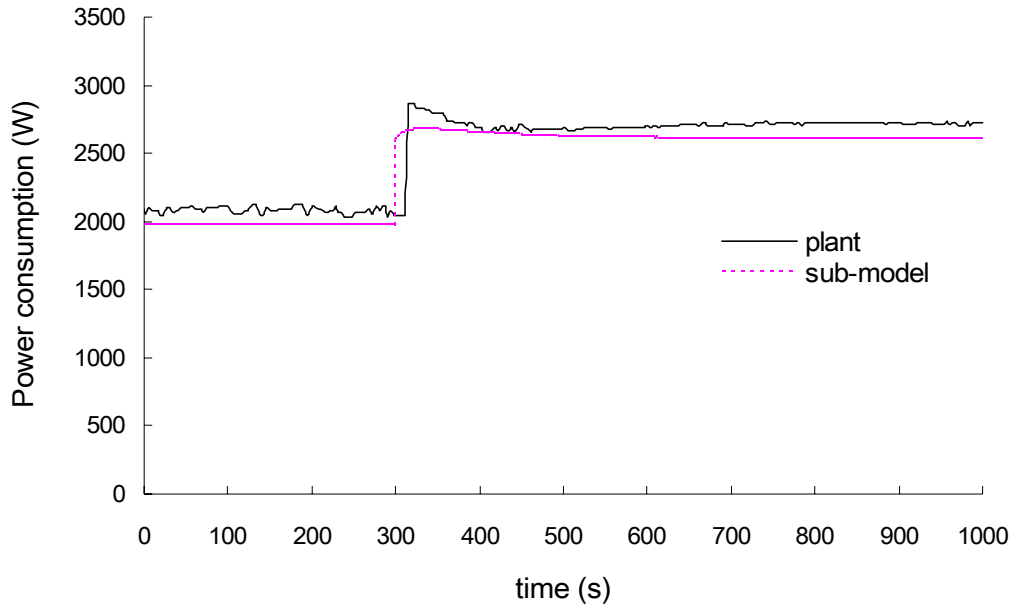


Figure 6.7 Open-loop responses of the sub-model and the plant (compressor power input) after being subjected to a step-change of compressor speed

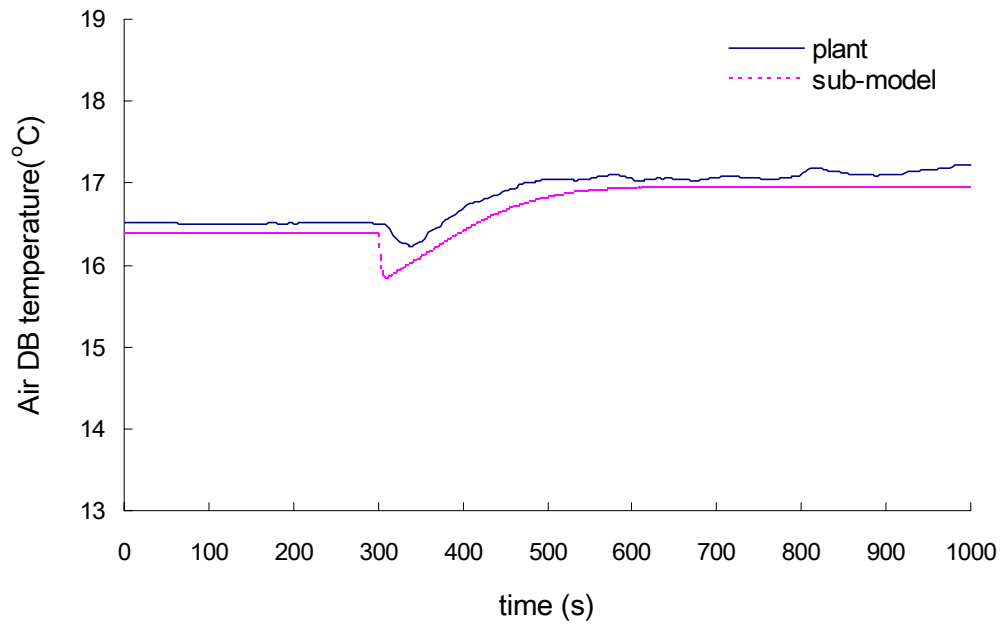


Figure 6.8 Open-loop responses of the sub-model and the plant (dry-bulb air temperature at evaporator exit) after being subjected to a step-change of compressor speed

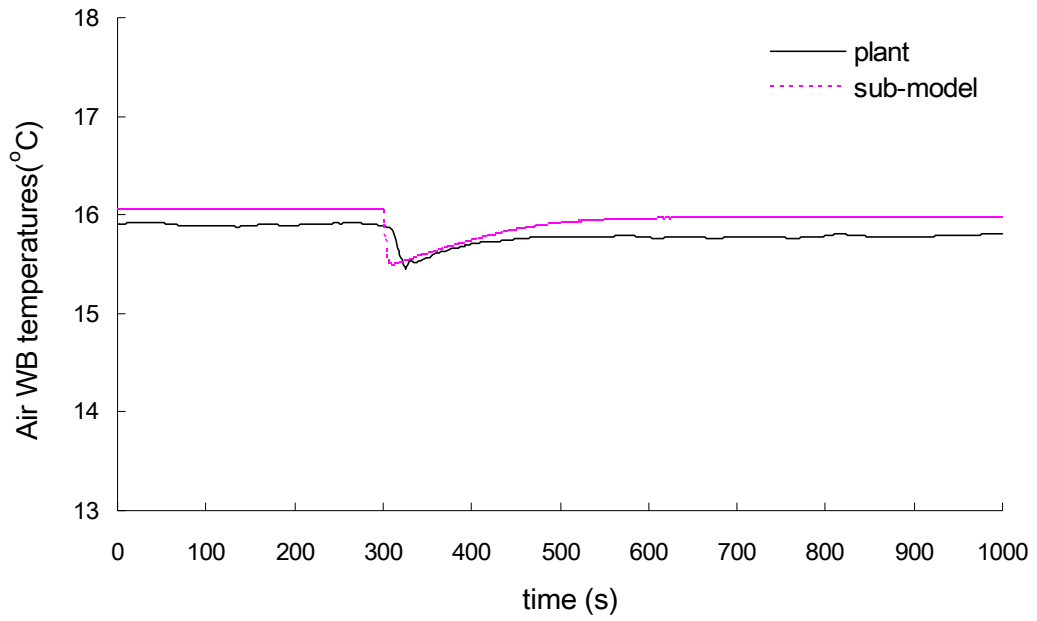


Figure 6.9 Open-loop responses of the sub-model and the plant (wet-bulb air temperature at evaporator exit) after being subjected to a step-change of compressor speed

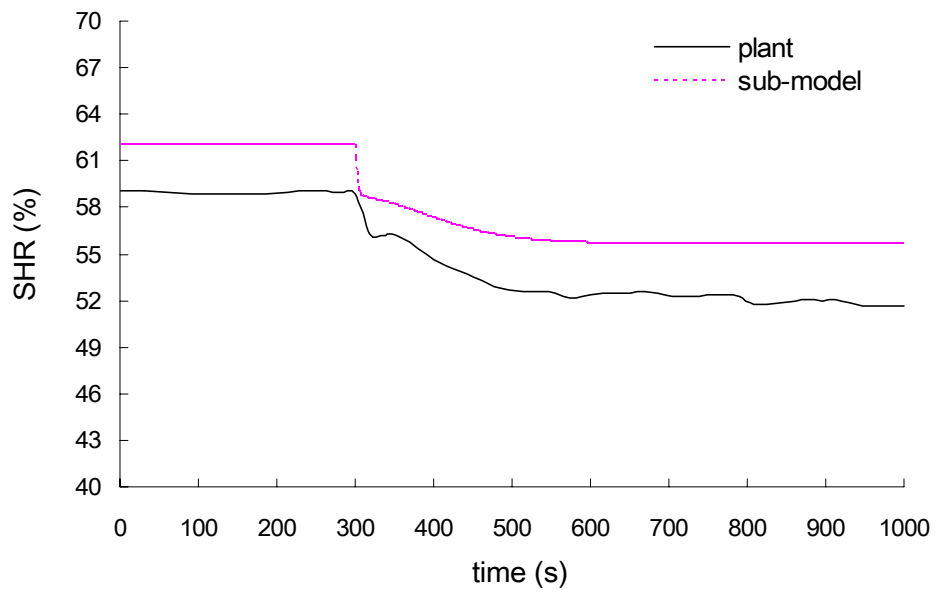


Figure 6.10 Open-loop responses of the sub-model and the plant (sensible heat ratio) after being subjected to a step-change of compressor speed

## 6.4 Summary

The dynamic mathematical model developed for the experimental DX VAV A/C system has been experimentally validated, through validating experimentally the constituent sub-model of its DX refrigeration plant, on the basis that the sub-model for the VAV air-distribution sub-system was developed using the correlations describing the operational performance of various components in the sub-system, which are either field-tested or available from manufacturers. As illustrated in Figures 6.3 to 6.10, the steady-state and transient open-loop responses from both the DX refrigeration plant and its dynamic mathematical sub-model agreed well. The deviation for the eight parameters' steady-state responses, as shown in these eight figures, before and after the step-change in compressor speed between the plant and sub-model were all within 6%. On the other hand, the responses from the sub-model and the plant during the transient period after the introduction of the step-change in compressor speed demonstrated acceptable agreements for these eight parameters, with the sub-model behaved in a similar way to that of the DX plant.

The experimentally validated dynamic mathematical model for the DX VAV A/C system is expected to be very useful in studying the dynamic behavior of, and in developing better control strategies for DX VAV A/C systems.

## **Chapter 7**

### **Simulated Closed-loop Responses Using the Validated Model**

#### **7.1 Introduction**

The objective of developing a dynamic model for a DX VAV A/C system is to provide an effective and time-saving tool for the research work on investigating its dynamic behavior and developing related control strategies. The simulation accuracy of the two constituent sub-models, respectively for the DX refrigeration plant and the VAV air-distribution sub-system, has been confirmed, as reported in Chapter 6. However, during the model validation process, only the open-loop responses from both the DX refrigeration plant and its sub-model were compared. The applicability of the complete system model for investigating the closed-loop responses of the experimental DX VAV A/C system, when all its existing inherent control loops are enabled, remains untested.

Therefore, it is necessary to obtain the closed-looped responses from the validated model to see whether it can also reasonably represent the experimental DX VAV A/C system with all its PI feedback control loops enabled. This chapter presents the simulated closed-loop responses after being subjected to step-changes, using the validated DX VAV A/C system model.

## **7.2 Operating conditions to obtain closed-loop responses**

As mentioned in Section 4.5, in the experimental DX VAV A/C system there were seven conventional PI control loops which may directly affect the operating conditions to obtain closed-loop responses. Among these seven loops, because the speed of condenser fan was fixed and the control loop for the condenser fan was out of action. In addition, it should be noted that the ventilation strategy of fixed outdoor air ratio is the most common and reliable ventilation strategy adopted by VAV systems up to date. In practice, this strategy is easy to implement, assuring high indoor air quality. Therefore, a fixed outdoor air ratio ventilation strategy has been adopted in the DX VAV A/C system, and its corresponding control loop was also out of action. The ratio of outdoor air volumetric flow rate to the total supply air volumetric flow rate was fixed at 20%.

The other remaining control loops in the experimental DX VAV A/C system are strongly coupled, acting intensely as the action of one loop can influence other loops. Therefore, it is usually challenging to achieve an overall quality control for the experimental DX VAV A/C system, even though the commissioning of each control loop may be easily carried out separately.

Suitable control parameters for various PI controllers input to the dynamic system model to obtain closed-loop responses are shown in Table 7.1. These were determined through trial and error. Set points for various operating parameters are shown in Table 7.2.

There are two conditioned spaces served by the DX VAV A/C system: *Space A* and *B*, with their respective pressure-independent VAV terminals. The closed-loop responses of the validated dynamic model representing the experimental DX VAV A/C system, with the aforementioned PI feedback control loops enabled, have been obtained after being subjected to: (1) a step-change in space internal thermal load; (2) a step-change in the set-point of space air temperature. The dry-bulb temperature and moisture content of outdoor air were assumed to be 35 °C and 24 g/kg *dry-air*, respectively. The condenser inlet air temperature was also assumed to be 35 °C.

The total simulated operation period is 5400 s, i.e., 90 min. It was assumed that at the start of simulation, i.e.,  $t=0$  s, the internal sensible load from occupants and equipment in *Space A* was 2160 W; and the internal latent load in *Space A* was 410 W, with a constant moisture generation rate of 12.24 g/m. The set point of air temperature in *Space A* was 25 °C. Ten minutes after starting time, i.e.,  $t=600$  s, the internal sensible load in *Space A* was step changed down to 1080 W, or a 50% reduction.

In *Space B*, at  $t=0$  s the internal sensible load and latent load from occupants and equipment were 1730 W and 410 W, respectively. Both remained unchanged throughout the whole simulated operation period. At  $t=3000$  s, the set-point of air temperature in *Space B* was step-changed from 25 °C down to 24 °C.

Table 7.1 Controllers' control parameters for obtaining closed-loop response

<b>PI Controller</b>	<b>Proportional action</b>	<b>Integration time <math>t_i</math> (unit: s)</b>
Space thermostat *	$PB=2$	800
Compressor	$K_p=-35.0$	500
EEV	$K_p=-8.0$	100
VAV terminal (built-in) *	$K_p=3.2$	23.5
Supply fan	$K_p=0.8$	5

\* Same for Space A or B

Table 7.2 Set points for various operating parameters

<b>Operating parameters</b>	<b>Set point</b>
Space A air temperature	25 °C
Space B air temperature	Step-changed from 25 °C to 24 °C at $t=3000$ s
Degree of superheat at evaporator exit	6 °C
Supply air temperature	15 °C
Supply air static pressure	535 Pa

### 7.3 Simulated results and analysis

Figure 7.1 shows the simulated closed-loop responses of air temperature variation in both *Space A* and *B* in response to the two step-changes introduced, at 10 minutes and 50 minutes respectively. For the first 10 minutes, the temperatures in both *Space A* and *B* were steady at 24.8 °C and 24.9 °C, respectively. At  $t=600$  s, the step-change



of internal sensible load was introduced in *Space A*. Therefore, air temperature in *Space A* started to gradually decrease. This in turn led to the actions of both the air temperature controller (thermostat) and the VAV terminal's flow controller in *Space A*. As seen from Figures 7.2 and 7.3, at  $t=640$  s, the damper in VAV terminal in *Space A* began to close step-by-step from its opening of  $38.4^\circ$ ; and therefore the flow rate of supply air entering *Space A* began to gradually reduce from  $775$   $m^3/h$ , in response to the changes in air temperature in *Space A*. Under the combined effect from the thermal capacitance of space air and the regulation of supply air flow rate to *Space A*, air temperature in *Space A* reached its lowest point of  $24.1$   $^\circ\text{C}$  at  $t=808$  s, and afterwards the air temperature in *Space A* began to rise slowly. It was brought close to and finally kept at its set-point, i.e.  $25$   $^\circ\text{C}$ , approaching the end of the operation period. The opening of terminal damper in, and the supply air flow rate to *Space A* were eventually kept at around  $58^\circ$  and  $330$   $m^3/h$ , respectively.

Before the step-change in *Space B* at  $t=3000$  s, air temperature in *Space B* was stable at  $24.86$   $^\circ\text{C}$ , while that in *Space A* was approaching its setting at  $24.98$   $^\circ\text{C}$  after the step-change at  $t=600$  s in *Space A*. At  $t=3000$  s, the set-point of air temperature in *Space B* was step-changed from  $25$   $^\circ\text{C}$  down to  $24$   $^\circ\text{C}$ . The deviation between actual air temperature in *Space B* and its setting called for the damper in VAV terminal in *Space B* to respond quickly by increasing its opening from  $49.2^\circ$  at the time of the step-change. As shown in Figures 7.2 and 7.3, at  $t=3085$  s, the terminal's damper in *Space B* was fully opened at  $0^\circ$ ; and the supply air flow rate to *Space B* increased to  $871$   $m^3/h$ , which was over the maximum flow rate set for the VAV terminal in *Space B*,  $850$   $m^3/h$  as given in Section 5.3.4. However, due to the combined effect from the flow controller and the hysteresis of damper linkage, the terminal's damper in *Space*

*B* remained fully open for about 100 *s*. Afterwards, the damper began to reduce its opening quickly so that the terminal's actual air flow rate could meet the demanded flow rate signaled from the thermostat controller in *Space B*. As a result, as seen in Figure 7.1 the air temperature in *Space B* was quickly reduced towards the new set-point after the step-change, and become stable at 24.1 °C 180 *s* after the step-change at  $t=3000$  *s*.

The gradual closing of VAV terminal's damper in *Space A* after  $t=640$  *s*, resulted in an increase of the overall flow resistance in the VAV air-distribution duct-work. It can be seen from Figure 7.8 which shows the simulated closed-loop responses of supply fan speed, that the supply fan, therefore, responded by reducing its speed from 1920 *rpm* in order to maintain the supply air static pressure at its set-point, i.e., 535 *Pa*. Due to the timely regulation of supply fan speed, the supply air static pressure was well controlled at  $535 \pm 5$  *Pa*, before the step-change in *Space B* at  $t=3000$  *s*, as shown in Figure 7.7. The supply fan speed was stabilized at 1825 *rpm* at  $t=3000$  *s*.

At  $t=3000$  *s*, the drastic increase of the opening of terminal's damper in *Space B* caused the supply air static pressure to reduce quickly, as seen in Figure 7.7. At  $t=3035$  *s*, the supply air static pressure reached its lowest value of 525 *Pa*. It can be observed in Figure 7.8 that in order to restore the supply air static pressure's set-point, supply fan speed was increased from 1824 to 1904 *rpm* within 103 *s*. After the damper began to close at  $t=3180$  *s*, the supply fan responded by reducing its speed rapidly in an attempt to maintain the set point of supply air static pressure. As seen from Figure 7.7, finally the supply air static pressure was again well-controlled

at its set point.

It is obvious that the total supply air flow would also be lower following the gradually closing of VAV terminal's damper in *Space A* after  $t=640$  s, as depicted in Figure 7.6 which shows the simulated closed-loop responses of total supply air flow rate. On the other hand, Figure 7.9 illustrates the simulated closed-loop responses of supply air temperature. It can be observed that supply air temperature started to decrease from  $15\text{ }^{\circ}\text{C}$  at  $t=640$  s, because of the fast reduction of air flow rate passing through the DX cooling coil. In order to maintain the supply air temperature at its set-point of  $15\text{ }^{\circ}\text{C}$ , the variable-speed compressor responded by gradually lowering its speed from  $105\text{ Hz}$  ( $\sim 6300\text{ rpm}$ ) at  $t=668$  s and was finally stabilized at  $72\text{ Hz}$  ( $\sim 4320\text{ rpm}$ ) at  $t=3000$  s, as shown in Figure 7.10. At  $t=1145$  s, supply air temperature reached its lowest value of  $14.65\text{ }^{\circ}\text{C}$ . Afterwards it rose slowly towards its set-point and was finally settled at  $14.95\text{ }^{\circ}\text{C}$  at  $t=3000$  s.

After  $t=3000$ s, the total supply air flow rate increased rapidly from  $887\text{ m}^3/\text{h}$ , and maintained its maximum value of  $1235\text{ m}^3/\text{h}$  for nearly 100 seconds. Then it began to gradually drop and was finally settled at  $1171\text{ m}^3/\text{h}$ . Resulting mainly from the variation of total supply air flow rate, supply air temperature began to rise from  $14.95\text{ }^{\circ}\text{C}$  at  $t=3000$  s, and reached its peak value of  $15.49\text{ }^{\circ}\text{C}$  at  $t=3132$  s, as shown in Figure 7.9. As seen in Figure 7.10, the compressor could timely vary its speed in order to maintain the supply air temperature's set point. Consequently, supply air temperature was slowly brought downwards to its set point and finally settled at  $15\text{ }^{\circ}\text{C}$ .

Since supply air temperature and static pressure were both well controlled and maintained at their respective set-points, disturbances in either of the two spaces had hardly effects on the operation parameters in the other space. As shown in Figures 7.1 to 7.3, the opening of VAV terminal's damper, supply air flow rate, and air temperature in *Space B* remained nearly unchanged during the period from  $t=0$  s to 3000 s; the same occurred for those in *Space A* from  $t=3000$  s to 5400 s. This proved that independent zoning control could be realized by using the DX VAV A/C system.

The gradual reduction of the total supply air flow rate after  $t=600$  s would lead to a lower heat transfer rate in evaporator. This caused the degree of refrigerant superheat at evaporator exit to decline from 6 °C at  $t=645$  s, as illustrated in Figure 7.11. Consequently, the EEV was called for to reduce its opening from 213 *pulse* ( $2.1726 \times 10^{-6} \text{ m}^2$ ) at  $t=647$  s, so that the degree of superheat can be controlled at its set-point of 6 °C, as shown in Figure 7.12. At  $t=3000$  s the EEV's opening was kept at 166 *pulse* ( $1.6932 \times 10^{-6} \text{ m}^2$ ) and the degree of superheat was well maintained at its set point.

After  $t=3000$  s, the degree of refrigerant superheat at the evaporator exit drastically responded to the sudden change of total supply air flow rate. Therefore, the EEV was called for to quickly increase its opening from 166 *pulse* ( $1.6932 \times 10^{-6} \text{ m}^2$ ), to 200 *pulse* ( $2.04 \times 10^{-6} \text{ m}^2$ ) at  $t=3144$  s. Finally the EEV opening was maintained at around 196 *pulse* ( $1.9992 \times 10^{-6} \text{ m}^2$ ) and the degree of superheat was controlled at its set-point of 6 °C.

In a DX air-cooling refrigeration plant equipped with a variable-speed compressor

and expansion valve, its evaporating pressure is determined jointly by its compressor speed, EEV opening, temperature and flow rate of air passing through its evaporator. The averaged air temperature across an evaporator would significantly affect its evaporating pressure. Therefore, as seen in Figures 7.9 and 7.13, the variation pattern in evaporating pressure was similar to that of supply air temperature. At  $t=1098\text{ s}$ , the evaporating pressure reached its lowest value at  $7.15\text{ Bar}$  ( $7.15 \times 10^5\text{ Pa}$ ); at  $t=3225\text{ s}$ , it reached its peak value at  $7.27\text{ Bar}$  ( $7.27 \times 10^5\text{ Pa}$ ).

Figure 7.14 presents the simulated closed-loop responses of condensing pressure. It can be observed that, after  $t=600\text{ s}$ , condensing pressure decreased from  $19.95\text{ Bar}$  ( $19.95 \times 10^5\text{ Pa}$ ) gradually towards a new steady-state value of  $17.52\text{ Bar}$  ( $17.52 \times 10^5\text{ Pa}$ ), because of the gradually reduced condensing load under the constant inlet temperature and flow rate of condenser cooling air. After  $t=3000\text{ s}$ , the condensing pressure quickly increased soon after the introduction of the step-change, and finally settled at a higher value of  $19\text{ Bar}$  ( $19.0 \times 10^5\text{ Pa}$ ) because of the increased condensing load from  $t=3000\text{ s}$  to  $5400\text{ s}$ .

As seen in Figure 7.6, during the first  $3000\text{ s}$ , the total supply air flow rate was approaching  $887\text{ m}^3/\text{h}$  at  $t=3000\text{ s}$ , 68% of total air flow rate at  $t=600\text{ s}$ . Since the outdoor air flow rate was fixed at 20% of total supply air flow rate during the whole simulated operation period, between  $t=600\text{ s}$  and  $3000\text{ s}$ , the heat gain from outdoor air was therefore correspondingly reduced. Consequently, the total thermal load was then reduced. As seen in Figure 7.16, in order to match the reduced total thermal load, the output cooling capacity from the DX refrigeration plant was also reduced, approaching  $6310\text{ W}$  at  $t=3000\text{ s}$ , which was 71% of the output cooling capacity at

$t=600$  s.

Although after  $t=3000$  s, the total internal thermal loads in both *Space A* and *B* remained unchanged, the heat gain due to inside-outside air temperature difference increased because of the reduced air temperature setting in *Space B*. As shown in Figure 7.16, after the step-change in *Space B* at  $t=3000$  s, the output cooling capacity from the DX refrigeration plant was increased by about 1.6 kW to compensate the increase of system's total thermal load.

Figure 7.15 depicts the simulated closed-loop responses of moisture content of supply air. Very often, the averaged surface temperature of a DX cooling coil or evaporator, is below air dew-point and hence off-coil air is close to saturation. Generally it can be assumed that off-coil air has a relative humidity of around 95%. Moreover, the moisture content of supply air could be assumed to be equal to that of off-coil air. Therefore, a similar variation pattern of supply air moisture content to that of supply air temperature has been demonstrated. Because the supply air temperature was well controlled at its setting around 15 °C, the moisture content of supply air was then maintained at its corresponding value of 10.5 g/kg dry-air with a rather small variation range during the whole simulated operation period. Figure 7.4 shows the simulated closed-loop response of air moisture contents both in *Space A* and *B*. It can be observed that although the moisture content of supply air was steady, the air moisture content in *Space A*, at  $t=3000$  s, was still increased because of unvaried internal latent load in, and the decreased supply air flow to *Space A*. Figure 7.5 shows the simulated closed-loop responses of space air relative humidity. It can be seen from Figure 7.5 that after the step-change was introduced into *Space A*

at  $t=600$  s, the air relative humidity in *Space A* rose rapidly from 57% to its peak value of 59.5% at  $t=792$  s. The occurrence of such a peak value was due to the quickly-reduced air temperature in *Space A* in the first few minutes after  $t=600$  s.

After  $t=3000$  s, because of the increase of supply air flow rate to *Space B*, air moisture content in *Space B* was still decreased slowly from 11.47 g/kg dry-air at  $t=3000$  s to the final steady-state value of 11.14 g/kg dry-air. However, since the final new steady-state air temperature in *Space B* was at a lower value of 24 °C, air relative humidity in *Space B* was finally higher than that before the introduction of the step-change at  $t=3000$  s.

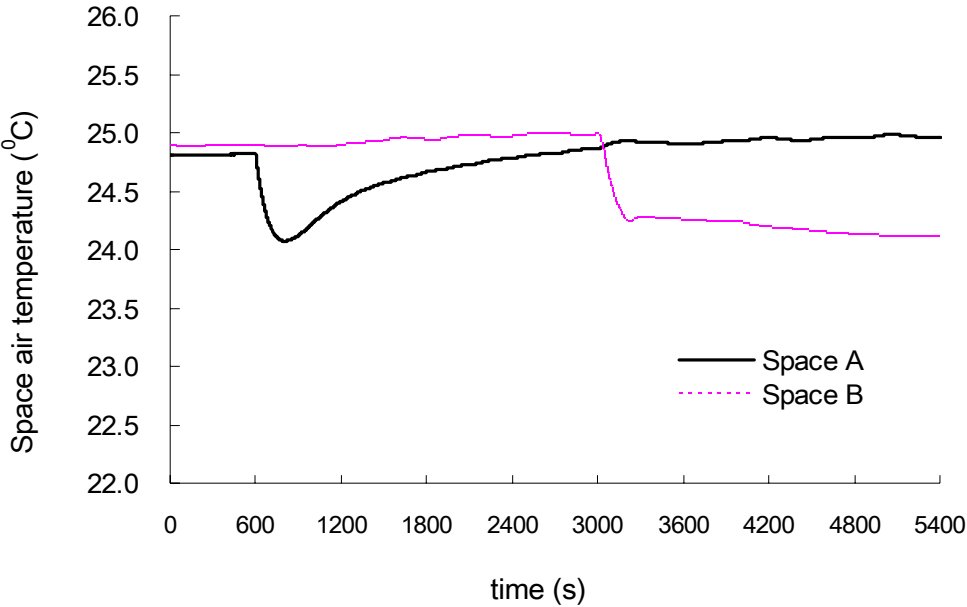


Figure 7.1 Simulated closed-loop responses (space air temperatures)

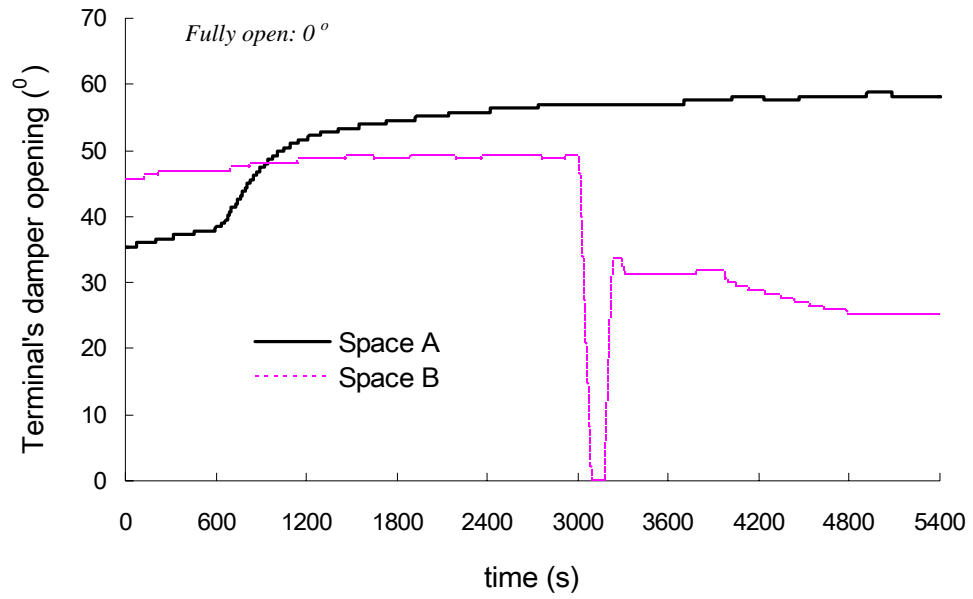


Figure 7.2 Simulated closed-loop responses (VAV terminal's damper opening)

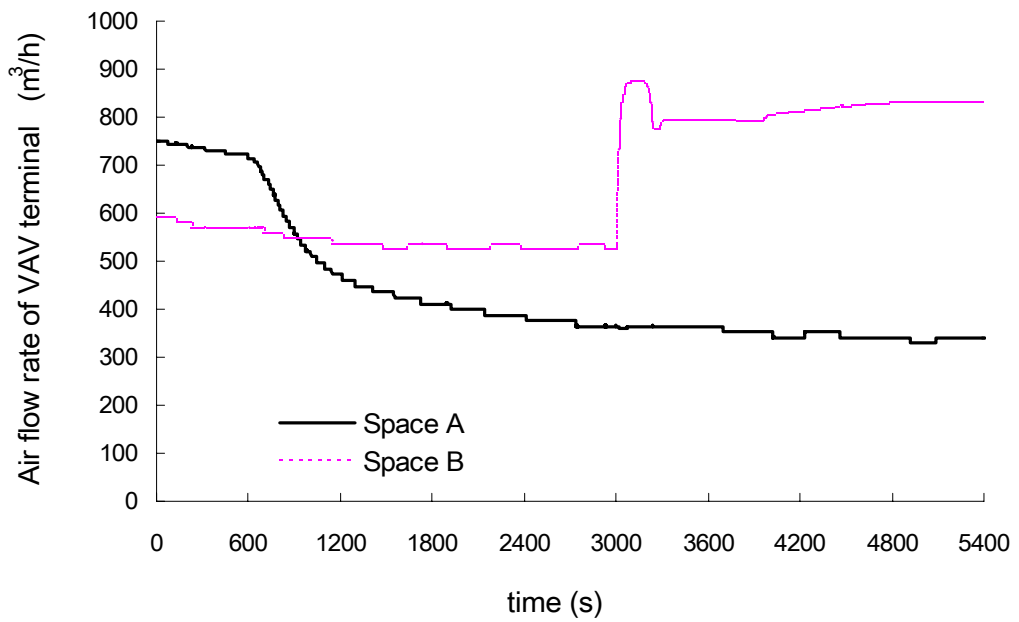


Figure 7.3 Simulated closed-loop responses (air flow rate of VAV terminal)



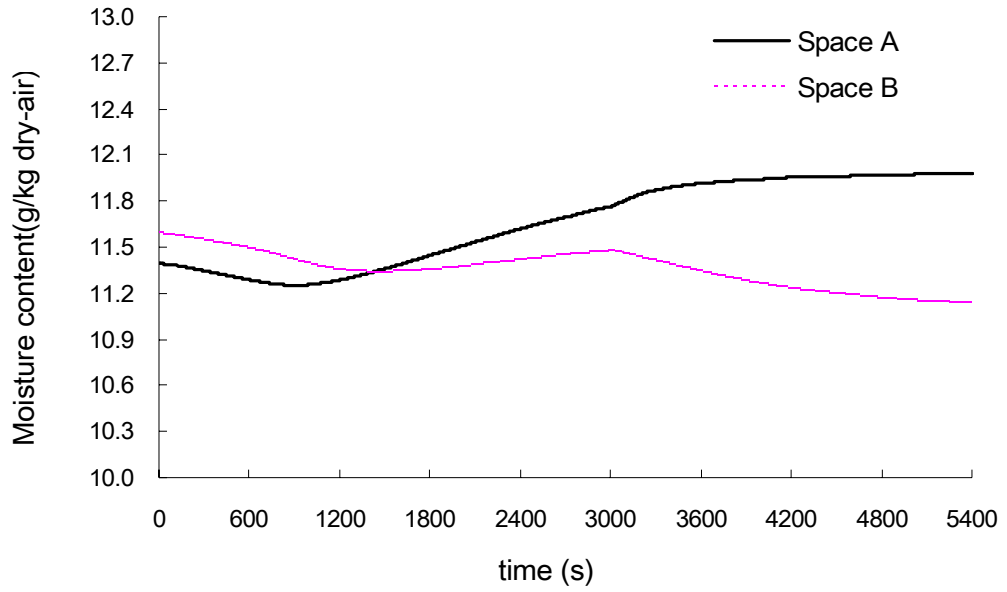


Figure 7.4 Simulated closed-loop responses (space air moisture content)

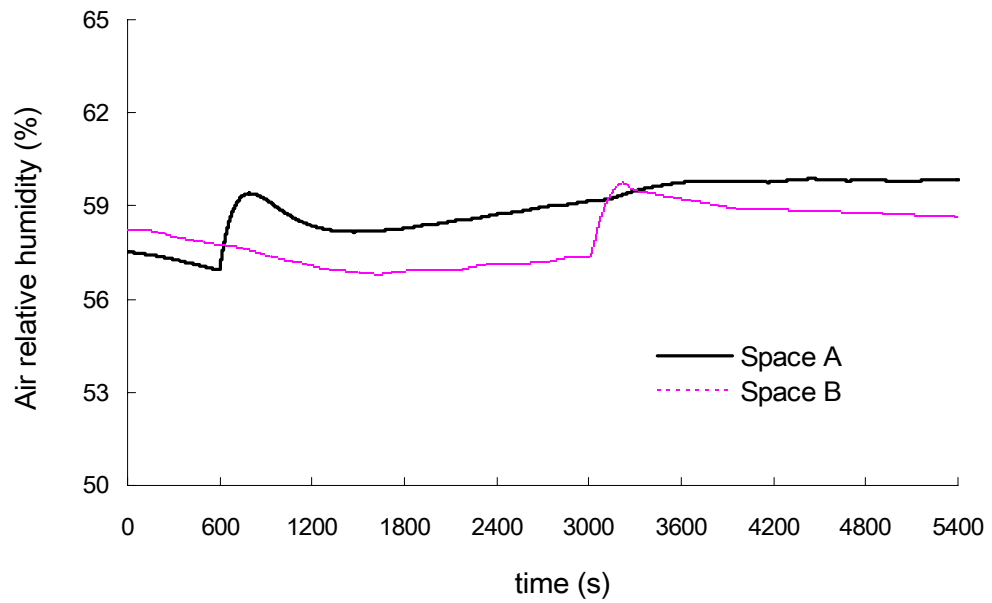


Figure 7.5 Simulated closed-loop responses (space air relative humidity)

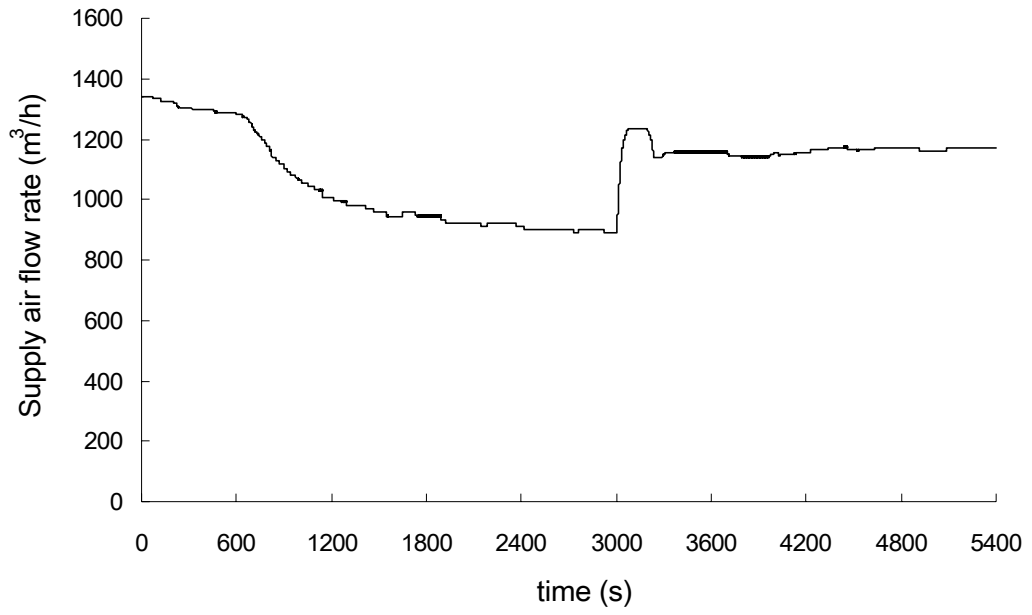


Figure 7.6 Simulated closed-loop response (total supply air flow rate)

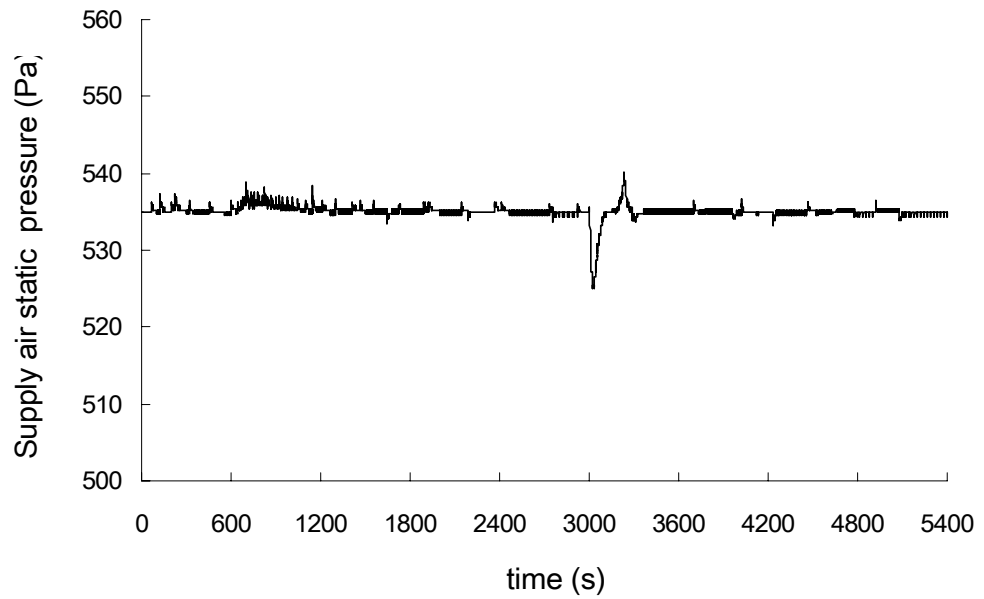


Figure 7.7 Simulated closed-loop response (supply air static pressure)

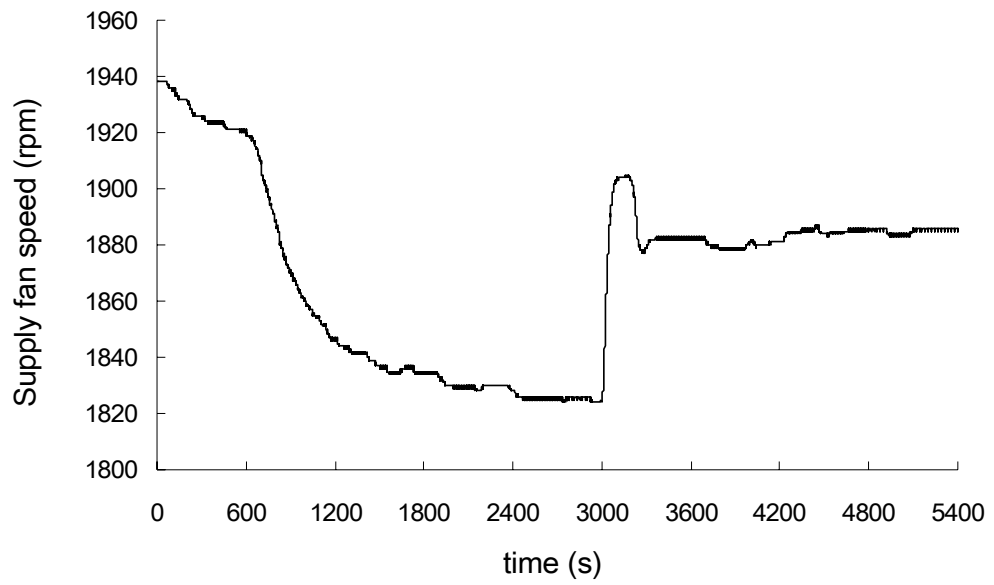


Figure 7.8 Simulated closed-loop response (supply fan speed)

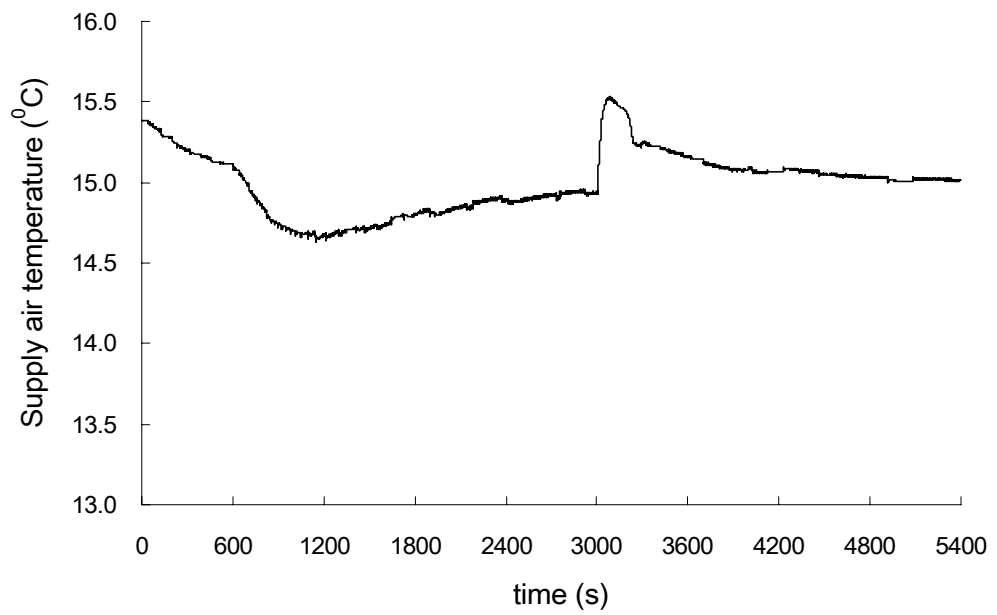


Figure 7.9 Simulated closed-loop response (supply air dry-bulb temperature)

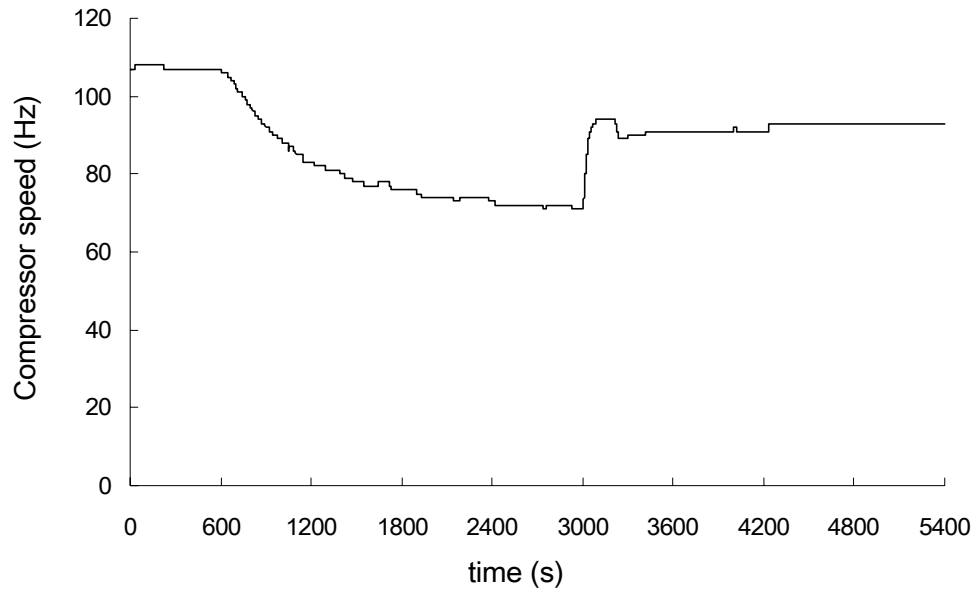


Figure 7.10 Simulated closed-loop response (compressor speed)

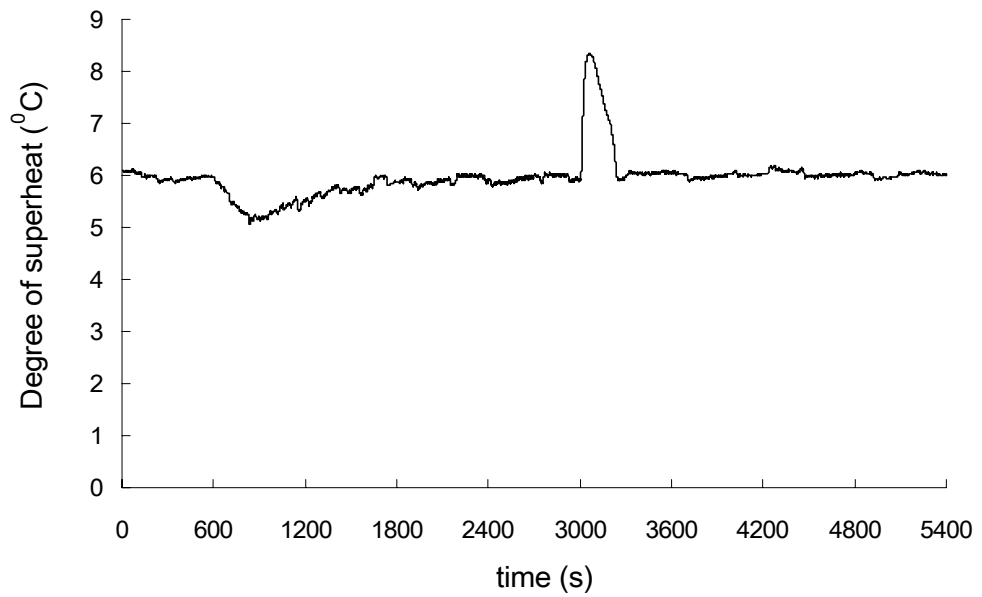


Figure 7.11 Simulated closed-loop response (degree of refrigerant superheat at evaporator exit)

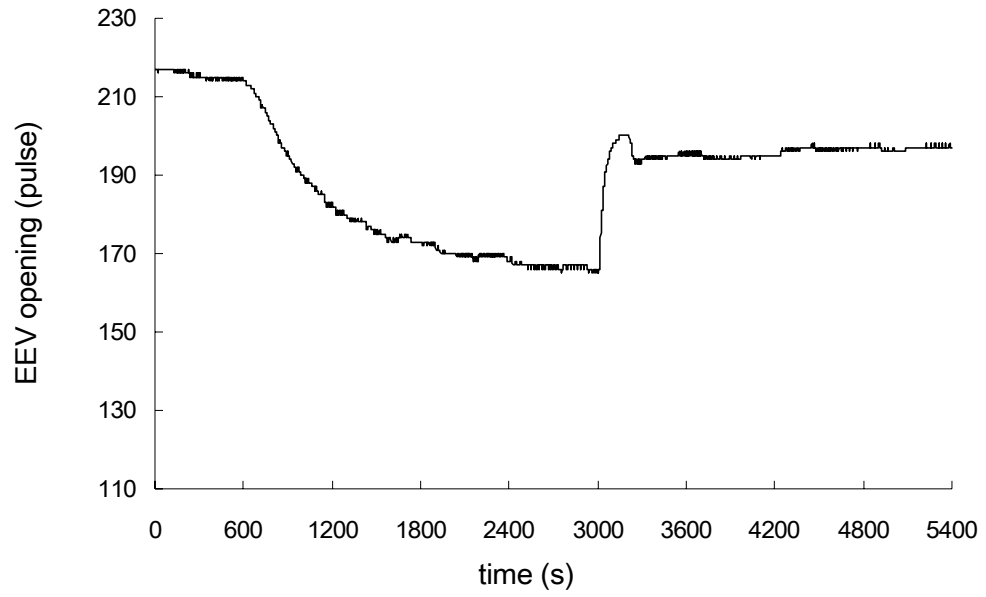


Figure 7.12 Simulated closed-loop response (EEV opening)

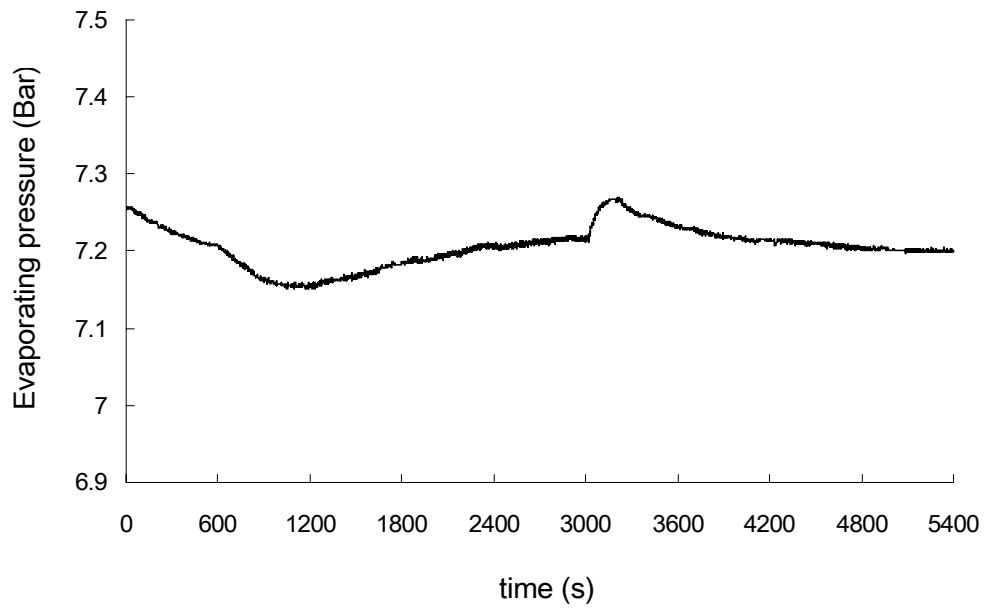


Figure 7.13 Simulated closed-loop response (evaporating pressure)

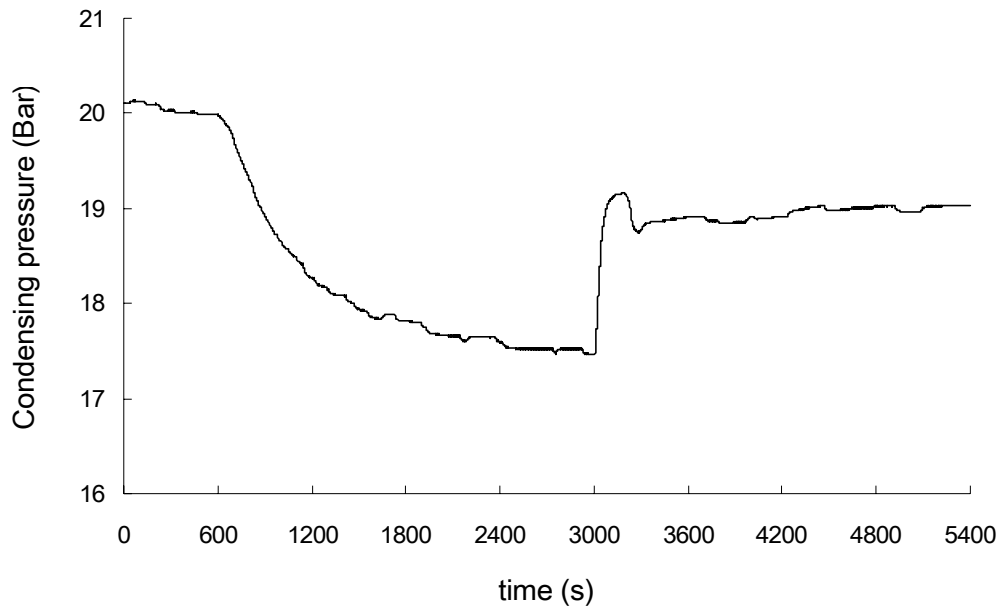


Figure 7.14 Simulated closed-loop response (condensing pressure)

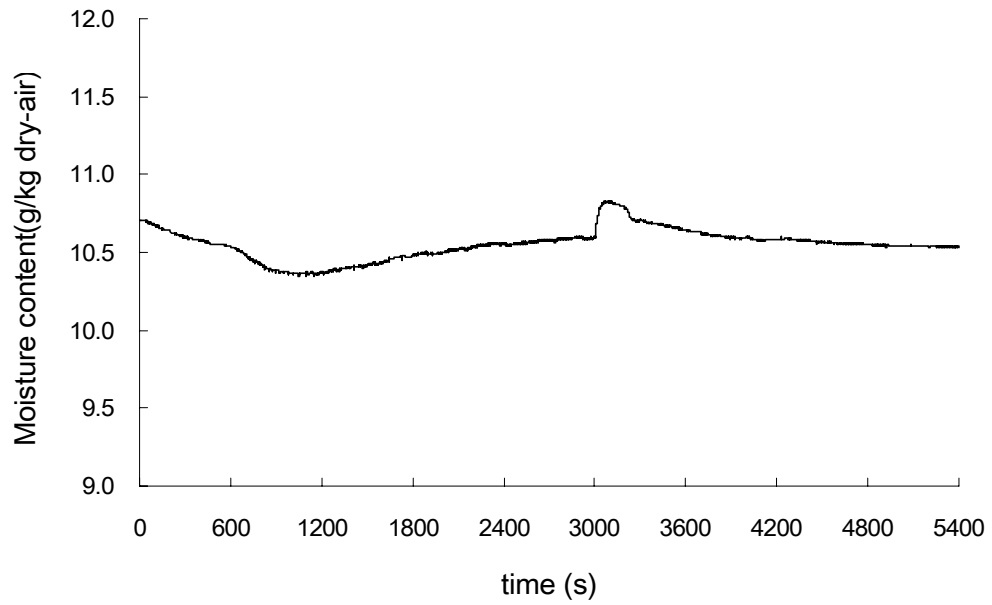


Figure 7.15 Simulated closed-loop response (supply air moisture content)

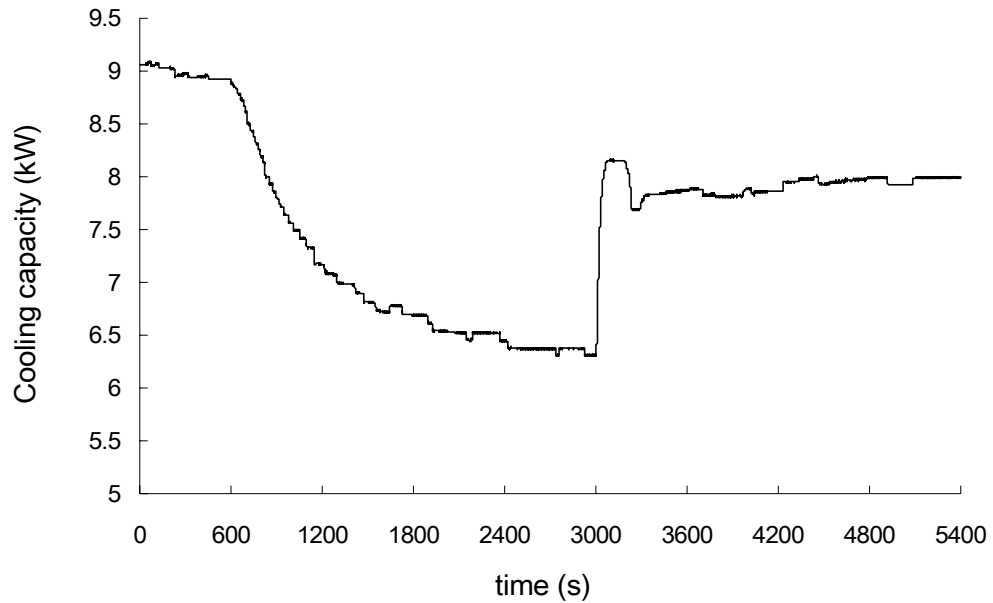


Figure 7.16 Simulated closed-loop response (cooling capacity)

#### 7.4 Summary

Following the model experimental validation which was mainly based on comparing the open-loop responses from both the DX refrigeration plant and its sub-model, this chapter presents the simulated closed-loop responses with various PI feedback control loops being enabled using the validated dynamic mathematical model for the experimental DX VAV A/C system, when the system was subjected to step-changes in both space internal thermal load and space air temperature set point. As seen in Section 7.3, the simulated closed-loop responses can correctly describe both the steady-state and transient behaviors of the DX VAV A/C system when various PI feedback control loops of the system were enabled. This suggested that the dynamic model would behave as expected in a similar manner to a real DX VAV A/C system

in both open-loop and closed-loop operational situations.

Therefore, the dynamic model developed could be used as a powerful, effective and convenient tool in understanding the dynamic characteristic of, and in developing appropriate control strategies for, DX VAV A/C systems. With the help of the dynamic model, a novel feedforward capacity controller for DX VAV A/C system has been developed and is reported in Chapter 8.



## **Chapter 8**

### **A Novel DDC-based Feedforward Capacity Controller for the DX VAV A/C System**

#### **8.1 Introduction**

As discussed in Chapter 3, the VRV technology featured with a variable-speed compressor and electronic expansion valve (EEV) is expected to be very useful for a DX VAV A/C system to address its difficulty to continuously match the output cooling capacity from its DX refrigeration plant with the varying cooling load in its VAV air-distribution sub-system. In a DX VAV A/C system equipped with a variable-speed compressor and an EEV, there should normally exist seven control loops for different system operational parameters, as detailed in Chapter 4. These seven control loops interact intensely within the DX VAV A/C system.

In a VAV air-distribution sub-system, the stability for both supply air temperature and static pressure is critical to eliminating the interferences from different conditioned spaces and their respective VAV terminals, which helps realize a satisfactory independent zoning-control for space air temperature. In a DX air cooling plant, continuously varying the flow rate and temperature of air entering its DX evaporator, as a result of the control actions for supply air static pressure and air temperatures in conditioned spaces, however, requires corresponding regulation in the output cooling capacity from the DX plant.

To match the plant's output cooling capacity with system's varying cooling load is a

pre-requisite for both keeping the supply air temperature stable and realizing the desirable zoning-control of space air temperature. On the other hand, controlling the opening of EEV and varying the speed of compressor may be used to regulate the output cooling capacity from a DX refrigeration plant. Conventionally, an EEV is used to control the degree of refrigerant superheat at the exit of evaporator, and a variable-speed compressor to control supply air temperature. Compressor speed and the opening of an EEV are coordinated so that a required plant's output cooling capacity may be achieved.

A DX air-cooled refrigeration plant with variable-speed compressor, is a nonlinear, multi-variable, time-varying and strong-coupled control object. Large variation of air flow rate passing through the DX evaporator of the plant, which is inherent for a DX VAV A/C system, deteriorates further its nonlinearity. It is therefore difficult for a standard PI controller having fixed control parameter settings for the variable-speed compressor to adapt itself to the wide range of system's operating conditions; the robust control of supply air temperature is then hard to achieve. Control action for supply air temperature may respond slowly to disturbance, and even become oscillatory under certain operating conditions. Some recent research work has addressed the problem of controlling DX refrigeration plants experiencing strong nonlinearity and continuously varying operating conditions, and the widely-reported approaches to improving control robustness included, for example, adaptive control [Seem 1997], artificial-neural-network (ANN) control [So et al. 1995]. Although these approaches have been demonstrated to be capable of improving the control performance of a DX refrigeration plant having strong nonlinear control characteristics, the HVAC industry has shown its reluctance to adopt these methods

as alternatives to PI controls. One of possible reasons is that these methods are relatively complex to configure and difficult to implement. For instance, a successful ANN control algorithm often requires extensive training data that are often difficult to obtain in practice.

On the other hand, for most DX A/C systems used in small-scaled buildings, their capacity control is in most cases based on simple on-off cycling, in response to the air temperature in conditioned-spaces they serve. Such an on-off cycling for regulating the output capacity often leads to poor environmental control and low operating efficiency.

With the rapid development of computer technology and DDC technique, the computational and communication capacities of the controllers available to HVAC industry have been greatly strengthened. A large number of operating parameters of HVAC equipment can be simultaneously real-time measured, monitored and processed. DDC provides a DX VAV A/C system with possibilities for exploring novel approaches to realize robust capacity control for its DX refrigeration plant.

This chapter reports on the development of a novel DDC-based feedforward capacity controller for the experimental DX VAV A/C system described in Chapter 4, for matching the output cooling capacity from its DX refrigeration plant with the varying cooling load in its VAV sub-system. The feedforward controller developed, replaced the original conventional PI feedback controller for compressor speed in the experimental DX VAV A/C system. It worked together with the EEV's PI feedback controller for regulating the output cooling capacity from the DX plant to maintain

supply air temperature stable at its desired value. Controllability tests for the feedforward capacity controller have been carried out in the experimental rig. The experimental results of the system's responses to the step-changes of space cooling load and space air temperature set-point respectively, are presented and discussed.

## **8.2 Development of the novel DDC-based feedforward capacity controller**

The control loops in a DX VAV A/C system may be divided into two parts. One includes various control loops for its VAV air-distribution sub-system; the other various control loops for its DX refrigeration plant. In a DX refrigeration plant equipped with a variable-speed compressor and an EEV, there are two control loops, respectively, for its compressor speed and its EEV opening. Although an EEV's opening may be controlled in response to room air temperature [Chen et al. 2005], in most cases, an EEV's opening should be regulated by a PI feedback control loop in response to the degree of refrigerant superheat at evaporator exit.

In a small-sized residential variable-speed air conditioner, its compressor speed is usually regulated by a feedback control loop in response to room air temperature. However, for a VAV A/C system, its supply air temperature should be maintained constant at its setting. Therefore, in a DX VAV A/C system, similarly, its supply air temperature, or the outlet air temperature from its DX cooling coil, should also be maintained constant at its set point, through appropriate capacity control actions on both compressor speed and the opening of EEV.

When, on the other hand, there are problems in accurately measuring the controlled parameters, a feedback controller can no longer be operative since the information required for feedback control actions is not available. For example, in short supply air ducts problems may be encountered in measuring the air temperature and water vapor content downstream and close to cooling coils, where the air is stratified with respect to velocity, temperature and water vapor content. In this case, a feedforward controller may provide an alternative solution [Deng 2002].

For the DDC-based feedforward controller reported in this chapter, it consisted of a numerical calculation algorithm (NCA), which was based on the energy balance between the air side and the refrigerant side in the DX cooling coil, using a number of real-time measured system operating parameters, and a dead-band for avoiding unstable compressor operation. They are described separately, as follows.

### **8.2.1 Numerical calculation algorithm (NCA) using real-time measured operating parameters**

A DDC-based pressure-independent VAV terminal has its built-in air flow sensor and can therefore provide the digital signal representing its current actual air flow rate. The air flow rate passing through the DX cooling coil in the experimental DX VAV A/C system,  $M_a$ , can be regarded as the summation of the air flow rates passing through individual VAV terminals. Therefore, the digital signal representing the total air flow rate passing through the cooling coil is easily obtainable.

Knowing the real-time measured dry-bulb and wet-bulb temperatures of the air entering the DX coil, the enthalpy of incoming air,  $h_{a,i}$ , can be evaluated using the air state equations [ASHRAE 2001]. On the other hand, based on the established psychrometric practices, air leaving the DX coil can be assumed at about 95% saturation. The temperature of air leaving the DX coil is assumed to be the supply air temperature setting minus a fixed air temperature rise due to the heat gain from the supply fan. Then the enthalpy of air leaving the DX coil,  $h_{a,l}$ , can be obtained similarly using the air state equations. Therefore, the required output cooling duty from the DX coil is given by:

$$Q_{c,a} = M_a (h_{a,i} - h_{a,l}) \quad (8.1)$$

The real-time measured pressure and temperature of superheated refrigerant at the suction of compressor are available from their respective measuring sensors available in the experimental DX VAV rig. The enthalpy of superheated refrigerant at the suction of compressor,  $h_{r,s}$ , can then be evaluated based on the measured pressure and temperature using the *A.C. Cleland* correlations for R22 [Cleland 1986]. Neglecting the energy loss in the refrigerant line between DX evaporator and compressor suction owing to good thermal insulation, the enthalpy of refrigerant leaving the DX evaporator is given by:

$$h_{r,l} = h_{r,s} \quad (8.2)$$

On the other hand, as mentioned in Chapter 5, normally the refrigerant subcooling in a condenser with a receiver is rather low, and the refrigerant in the receiver can be assumed to be the saturated liquid refrigerant at condensing pressure. Therefore after

having the real-time measured condensing pressure, the enthalpy of refrigerant leaving the receiver,  $h_{r,c}$ , is obtained using the R22 State Equations. Neglecting also the energy loss in refrigerant line and approximating the refrigerant throttling process in the EEV as being isenthalpic, the enthalpy of refrigerant entering the DX evaporator is given by:

$$h_{r,i} = h_{r,c} \quad (8.3)$$

Therefore, the specific output cooling capacity from the DX refrigeration plant can be calculated by:

$$q_{c,r} = (h_{r,l} - h_{r,i}) \quad (8.4)$$

In order to maintain the temperature of air leaving the DX cooling coil at its setting, the output cooling capacity from the DX coil, based on the principle of energy balance between the air side and the refrigerant side in the DX cooling coil, should be equal to the required cooling duty from air side, i.e.,

$$Q_{c,r} = Q_{c,a} \quad (8.5)$$

Hence, the required refrigerant mass flow rate through the DX evaporator, to be provided by compressor, is obtained:

$$M_r = \frac{Q_{c,r}}{q_{c,r}} \quad (8.6)$$

Meanwhile, the specific volume of superheated refrigerant entering compressor,  $v_s$ , can be obtained from measured pressure and temperature at compressor suction using the R22 State Equations. The swept volume of the rotor compressor,  $V_{com}$ , can be calculated using the related compressor's geometric parameters as follows:

$$V_{com} = \pi r^2 l \varepsilon (2 - \varepsilon) \quad (8.7)$$

where  $l$  is the stroke of cylinder;  $r$  the radius of rotor and  $\varepsilon$  the rotor relative eccentricity. On the other hand, the compressor's displacement coefficient,  $\lambda$ , can be determined using Equations (5.7) to (5.9) Therefore, the required compressor speed can be determined by:

$$n = \frac{M_r \times v_s}{V_{com} \times \lambda} \quad (8.8)$$

Then the input frequency to the variable-frequency drive for compressor's motor,  $F$ , can be obtained by:

$$F = \frac{n \times PL}{1 - s} \quad (8.9)$$

where  $s$  is the slip factor of the motor; and  $PL$  number of the electrode couple of the motor.

The following systems' operating parameters must be measured real-time so that the NCA may be completed: on-coil dry-bulb air temperature; the total supply air flow rate (obtained by summing up the air flow rates of individual VAV terminals); the degree of refrigerant superheat; condensing and evaporating pressures in the DX refrigeration plant. It should be noted that in order to assess the accuracy of the feedforward controller, the measurement of supply air temperature was also taken downstream of the supply fan in the experimental rig. This was for the investigation and validation purpose only since the controller was designed to operate without this measurement.



## **8.2.2 The dead-band for avoiding unstable compressor operation**

The feedforward controller based only on the NCA presented in Section 8.2.1, may be used to regulate compressor speed. On the other hand, EEV's opening is regulated by an existing PI feedback controller to maintain the degree of refrigerant superheat at the exit of the DX evaporator. Preliminary tests for compressor speed control using the feedforward controller based only on the NCA suggested that the control actions from both the feedforward controller and the PI feedback controller for the EEV were strongly coupled, leading to a number of problems for controlling compressor speed.

### **8.2.2.1 Problems for controlling compressor speed based only on the NCA**

There were two problems. Firstly, the feedforward controller for compressor speed depended largely on the refrigerant state at compressor suction, which however was also greatly influenced by the degree of opening of the EEV. Meanwhile regulating compressor speed also greatly influenced the degree of refrigerant superheat. This could significantly deteriorate the control of the degree of refrigerant superheat by the EEV. Therefore, in order to stabilize plant's operation, the coupling effect of the two control loops must be minimized or eliminated if at all possible.

Secondly, the NCA based feedforward controller for compressor speed was prone to disturbances including the measuring noise for system's operating parameters such as supply air flow rate. However, measuring noise and uncertainty, as well as the

deviation of numerical calculation, cannot be normally avoided. Moreover, in a real DX VAV A/C system, various operating parameters such as supply air flow rate can in fact hardly be maintained absolutely constant even when the system's steady state operation has been reached. Therefore, if compressor speed was determined solely through the NCA using those real-time measured operating parameters, it was virtually impossible to prevent compressor speed from fluctuating.

Figures 8.1 to 8.4 show results of one of the preliminary tests to illustrate the extent of the two problems. Prior to starting the test, the DX VAV A/C system was operated for a long time, so that its steady-state operation was achieved and then any external disturbances to the system could be regarded as being eliminated. The test was conducted from  $t=0$  s to 2400 s using the experimental rig described in Chapter 4. At  $t=240$  s, the NCA-based feedforward controller for compressor speed was employed to replace its original PI controller. During the test, all operating conditions of the DX VAV A/C system remained unchanged and no other external disturbances were introduced. Therefore, operating parameters including compressor speed, EEV opening and the degree of refrigerant superheat after  $t=240$  s would have stayed steady if the above two problems did not exist, or the NCA-based feedforward controller for compressor speed satisfactorily worked.

However, it can be observed from Figure 8.1 that the measured supply air flow rate fluctuated with a notable range mainly due to the continuous fine-tunings for both the openings of VAV terminals and the speed of supply fan in the VAV air-distribution subsystem. As a result, compressor speed after  $t=240$  s when the NCA-based feedforward controller for compressor speed was enabled, fluctuated, as

shown in Figure 8.2. Consequently, as discussed earlier, the degree of refrigerant superheat at the exit of DX evaporator, controlled by the EEV's feedback PI control loop and having a set point of 9.0 °C, was also greatly influenced by the fluctuation of compressor speed and became unstable after  $t=240$  s, as depicted in Figure 8.3. Correspondingly, the oscillation of EEV opening occurred after  $t=240$  s, as seen in Figure 8.4.

From the test results shown in Figures 8.1 to 8.4, it became obvious that certain supplementary measures were necessary to improve the performance of the NCA based feedforward controller for regulating compressor speed. Hence a dead-band for compressor speed regulation has been developed, as an essential part of the feedforward controller to stabilize the operation of compressor.

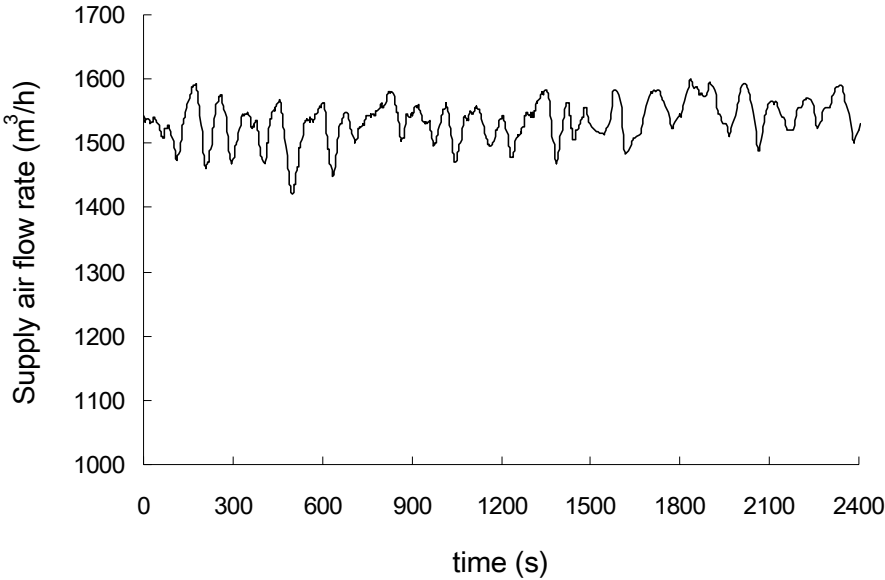


Figure 8.1 Measured total supply air flow rate

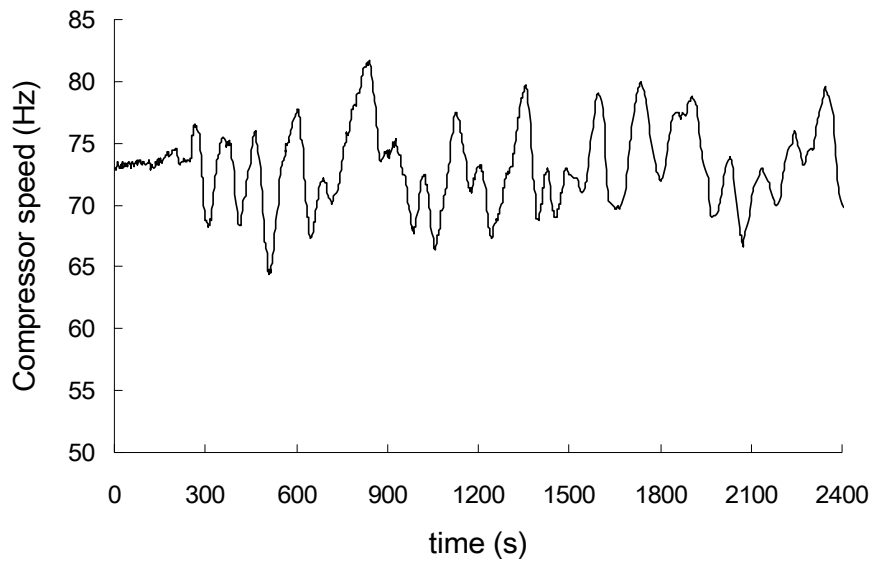


Figure 8.2 Measured compressor speed regulated by NCA only based feedforward controller

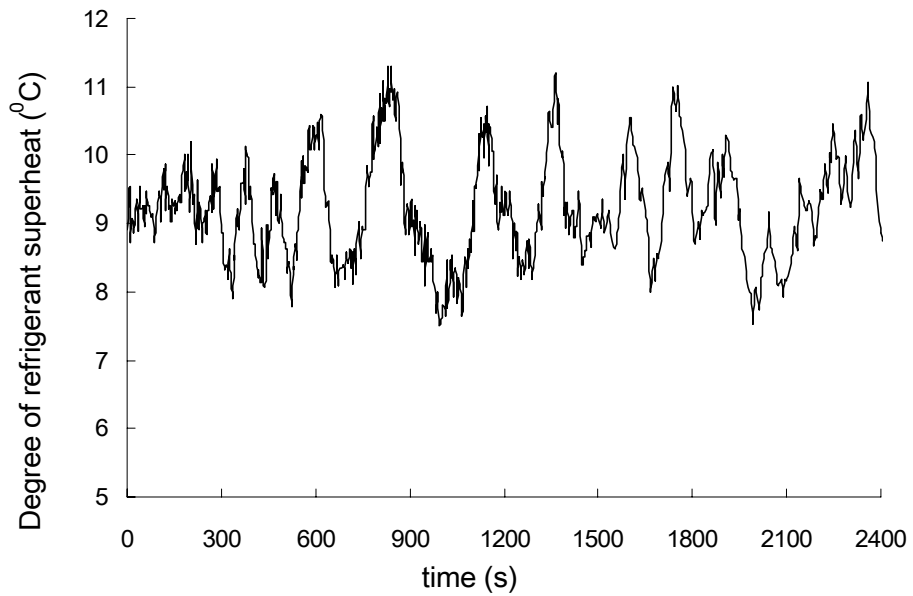


Figure 8.3 Measured degree of refrigerant superheat

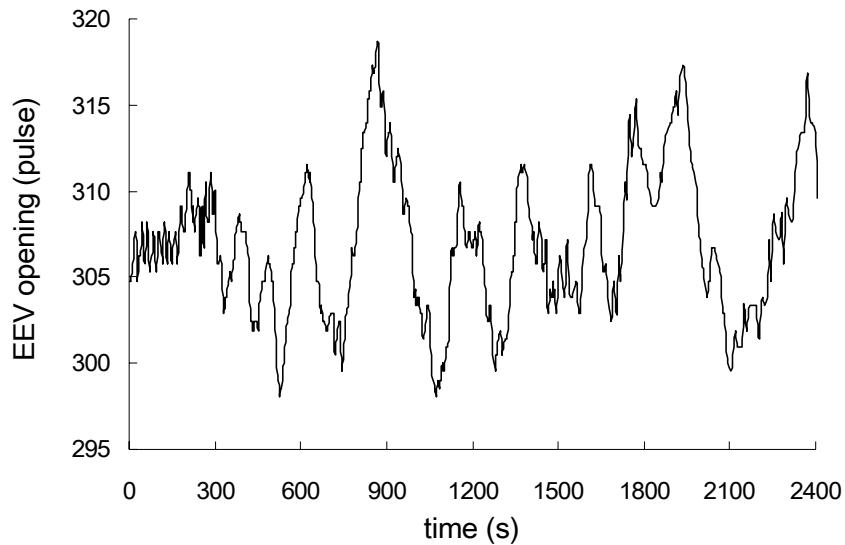


Figure 8.4 Measured EEV opening

### 8.2.2.2 Introduction of the dead-band

Both the opening of EEV and the speed of compressor would affect the output cooling capacity from a DX refrigeration plant. The actual refrigerant mass flow rate entering the DX coil is regulated by the opening of EEV.

In fact, the change of the degree of refrigerant superheat at the exit of a DX evaporator reflects directly the variation of required cooling duty from the air side of the DX evaporator. When the required cooling duty is greater than the output cooling capacity from the DX evaporator, the degree of refrigerant superheat becomes greater, and vice versa. Therefore an EEV is correspondingly initiated to increase its opening to allow more refrigerant flowing into a DX coil when the degree of refrigerant superheat is above its set point, vice versa. When compressor speed is fixed, an EEV solely has the capability of regulating a coil's output cooling capacity to deal with a relatively small range of variation in cooling duty. Moreover, an EEV

itself can usually fine-tune refrigerant flow. For example, for the EEV in the experimental rig, its smallest change in opening is 1/480 of its full opening. It can therefore be said that an EEV makes possible the accurate matching between output cooling capacity of a DX refrigeration plant and system's cooling load.

Therefore, due to the strong coupling effect of the two controllers, i.e., the feedback PI controller for EEV's opening and the NCA based feedforward controller for compressor speed, it was considered necessary to introduce a dead-band, to be a part of the feedforward controller, for regulating compressor speed. Such a dead-band would allow a conditional temporary decoupling of the actions from the two controllers by locking up compressor speed on the condition that the variation of speed is within a pre-determined dead-band. Hence, compressor speed will be discretely, rather than continuously, regulated because of the introduction of the dead-band, and the opening of EEV is continuously regulated. The dead-band used in this study was  $\pm 5\%$  of the current compressor speed, which was determined using trial-and-error method, so that a reasonable balance between control stability and control sensitivity can be achieved.

With the introduction of the dead-band, the complete feedforward controller would then consist of both the NCA and the dead-band for regulating compressor speed.

### **8.2.3 Complete control for the DX VAV A/C system**

The feedforward controller developed for regulating compressor speed, worked together with the conventional PI feedback controller for the opening of EEV to

jointly control the output cooling capacity from the DX refrigeration plant so that supply air temperature can be maintained stable at its setting under the joint control by the two controllers. Varying compressor speed provided first-layer or macro-tuning control for cooling capacity whereas modulating EEV's opening second-layer or micro-tuning control for cooling capacity. The feedforward controller for compressor speed appeared logic to track disturbances so that pre-emptive actions may be initiated. External disturbances of significant amplitudes can be counteracted by rapidly changing compressor speed. On the other hand, with the dead-band, the calculated compressor speed fluctuation due to measuring noise and uncertainty, etc., may be eliminated.

Other existing PI feedback control loops in the VAV air-distribution sub-system, such as the controls of the supply air static pressure, the air flow rate of VAV terminals and the space air temperature, remained functional as usual.

### **8.3 Approach to realize the feedforward controller in the experimental station**

As reported in Chapter 4, a LabVIEW logging & control (L&C) program has been developed specifically for the experimental DX VAV A/C rig. The L&C program provided an independent self-programming module (SPM) by which the novel feedforward controller developed for the DX VAV A/C system has been realized through programming using the LabVIEW language.

In activating the novel feedforward capacity controller developed, the status of

compressor speed control in the experimental rig was switched to “Prog” condition, as shown in Figure 8.5. Under the “Prog” condition, the original PI controller for regulating compressor speed in the experimental rig was disabled but acted only as a digital-analog converter. The SPM developed for the feedforward controller was then activated. As shown in Figure 8.6, by processing the measured parameters according to the procedures described in Section 8.2, compressor speed was finally determined and then communicated to the digital-analogue converter, i.e., the original PI controller, which produced a DC control signal for activating the variable-frequency drive of compressor motor for speed change. Other PI feedback control loops in the DX VAV A/C system all remained functional as usual.

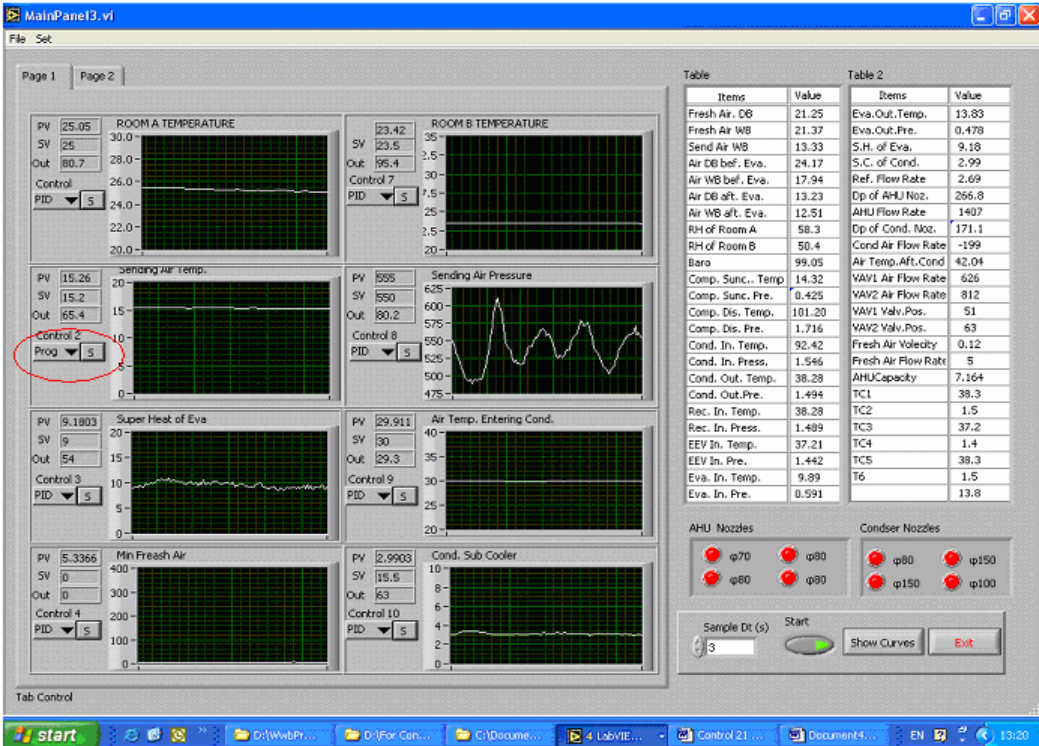


Figure 8.5 Interface of the L&C program for testing the feedforward controller developed



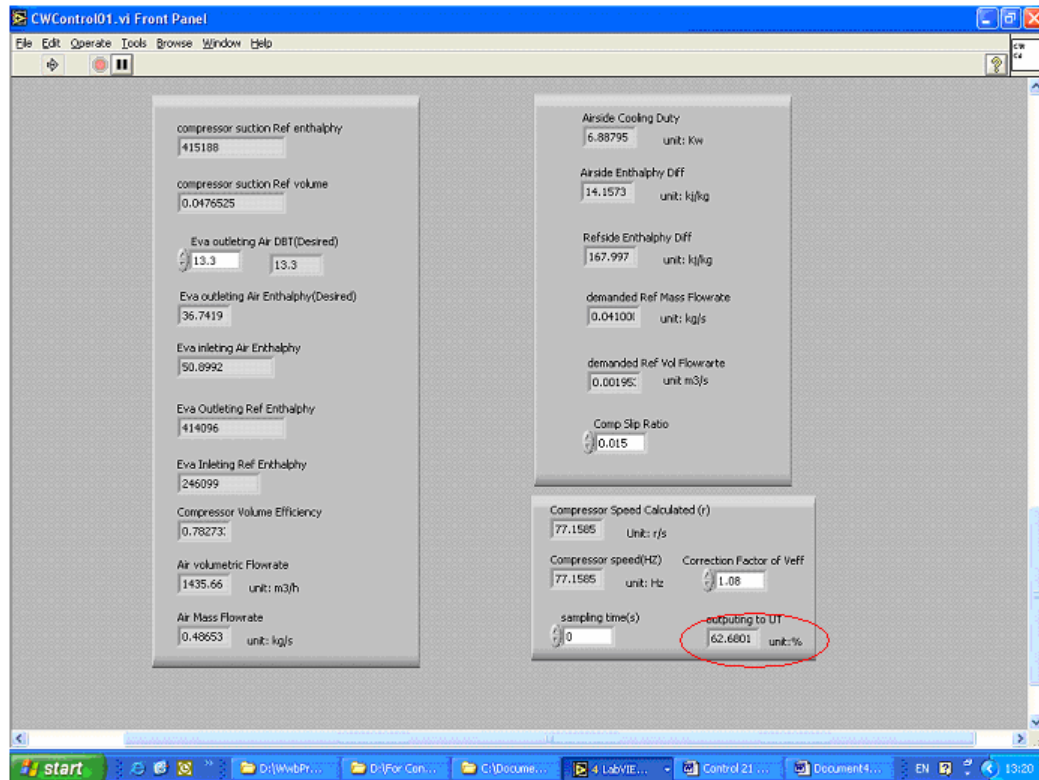


Figure 8.6 Interface of the self-programming module for testing the feedforward controller developed

#### 8.4 Controllability tests for the feedforward controller developed

Controllability tests for the novel feedforward controller developed for the experimental DX VAV A/C system have been carried out using the experimental rig. As described in Chapter 4, there were two pressure-independent VAV terminals, Terminal A and B, serving respectively two equally-sized conditioned spaces, Space A and B, in the experimental DX VAV A/C system. The results of two separate tests, i.e., Test 01 where the internal cooling load in Space A was subjected to a step-change, and Test 02 where the set point of air temperature in Space A was also subjected to a step-change, were selected for discussion as follows.

For the controllability tests, the condenser fan speed was kept unchanged, and the openings of outdoor and return dampers were fixed. The variable-speed rotor compressor in the experimental rig was controlled by the novel feedforward controller. The control parameters of other PI feedback controllers in the experimental DX VAV A/C system are given in Table 8.1.

Table 8.1 Control parameters of the PI feedback controllers in the experimental DX VAV A/C system

<b>PI Controller</b>	<b>P</b>	<b>I (s)</b>
EEV	430.0 °C	60
Supply fan	380.0 Pa	19
Terminal A	5.0 °C	240
Terminal B	5.0 °C	240

The air temperature entering the air-cooled condenser was maintained at 30 °C, and the condenser air flow rate at 3250 m<sup>3</sup>/h. The set points for the degree of refrigerant superheat at the exit of the DX evaporator, and for the supply air static pressure were 9 °C and 550 Pa, respectively. The design supply air temperature was set at 15 °C. Other operating conditions for both Test 01 and 02 are given in Table 8.2.

Table 8.2 Operating conditions of the two controllability tests

Test		01	02
Space A	Sensible load (W)	Step change from initial 1200 W at $t=0$ s to 2200 W at $t=300$ s	2000
	Latent load (W)	1600	1400
	Temperature set point ( $^{\circ}\text{C}$ )	25	Step change from initial $23.5^{\circ}\text{C}$ at $t=0$ s to $25^{\circ}\text{C}$ at $t=420$ s
Space B	Sensible load (W)	2200	2300
	Latent load (W)	600	400
	Temperature set point ( $^{\circ}\text{C}$ )	23.5	23

#### 8.4.1 Results of Test 01

The duration for Test 01 was 3000 seconds. Before the test started at  $t=0$  s a steady-state operation was reached. At  $t=300$  s the space sensible cooling load in Space A was step increased by 1000 W from 1200 W to 2200 W, a 35% increase of the total space cooling load of 2800 W.

Figure 8.7 shows the time-variation of air temperatures in both Space A and B in response to the step increase. Before the step-change was introduced, air temperatures in both Space A and B were kept at their respective set points,  $25^{\circ}\text{C}$  and  $23.5^{\circ}\text{C}$ . Mainly due to the heat capacitance of space air, air temperature in

Space A started to rise at  $t=430$  s, i.e., 130 seconds after the introduction of the step-change. From Figure 8.8, it can be observed that VAV Terminal A was then activated timely to step by step increase its opening from  $32^\circ$ . Accordingly the air flow rate passing through Terminal A was increased, as shown in Figure 8.9, in order to bring air temperature in Space A back to its set point. On the other hand, the increase of the opening of Terminal A decreased supply air static pressure. The supply fan therefore responded to increase its speed rapidly, as shown in Figure 8.10. As a result, the supply air static pressure was maintained at its set point throughout the durations of the test, as illustrated in Figure 8.11.

The gradual increase of supply air flow rate, as illustrated in Figure 8.12, suggested an increased cooling duty for the DX coil. It can be seen from Figure 8.13 that the compressor's feedforward controller, therefore, responded to discretely increase compressor speed. During the period when the compressor speed was not altered because of the action by the dead-band, the increase of supply air flow rate also led to the increase of the degree of refrigerant superheat at DX coil's exit. Correspondingly the EEV was regulated by its PI controller to increase gradually its opening, as shown in Figure 8.14. It can be seen from Figure 8.15 that at  $t=550$  s the degree of refrigerant superheat reached its maximum at  $11.3^\circ\text{C}$ ; but afterwards, decreased because of the sudden increase of compressor speed from  $64\text{ Hz}$  ( $\sim 3840$  rpm) to  $69\text{ Hz}$  ( $\sim 4140$  rpm). At  $t=736$  s the degree of refrigerant superheat returned to its set point. Due to the combined actions from the two controllers, the variation of the degree of refrigerant superheat was limited to within  $9 \pm 2.5^\circ\text{C}$ , which was mild and therefore acceptable. After  $t=2000$  s when a new steady operation for the DX VAV A/C system was achieved, both compressor speed and EEV's opening were

kept unchanged, and the degree of refrigerant superheat was maintained at its set point.

It can be observed in Figure 8.16 that the averaged DX refrigeration plant's cooling capacity after  $t=2000$  s was about 1000 W greater than that before the introduction of the step-change at  $t=300$  s. This agreed with the step-change in the system's cooling load introduced. With the feedforward controller developed, it was possible for the DX refrigeration plant to timely vary its output cooling capacity to match its cooling load. Consequently, the design supply air temperature of 15 °C was well maintained, with deviations of less than 0.3 °C, as shown in Figure 8.17.

It can be observed from Figure 8.7 that the maximum deviation of air temperature in Space A was less than 0.5 °C during transit period. During steady-state period, the deviation was within  $\pm 0.15$  °C. Such a control accuracy was satisfactory. On the other hand, with more air flowing into Space A, its air relative humidity decreased accordingly from 64% and finally stabilized at a lower value of 59%, as depicted in Figure 8.18.

Maintaining both static pressure and temperature of supply air at their respective set points effectively inhibited the interference of controlled parameters between the two terminals, or conditioned spaces. It can be seen that both the opening and air flow rate for Terminal B were almost free of the influence from the actions of Terminal A, as shown in Figures 8.8 and 8.9. Air temperature in Space B was well controlled at  $23.5 \pm 0.15$  °C, as shown in Figure 8.7; and its relative humidity kept stable at 52%, as shown in Figure 8.18, throughout the duration of the test.

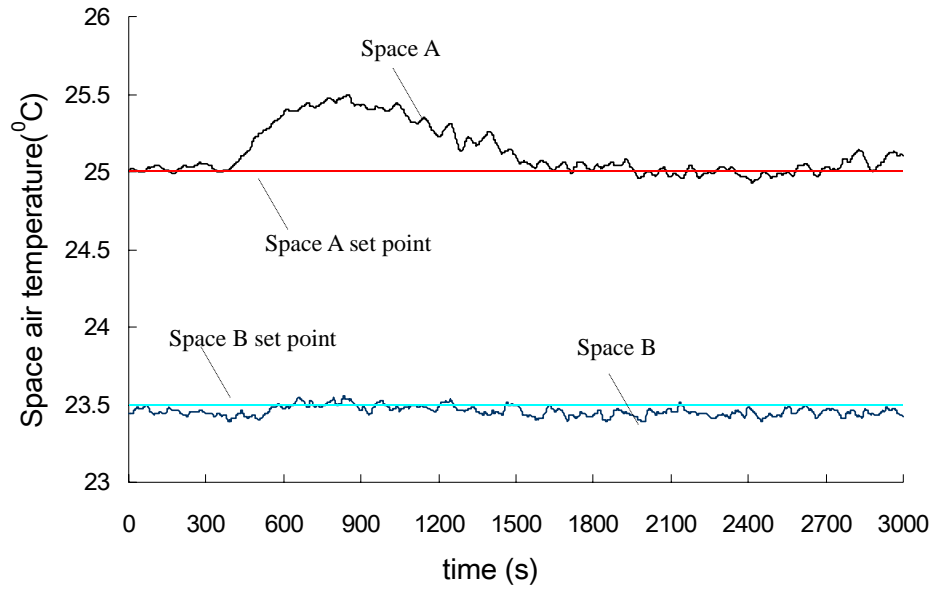


Figure 8.7 Space air temperatures vs. time (Test 01)

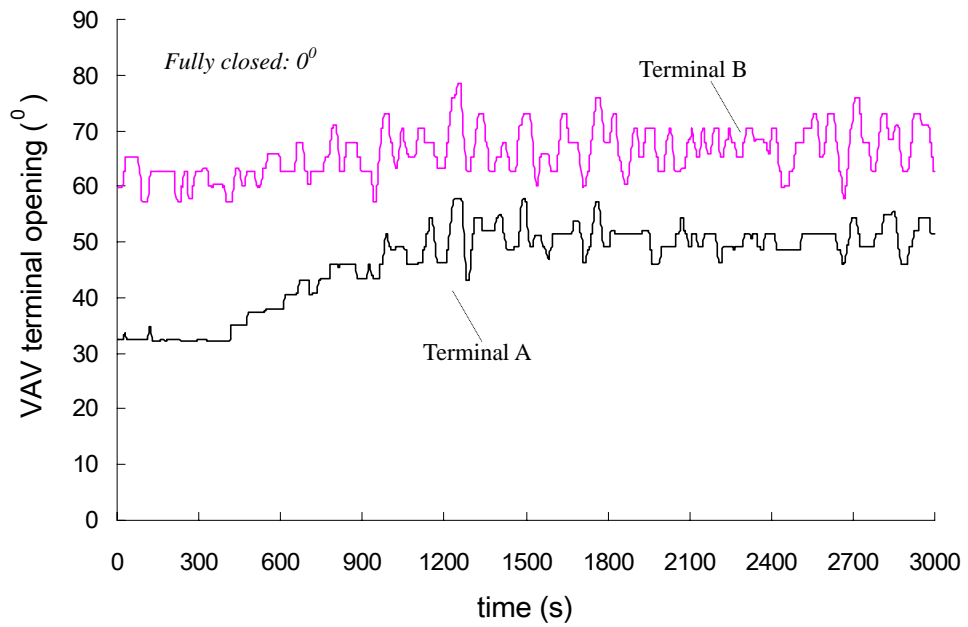


Figure 8.8 VAV terminal openings vs. time (Test 01)

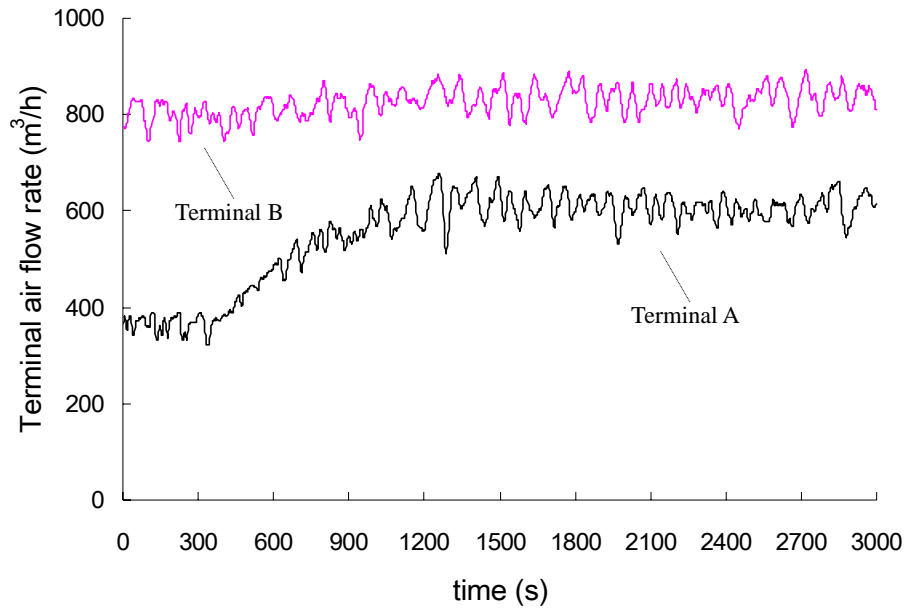


Figure 8.9 VAV terminal air flow rates vs. time (Test 01)

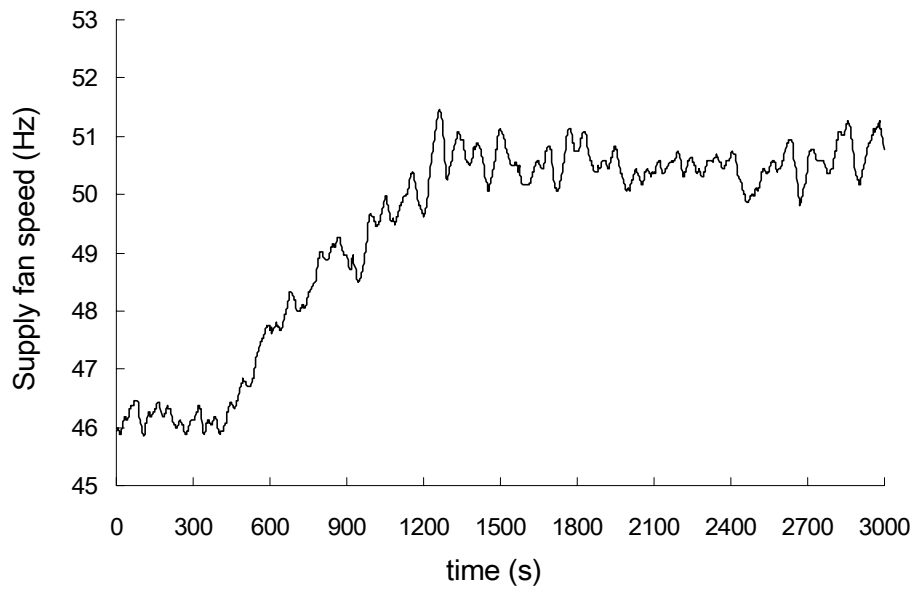


Figure 8.10 Supply fan speed vs. time (Test 01)

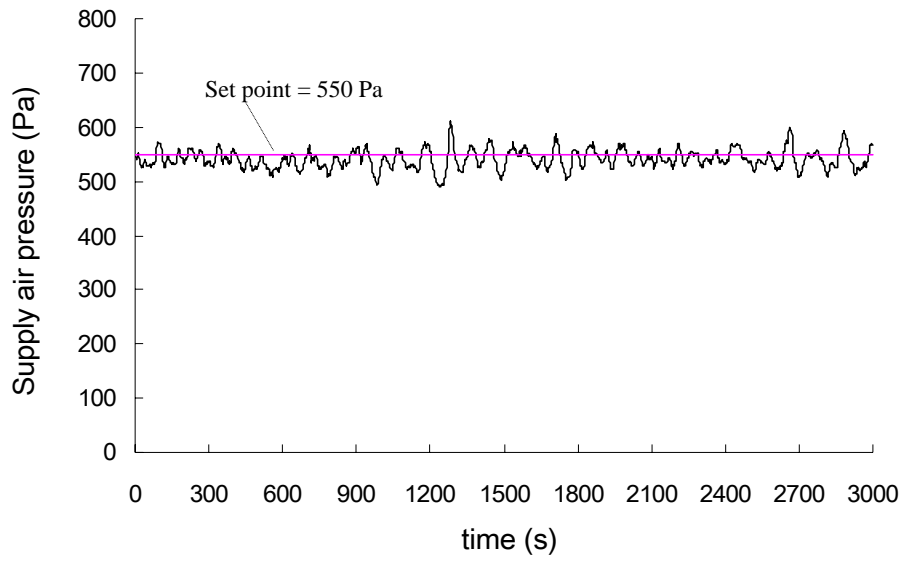


Figure 8.11 Supply air pressure vs. time (Test 01)

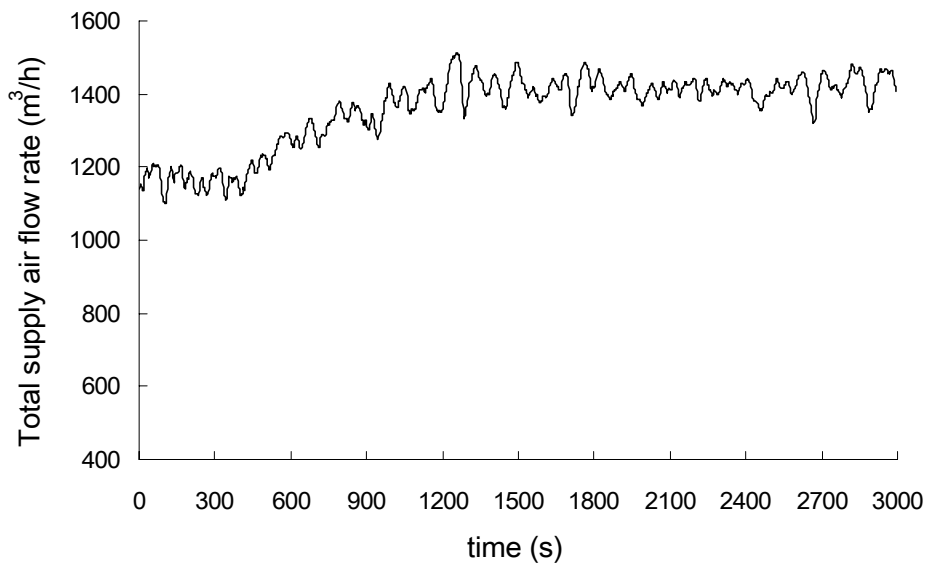


Figure 8.12 Total supply air flow rate vs. time (Test 01)



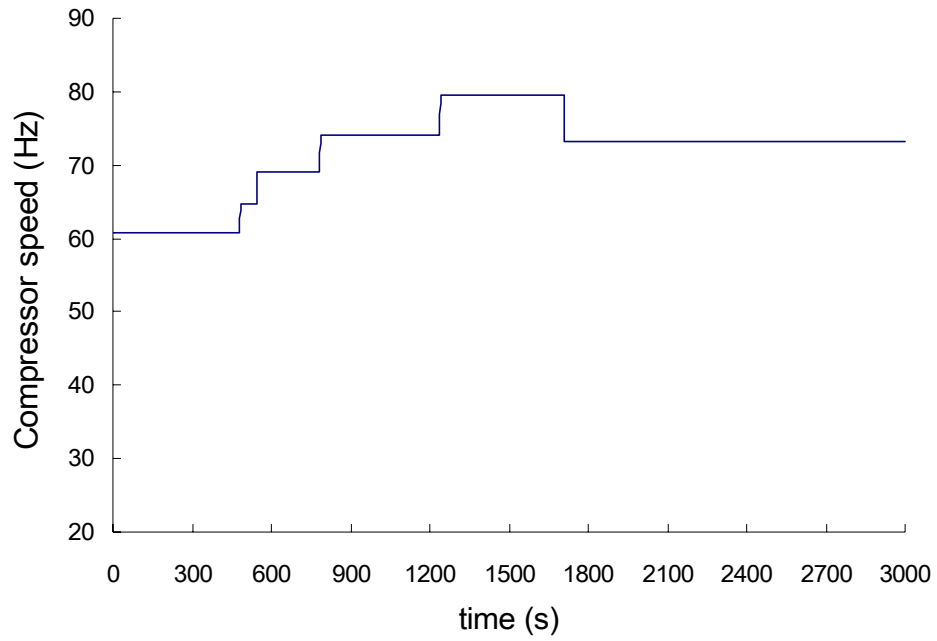


Figure 8.13 Compressor speed vs. time (Test 01)

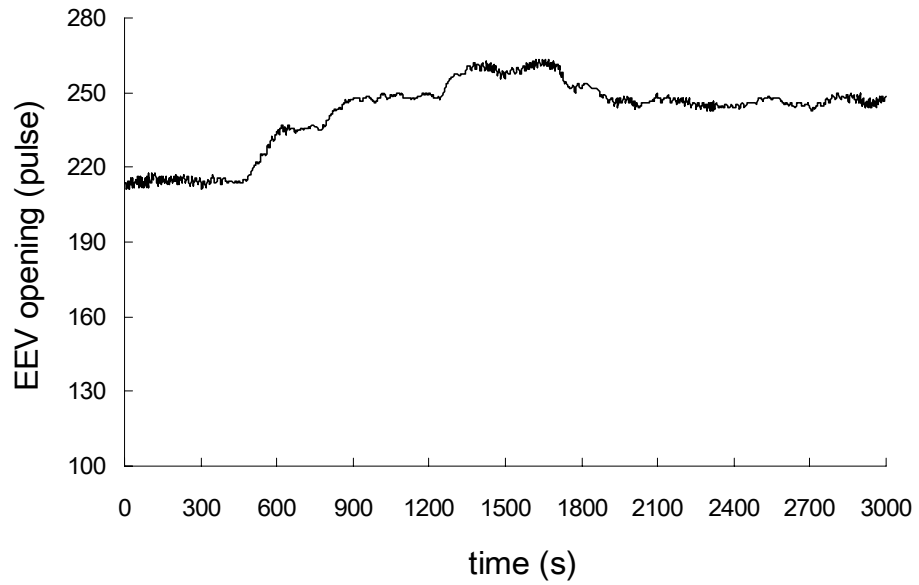


Figure 8.14 EEV opening vs. time (Test 01)

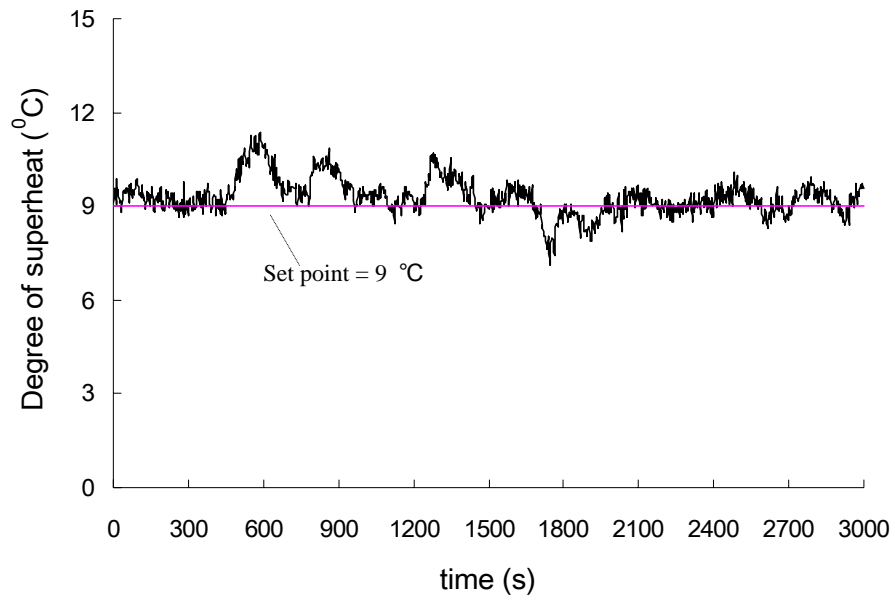


Figure 8.15 Refrigerant superheat at the exit of evaporator vs. time (Test 01)

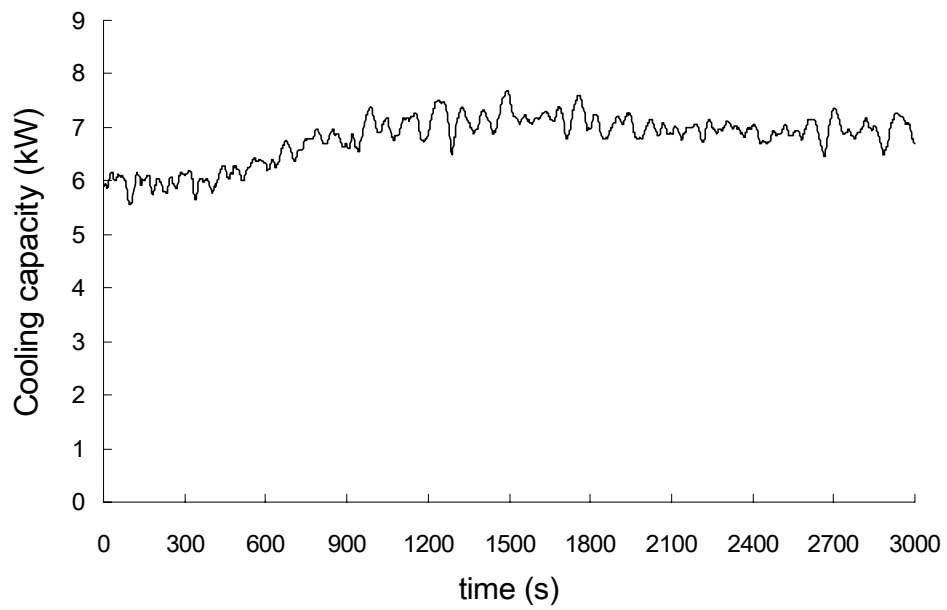


Figure 8.16 Plant's cooling capacity vs. time (Test 01)

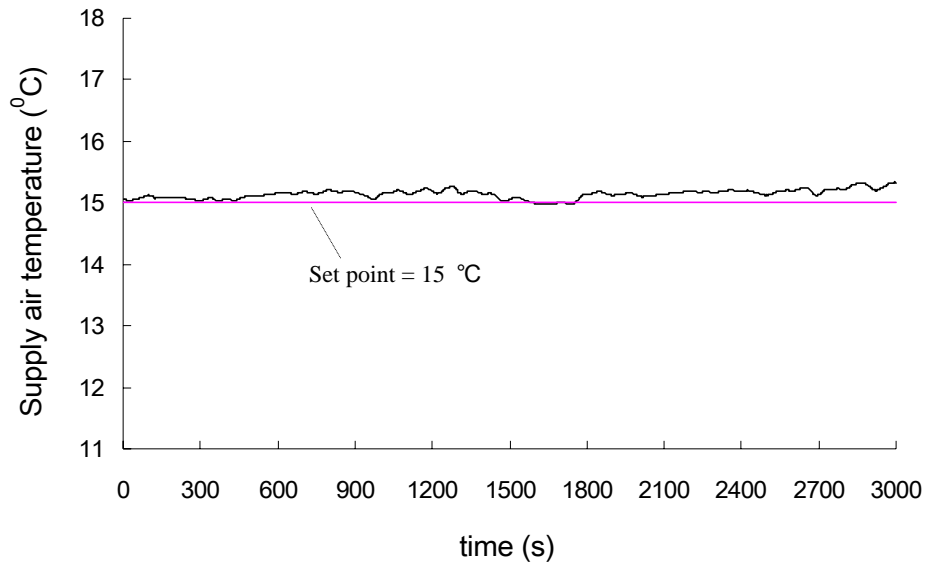


Figure 8.17 Supply air temperature vs. time (Test 01)

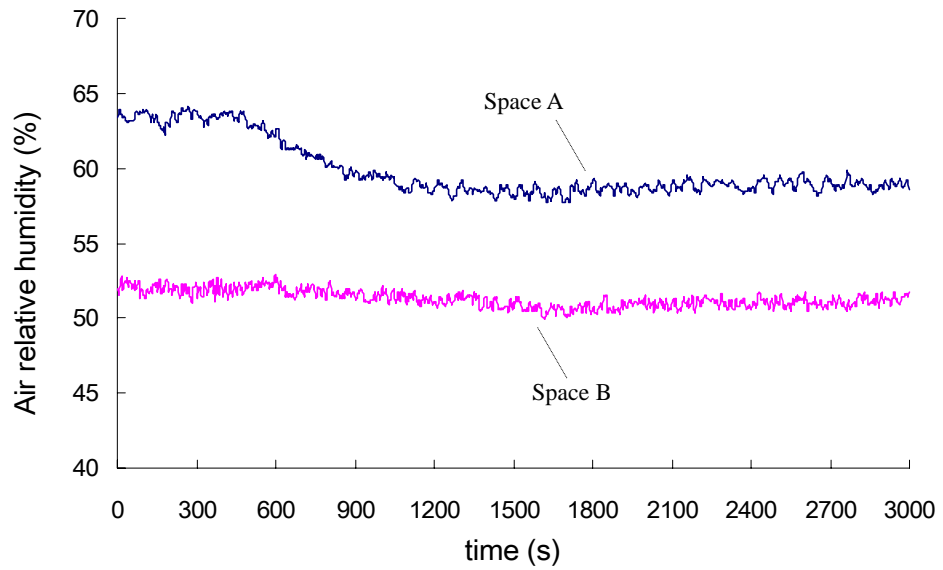


Figure 8.18 Air relative humidity in both Spaces vs. time (Test 01)

### 8.4.2 Results of Test 02

The duration of Test 02 was 2100 seconds. Initially, air temperatures in both Space A and B were stabilized at their respective set points, 23.5 °C and 23 °C. At  $t=420$  s the set point of air temperature in Space A was step changed to 25 °C with all other system's operating conditions kept unchanged. Figures 8.19 to 8.30 depict the responses of the DX VAV A/C system to such a step-change, under the control of the feedforward capacity controller and other existing PI feedback controllers.

Figure 8.19 shows the time-variation of air temperatures in both Space A and B. The responses of the openings of both Terminal A and B are illustrated in Figure 8.20. The opening of Terminal A was 60° at  $t=420$  s. Afterwards it quickly responded to the step-change by reducing its opening to 32° within 30 seconds. Accordingly, its air flow rate was significantly decreased from 670  $m^3/h$  to 350  $m^3/h$ , as shown in Figure 8.21. Meanwhile, as shown in Figures 8.22 and 8.23, the supply fan lowered rapidly its speed for maintaining the set point of supply air static pressure. Although the peak supply air static pressure of 680 Pa occurred at  $t=460$  s, the supply air static pressure was quickly pulled back and well maintained at its set point, with steady deviations of less than  $\pm 40$  Pa.

The large variation of supply air flow rate immediately after  $t=420$  s, as shown in Figure 8.24, called for the compressor to quickly decrease its speed. It can be seen in Figure 8.25 that the feedforward controller responded to suddenly reduce the speed of compressor from the initial 72 Hz (~4320 rpm) to 55 Hz (~3300 rpm) at  $t=460$  s. The significant decrease of supply air flow rate and compressor speed caused the

degree of refrigerant superheat to decrease rapidly, reaching its minimum value of  $5.1\text{ }^{\circ}\text{C}$  at  $t=504\text{ s}$ , as shown in Figure 8.27. Consequently, the EEV was activated by its PI feedback controller to quickly reduce its opening from the initial  $305\text{ pulse}$  in order to maintain the degree of refrigerant superheat at its set point of  $9\text{ }^{\circ}\text{C}$ . The minimum opening of  $261\text{ pulse}$  for the EEV was resulted in at  $t=630\text{ s}$ , as shown in Figure 8.26. Eventually after  $t=1650\text{ s}$  the degree of refrigerant superheat was stabilized at its set point with deviations of less than  $0.8\text{ }^{\circ}\text{C}$ . Overall, the control performance for the degree of refrigerant superheat was satisfactory.

Figure 8.28 shows the time-variation of the output cooling capacity from the DX refrigeration plant. Due to the joint controls for compressor speed and EEV's opening, the plant's cooling capacity decreased rapidly from its initial  $6.8\text{ kW}$  to the minimum  $5.5\text{ kW}$  within  $50\text{ second}$  after the introduction of the step-change. Afterwards, output cooling capacity began to rise slowly. Consequently, the supply air temperature was well controlled at  $15 \pm 0.3\text{ }^{\circ}\text{C}$  without any obvious deviation, as shown in Figure 8.29.

From Figure 8.19 it can be seen that air temperature in Space A increased gradually after its set point was changed. Finally, it was well controlled at its new set point of  $25 \pm 0.15\text{ }^{\circ}\text{C}$ . On the other hand, air relative humidity in Space A was changed from its initial  $60\%$  before the step-change to  $57\%$  after the step-change due to the increase of space air temperature, as shown in Figure 8.30.

When the supply air temperature was controlled at its set point, increased air temperature in Space A would require a lower air flow rate passing through Terminal

A under the new steady-state operation. This was in agreement with the test results depicted in Figure 8.21. Correspondingly, since supply air static pressure was well controlled at its set point throughout the duration of the test, and the opening of Terminal A was finally kept at a lower value of around 43°, as shown in Figure 8.20.

Similar to the results in Test 01, air temperature in Space B, air flow rate and opening of Terminal B were hardly influenced by the action from Terminal A because constant supply air temperature and static pressure were effectively maintained, as shown in Figures 8.19 to 8.21. Independent zoning control using the DX VAV A/C system has been achieved. Air temperature in Space B was well controlled at  $23 \pm 0.15$  °C, with the air relative humidity in Space B maintained at around 51% throughout the test.

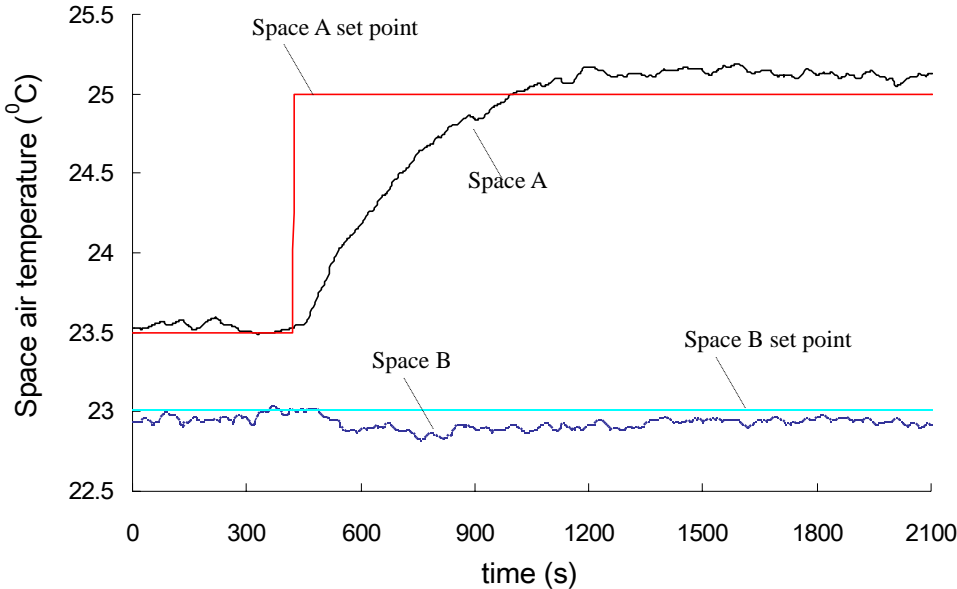


Figure 8.19 Space air temperatures vs. time (Test 02)

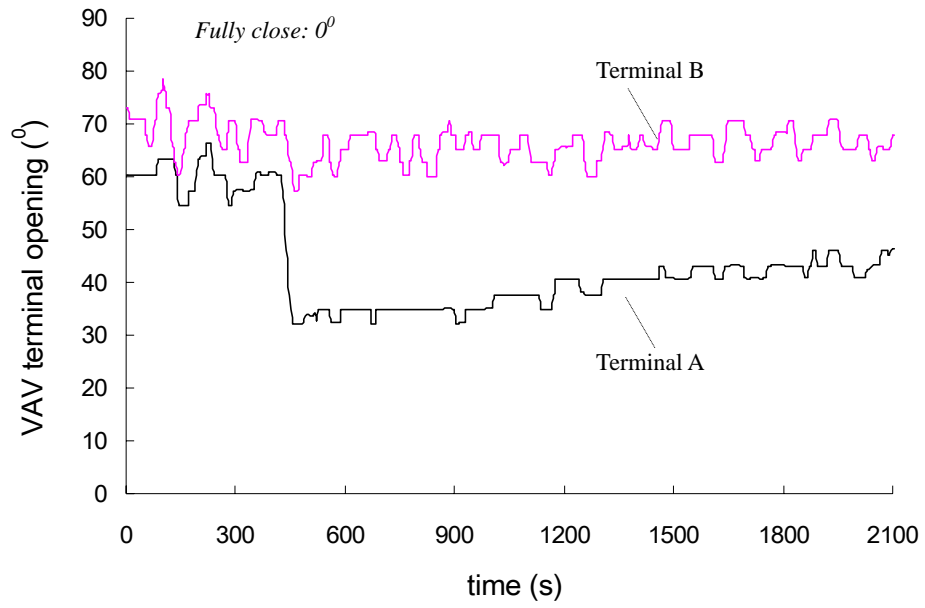


Figure 8.20 VAV terminal openings vs. time (Test 02)

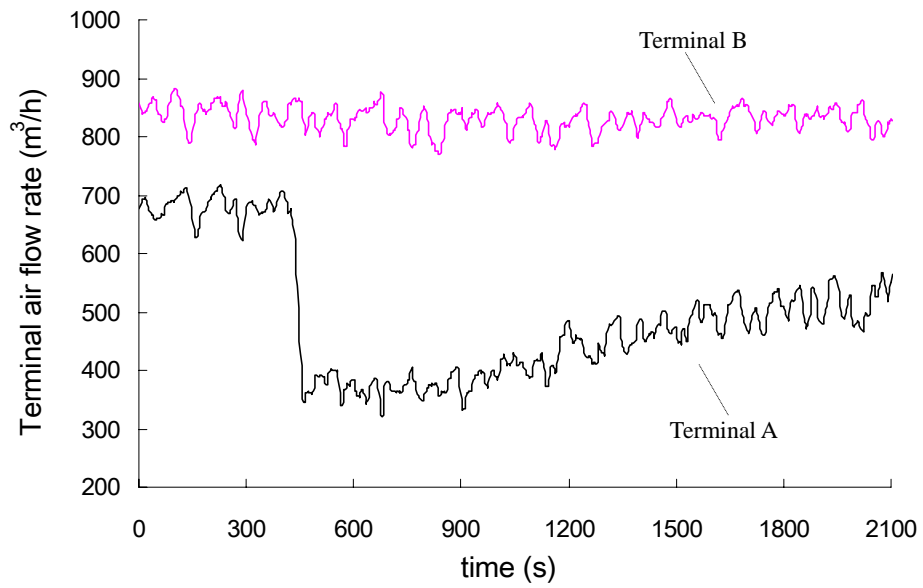


Figure 8.21 VAV terminal air flow rates vs. time (Test 02)

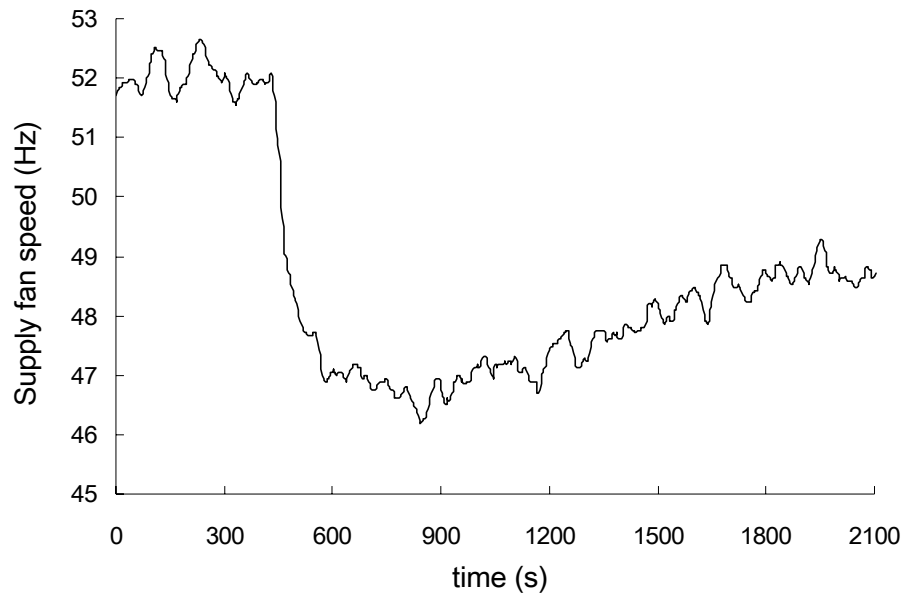


Figure 8.22 Supply fan speed vs. time (Test 02)

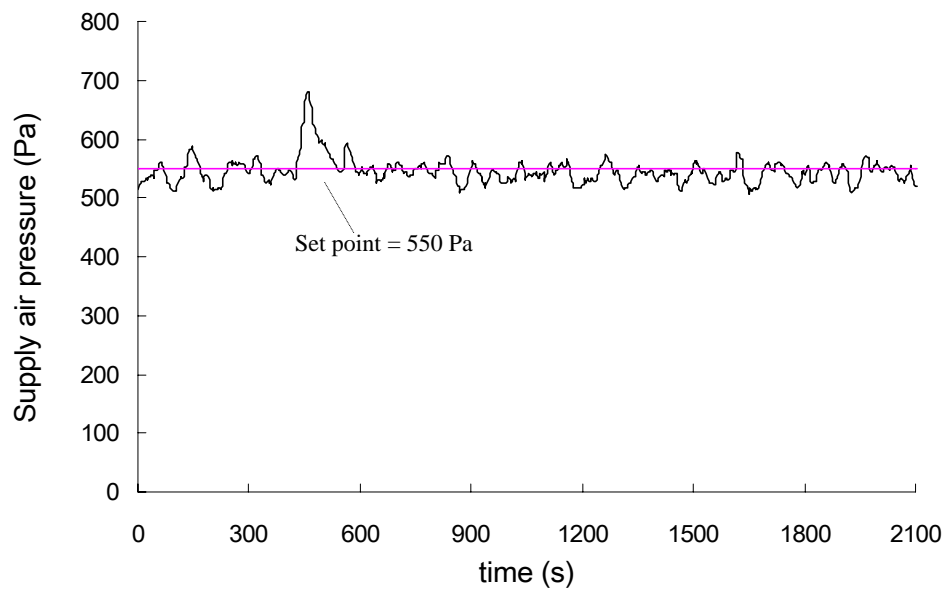


Figure 8.23 Supply air pressure vs. time (Test 02)



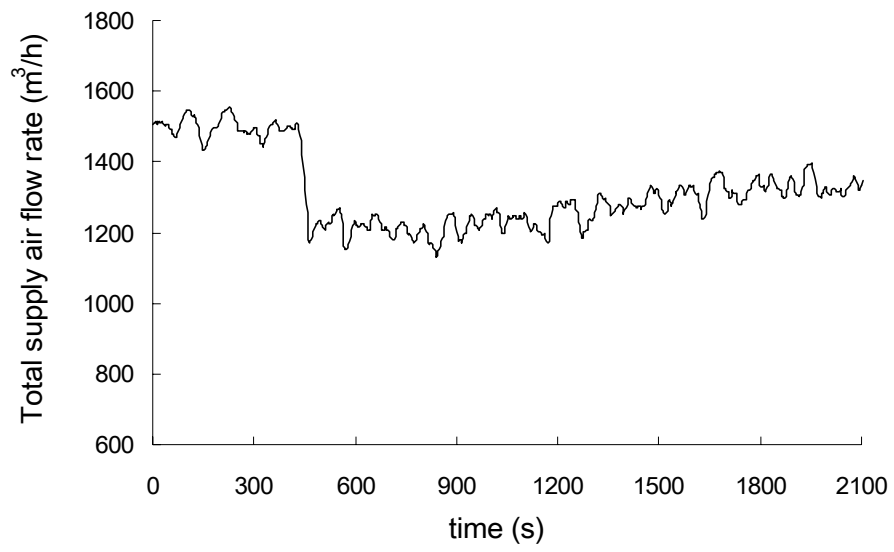


Figure 8.24 Total supply air flow rate vs. time (Test 02)

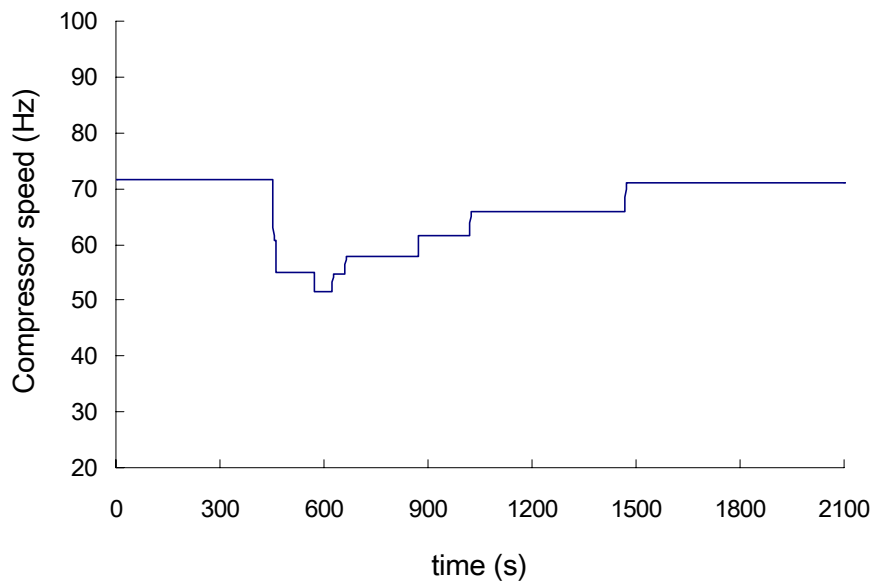


Figure 8.25 Compressor speed vs. time (Test 02)

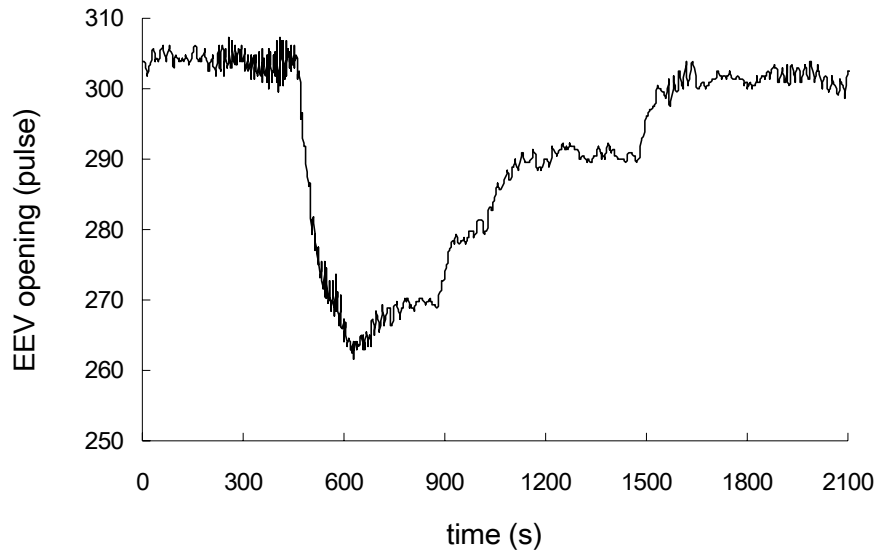


Figure 8.26 EEV opening vs. time (Test 02)

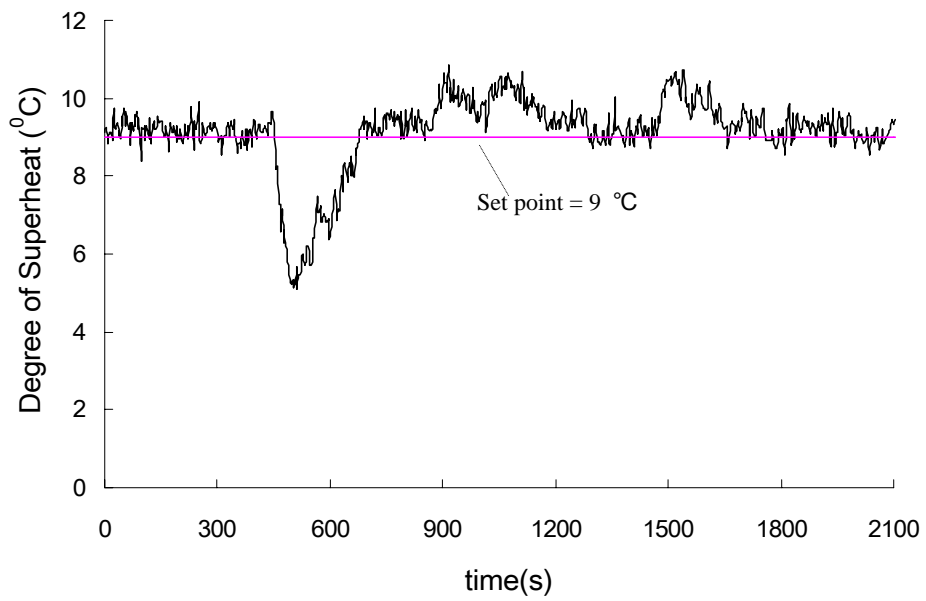


Figure 8.27 Refrigerant superheat at the exit of evaporator vs. time (Test 02)

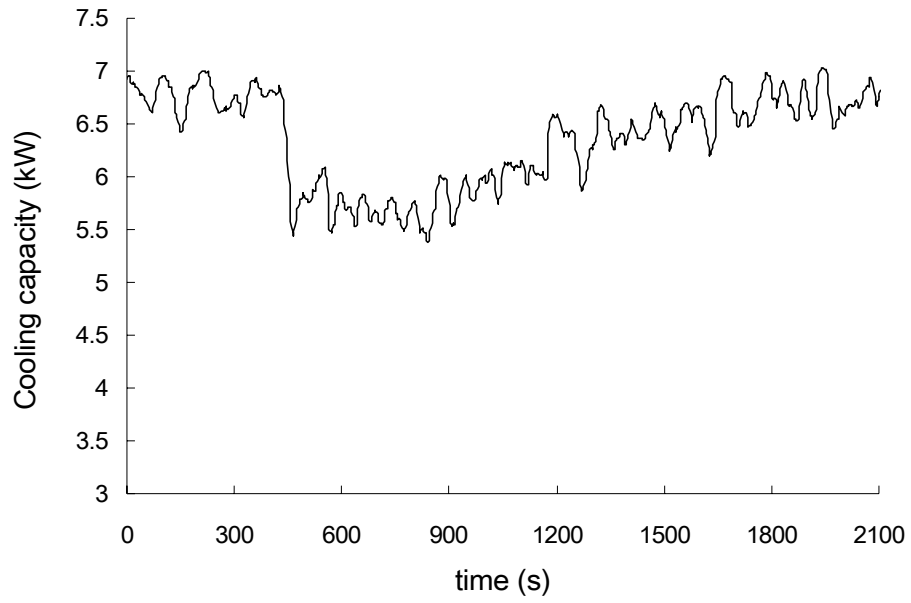


Figure 8.28 Plant's cooling capacity vs. time (Test 02)

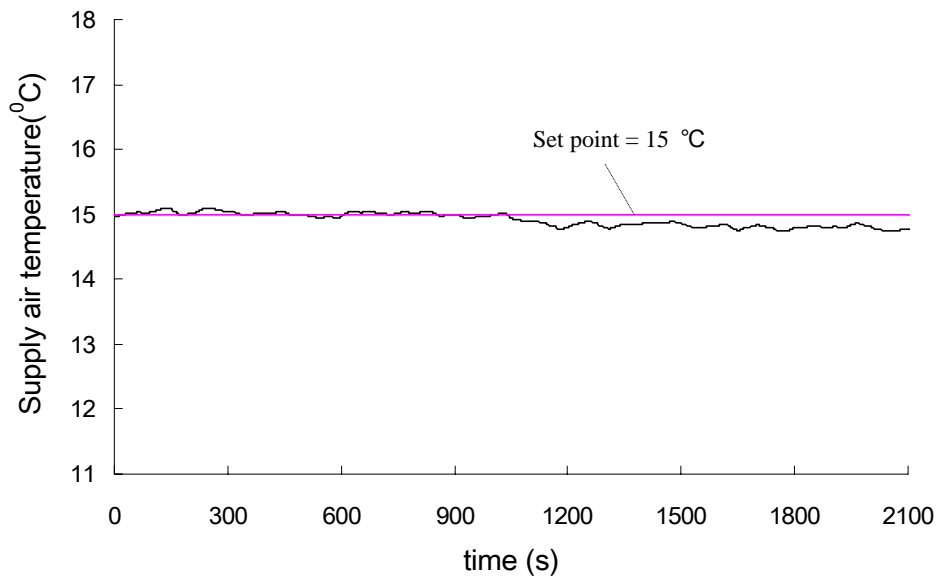


Figure 8.29 Supply air temperature vs. time (Test 02)

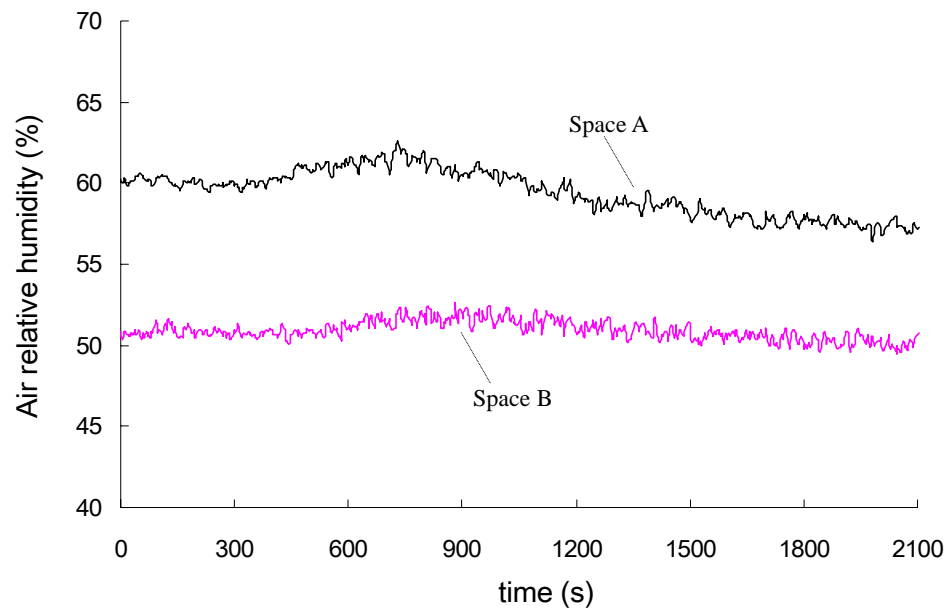


Figure 8.30 Air relative humidity in both Spaces vs. time (Test 02)

## 8.5 Summary

By applying the powerful ability of real-time measuring, computation and communications of DDC technology, a novel feedforward capacity controller has been successfully developed for the experimental DX VAV A/C system. Compressor speed was regulated by the feedforward controller, for matching the output cooling capacity from the DX refrigeration plant with the varying cooling load in the VAV air-distribution sub-system. The feedforward controller consisted of both a NCA, which was fundamentally based on the principle of energy balance using a number of real-time measured system's operating parameters, and a dead-band for decoupling the two controllers for compressor speed and EEV's opening.

The EEV was controlled by a conventional PI controller in response to the change of degree of refrigerant superheat at DX coil's exit. The compressor's feedforward controller, coordinated with the EEV's PI feedback controller, continuously regulated the output cooling capacity from the DX refrigeration plant. In the VAV air-distribution sub-system, controls for supply air static pressure, air flow rate of VAV terminals and space air temperatures were all achieved using conventional PI feedback controllers.

The novel feedforward capacity controller was implemented in the experimental DX VAV A/C rig described in Chapter 4. Controllability tests for the feedforward controller have been carried out, and the results of two tests were reported and discussed in this chapter. Test 01 was for investigating the system's response to a step-change in space cooling load, and Test 02 to the step-change in the set point of indoor air temperature.

The results of the controllability tests showed that using the feedforward capacity controller together with other conventional PI controllers, the controls of supply air temperature, supply air static pressure, space air temperatures were all highly satisfactory. External disturbances of significant amplitudes can be effectively counteracted by the pre-emptive action of compressor speed. Therefore, the novel feedforward capacity controller has been proved to be workable and advantageous. This opened up a new approach for studying the control for DX VAV A/C systems. On the other hand, because the feedforward controller for compressor speed is developed based on the energy balance of a DX evaporator, such a controller is

expected to be significantly advantageous with respect to control robustness, compared to conventional feedback controllers based on controlled objects' transfer functions.

## **Chapter 9**

### **Conclusions and future work**

#### **9.1 Conclusions**

A DX VAV A/C system consists of a direct expansion (DX) refrigeration plant and a variable-air-volume (VAV) air-distribution sub-system. The evaporator in the DX refrigeration plant is used directly as the DX cooling coil in the VAV air-distribution sub-system to simultaneously cool and dehumidify the air passing through the DX cooling coil. Compared to conventional chilled-water based central A/C systems, a DX VAV A/C system is more energy efficient, owing to a higher evaporating temperature in the DX refrigeration plant and a lower fan power consumption during part-load operations. It can therefore help reduce peak power demand. Furthermore, a DX VAV A/C system generally costs less to own and maintain.

##### **9.1.1 The problem encountered**

However, the difficulty in accurately matching the output cooling capacity from its DX refrigeration plant with the varying cooling load in its VAV air-distribution sub-system has been the main deterrence to the wide application of a DX VAV A/C system. Capacity control methods currently adopted by DX VAV A/C systems, such as on-off cycling refrigeration plant, hot-gas bypass and staging-control, were not totally satisfactory because of either poor control accuracy or poor energy efficiency. The advanced variable-refrigerant-volume (VRV) technology has been recognized to

be a promising way to solve the capacity-load matching problem for a DX VAV A/C system. The use of both a variable-speed compressor and an EEV in its DX refrigeration plant could help a DX VAV A/C system to realize an accurate capacity control so that a stable control of supply air temperature, which is critical for normal operation for a VAV A/C system, could be achieved.

### **9.1.2 The experimental rig and dynamic mathematical model developed**

In order to study the operating performance of a DX VAV A/C system having a variable-speed compressor and an EEV, and to develop suitable capacity control strategies to address the problem of capacity-load matching, an experimental rig and a dynamic mathematical model have been developed for the experimental DX VAV A/C system with two conditioned spaces.

The experimental rig has been set up in the HVAC Laboratory of The Hong Kong Polytechnic University. The experimental rig consisted of a DX refrigeration plant having a variable-speed rotor compressor and an EEV, and a VAV air-distribution sub-system including two identical conditioned spaces respectively, served by two pressure-independent VAV terminals. Using high-accuracy measuring sensors and a computerized data acquisition system, a large number of operating parameters can be real-time measured, monitored and curve-data displayed. Twelve conventional PI controllers were provided in the experimental rig so that any required experimental operating conditions could be created. A logging & control (L&C) supervisory program has been developed specifically for this experimental rig using the



LabVIEW programming platform. An independent self-programming module (SPM) by which new algorithms may be implemented through programming was available in the L&C program.

A representative dynamic mathematical model has been developed for the experimental DX VAV A/C system. The complete dynamic model for the experimental DX VAV A/C system consisted of two constituent sub-models for its DX refrigeration plant and its VAV air-distribution sub-system, respectively. The model is component-based and of partial-lumped-parameter type. It took into account the dynamic behaviors of both the DX refrigeration plant and the VAV air-distribution sub-system simultaneously. The dynamic model has been developed based on the principle of mass and energy conservation, and using the correlations describing the operational performance of various components in the experimental DX VAV A/C system, which were either field-tested or available from manufacturers. Mathematical correlations representing the control logics of various controllers were also included. The dynamic model so developed was expected to be very useful in understanding the transient behaviors of, and in developing advanced control strategies for, DX VAV A/C systems.

### **9.1.3 Model validation and simulated closed-loop responses**

The complete dynamic model for the experimental DX VAV A/C system has been experimentally validated using the experimental rig. Experimental work to obtain the open-loop responses of the DX refrigeration plant after being subjected to step

changes in its major operating parameters has been carried out. Experimental open-loop responses for all major operational parameters from the DX plant agreed well with the simulated open-loop responses from the dynamic sub-model representing the DX refrigeration plant, suggesting that the dynamic model has been successfully experimentally validated.

Using the validated model, the simulated closed-loop responses of the experimental DX VAV A/C system with its conventional proportional-integral (PI) control loops enabled, after being subjected to step changes in space internal cooling load and indoor air temperature set-point, have been studied. The closed-loop responses obtained suggested that the validated dynamic model would behave in a similar manner to that a real DX VAV A/C system would, when all its control loops were enabled. This further confirmed that the model developed was correct and could be helpful for studying control issues for DX VAV A/C systems.

#### **9.1.4 Novel feedforward capacity controller**

Taking the advantages of the powerful calculation and processing capacity of DDC technology, a novel feedforward capacity controller has been developed for the experimental DX VAV A/C system. Compressor speed was regulated by the feedforward controller, for matching the output cooling capacity from the DX refrigeration plant with the varying cooling load in the VAV air-distribution subsystem. The feedforward controller consisted of both a numerical calculation algorithm (NCA), which was fundamentally based on the principle of energy balance

using a number of real-time measured system's operating parameters, and a dead-band for decoupling the control actions from both the feedforward capacity controller and the conventional PI feedback controller for regulating the opening of the EEV.

The novel feedforward capacity controller has been implemented in the experimental rig; and controllability tests have been carried out. The results of the controllability tests showed that using the feedforward controller in conjunction with other conventional PI feedback controllers in the DX VAV A/C system, the control performance for supply air temperature, supply air static pressure, space air temperatures were all highly satisfactory. On the other hand, using the feedforward controller, external disturbances of significant amplitudes can be effectively counteracted by the pre-emptive action of compressor speed. Therefore, the novel feedforward capacity controller has been proved to be workable and advantageous. The successful development of the feedforward capacity controller has opened up a new approach for studying the control for DX VAV A/C systems.

#### **9.1.5 Main contributions**

In this thesis, a complete dynamic mathematical model for a DX VAV A/C system has been developed for the first time. With the model developed, the dynamic behaviors of a DX VAV A/C system can be thoroughly investigated and new control strategies proposed and tested. With the aid of modeling and experimental work, a novel feedforward capacity controller has been proposed and experimentally tested,

so that the problem of accurate capacity-load matching, which has been the main deterrence to the wide application of DX VAV A/C systems, has been solved.

The following are the long term academic and industrial significances for the outcomes of the thesis:

- The complete dynamic mathematical model developed would provide researchers in the field of air conditioning and refrigeration with a powerful tool in studying the inherent behaviors of, and in improving design and control of a DX VAV A/C system. The model developed may also be integrated into those well-known large building energy simulation packages such as EnergyPlus, etc.
- The novel capacity controller developed can help pave the way for large-scaled applications for DX VAV A/C systems, so that the energy utilization efficiency for building air conditioning can be significantly improved, contributing substantially to the sustainable development.

## **9.2 Proposed future work**

It is noted that the accuracy of an HVAC system model depends, to a certain extent, on the accuracy of its components models. With the continuing development of the models for system components, the dynamic mathematical model developed for the experimental DX VAV A/C system and reported in this thesis should be updated accordingly. For example, a better model for a conditioned space, which can both accurately reflect the real-time influence from the changes in an ambient

environment on the system's cooling load and properly account for the thermal storage of the space envelope and furniture, should be preferred so as to further improve the overall accuracy of dynamic modeling.

Although the novel feedforward capacity controller for the experimental DX VAV A/C system has been successfully developed, more case studies should be undertaken to explore its advantages over other existing conventional capacity controllers for DX VAV A/C systems. Moreover, the feedforward controller developed may be further refined by using an optimized dead-band or by applying fault-detection-diagnosis techniques for regulating compressor speed, so that its reliability and robustness can be further strengthened. On the other hand, the results obtained from controllability experiments could also be used to further verify the robustness of the mathematical model developed for the DX VAV A/C system.

## References

1. AEC 1989  
Alternative Energy Corporation  
*Industrial energy savers-chiller optimization and energy efficient chillers.*  
North Carolina: Alternative Energy Corporation (1989)
2. Ahemd et al. 1998a  
Ahmed O., Mitchell J. W., Klein S.A.  
Feedforward-feedback controller using general regression neural network (GRNN) for laboratory HVAC system, Part I - pressure control. *ASHRAE Trans.*, Vol. 104, part 2, pp. 613-625 (1998)
3. Ahemd et al. 1998b  
Ahmed O., Mitchell J. W., Klein S. A.  
Feedforward-feedback controller using general regression neural network (GRNN) for laboratory HVAC system, part II: cooling control. *ASHRAE Trans.*, Vol. 104, part 2, pp. 626-633 (1998)
4. Ahemd et al. 1998c  
Ahmed O., Mitchell J. W., Klein S. A.  
Feedforward-feedback controller using general regression neural network (GRNN) for laboratory HVAC system, part III: heating control. *ASHRAE Trans.*, Vol. 104, part 2, pp. 634-642 (1998)
5. Ahmed 1991  
Ahmed O.  
DDC applications in variable-water-volume systems. *ASHRAE Trans.*, Vol. 97, part 2, pp. 751-758 (1991)
6. Alcalá et al. 2005  
Alcalá R., Casillas J., et al.  
A genetic rule weighting and selection process for fuzzy control of heating, ventilating and air conditioning systems. *Engineering Applications of Artificial Intelligence*, Vol. 18, No. 3, pp. 279-296 (2005)
7. Andrade and Bullard 2002  
Andrade M. A., Bullard C. W.  
Modulating blower and compressor capacities for efficient comfort control. *ASHRAE Trans.*, Vol. 108, part 1, pp. 63-67 (2002)
8. Angelov 2003  
Angelov P. P.  
An evolutionary approach to fuzzy rule-based model synthesis using indices for rules. *Fuzzy Sets and Systems*, Vol.137, No. 3, pp. 325-338 (2003)

9. ASHRAE 2000  
ASHRAE  
*ASHRAE Handbook: HVAC systems and equipment*. American Society of Heating, Refrigerating and Air-conditioning Engineers, Inc., Atlanta, USA, (2000)
  
10. ASHRAE 2001  
ASHRAE  
*ASHRAE Handbook: Fundamentals*. American Society of Heating, Refrigerating and Air-conditioning Engineers, Inc., Atlanta, USA, (2000)
  
11. Atkinson 1987  
Atkinson G. V  
Rooftop variable air volume control. *Consulting-specifying Engineer*, Vol.1, No.3, pp. 93-98 (1987)
  
12. Avery 1996  
Avery G.  
Control of VAV systems with DX cooling: A digital to analog conversion. *ASHRAE Journal*, Vol. 38, No. 2, pp. 59-61 (1996)
  
13. Baughn and Roby 1992  
Baughn J. W., Roby J. L.  
Enhanced turbulent heat transfer in circular ducts with transverse ribs. *American Society of Mechanical Engineers, Heat Transfer Division, (Publication) HTD, Vol. 202, Enhanced Heat Transfer*, pp. 9-15 (1992)
  
14. Bensafi et al. 1997  
Bensafi A., Borg S., Parent D.  
CYRANO: a computational model for the detailed design of plate-fin-and-tube heat exchangers using pure and mixed refrigerant. *Int J. Refrig.*, Vol. 20, No. 3, pp. 218-228 (1997)
  
15. Bordick and Gilbride 2002  
Bordick J., Gilbride T. L.  
Focusing on buyer's needs: DOE's engineering technology programme. *Energy Engineering*, Vol. 99, No. 6, pp. 18-38 (2002)
  
16. Browne and Bansal 2002  
Browne M. W., Bansal P. K. Transient simulation of vapour-compression packaged liquid chillers. *Int. J. Refrig.*, Vol. 25, No. 5, pp. 597-610 (2002)
  
17. Carrado and Mazza 1991  
Carrado V., Mazza A.  
*Axial fan*. IEA Annex 17 Report, Politecnico di Torino, Italy (1991)

18. Cavallini et al. 2001  
Cavallini A., Censi G., Delcol D., et al.  
Experimental investigation on condensation heat transfer and pressure drop of new HFC refrigerants (R134a, R125, R32, R410A, R236ea) in a horizontal smooth tube. *Int. J. Refrig.*, Vol. 24, No. 1, pp. 73-87 (2001)
19. Chan and Halselden 1981a  
Chan C. Y., Haselden G. G.  
Computer-based refrigerant thermodynamic properties, Part 1: Basic equations. *Int. J. Refrig.*, Vol. 4, No. 4, pp. 7-12 (1981)
20. Chan and Halselden 1981b  
Chan C. Y., Haselden G. G.  
Computer-based refrigerant thermodynamic properties, Part 2: Program listings. *Int. J. Refrig.*, Vol. 4, No. 4, pp. 52-60 (1981)
21. Chan and Halselden 1981c  
Chan C. Y., Haselden G. G.  
Computer-based refrigerant thermodynamic properties, Part 3: Use of the program in the computation of standard refrigerant cycles. *Int. J. Refrig.*, Vol. 4, No. 4, pp.131-134 (1981)
22. Chen 1999  
Chen W.  
*Research on the characteristic and control strategy of multi-evaporator VRV air conditioning system*. Master thesis, Shanghai Jiao Tong University, China [In Chinese] (1999)
23. Chen et al. 2005  
Chen W., Zhou X., Deng S. M.  
Development of control method and dynamic model for multi-evaporator air conditioner (MEAC). *Energy conversion and management*, Vol. 46, No. 3, pp. 451-465 (2005)
24. Chi and Didion 1982  
Chi J., Didion D.  
A simulation model of the transient performance of a heat pump. *Int. J. Refrig.*, Vol. 5, No. 3, pp. 176-184 (1982)
25. Clark, 1985  
Clark D. R., Hurley C. M., Hill C. R.  
Dynamic models for HVAC system components. *ASHRAE Trans.*, Vol. 91 part 1B, pp. 737-751 (1985)
26. Cleland 1986  
Cleland A. C.  
Computer sub-routines for rapid evaluation of refrigerant thermodynamic properties. *Int. J. Refrig.*, Vol. 9, No. 9, pp.346-351 (1986)



27. Cleland 1994  
Cleland A. C.  
Polynomial curve-fits for refrigerant thermodynamic properties: extension to include R134a. *Int. J. Refrig.*, Vol. 17, No. 4, pp. 245-249 (1994)
28. Coad 1984  
Coad W. J.  
DX problems with VAV. *Heating/Piping/Air Conditioning*, Vol. 56, No. 1, pp. 134-139 (1984)
29. Coad 1996  
Coad W. J.  
Indoor Air Quality: A Design Parameter. *ASHRAE Journal*, Vol. 38, No. 6, pp. 39-47 (1986)
30. Corberan and Melon 1998  
Corberan J. M., Melon M. C.  
Modeling of plate finned tube evaporators and condensers working with R134a. *Int. J. Refrig.*, Vol. 21, No. 4, pp. 273-284 (1998)
31. Damasceno and Rooke 1990  
Damasceno G. S., Rooke S. P.  
Comparison of three steady-state heat pump computer models. *ASHRAE Trans.*, Vol. 96, part 2, pp. 191-204 (1990)
32. Davidge 1991  
Davidge B.  
Demand controlled ventilation in office buildings. *Proceeding of 12th AIVC conference*, AIVC, pp. 105-111(1991)
33. Deng 2000  
Deng S. M.  
A dynamic mathematical model of a direct expansion (DX) water-cooled air conditioning plant. *Building and Environment*, Vol. 35, No. 7, pp. 603-613 (2000)
34. Deng 2002  
Deng S. M.  
The application of feedforward control in a direct expansion (DX) air conditioning plant. *Building and Environment*, Vol. 37, No. 1, pp. 35-40 (2002)
35. Desta et al. 2005  
Desta T. Z., Brecht A. V., et al.  
Modelling and control of heat transfer phenomena inside a ventilated air space. *Energy and Buildings*, Vol. 37, No. 7, pp. 777-786 (2005)

36. Ding et al. 1992  
Ding G. L., Zhang C., Li H.  
Polynomial curve-fitting method for refrigerant thermodynamic saturation properties. *Journal of Shanghai Jiao Tong University*, Vol. E-4, No. 2, pp.73-77 (1992) [In Chinese]
37. Domanski 1991  
Domanski P. A.  
Simulation of an evaporator with nonuniform one-dimensional air distribution. *ASHRAE Trans.*, Vol. 97, part 1, pp. 793-802 (1991)
38. Domanski and McIinden 1992  
Domanski, P., McIinden M.  
A simplified cycle simulation model for the performance rating of refrigerants and refrigerant mixtures. *Int. J. Refrig.*, Vol. 15, No. 2, pp.81-88 (1992)
39. Donnini et al. 1991  
Donnini G., Haghihghat F., et al.  
Ventilation control of indoor air quality, thermal comfort and energy conservation by carbon dioxide measurement. *Proceeding of 12th AIVC conference*, AIVC, pp. 311-331 (1991)
40. Doty 2001  
Doty S.  
Applying DX equipment in humid climates. *ASHRAE Journal*, Vol. 43, No.3, pp. 30-34 (2001)
41. Dutta and Yanagisawa 2001  
Dutta A.K., Yanagisawa T, et al.  
An investigation of the performance of a scroll compressor under liquid refrigerant injection, *Int. J. Refrig.*, Vol. 24, No. 6, pp. 577-587 (2001)
42. Englander and Norford 1992  
Englander, S., Norford L.  
Saving fan energy in VAV systems - part 2: supply fan control for static pressure minimization using DDC zone feedback. *ASHRAE Trans.*, Vol. 98, part 1, pp. 19-32(1992)
43. EnergyPlus 2004  
<http://www.eere.energy.gov/buildings/energyplus/>
44. Eric et al. 2002  
Eric W., Saavedra O. C., et al.  
Experimental analysis and simplified modeling of a hermetic scroll refrigeration compressor. *Applied Thermal Engineering*, Vol. 22, No. 2, pp.107-120 (2002)

45. Gray and Webb 1986  
Gray D.L., Webb R.L.  
Heat transfer and friction correlations for plate finned-tube heat exchangers having plain fins. *Proc. of The Eighth International Heat Transfer Conference*, San Francisco: American Society of Mechanical Engineers (1986)
46. Haessig 1995  
Haessig D.L.  
A solution for DX VAV air handlers. *Heating/Piping/Air Conditioning*, Vol. 67, No. 5, pp. 83-86 (1995)
47. He et al. 2005  
He M., Cai W. and Li S.  
Multiple fuzzy model-based temperature predictive control for HVAC systems. *Information Sciences*, Vol. 169, No.1, pp. 155-174 (2005)
48. Hesse and Kruse 1988  
Hesse U., Kruse H.  
Prediction of the behavior of oil refrigerant mixtures. *Proceedings of the Purdue Refrigeration Conference*, Purdue University (1988)
49. Hong and Webb 1996  
Hong T. K., Webb R. L.  
Calculation of fin efficiency for wet and dry fins. *Int. J. HVAC&R Research*, Vol. 2, No. 1, pp. 27-41 (1996)
50. Hong and Jiang 1997  
Hong T. Z., Jiang Y.  
A new multizone model for the simulation of building thermal performance. *Building and Environment*, Vol. 32, No. 2, pp. 123-128 (1997)
51. House 1995  
House J. M.  
System approach to optimal control for HVAC and building systems. *ASHRAE Trans.*, Vol. 101, part 2, pp. 647-660 (1995)
52. Hung 1999  
Hung C.Y.S., Lam H.N., Dunn A.  
Dynamic performance of an electronic zone air temperature control loop in a typical variable-air-volume air conditioning system. *Int. J. HVAC&R Research*, Vol. 5, No. 4, pp. 317-337 (1999)
53. International Institute of Refrigeration 1992  
International Institute of Refrigeration  
Booklet on R134a. *International Institute of Refrigeration*, Paris, France (1992)

54. Jabobs 2002  
Jabobs P.C.  
Sizing single-package rooftop units for optimum performance. *HPAC Engineering*, Vol. 74, No. 8, pp. 57-60 (2002)
  
55. Jacob et al. 1987  
Jacob F.E., Fisher R.D. and Flanigan L.J.  
Experimental validation of the duct sub-model for the SP43 simulation model. *ASHRAE Trans.*, Vol. 93, part 1, pp. 1499-1514 (1987)
  
56. Janu et al. 1995  
Janu, G. J., Wenger J. D., et al.  
Outdoor air flow control for VAV systems. *ASHRAE Journal*, Vol. 37, No.4, pp. 62-68 (1995)
  
57. Jabardo et al. 2002  
Jabardo J.M.S., Mamani W.G. and Ianella M.R. Modeling and experimental evaluation of an automotive air conditioning system with a variable capacity compressor. *Int. J. Refrig.* Vol. 25, No. 8, pp. 1157-1172 (2002)
  
58. Jolly et al. 1990  
Jolly P., Jia X., Clements S.  
Heat pump assisted continuous drying, Part 1: simulation model. *Int. J. Energy Research*, Vol. 14, No. 7, pp. 757-770 (1990)
  
59. Jolly et al. 2000  
Jolly P. G., Tso C. P., et al.  
Simulation and measurement on the full-load performance of a refrigeration system in a shipping container. *Int. J. Refrig.*, Vol. 23, No. 2, pp. 112-126, (2000)
  
60. Kalman 1995  
Kalman I. K., Sui L., et al.  
Temperature and humidity control during cooling and dehumidifying by compressor and evaporator fan speed variation. *ASHRAE Trans.*, Vol. 101, part 1, pp. 292-304 (1995)
  
61. Kandlikar 1990  
Kandlikar S. G.  
A general correlation for saturated two-phase flow boiling heat transfer inside horizontal and vertical tubes. *Journal of Heat Transfer*, Vol. 112, No. 2, pp.219-228 (1990)
  
62. Kays and London 1984  
Kays W. M., London A. L.  
*Compact heat exchangers*. McGraw-Hill Book Company, New York, U.S.A. (1984)

63. Kenneth 1997  
Kenneth E. G.  
Rooftop HVAC. *HPAC Engineering*, Vol. 69, No. 7, pp. 51-55 (1997)
64. Khattar 1999  
Khattar M.  
Impact of HVAC control improvement on supermarket humidity levels. *ASHRAE Trans.*, Vol. 105, part 1, pp. 521-532 (1999)
65. Khoo and Levermore 1998  
Khoo I., Levermore G. J., et al.  
Variable-air-volume terminal units II: dynamic model. *Building Services Engineering Research & Technology*, Vol. 19, No. 3, pp. 163-169 (1998)
66. Klein et al. 1990  
Klein S.A., et al.  
*TRNSYS: A transient system simulation program*, Version 13.1. University of Wisconsin-Madison, U.S.A (1990)
67. Klein 1994  
Klein S. A.  
*TRNSYS reference manual*, Type 31: pipe or duct. pp. 4.5.41-4.5.45 (1994)
68. Kirkman 1984  
Kirkman W. M.  
Benefits of using direct expansion air conditioning systems with rotary screw compressors. *Plant Engineering*, Vol. 38, No. 22, pp. 43-45 (1984)
69. Koury et al. 2001  
Koury R. N. N., Machado L. and Ismail K. A. R. Numerical simulation of a variable speed refrigeration system. *Int J Refrig.* Vol.24, No.2, pp. 192-200 (2001)
70. Lam 2000  
Lam C. J.  
Energy analysis of commercial buildings in subtropical climates. *Building and Environment*, Vol. 35, No. 1, pp. 19-26 (2000)
71. LBL 1982  
Lawrence Berkeley Laboratory  
*LBL: DOE-2, Engineering Manual*, Version 2.1e. Lawrence Berkeley Laboratory, Berkeley, CA (1982)
72. Lebrun 1995  
Lebrun J.  
Bring simulation to application. *Final proposal for IEA Annex 30*, University of Liege, Belgium (1995)

73. Legg 1986  
Legg R. C.  
Characteristics of single and multi-blade dampers for ducted air systems. *Building Services Engineering Research & Technology*, Vol. 7, No. 4, pp. 129-145 (1986)
74. Lenarduzzi and Yap 1998  
Lenarduzzi F. J., Yap S. S.  
Measuring the performance of a variable-speed drive retrofit on a fixed-speed centrifugal chiller. *ASHRAE Trans.*, Vol. 104, part 2, pp.658-667 (1998)
75. Lida et al. 1982  
Lida K., Yamamoto T., et al.  
Development of an energy-saving-oriented variable capacity system heat pump. *ASHRAE Trans.*, Vol. 88, part 1, pp. 441-450 (1982)
76. Liu et al. 2003  
Liu Z., Tang G., Zhao F. Dynamic simulation of air-source heat pump during hot-gas defrost. *Applied Thermal Engineering* Vol.23, No.6, pp. 675-685 (2003)
77. Lorenzetti and Norford 1994  
Lorenzetti D.M., Norford L.K.  
Pressure set point control of adjustable speed fans. *Journal of solar energy engineering-Transactions of the ASME*, Vol. 116, No. 3, pp. 158-163 (1994)
- 78.. Lsiburek 2002  
Lsiburek J.  
Residential ventilation and latent loads. *ASHRAE Journal*, Vol. 44, No. 4, pp. 18-22 (2002)
79. MacArthur 1984  
MacArthur J. W.  
Transient heat pump behavior: a theoretical investigation. *Int. J. Refrig.*, Vol. 7, No. 2. pp. 123-127 (1984)
80. Mahmoud and Ben-Nakhi 2003  
Mahmoud M. A. and Ben-Nakhi A. E.  
Architecture and performance of neural networks for efficient A/C control in buildings. *Energy Conversion and Management*, Vol. 44, No. 20, pp.3207-3226 (2003)
81. Martz et al. 1996  
Martz W. L., Burton C. M., Jacobi A. M.  
Local composition modeling of the thermodynamic properties of refrigerant and oil mixtures. *Int. J. Refrig.*, Vol. 19, No. 1, pp. 25-33 (1996)

82. Masato et al. 2000  
Masato K., Yoshiaki K., et al.  
Physical model of an air-conditioned space for control analysis. *ASHRAE Trans.*, Vol. 106, part 2, pp. 304-317 (2000)
83. Matthew and Banasal 1998  
Matthew W. B., Banasal P. K.  
Challenges in modeling vapor-compression liquid chillers. *ASHRAE Trans.*, Vol. 104, part 1B, pp. 474-486 (1998)
84. McQuiston 1978  
McQuiston F. C.  
Heat, mass and momentum transfer data for five plate-fin-tube heat transfer surfaces. *ASHRAE Trans.*, Vol. 84, No. 1, pp. 266-293 (1978)
85. Mei and Levermore 2002  
Mei L., Levermore G. J.  
Simulation and validation of a VAV system with an ANN fan model and a non-linear VAV box model. *Building and Environment*, Vol. 37, No. 3, pp. 277-284 (2002)
86. Nakashima et al. 1985  
Nakashima Y., Lijima H., et al.  
Reversible-flow-type linear expansion valve for heat pump. *ASHRAE Trans.*, Vol. 91, part 2, pp. 1555-1568 (1985)
87. NTIS 1986  
National Technical Information Service  
*NTIS: HVACESIM+, Building systems and equipment simulation program reference manual*. National Technical Information Service, U.S. Department of Commerce (1986)
88. Okada et al. 1992  
Okada T., Yoshikawa T., et al.  
Research and development of a home use VAV air-conditioning system. *ASHRAE Trans.*, Vol. 98, part 2, pp. 133-139 (1992)
89. Pavlovas 2004  
Pavlovas V.  
Demand controlled ventilation: A case study for existing Swedish multifamily buildings. *Energy and Buildings*, Vol. 36, No.10, pp.1029-1034 (2004)
90. Park et al. 2001  
Park Y. C., Young C. K., et al.  
Performance analysis on a multi-type inverter air conditioner. *Energy Conversion and Management*, Vol. 42, No. 13, pp. 1607-1621 (2001)

91. Pierre 1964  
Pierre B.  
Flow resistance with boiling refrigerant-part 1. *ASHRAE Journal*, Vol. 6, No. 9, pp. 58-65 (1964)
  
92. Qian and Zheng 2003  
Qian F. and Zheng Z.  
VAV air conditioning system in middle and small buildings. *Journal of HV&AC*, Vol.33, No.3, pp118-119 (2003) [In Chinese]
  
93. Reeves 1996  
Reeves K.  
Understanding direct digital controls for HVAC systems. *Cost Engineering*, Vol. 38, No. 8, pp. 28-32 (1996)
  
94. Scalabrin and Bianco 1994  
Scalabrin G., Bianco G.  
Experimental and thermodynamic analysis of a variable-speed open reciprocating refrigeration compressor. *Int. J. Refrig.*, Vol. 17, No. 1, pp.68-75 (1994)
  
95. Schell 1998  
Schell M.  
Saving energy and optimizing air quality using carbon dioxide. *Energy Engineering*, Vol. 95, No. 2, pp. 19-34 (1998)
  
96. Schmidt 1945  
Schmidt T. E.  
La production calorifique des surfaces munies d'ailettes. *Bulletin De L'Institu international du Froid Annexe G-5* (1945)
  
97. Seem et al. 2000  
Seem J. E., House J. M., et al.  
Damper control system for preventing reverse airflow through the exhaust air damper of variable-air-volume air-handling units. *ASHRAE Trans.*, Vol. 106, part 2, pp. 106-115 (2000)
  
98. Seem 1997  
Seem J. E.  
Implementation of a New Pattern Recognition Adaptive Controller Developed Through Optimization. *ASHRAE Trans*, Vol. 103, part 1, pp. 494-506 (1997)
  
99. Shaw and Luxion 1988  
Shaw A., Luxion R. E.  
A comprehensive method of improving part load conditioning performance. *ASHRAE Trans.*, Vol. 94, part 2, pp. 442-457 (1988)



100. Shaw and Luxion 1993  
Shaw A. and Luxion R. E.  
Intergration of dehumidification into life-cycle system design. *Proc. Int. Conf. Building design, technology and occupant well-being in tempera climates*, Brussels, ASHRAE, Atlanta, GA (1993)
101. Shelquist and Randy 2001  
Shelquist P., Randy A.  
Ventilation control strategies. *ASHRAE Journal*, Vol. 43, No. 9, pp.30-35 (2001)
102. Shepherd 1999  
Shepherd K.  
*VAV air conditioning systems*, Blackwell Science Ltd, London (1999)
103. Shirey 1993  
Shirey D. B.  
Demonstration of efficient humidity control techniques at an art museum. *ASHRAE Trans.*, Vol. 99, part 1; pp. 694-670 (1993)
104. Silver et al.1990  
Silver S. C., Fine P. J., et al.  
Performance monitoring of DX rooftop cooling equipment. *Energy Engineering: Journal of the Association of Energy*, Vol. 87, No. 5, pp.32-41 (1990)
105. So et al. 1995  
So A. T. P, Chow T. T., Chan W. L., et al  
Neural-Network-Based Identifier/Controller for Modern HVAC Controller. *ASHRAE Trans.*, Vol. 101, part 2, pp. 14-31 (1995)
106. So et al. 1997  
So A. T. P., Chan W. L., et al.  
Self-learning fuzzy air handling system controller. *Building Services Engineering Research & Technology*, Vol. 18, No. 2, pp. 99-108 (1997)
107. Song and Hu 2002  
Song Q., Hu W. J.  
Robust neural network controller for variable airflow volume system. *Proceedings of the American Control Conference*, Vol. 1, pp. 418-423 (2002)
108. Stephenson and Mitalas 1967  
Stephenson D. G., Mitalas G. P.  
Room thermal response factors. *ASHRAE Trans.*, Vol. 73, part 2. pp. 31-38 (1967)

109. Stephenson and Mitalas 1971  
Stephenson D. G., Mitalas G. P.  
Calculation of heat conduction of transfer functions for multilayer slabs. *ASHRAE Trans.*, Vol. 77, part 2, pp. 117-123 (1971)
110. Thomas 1997  
Thomas E. C.  
VAV systems--what makes them succeed? What make them fail? *ASHRAE Trans.*, Vol. 103, part 2, pp. 814-821 (1997)
111. Tobias 1973  
Tobias J. R.  
Simplified transfer function for temperature response of fluids flowing through coils, pipes or ducts. *ASHRAE Trans.*, Vol. 79, part 1, pp. 19-22 (1973)
112. Tung and Deng 1997  
Tung D. S. L., Deng S. M.  
Variable-air-volume air-conditioning system under reduced static pressure control. *Building Services Engineering Research & Technology*, Vol. 18, No. 2, pp. 77-83 (1997)
113. Turaga et al. 1988  
Turaga M., Lin S., Fazio P. F.  
Correlations for heat transfer and pressure drop factors for direct expansion air cooling and dehumidifying coils. *ASHRAE Trans.*, Vol. 94, part 2, pp. 616-629 (1988)
114. UI 1983  
University of Illinois  
*UI: BLAST 3.0*, Building loads analysis and system thermodynamics program user manual. Department of Mechanical and Industrial Engineering, University of Illinois, Urbana, U.S.A (1983)
115. Underwood 2000  
Underwood C. P.  
Robust control of HVAC plant I: modeling. *Building Services Engineering Research and Technology*, Vol. 21, No. 1, pp. 53-61 (2000)
116. Urashima 1993  
Urashima H.  
Modern multi-split system air conditioners for buildings. *Hitachi Review*, Vol. 42, No. 2, pp. 67-70 (1993)
117. Vargas and Parise 1995  
Vargas J. V. C., Parise J. A. R.  
Simulation in transient regime of a heat pump with closed-looped and on-off control. *Int. J. Refrig.*, Vol. 18, No. 4, pp. 25-243 (1995)

118. Wang and Burnett 1998  
Wang S., Burnett J.  
Variable-air-volume air-conditioning systems: Optimal reset of static pressure setpoint. *Building Services Engineering Research & Technology*, Vol. 19, No. 4, pp. 219-231 (1998)
119. Wang 1999  
Wang S.  
Dynamic simulation of building VAV air-conditioning system and evaluation of EMCS on-line control strategies. *Building and Environment*, Vol. 34, No. 6, pp. 681-705 (1999)
120. Wang et al. 1999  
Wang C. C., Lee C. J., Chang C. T., et al.  
Heat transfer and friction correlation for compact louvered fin-and-tube heat exchangers. *Int. J. Heat and Mass Transfer*, Vol. 42, No. 11, pp. 1945-1956 (1999)
121. Wang et al. 2000  
Wang C. C., Lin Y. T., Lee C. J.  
Heat and momentum transfer for compact louvered fin-and-tube heat exchangers in wet conditions. *Int. J. Heat and Mass transfer*, Vol. 43, No. 18, pp. 3443-3452 (2000)
122. Webb 1990  
Webb R. L.  
Air-side heat transfer correlations for flat and wavy plate fin-and tube geometries. *ASHRAE Trans.*, Vol. 96, part 2, pp. 445-449 (1990)
123. Welsby et al. 1988  
Welsby P., Devotta S., and Diggoy P. J.  
Steady- and dynamic-state simulations of heat-pumps, Part 1: literature review. *Applied Energy*, Vol. 31, No. 3, pp. 189-203 (1988)
124. Wilson 1995  
Wilson H. W.  
VAV mixed air plenum pressure control. *Heating/Piping/Air Conditioning*, Vol. 67, No. 8, pp. 53-55 (1995)
125. Wu and Cai 2000  
Wu J., Cai W.  
Development of an Adaptive Neuro-Fuzzy method for supply air pressure control in HVAC system. *Proceedings of the IEEE International Conference on Systems, Man and Cybernetics*, Vol. 5, pp. 3806-3809 (2000)
126. Yang and Lee 1991  
Yang K. H, Lee M. L.  
Analysis of an inverter-driven air-conditioning system and its application in a hot and humid area. *Int. J. of Energy Research*, Vol. 15, No. 5, pp.357-365 (1991)

127. Youn et al. 2002  
Youn C. P., Kim Y., et al.  
Thermodynamic analysis on the performance of a variable speed scroll compressor with refrigerant injection. *Int. J. Refrig.*, Vol. 25, No. 8, pp.1072-1082 (2002)
128. Zaheer and Zheng 1994  
Zaheer-uddin M., Zheng G. R.  
A dynamic model of a multizone VAV system for control analysis. *ASHRAE Trans.*, Vol. 100, Part 1, pp. 219-229 (1994)
129. Zamboni et al. 1991  
Zmaboni M., Gerchtold O., et al.  
Demand control ventilation: An application to auditoria. *Proceeding of 12th AIVC conference*, AIVC, pp. 143-145 (1991)
130. Zhang 1986  
Zhang Z. Y.  
*Principle and equipment for refrigeration*. Mechanical industry press, Ltd., Beijing, China. [In Chinese] (1986)
131. Zhang et al. 2000  
Zhang C. L., Ding G. L., Li H.  
An implicit curve-fitting method for thermodynamic property of refrigerant gas. *Journal of Engineering Thermodynamic*, Vol. 21, No. 5, pp. 533-536 (2000)
132. Zivi 1964  
Zivi S. M.  
Estimation of steady-state steam void-fraction by means of the principle of minimum entropy production. *Journal of Heat Transfer*, Vol. 86, No. 3, pp. 247-252 (1964)

## Appendix A

### Photos of the Experimental Rig

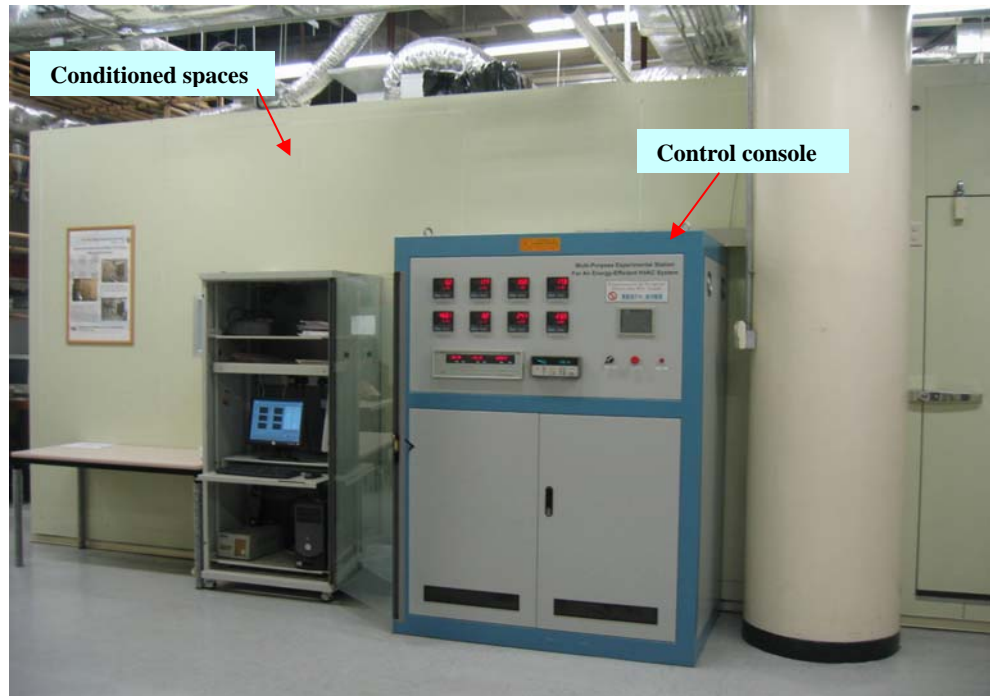


Photo 1 Overview of the experimental rig (1)

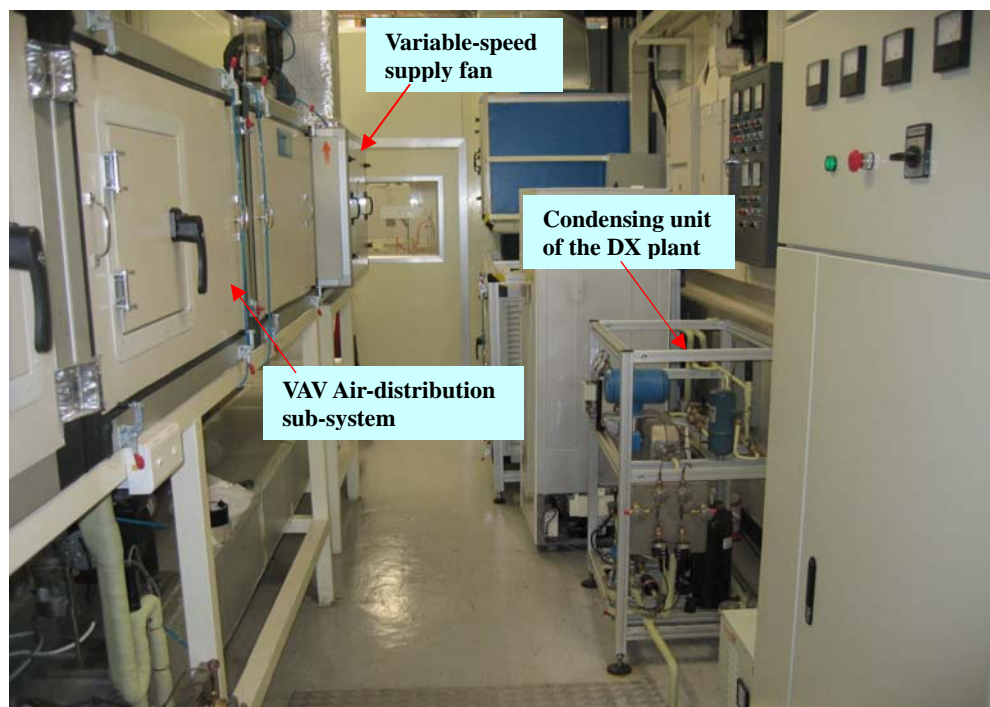


Photo 2 Overview of the experimental rig (2)

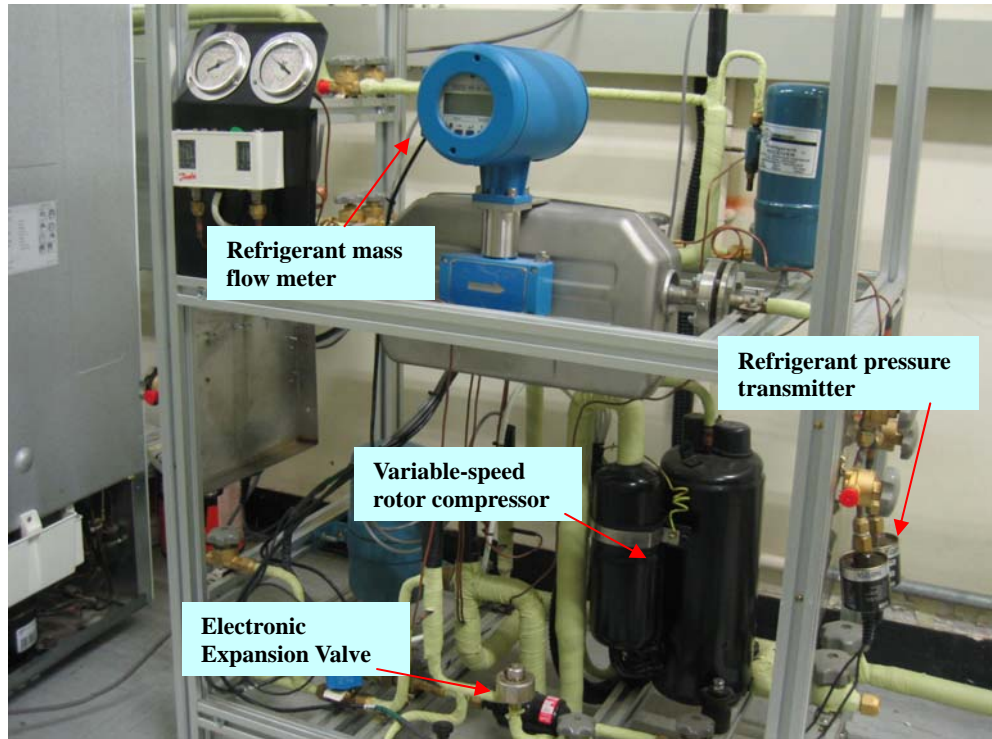


Photo 3 Condensing unit of the DX plant

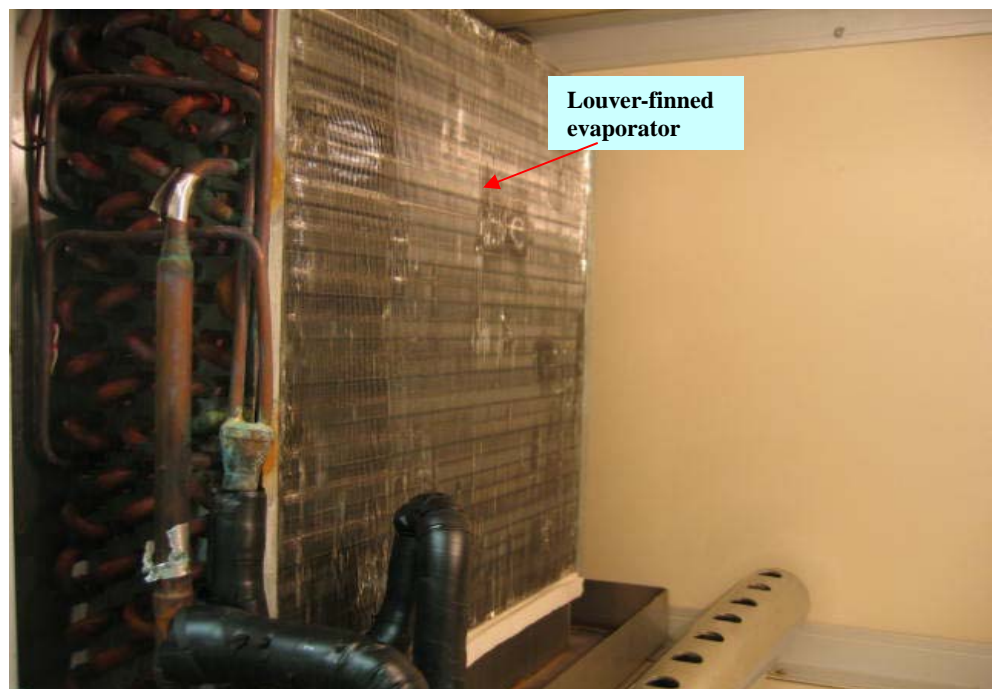


Photo 4 DX cooling coil in the VAV air-distribution sub-system

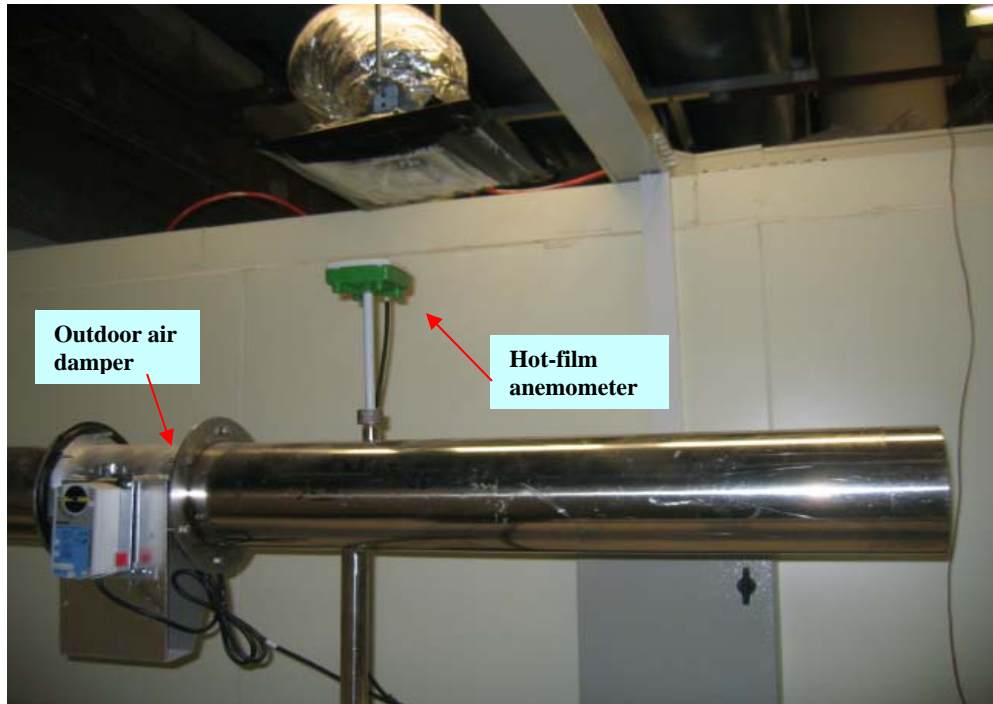


Photo 5 Outdoor air induction

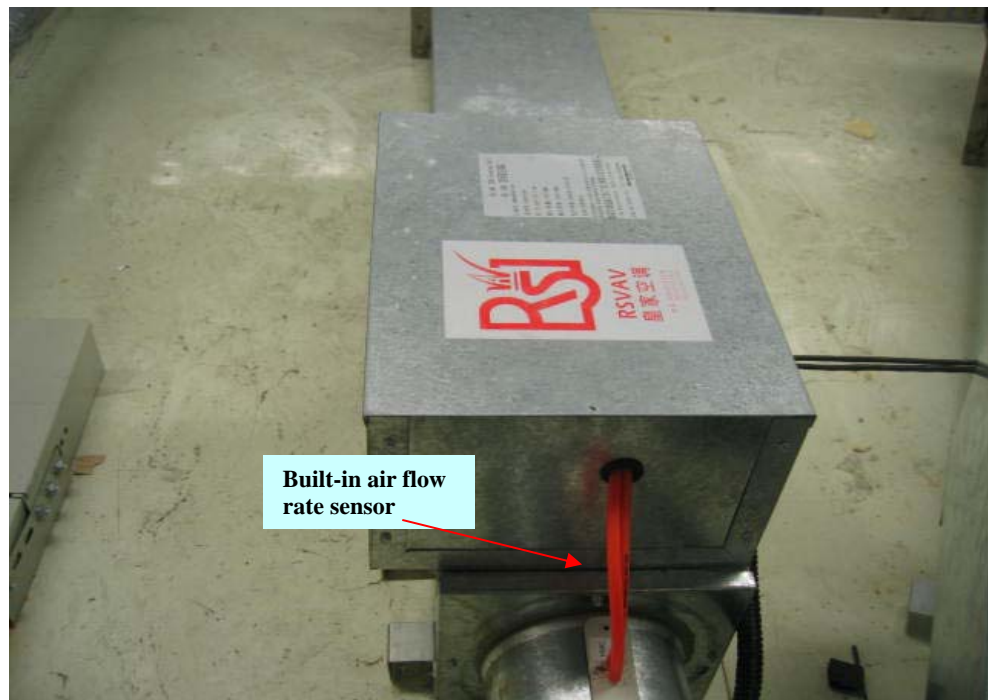


Photo 6 Box of VAV terminal



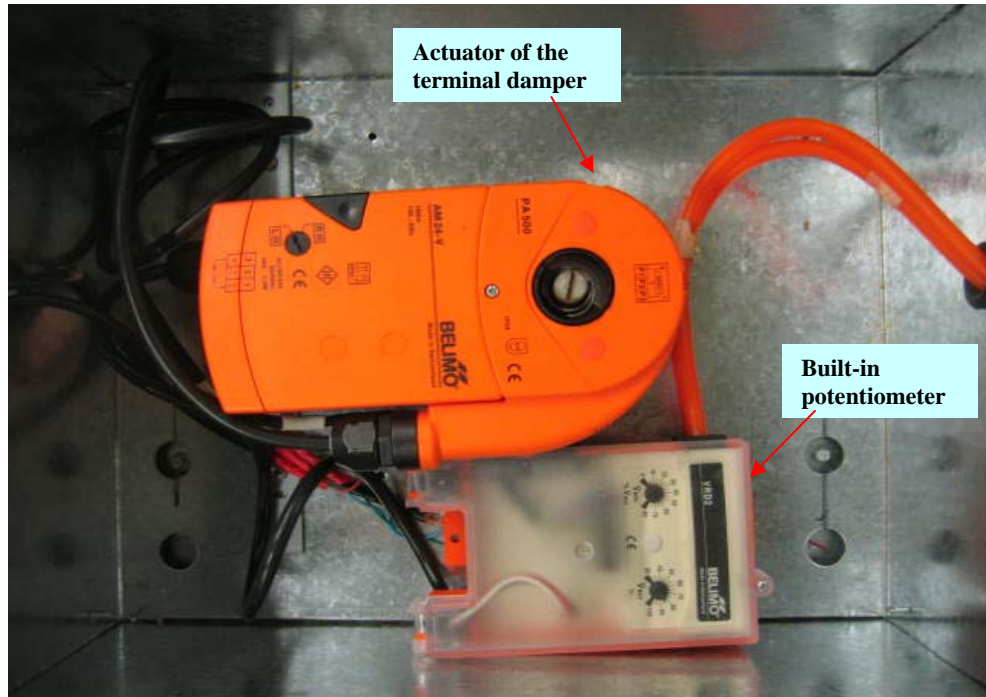


Photo 7 Controller of VAV terminal



Photo 8 Load generation unit inside conditioned spaces



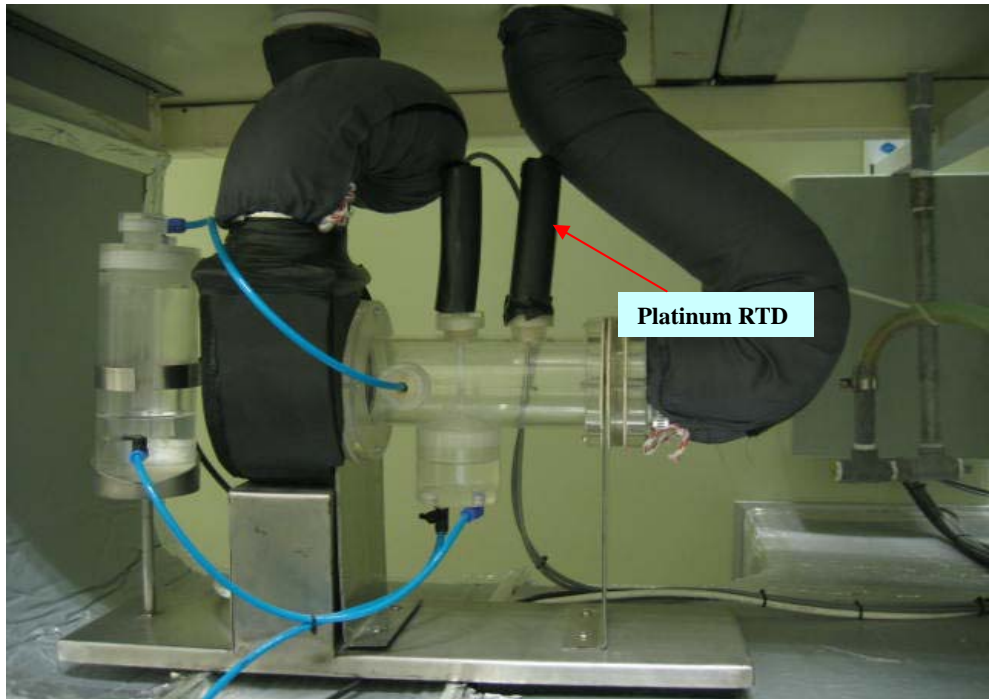


Photo 9 Air sampling device



Photo 10 Manometers for measuring supply air static pressure

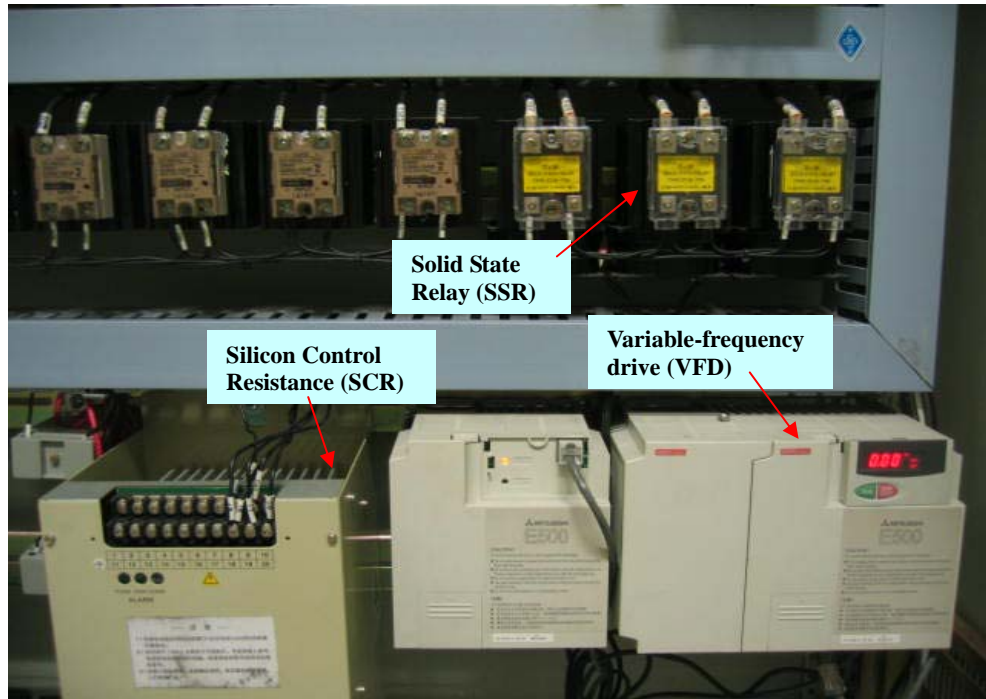


Photo 11 SCR, SSR and VFD

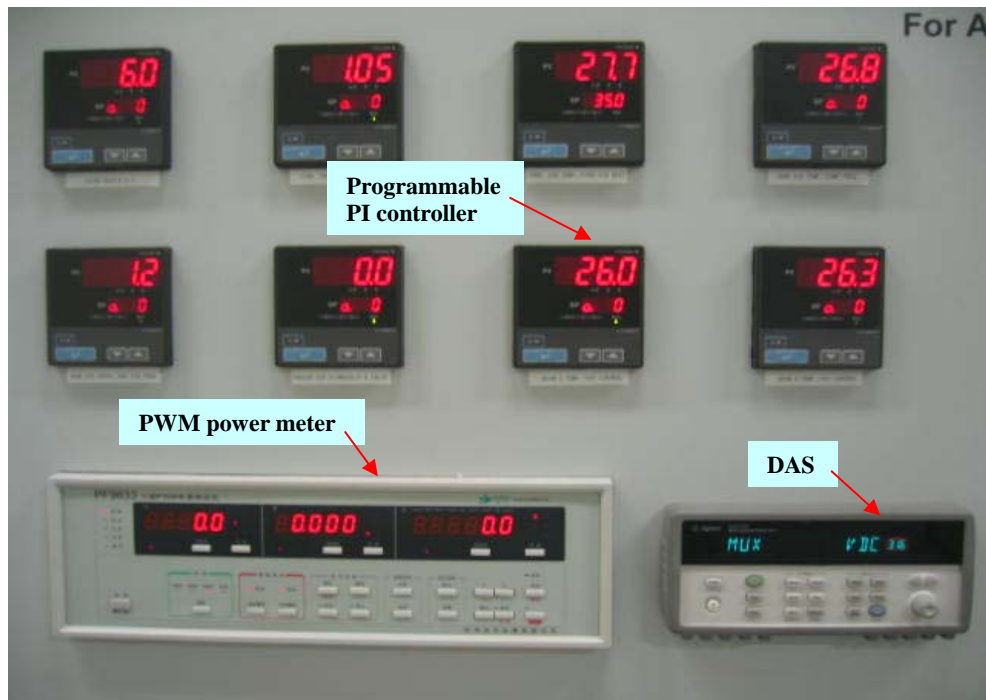


Photo 12 Control panel

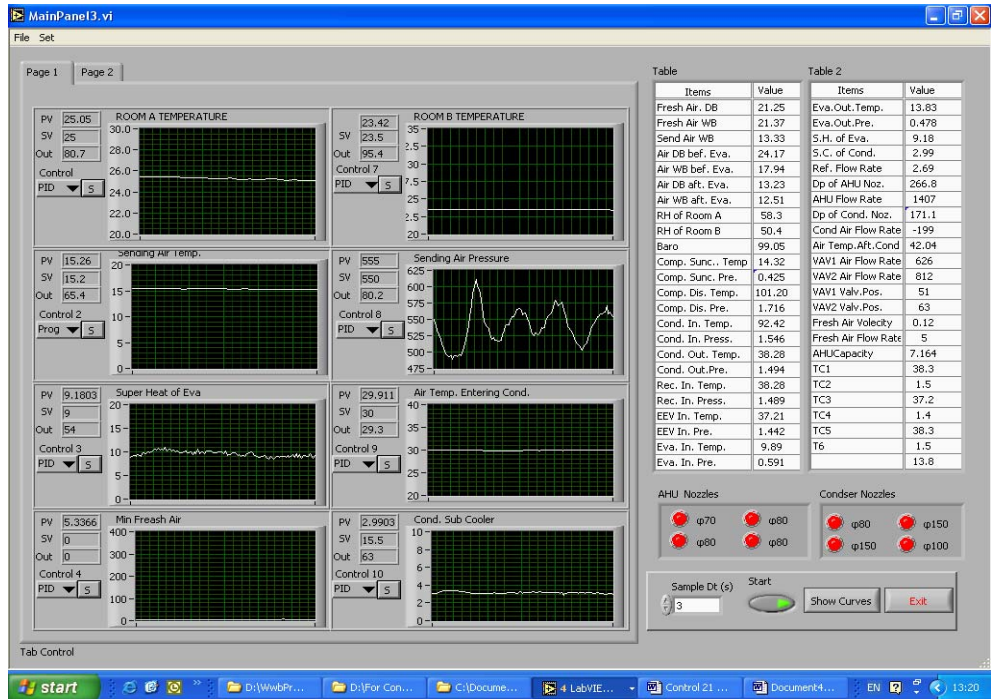


Photo 13 Logging & control supervisory program

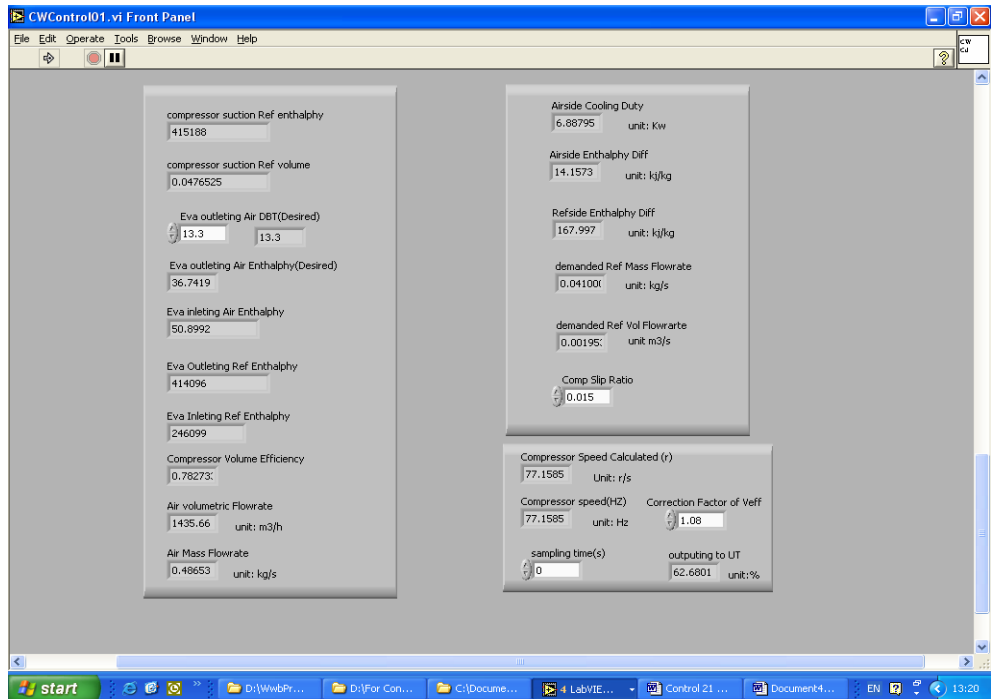


Photo 14 Self-programming Module (SPM)

## Appendix B

### Publications Arising From the Thesis

#### I. Journal papers

- **Wu Chen** and Shiming Deng. Dynamic mathematical modeling of a DX VAV A/C system–Part I : modeling DX plant. Submitted to *Building and Environment*.
- **Wu Chen** and Shiming Deng. Dynamic mathematical modeling of a DX VAV A/C system–Part II: modeling VAV air-distribution sub-system. Submitted to *Building and Environment*.
- **Wu Chen** and Shiming Deng. Dynamic mathematical modeling of a DX VAV A/C system–Part III: model validation and simulated closed-loop responses. Submitted to *Building and Environment*.
- Zheng Li, **Wu Chen**, Shiming Deng and Zhongping Lin. The characteristics of space cooling load and indoor humidity control for residences in the subtropics. In press, *Building and Environment*.
- **Chen Wu**, Zhou Xingxi, Deng Shiming. Development of control method and dynamic model for multi-evaporator air conditioners (MEAC). *Energy Conversion and Management*, Vol. 46, No. 3, pp. 451-465, 2004.

#### II. Manuscripts

- **Wu Chen** and Shiming Deng. A novel feedforward capacity controller for a DX VAV A/C system. To be submitted to *International Journal of Refrigeration*.

#### III. Conference papers

- **Wu Chen**, Zheng Li and Shiming Deng. Capacity control of a DX VAV system and its modeling. *Proc. of 10<sup>th</sup> International Refrigeration and Air*

*Conditioning Conference at Purdue*, pp. 01-05 (R009) Indianapolis, USA, 12–15 July, 2004.

- Zheng Li, **Wu Chen** and Shiming Deng. Indoor humidity control with DX A/C systems in subtropical residences. *Proc. of the 26<sup>th</sup> AIVC International Conference*, pp. 229-234, Brussels, Belgium, 21-23 Sep., 2005.